Issue No. 225 October 2002

BARC

NEWSLETTER

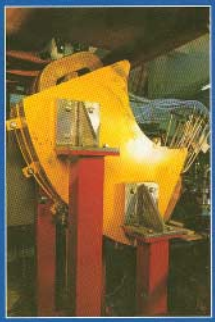


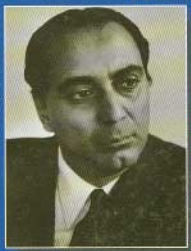


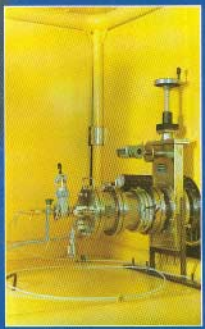

सत्यमेव जयते

BHABHA ATOMIC RESEARCH CENTRE

Founder's Day Special Issue

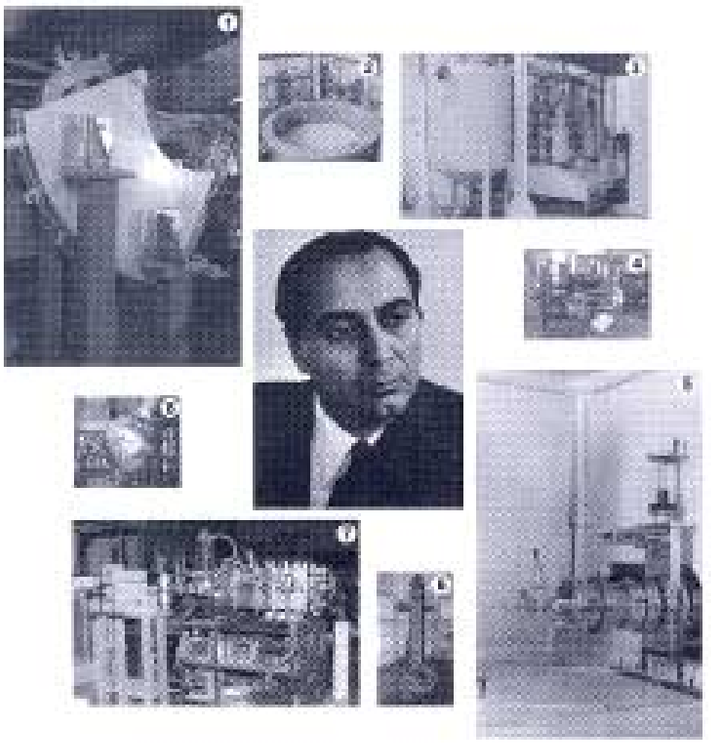

1. The 90°-analysing magnet.
2. Agitation tank used for ^{231}Pa Recovery Plant.
3. Vacuum station used for ^{231}Pa Recovery Plant.
4. Scattering chamber used for RBS measurements.
5. SNICS II ion source.
6. High voltage column section of FOTIA.
7. LAPSIS in the Pelletron Beam hall.
8. The 70° pre injector magnet.

सत्यमेव जयते

Government of India

BHABHA ATOMIC RESEARCH CENTRE

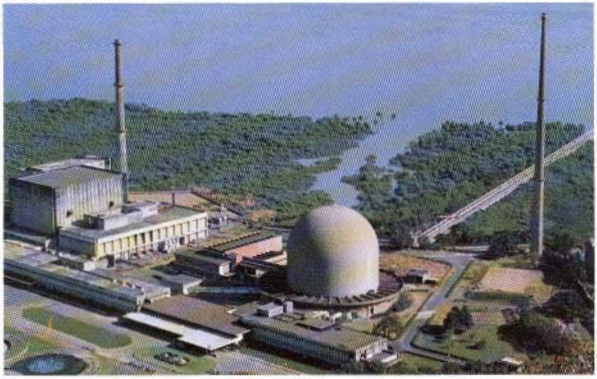

BARC Founder's Day Special Issue

October 2002 Issue No. 225

DEDICATED TO THE MEMORY OF

Homi Jehangir Bhabha

(1906 - 1966)

Founder and Architect of
Indian Atomic Energy Programme

Editorial Staff

CHIEF EDITOR
Dr Vijai Kumar

MANAGING EDITOR
T.C. Balan

Computer Graphics, Design & Layout
P.A.S. Warrier

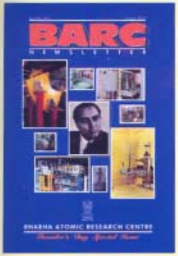

Newsletter on the Web

Available at
URL:http//www.barc.ernet.in

"When nuclear energy has been successfully applied to power production in, say, a couple of decades from now, India will not have to look abroad for its experts, but will find them ready at hand."

- **Homi Bhabha**

Issue No. 225 October 2002

BARC NEWSLETTER

Founder's Day Special Issue

Contents

Page 15

Page 27

Page 29

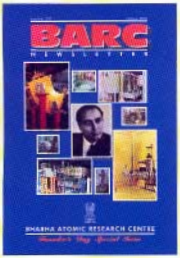

"We meet today at the beginning of a new chapter in our history. We have great hopes that this new chapter will be a glorious one. The development and use of atomic energy is a question of national importance. We hope to establish soon an Atomic Research Centre comparable with those in the most advanced countries."

- Homi Bhabha

Contents contd..


page 54


page 79


page 97

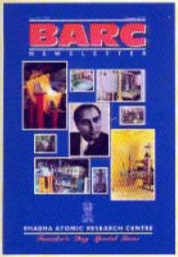

Contents *contd..*

"A scientist does not belong to a particular nation. He belongs to the whole world. The doors of science should be kept open to all those who work for the welfare of humanity."

- Homi Bhabha


page 99


page 108

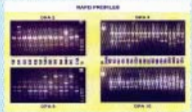
page 131

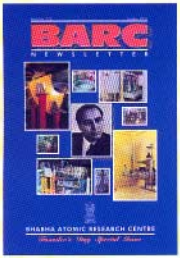

Contents *contd..*

"I know quite clearly what I want out of my life. Life and my emotions are the only things I am conscious of. I love the consciousness of life and I want as much of it as I can get. But the span of one's life is limited. What comes after death no one knows. Nor do I care. Since, therefore, I cannot increase the content of life by increasing its duration, I will increase it by increasing its intensity."

- Homi Bhabha

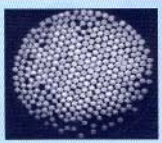
page 141

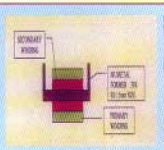

page 152


page 166

An Ideal Thyratron-Less Repetitive TE- Laser Pulser

Dhruba Jyoti Biswas
Laser and Plasma Technology Division
Bhabha Atomic Research Centre

Abstract

Laser and Plasma Technology Division has developed a thyratron-less, repetitive, transversely-excited (TE) laser pulser that has complete latch proof operation capability with D-C resonant charging. Thyratrons, a crucial component of the LIS programme of the DAE, are not manufactured in India and embargo applies to their sale. The heart of this novel TE laser pulser is a rotating dielectric spark gap, which has been conceived, developed, and operated in our laboratory. Its unique geometry has been fully exploited to obtain diode-less operation of the pulser and also to drive two high repetition rate TE lasers either simultaneously or with a variable delay.

Introduction

The TE laser pulser performs the crucial job of subjecting the gaseous medium to a transverse electric discharge leading to the inversion of population. The function of a pulser in the operation of a pulsed gas laser begins with the drawing of energy from the source and ends with the realisation of most of this as the internal energy of the (lasing) gas. Undoubtedly therefore, the overall efficiency of the laser depends quite strongly on the performance of the pulser. In the operation of pulsed gas lasers, energy is initially stored in a condenser, which is then made to discharge rapidly into the laser load with the help of a fast high voltage high current switch. The performance of the pulser during the charging process thus dictates the wall plug efficiency of the laser. Lesser the energy expended by the pulser while drawing energy from the source, the better the efficiency of the laser.

A typical pulse generator for a TE laser is shown in Fig 1. A DC high voltage supply charges up a condenser through a charging element, normally a resistance or an inductance. The charging bypass provides a path for the charging current. Once the condenser is charged to the required voltage, the rapid closure of the high voltage and high current switch enables the condenser to deliver its stored energy into the laser load before glow to arc transition can occur. The charging bypass must offer an impedance that is many times more than that of the laser load lest this should eat up a significant fraction of the energy stored in the condenser lowering, thereby, the plug in efficiency of the laser. At the same time its impedance should be much less than that of the charging element so that the current flowing through the conducting switch from the source following a discharge can be kept low for a given repetition rate. In the single shot operation, the condenser is normally

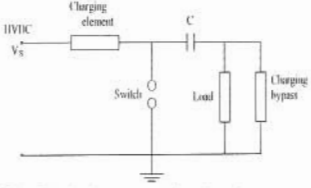

Fig.1 : Typical pulse generator for a TE gas laser

charged resistively and a spark gap is traditionally used as a switch. For repetitive operation, however, more efficient charging by means of inductance is employed and a thyratron replaces the spark gap. Following a discharge when the switch is still in a state of conduction, all the charging current delivered by the power supply gets diverted through this conducting switch. This current must be kept lower than the hold over current of the switch to ensure its recovery. Low charging current limits the maximum achievable repetition rate from the pulser. An ideal pulser would be one that allows recovery of the switch however high the charging current, and in turn repetition rate, is. We have conceived, developed, and operated in our laboratory a so-called 'ideal TE gas laser pulser' the repetitive operation of which is not hindered by the recovery problem of the switch. It is imperative that an account of this work here follows a brief review of the D-C resonant charging scheme on which a conventional repetitive TE gas laser pulser is normally based. Interested readers are referred to a review article [1] for a deeper insight to the various aspects of charging and discharging processes of a TE-laser pulser.

Direct - Current (D-C) Resonant Charging

The main condenser can be charged to the required voltage, ranging within tens of kV depending on the type of the TE laser load, normally in two different ways: resistively or resonantly by a DC source although resonant charging of a condenser by an AC source is also not uncommon. Resistive charging not only suffers from poor charging efficiency but also offers low charging frequency as the recovery problem of the switch assumes greater significance here [1]. The charging of the condenser through an inductance, commonly known as D-C resonant charging, finds wide application in the repetitive operation of TE gas lasers because of its inherent high plug-in efficiency [2] and high repetition rate capability [3].

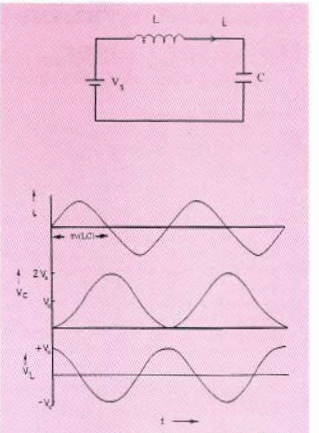

Fig. 2 : a) Typical D-C resonant charging network b) The charging current (i), the voltage across the capacitor (V_c), and the voltage across the inductance (V_L) as a function of time (t).

The Kirchoff's loop equations in a typical D-C resonant charging circuit (as shown in Fig 2a), considering an ideal case where there is no resistance in the charging loop and a D- C source (V_s) charges the capacitance C through an inductance L, can be written as follows:

$$V_S - L(di/dt) - (q/C) = 0 \quad (1)$$

Substituting $i = (dq/dt)$, we obtain

$$(d^2q/dt^2) + q/(LC) - V_S/L = 0 \quad (2)$$

The solution of the above equation can be shown to be

$$q = V_S C\,(1 - \cos(\omega t)) \quad (3)$$

where ω, the resonant frequency of the circuit, is given by

$$\omega = 1/(\sqrt{(LC)}) \quad (4)$$

The expressions for current (i) and voltages across the condenser (V_C) and the inductance (V_L) can be worked out to be,

$$i = dq/dt = V_S C\omega \sin(\omega t) \quad (5)$$

$$V_C = V_S (1-\cos(\omega t)) \quad (6)$$

$$V_L = V_S \cos(\omega t) \quad (7)$$

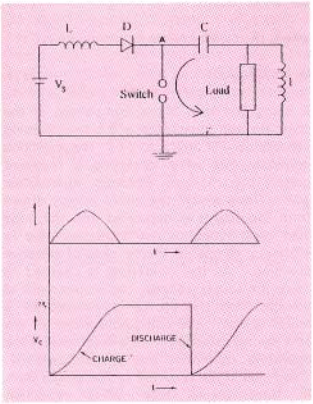

Fig. 3 a) Typical resonantly charged TE laser pulser
b) The charging current and voltage across the condenser in the above figure

The current and the voltages represented by the above equations are illustrated in Fig 2b. Understandably, the sum of voltages across the inductance and the condenser at any instant equals the supply voltage V_S. It can be seen from this figure that during a half cycle when the charging current is in the forward direction, the condenser acquires a voltage twice that of the supply. During the next half cycle, the current flows in the reverse direction and the condenser loses all its charge. If, however, a diode were introduced in the circuit (Fig 3a) to arrest the flow of reverse current the condenser would then retain its voltage. This figure also shows the discharge path of the condenser that includes the switch and the load. As the switch closes, condenser discharges through it into the load and the voltage across it drops to zero. The current flows in the forward direction once again and the condenser acquires twice the supply voltage and so on (Fig 3b).

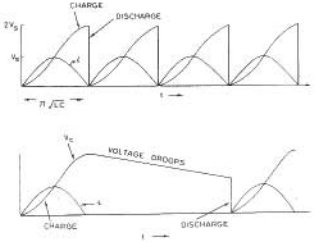

Fig. 4 : Few charging and discharging waveforms and the charging current (i) in a resonantly charged pulser
(a) Operation at 100% duty cycle
(b) Operation at a lower duty cycle, the droop in the voltage across the condenser is apparent here.

The time required for the condenser to get charged to $2V_S$ is $\pi\sqrt{(LC)}$, half the period of oscillation. Thus at 100% duty cycle, i.e., the condenser discharges as soon as its acquired voltage is $2V_S$, the repetition rate is double the resonant frequency of the D-C resonant charging network (Fig.4a). If, however, the network is operated at a lower duty cycle, i.e., the condenser discharges long after acquiring the peak voltage, the voltage across it would then droop (Fig 4b). This is because current, though small, may flow for longer duration through the voltage measuring circuitry. The voltage may also fall due to the flow of minority current in the reverse biased diode. This effect would assume significance in the operation at a very low duty cycle.

Immediately following a discharge, as the switch is still in the state of conduction, the power supply makes a short through it (Fig5a). However, unlike in the case of R-C charging, where the peak charging current

(i=V_S/R) appears immediately after the discharge, the charging current here builds up from zero value and can be expressed by the following equation:

$$\Delta i(t) = V_S \times \Delta t/L \quad (8)$$

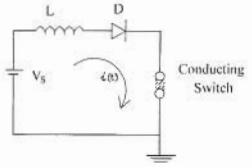

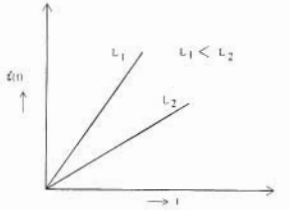

Fig. 5 : a) The power supply making a short through the conducting switch
b) Short circuit current as a function of time for two different values of charging inductance L.

The build up of the short circuit current (shown in the Fig 5b for two values of charging inductance) should be such that it does not exceed the hold over current of the switch until it's complete recovery. Higher the inductance, slower the rise of the current and better is the chance of the recovery of the switch although at the expense of the maximum achievable repetition rate, f_{max}, which is given by

$$f_{max} = 1/[2\pi\sqrt{(LC)}] \quad (9)$$

As is seen from eqn.5, the same recovery condition of the switch can also be met for smaller values of V_S. However, V_S is fixed from the consideration of the laser load and cannot be utilised to control rise of the short circuit current. Thus for a particular load and a given switch, the value of L needs to be appropriately fixed to ensure recovery of the switch.

The efficiency (η) of resonant charging is given by the following expression [3].

$$\eta = 1 - \pi/(4Q), \quad (10)$$

where the Quality factor Q is defined as

$$Q = 2\pi f_{max} L/R \quad (11)$$

R being the total ohmic component of the charging loop impedance and L the charging inductance. If $R/(f_{max}L) << 1$, the condition generally met while designing a resonant pulser, the charging efficiency approaches 100%. Thus almost the entire energy drawn from the source is deposited into the laser load contributing to the increased plug in efficiency compared to the case of resistive charging. As the condenser is charged to twice the supply voltage, the requirement of voltage from the source is lowered by a factor of half. The charging current arrives at a low rate starting from a zero value if the operating conditions are chosen properly. This helps in the recovery of the switch that, in turn, allows high pulse repetition frequency (prf).

This scheme too suffers from few short-comings. If the prf is considerably lower than the resonant frequency of the network, i.e., the pulser is operated at a low duty cycle, the discharge voltage may droop considerably. Secondly, the value of L cannot be made arbitrarily small as then the rapid build up of the short circuit current would prevent the conducting switch to go into the off state following a discharge. This effect, which limits the maximum achievable repetition rate, has been the subject of investigation in a number of studies [4,5] aimed at enhancing the repetition rate capability of a resonant charging network. The central point of these studies is to isolate the power supply during a discharge so that flow of short circuit current through the conducting switch is prevented. The most

effective means of controlling the rise of short circuit current without jeopardising the repetition rate capability of the pulser network is to introduce a second switch in the charging loop, [6-8] commonly known as command resonant charging

Command Resonant Charging:

Schematic diagram of a pulser based on command resonant charging is as shown in Fig 6. As is seen, a second switch S_2 is now introduced in the charging loop. The operation of the circuit can be explained as follows. When a trigger pulse T_2 arrives in

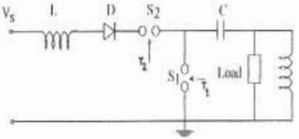

Fig. 6 : Typical command resonant charged TE laser pulser network

the charging switch S_2, it closes and the condenser C gets charged. As the charging current becomes zero, this switch automatically turns off isolating the power supply from the rest of the circuit. At this point, a second trigger T_1 arrives at the discharge switch S_1, which then closes enabling the condenser to discharge through it into the load. During and following a discharge, the switch S_2, which is in the off state, forbids the flow of any short circuit current enabling S_1 to recover within its deionisation time. Thus in this mode of operation, maximum achievable repetition rate is not limited by the switch latch up problem. Simply lowering the value of L can reduce charge-up time of the condenser. Few charging and discharging waveforms in this mode of operation are shown in Fig 7. As the condenser is charged on command here, this network can be operated at any duty cycle with almost no voltage droop. The condenser can be made to charge just before it has to be discharged. This increases the life of both the discharge switch as well as the storage capacitor as the hold off voltage

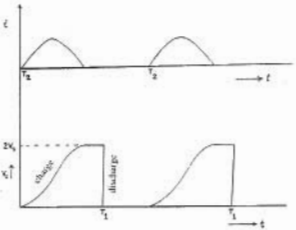

Fig. 7 : The charging current (i) and few charging and discharging waveforms in a command resonant charged pulser network

appears across them briefly. The droop free operation of this pulser has been illustrated in Fig 8 for a duty cycle of 10%. The resonant frequency shown here is 1kHz while the operating frequency is 100 Hz. 8 ms after a discharge the trigger arrives in S_2 allowing the condenser to be fully charged within 1 ms. The condenser holds the charge for 1 ms when the second trigger arrives in S_1 causing it to discharge into the load. The voltage droop in a similar operation with conventional resonant charging network can be seen in Fig 4b.

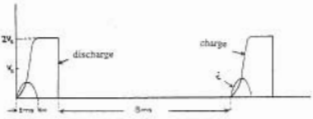

Fig. 8 : Droop free operation in a command charged pulser network at a low duty cycle operation

This method of charging too, however, is not devoid of disadvantages. Firstly, both the anode and the cathode of the charging switch have to be maintained at high voltages. High voltage isolation transformer is therefore required for the filaments. Much art is also needed in the design of the grid and bias circuits. False triggering of the charging switch also cannot be ruled out which can be caused by the electromagnetic

noise associated with the high voltage high current discharge pulse initiated by the closure of the discharge switch. This would mean that both the switches are simultaneously in conduction once again bringing in the switch latch up problem with a much graver consequence as the value of charging inductance is kept low to make the command resonant charging high repetition rate compatible.

An Ideal Repetitive TE Laser Pulser

We have seen that short circuit proof operation of a pulser based even on a command resonant charging network cannot be guaranteed. This makes the switches, normally two thyratrons, vulnerable to damage. Thyratrons are expensive, have limited life, and embargo applies to their sale in India. Against this background we have conceived, designed, developed, and operated a novel, inexpensive, and simple switch that as a driver of a resonantly charged TE laser pulser offers complete latch proof operation. By exploiting the unique geometry of this device we have achieved a number of advantages that even a command resonant charged pulser cannot match [9-14]. The heart of this device is a suitably configured circular dielectric plate that rotates between the electrodes of an ordinary spark gap. Such rotation intrinsically isolates the power supply from the rest of the circuit during a discharge and, as explained below, is instrumental in making a TE-laser pulser driven by this switch a near ideal one.

Rotating Dielectric Spark Gap:

The rotating disc, the most important part of this switch, is shown in Fig 9. The disc is a circular plate of ~20 cm diameter with even number of equidistant holes (~6mm diameter) drilled along a circle close to its periphery. By mounting the disc on a motor, it can be so rotated that the holes pass symmetrically between the electrodes of the spark gap. The operation of this switch can be easily understood by considering a

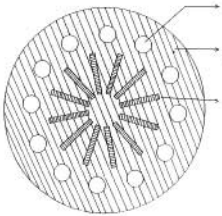

Fig. 9 : Schematic diagram of a rotating dielectric disc

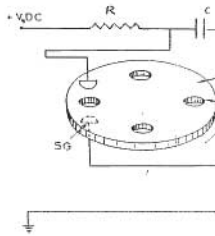

Fig. 10 : Resistively charged pulser network driven by a rotating dielectric spark gap

resistively charged pulser as shown in Fig 10. Within the travel time between two adjacent holes the condenser C gets charged close to the supply voltage V_0, which is more than the air breakdown voltage of the spark gap. Every time a hole appears between the electrodes of the spark gap, it closes allowing the condenser to discharge into the load. Following a discharge, the appearance of the dielectric between the electrodes truncates the flow of any charging current through the switch causing thereby its forced recovery. The charging current thus can assume very high value reducing thereby the charging time of the condenser. If the rotation speed of the dielectric plate is made compatible with the charge up time of the condenser, the repetition rate would then be accordingly enhanced. In contrast, the repetitive operation capability of a

conventional spark gap when used with this pulser is restricted, as the charging current has to be less than the holdover current of the switch. In the operation with rotating dielectric spark gap as the switch, ~2kW of power was dissipated into a dummy load at a repetition rate of 300Hz [9]. The fins on the dielectric disc, when rotated, blow air jet into the spark gap and facilitate, thereby, such high repetition rate operation of the switch.

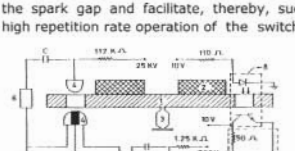

Fig. 11 : Schematic diagram of the rotating dielectric spark gap driven resistively charged pulser along with optical sensor based triggering circuitry. 1 Rotating dielectric disc, 2. Fins, 3. Motor, 4. Triggerable spark gap, 5. Trigger, 6. Load, 7. Pulse transformer, 8. Opto electronic sensor, 9. Current amplifier, 10. SCR

In the un-triggered mode of operation, the large jitter associated with the fluctuation of the breakdown voltage marred the performance of the pulser. The triggering of the switch was accomplished by mounting a light emitting diode and a photo detector face to face on either side of the rotating dielectric in such a way that whenever a hole passed between them another hole also passed between the electrodes of the spark gap (Fig 11). At every such coincidence, the detector received light from the emitter and gave out a pulse, which after processing was used to trigger the spark gap. In the triggered mode of operation the jitter significantly reduced to ~ 25 nsec [10].

As demonstrated in ref 11, a rotating dielectric spark gap also has latch proof operation capability when used with resonantly charged pulsers. However, such an operation is not possible utilising a simple circuit as of Fig 10 where the charging resistance is replaced by an inductance. This is because following a discharge the short circuit current (i) can build up during the travel time of the hole (t) between the electrodes of the conducting switch. For a TE laser load, this current and hence the energy stored in the charging inductor can be appreciable [11]. As the flow of this current is intercepted by the moving dielectric, the inductor releases the stored energy causing the dielectric plate to ignite. The energy stored can be reduced by increasing the value of L (as $E = \frac{1}{2}(Li^2) = (V_s^2t^2)/(2L)$, from eqn 6). This, however, is not a practical solution as it would be at the expense of the achievable repetition rate.

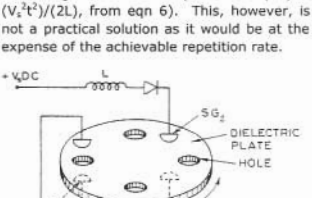

Fig. 12 : Short circuit proof operation of the resonantly charged pulser when driven by a rotating dielectric spark gap

An elegant solution to this problem is to incorporate a second spark gap in the charging loop and rotate the same dielectric plate between the electrodes of both the spark gaps in such a way that holes appear in them exactly out of phase (Fig 12). The operation of this circuit can be explained in the following manner. When a hole gets aligned with the charging spark gap SG_2, it closes allowing the condenser to be charged to $2V_s$ in a time $(\pi\sqrt{(LC)})$ which is made smaller than the travel time of the hole inside the gap by proper choice of L. After the passage of the hole, the appearance of the dielectric in the gap of this switch virtually cuts off the power supply from the rest of the circuit. A hole now appears between the electrodes of the discharge spark gap (SG_1) when it closes allowing the condenser to discharge into the load. During

and immediately following the discharge, which is normally very short lived for a TE laser load, the open switch SG_2 prevents any short circuit current from flowing through SG_1. The discharge switch thus readily recovers, as the inductor now does not store any energy during its conduction. The condenser would get charged once again when a second hole gets aligned with SG_2 and so on. In this mode of operation the pulser delivered ~3.2kW of power at a repetition rate of 200 Hz into a dummy load which resembled a typical TEA CO_2 laser.

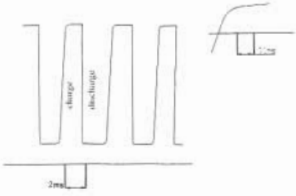

Fig. 13 : Few charging and discharging waveforms of the short circuit proof operation of the resonantly charged pulser shown in Fig. 18. The inset shows the charging of the condenser in an expanded time scale.

Few charging and discharging waveforms shown in Fig 13 conform to the above description. The jitter in the operation of both SG_1 and SG_2 is apparent from this figure. When this pulser is used to drive a laser, the fluctuation in the closing of charging switch can be ignored, as it does not affect the performance of the laser. Therefore triggering of the discharge switch alone suffices which is accomplished using the optical sensor based mechanism described in ref 9. Proper positioning of the holes with respect to the spark gaps such that the condenser discharges soon after acquiring the peak voltage ensures droop free operation with this device.

The rotating dielectric spark gap switch can also drive simultaneously two high repetition rate lasers [12]. The two lasers can be operated synchronously or with a delay that can be as large as a millisecond. Schematic diagram of the circuit is shown in Fig 14. The

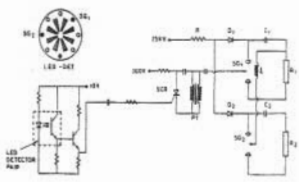

Fig. 14 : Rotating dielectric spark gap as a driver of two resistively charged high repetition rate lasers.Inset shows the positions of the holes with respect to the discharge gap SG_1 and SG_2

same dielectric is rotated between the electrodes of SG_1 and SG_2 in such a way that holes appear in them simultaneously. SG_1, triggered by the optical sensor based technique, causes the condenser C_1 charged to the supply voltage to discharge into the load R_1 while a pulse derived from this first pulser triggers SG_2 causing C_2 to discharge into the load R_2. A delay up to few microseconds between the two discharges has been obtained by varying the value of *l*. The diodes D_1 and D_2 are required to isolate the two discharge circuits. A larger delay, ranging from several microseconds to more than a millisecond, has also been obtained by positioning SG_1 and SG_2 with respect to the dielectric such that when a hole arrives in SG_1, another hole is yet to arrive in SG_2. The time interval between the arrivals of the two holes between the electrodes of their respective spark gaps is the delay between the two discharges. Triggering both SG_1 and SG_2 has considerably reduced the jitter in such operation. The voltage enhanced pulse from the optical sensor triggers SG_1 directly and SG_2 after being delayed by a delay generator. The performance of this device has been tested by switching a total of 2.5 kW of power at 200Hz into two identical dummy loads resembling a typical TE laser in terms of resistance. Though resistive charging has been employed in this operation, resonant charging can be used for better efficiency. We note here that this technique can be, in principle, employed for synchronisation of more than two lasers.

The unique geometry of the rotating dielectric spark gap also allows diode-less operation of a command resonant charging network [13]. In a conventional switch, thyratron, spark gap or SCR driven resonant charging pulser, the presence of diode is mandatory to arrest the flow of reverse current so as to maintain the voltage on the condenser (refer to Fig 3a). These diodes, which should be capable of withstanding high voltages and high currents, when form a part of the pulsers meant for repetitive operation of typical TE lasers are expensive and prone to damage, more so in the event of a short circuit. The principle of diode less operation can be understood by referring to Fig 15.

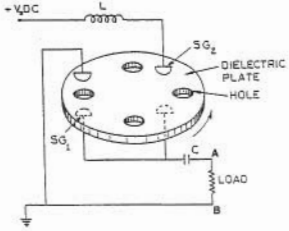

Fig. 15 : Diode-less operation of a resonantly charged pulser network driven by a RDSG

SG_1 and SG_2 are so located that when the dielectric rotates, holes appear in them exactly out of phase. As a hole gets aligned with SG_2, it closes allowing the condenser to get charged through L. If the time of passage of the hole between the electrodes of SG_2 exactly equals the time taken by the condenser to get charged fully ($=\pi\sqrt{(LC)}$) the appearance of the moving dielectric in the gap thereafter forces the switch to go into the off state preventing the flow of any reverse current thus rendering the usage of a diode superfluous. As a second hole gets aligned with SG_1 it closes and the condenser discharges into the load. A pulser has been operated in this mode at a repetition rate of 600 Hz with a dummy load resembling a typical TE laser. Few charging and discharging waveforms at this repetition rate are shown in Fig 16. It would be seen that the voltage of the condenser has dropped to about 90% of its initial value at the time of a discharge. This indicates that some reverse current had flown through SG_2 before the moving dielectric appeared between its electrodes and blocked it. Such a situation can be overcome by adjusting the charge up time of the condenser by making use of a variable choke or alternately by adjusting the rotation speed of the motor.

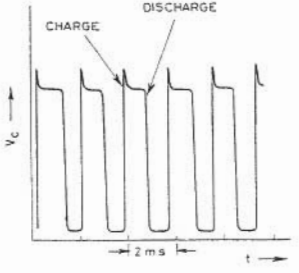

Fig. 16 : Few charging and discharging waveforms for the diode-less pulser

The geometry of this switch allows an easy scalability of the maximum achievable repetition rate. The repetition rate (f) in Hz here can be written as

$$f = n \times s \qquad (12)$$

where n is the number of holes on the disc and s is the number of rotations per second. Increasing n or s or both, therefore, can increase the repetition rate, however, up to a certain limit. If holes are too close the device no longer remains compatible with resonant charging. On the other hand, the speed of rotation increases at the expense of the mechanical stability of the device. Further increase in the repetition rate is possible by increasing the number of discharge gaps [14]. The schematic diagram of the circuit where a repetition rate of 1.2 kHz has been achieved with a rotating dielectric switch utilising two pairs of discharge gaps SG_2 and SG_3 is shown in Fig 17. Reliable short circuit proof operation was

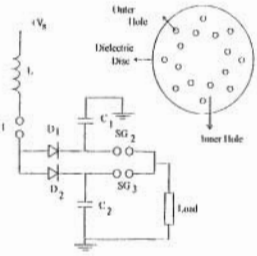

Fig. 17 : Schematic diagram of the pulser used to obtain KHz repetition rate with rotating dielectric spark gap. The inset shows the staggered configuration of the holes

achieved with resonant charging by staggering the holes into an inner and an outer circle. The outer holes were aligned with the charging gap (SG_1) while the inner holes were aligned with the discharge gaps. The condensers C_1 and C_2 get charged whenever SG_1 conducts and C_1 discharges through SG_2 and C_2 through SG_3 with a delay determined by the location of SG_2 and SG_3 with respect to the passing holes. Diodes $D_1$and D_2 prevent the condensers from discharging through the same gap.

Conclusions

We have shown that the repetition rate operation capability of an ordinary spark gap can be greatly enhanced simply by rotating a suitably configured dielectric plate between its electrodes. Such a rotating dielectric spark gap has been shown to provide complete latch proof operation of a repetitive TE laser pulser with D-C resonant charging. This is indeed an achievement because complete short circuit proof operation cannot be guaranteed even with the popular method of command resonant charging. Further in this operation a rotating dielectric spark gap replaces two (expensive) thyratrons mandatory for command resonant charging. The unique geometry of this switch has been exploited to use it as a driver of i) a diode less resonantly charged pulser, ii) more than one high repetition rate lasers synchronously or with desired delay and iii) of a repetitive pulser in the KHz range.

Acknowledgement

The author acknowledges the keen interest shown and active support extended by N. Venkatramani, Head, Laser and Plasma Technology Division, BARC.He also gratefully acknowledges the contributions of U.K. Chatterjee, former Head, L&PT Div and his co-worker J. P. Nilaya. The author thanks B. S. Narayan for his collaboration towards achieving optical sensor based triggering of the rotating dielectric spark gap. He also thanks his colleagues, at CAT and BARC, N. S. Benerji, A. Kumar, S. K. Sarkar, A. K. Nath, and U. Nundy for many useful discussions and R. A. Nakhwa for excellent technical assistance.

References

1. D. J. Biswas and J. P. Nilaya, Prog. Quantum Electron **26,** pp 1-63 (2002)
2. P. K. Bhadani, Rev Sci Instrum **60**, 605 (1989).
3. J. V. Lebacqz and H. J. White, Pulse generators, ed: G. N. Glasoe and J. V. Lebacqz , Vol 5, p-275 (McGraw Hill, NewYork, 1948).
4. R. C. Sze and E. Seegmiller, IEEE J Quant Electron, **QE-17**, 81(1981).
5. S. Black and T. R. Borkes Digest of Technical papers, 2nd international pulsed power conference, Lubbock, Texas, June 1979.
6. K. R. Rickwood and J. McInnes, Rev Sci Instrum **53**, 1667 (1982).
7. T. Kan, D. Ball, E. Schmitt, and J. Hill, Appl Phys Lett **35**, 676 (1979).
8. G. J. Scoles and B. P. Newton, Proc of 11th modulator symposium, Sept 1973 (technical reprint no 78, English electric valve co., Chelmsford, U. K).
9. J. P. Nilaya, D. J. Biswas, B. S. Narayan, and U. K. Chatterjee, Rev Sci Instrum, **65**, 3590 (1994).

10. J. P. Nilaya, Ph.D thesis, University of Mumbai (2001). D. J. Biswas, J. P. Nilaya, and U. K. Chatterjee, Rev Sci Instrum **66**, 4813 (1995).
11. D. J. Biswas, J. P. Nilaya, and U. K. Chatterjee, Opt Eng **36**, 588 (1997).
12. D. J. Biswas and J. P. Nilaya, Rev Sci Instrum **72**, 2505 (2001).
13. J. P. Nilaya and D. J. Biswas, Proc of National laser symsposium, PRL, Ahmedabad, India, p-48 (1998).

Dr Dhruba J. Biswas was conferred the Homi Bhabha Science & Technology Award for the year 2000 for his outstanding contributions in laser technology and related fields.

About the author ...

Dr Dhruba J. Biswas *received his M.Sc (physics) degree from I.I.T. Kharagpur in 1978 and joined the erstwhile MDRS, BARC in 1979 after graduating from the 22nd Training School batch. His experimental work on optical chaos fetched him the doctorate degree from the Heriot-Watt University, Edinburgh, in 1986 where he was on a two-year sabbatical. His current research interest includes physics and technology of mid-infrared gas lasers including optically pumped molecular lasers and laser induced physical processes. He has to his credit 64 scientific papers, including 5 review papers, in refereed international physical journals. He is a recognised Ph.D (physics) guide of Mumbai University. He is recipient of the INSA young scientist medal (Physics, 1987), A. K. Bose Memorial award of INSA (Physical Science, 1989), N. S. Satyamurthy Memorial Award of IPA (1991), and Associate-ship of International Centre for Theoretical Physics, Italy (1994-2001).*

Design and Development of Drive Mechanisms for Adjuster Rods, Control Rods and Shut-off Rods of Tarapur Atomic Power Projects-3&4

Manjit Singh, D. N. Badodkar, N. K. Singh, N. S. Dalal, M. K. Mishra, C. B. Kothari, and G. Veda Vyas
Division of Remote Handling & Robotics
Bhabha Atomic Research Centre

Introduction

BARC and Nuclear Power Corporation of India Ltd (NPCIL) had entered into Memorandum of Understanding (MoU) for design and development of drive mechanisms for adjuster rods, control rods & shut-off rods of Tarapur Atomic Power Projects-3&4. The development work was taken up at DRHR, BARC.

An electromechanical, cable winch type drive mechanism with advance features has been developed for this purpose incorporating a number of advanced features. Design of this mechanism is significantly different from the mechanisms used in Dhruva, Kamini and 220 MWe PHWR's.

A prototype drive mechanism has been manufactured, assembled and tested on full-scale test station at BARC. The prototype mechanism has been tested for its functional testing, performance optimization and life cycle testing for design validation. After successful testing, the design including detailed drawings, technical specifications have been issued to NPCIL for production of drive mechanisms for reactor use. Test results during development and qualification stage have also been issued to NPCIL. This development work at BARC was also organized to meet the TAPP-3&4 project schedule requirements.

Functional Requirements

The drive mechanism is designed to meet the following functional requirements:

- Raising, lowering & holding of the rod
- Position indication: continuous and end limits
- Scram characteristics
- Size constraints
- Environmental conditions
- Remote engagement/disengagement
- Limited reactivity addition capability
- Fail-safe, non-reverse scram characteristics
- Service life requirements
- Trips, alarms & indications to check safe operation & healthiness
- Reliable, non-dependent on external power source for safety action
- Minimum periodic maintenance

Description

Shut-off Rod Drive Mechanism (SRDM)

Shut-off rod drive mechanism forms a part of Shut Down System No. 1 (SDS#1). The purpose of this is to provide shutdown capability to the reactor, when desired, under normal operating conditions as well as under undesirable conditions in the plant which calls for a reactor trip, with adequate margin so as to hold the reactor in shut down condition for prolonged period.

SRDM, being the most important safety system of the Nuclear Power Plant, it calls for a very high reliability of operation as well as effectiveness, which are mainly governed by its ability to operate within a very short interval and the magnitude of the negative reactivity worth it can impart to the reactor. The shut-off rod drive mechanism consists of a drive motor, worm gear unit, an electromagnetic clutch, set of spur gears as

reduction unit-I, sheave and sheave shaft assembly, mechanism housing assembly, potentiometer assembly, reduction unit-II, hydraulic dashpot assembly, limit switch assembly and reed switch assembly. Selection of drive motor for all the drive mechanism is based on the requirements of its reliable operation, material used in the construction to be radiation resistant, maintenance free and having required torque rating under all the operating conditions. The drive motor is custom built to meet these requirements and also the mounting arrangements to suit the mechanism layout. The drive motor is a three-phase induction motor rated at 220 volts (line), 50 Hz, 4 pole and 120 watts output. The electromagnetic clutch acts as a coupling between drive motor cum worm gear unit and a set of spur gears connected to the sheave. When energized, clutch couples the drive motor to the sheave and enables 'drive out' of the rod with the motor. At the parking location, the motor is cut-off but the energized clutch holds the rod in position by irreversible feature of worm gear unit. EM clutch is fed from 90 volts DC supply. Under SDS#1 trip, clutch is de-energized making rod to fall freely under gravity. The free fall is further assisted by the initial accelerating spring. The shut-off rod element contains an orifice at its top end, which comes into action at 80% downward travel of the rod and limits its free fall speed. At the end of 90% travel, hydraulic dashpot comes into action (through set of pick-up rings) which brings the rod to a smooth stop at 100% position. A mechanical stopper is provided in the mechanism to avoid damage of the dashpot vanes at the end of rod travel. Provision is made in the dashpot vane such that it offers negligible resistance during the rod withdrawal. A spiral spring is attached to the dashpot shaft, which is used to reset it as soon as the rod withdrawal starts. This feature makes the system ready to offer damping in case of SDS#1 trip, anytime during and after rod withdrawal. The drive mechanism is provided with two types of position indications: Indirect actuation (continuous position and 90% discrete position) and Direct actuation for end limits. Two sets of multi-turn potentiometers, connected to sheave shaft through set of spur gears, are used. These potentiometers are connected to RRS for continuous position as well as for generation of 'fully OUT' and 'fully IN' signals for interlocks and displays. Another set of three single turn potentiometers connected to the dashpot monitors the dashpot vane movement from 100% to 90% to check the re-setting of the dashpot. One set of discrete position indicators, consisting of three microswitches is provided on dashpot shaft to provide indication corresponding to 90% travel of the rod. The direct actuation indication consists of two sets of three magnetic reed switches, which are actuated by a magnet mounted on the push tube. During rod withdrawal, the push tube is lifted up bringing the magnet in line with the reed switches, which gets actuated in proximity of magnet. Similarly, when rod leaves the parking position, push tube along with magnet moves down, switching off the reed switch, indicating that rod has left the parking position. Signal from reed switches is used to cut-off the power to the motor, when rod is moved up. In case magnetic reed switches fail, a mechanical stopper provided in the mechanism prevents further rod withdrawal and power supply to motor is cut-off through over-current protection. The reed switches are also used to calibrate the potentiometers.

Control Rod Drive Mechanism (CRDM)

Control Rod Drive Mechanism forms a part of reactor regulating system. The purpose of CRDM are: to cause rapid power reduction when required (reactor step back), to compensate for the reactivity gain following transition from full power to hot standby condition and to bring average Zone Control Compartment level into normal operating range. For reactor regulation purpose, the control rods are driven into and out of the core by Reactor Regulating System (RRS). During reactor step back, the control rods are dropped partially or fully into the reactor core by RRS. During reactor trip, control rods are also dropped into the core along with

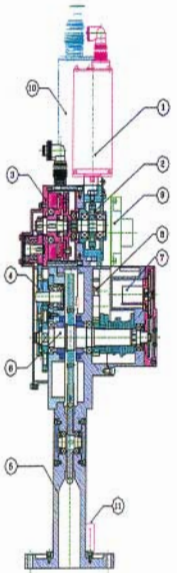

Shut-off Rod/Control Rod Drive Mechanism

Sub-assemblies:

1. Motor sub-assembly
2. Worm gear sub-assembly
3. Electromagnetic clutch sub-assembly
4. Reduction Unit-I sub-assembly
5. Mechanism housing sub-assembly
6. Sheave shaft sub-assembly
7. Potentiometer sub-assembly
8. Reduction unit-II sub-assembly
9. Hydraulic dashpot sub-assembly
10. Limit switch sub-assembly
11. Reed switch sub-assembly

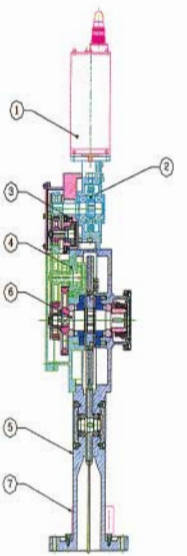

Adjuster Rod Drive Mechanism

Sub-assemblies:

1. Motor sub-assembly
2. Worm gear sub-assembly
3. Potentiometer sub-assembly
4. Reduction unit sub-assembly
5. Mechanism housing sub-assembly
6. Sheave shaft sub-assembly
7. Reed switch sub-assembly

shut-off rods of shutdown system no. 1 (SDS#1).

The drive mechanisms for control rods and shut-off rods are identical. However, the absorber element for control rod differs from that of shut-off rod. The bottom attachment of shut-off rod is fully open while that of control rod contains an orifice plate to limit its free fall speed.

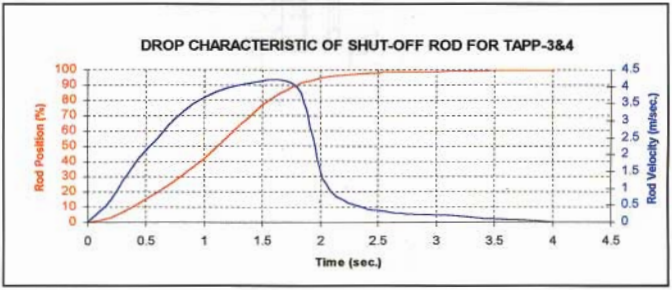

Drop characteristic of Shut-off Rod for TAPP-3&4

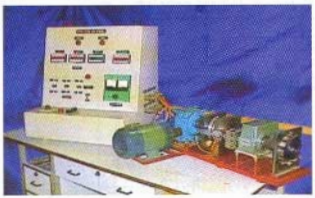

Test Rig for qualification of Spiral Spring, Rotary Switchgear and Potentiometer

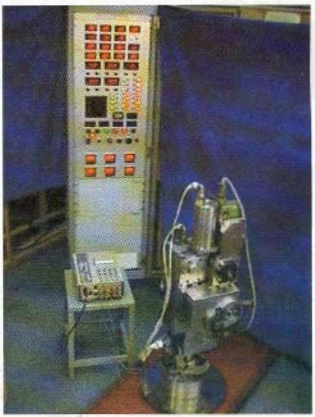

Full Scale Test Station

Seal Test Rig

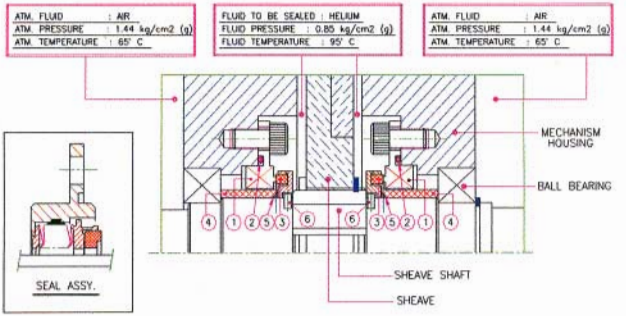

MECHANICAL SHAFT SEALS FOR SHEAVE SHAFT

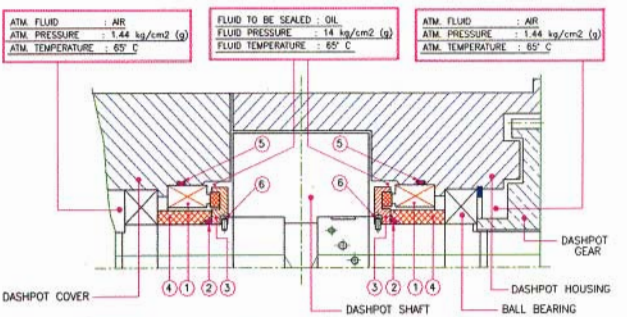

MECHANICAL SHAFT SEALS FOR HYDRAULIC DASHPOT

S.No	DESCRIPTION	MATERIAL
6	ANTI-ROTATION PIN	S.S.316
5	'O' RING	VITON
4	SLEEVE	S.S. 17-4 PH
3	MATING RING COMPOSITE (ROTATING)	T.C.+TITANIUM
2	'O' RING	VITON
1	SEAL ASSY. (STATIONARY)	CARBON FACE

Adjuster Rod Drive Mechanism (ARDM)

Adjuster rod drive mechanism forms a part of RRS. The purpose of ARDM are: to provide Xenon override capability during reactor start-up, flux flattening and reactivity shim during extended fuelling machine outages. During normal reactor operation, adjuster rods remain within the reactor core. For regulating purpose, the adjuster rods are driven out and into the core by RRS, as and when required.

Adjuster rod drive mechanism is designed for raising and lowering of adjuster rods at controlled speeds and does not contain electromagnetic clutch or hydraulic dashpot.

ARDM consists of drive motor, worm gear unit, potentiometer, set of spur gears as reduction unit, sheave and sheave shaft assembly, mechanism housing assembly and reed switch assembly.

Basic design specifications are given in Table-1.

Table 1 : Basic Design Specifications

Number of shut-off rods	: 28
Number of control rods	: 4
Number of adjuster rods	: 17
Reactivity worth of shut-off rods	: 72 mk
Total travel of shut-off rod / control rod	: 6600 mm
Weight of shut-off rod / control rod	: 50 kg
Time to raise shut-off rod / control rod (at max speed)	: 150 ± 10 s
Reactivity addition rate during withdrawal of rods	: ≤ 0.33 mk/s
Max linear speed during withdrawal of shut-off rod/control rod	: 56.5 mm/s
Drop time for 5940 mm (90% travel) of shut-off rod (*)	: 1.8 ± 0.1s
Speed variation of adjuster rods / control rods	: Upto 1:10
Weight of adjuster rod	: 15 kg
Time to raise adjuster rod at max speed	: 70 ± 10 sec
Drop time for 5940 mm (90% travel) of control rod	: 4 sec approx.
Partial drop distance for stepback function of control rod	: Anywhere upto 100% drop
Max ambient temperature for machanisms	: 65°C
Max radiation field for mechanisms	: 10 R/hr
Applicable code	: ASME Section III, Sub-sec NB for OBE & SSE

(*) Excluding signal processing and actuation delay

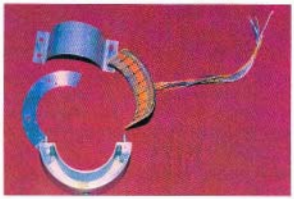

Reed Switch Assembly - parts

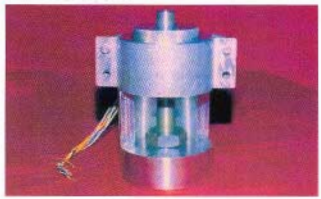

Fixture for checking actuation of Reed Elements

Reed Switch Assembly - before potting

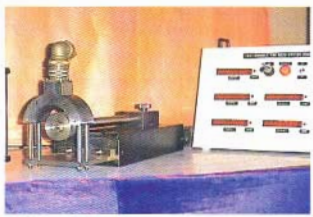

Test Console for qualification of Reed Switch Assembly

Salient Design Features

- 28 shut-off rods constitute the Primary Shutdown System (SDS#1). While 4 control rods and 17 adjuster rods constitute a part of Reactor Regulating System. The unavailability of the Primary Shutdown System shall not exceed 10^{-3}/year/year.
- Heavy water is used for cooling of shut-off rods, control rods and adjuster rods. The perforated guide tube surrounds the absorber rod in each case.
- The drive mechanism is flange mounted on top of guide tube extension and it forms part of pressure boundary for heavy water moderator system.
- The drive motor, used in the drive mechanism, is a custom built design operating on 3 phase, 220 Volts (line), 50 Hz. The drive motor for control rods and adjuster rods are designed for variable speeds (10% to 100%).
- Simplified absorber element design to facilitate easy inspection and replacement of wire rope used for attaching the absorber element to the drive mechanism.
- The electromagnetic clutch operates on 90V DC. Clutch design and torque capacity suitable to permit partial release of shut-off rod from parking position for checking healthiness of drive mechanisms. Clutch design and torque capacity are also suitable to permit re-arresting control rod after release for reactor stepback function.
- 90% free fall of shut-off rod/control rod for highest reliability and consistent performance. Maximum free fall speed of shut-off rod element is limited through the use of an orifice at its top end, which is effective during 80% to 90% downward travel. In case of control rod, the maximum free fall speed is limited through the use of an orifice at its bottom end.

- Hydraulic dashpot incorporates an oil window connected to low pressure side. Above the oil level, window has adequate space for expansion of oil at high ambient temperature.
- The conventional single vane replaced by double vane to balance forces on dashpot shaft arising from high oil pressure during damping action.
- A screw for controlling oil bypass from high pressure side to low pressure side for adjusting damping characteristics of dashpot.
- Modular design of drive mechanism layout to permit in-situ maintenance/ replacement for individual sub-assemblies e.g. motor and worm gear, clutch, dashpot, switchgear, potentiometer etc without opening moderator pressure boundary.
- Better lubrication for gears, bearings, pick-up rings and spiral springs for long wear life.
- Rope sheave in place of rope-drum to eliminate chances of wire rope coming off the drum groove.
- Provision of single turn triplicate potentiometer on dashpot shaft to monitor retrieval of spiral spring while the rod is being raised. Raising of the rod will get inhibited incase of unsatisfactory retrieval of dashpot shaft. Rationality checks on potentiometer signal shall be done to detect potentiometer failure.
- Provision of multi-turn dual potentiometer to monitor continuous position of rods. Rationality checks on potentiometer signal shall be done to detect potentiometer failure.
- Provision of rugged triplicated switchgear unit to monitor shut-off rod drop time for 90% fall.
- Gear reduction trains for potentiometer and limit switches are eliminated.
- Provision of one set of triplicated reed switches (directly actuated) to indicate shut-off rod fully out position and to cut-off the drive motor power. Second set of reed switches are used for RRS.

Testing of Prototype Drive Mechanism

Testing for Performance and Design Optimization

- Testing for full travel to establish the drive motor rating.
- Testing of EM Clutch for optimum performance (Minimum voltage at which the rod slips, delay time, temperature rise of the coil under continuous operation, effect of elevated temperature around mechanism, etc.).
- Optimization of orifice in the top attachment of shut-off rod element for rod drop dynamics.
- Effect of water level variation in tank (calandria) on rod drop dynamics.
- Optimization of orifice in the bottom attachment of control rod element for rod drop performance and clutch re-setting for partial drop qualification.
- Optimization of partial release characteristics of shut-off rod for on-line testing.
- Performance testing of dashpot using oil of different viscosity, effect of internal clearances, effect of oil by-pass screw adjustments on rod drop dynamics and effect of elevated ambient.
- Rod drop characteristics with tank water (simulating calandria) at 80°C and elevated temperature around mechanism to 65°C.

Qualification of Special Hardware Items on Test Rigs

- Simulated testing and qualification of dynamic shaft seals used in sheave chamber & dashpot for 50,000 cycles.
- Simulated testing and qualification of spiral spring, rotary switch-gear (Limit Switch) and potentiometers for 10^4 cycles.
- Simulated testing and qualification of reed switch unit for 10^6 cycles.
- Qualification of drive motor and electro-magnetic clutch.
- Qualification of wire rope & its crimped terminals (swaging is done using portable pneumatically operated cable swager).

Life Cycle Testing for Design Qualification

In order to qualify the design, prototype drive mechanism has been manufactured, assembled and tested on full-scale test station at BARC.

- Prototype SOR P-II has been successfully tested for more than 5000 drops for design validation and optimisation of scram characteristics, resulting in consistent performance.
- On-line testing of SOR P-II has also been successfully completed for more than 3000 cycles. During on-line testing, rod was held at park 'UP' position and the voltage to EM clutch was reduced to zero for short time. In each cycle, rod was released to fall three times consecutively (by pressing the trigger three times) and the rod travel was noted down. Rod travel corresponding to first trigger in each cycle is spring assisted. After releasing the rod three times, rod is taken up by the drive motor till it reaches the park 'UP' position. This completes one cycle. Thus, during on-line testing for 3000 cycles, rod has been released for total 9000 times. The rod travel corresponding to 1st, 2nd and 3rd trigger was around 100mm, 70mm and 70mm respectively. Results showed consistent performance.
- Partial release test of Control Rod (for stepback function) for about 60% travel has been successfully completed for about 1000 cycles.
- Prototype adjuster rod drive mechanism has been successfully cycle tested for more than 5000 cycles.

References

Design Basis Report on Shut-off Rod Mechanism: TAPP-3&4/DBR/31450/01 Rev. 2
Technical specification for manufacture of drive mechanisms of TAPP-3&4: No. PB-E-610.
Technical specification for Drive motor of SRDM for TAPP-3&4: No. PB-E-625
Test Report on Life Cycle testing of SOR for TAPP-3&4, Issue: Aug. 2001
Test Report on 'On-line testing of SOR for TAPP-3&4', Issue: Nov. 2001

Acknowledgement

The team members of Control Mechanism Section, DRHR, are grateful to the Head, DRHR, for giving the opportunity to work on this development work and giving guidance on regular basis.

Members of CMS, DRHR, are also thankful to the Director, A&MG and E&IG, for his continuous encouragement and support.

Mr D.N. Badodkar was conferred the BARC Technical Excellence Award for the year 2000 for his highly commendable contributions in the field of special purpose drives and reactor control mechanisms.

About the authors ...

Mr Manjit Singh *is Head, Division of Remote Handling & Robotics (DRHR), BARC, Trombay, Mumbai. He joined BARC Training School in 1972. Mr Manjit Singh is the recipient of Dr. Homi Bhabha award for securing Ist rank in BARC Training School. He has also received 'BARC Technical Excellence Award 1997'. He has pioneered the development of remotised tools for in-service inspection of coolant channels of 220 MWe PHWRs in India. He has been responsible for design, development and supply of BARCIS Systems to NPCIL. He has pioneered the development cable winch type control mechanisms for use in research and power reactors in India. He has been responsible for design and development of Shut-off Rod Drive Mechanisms for Dhruva, Safety Plate Drive Mechanisms for KAMINI and Shut-off Rod Drive Mechanisms for NAPP. He has also been responsible for the design & development of Shut-off Rod, Adjuster Rod and Control Rod Drive Mechanisms for TAPP-3&4.*

Mr D. N. Badodkar *of Division of Remote Handling & Robotics, BARC, was conferred the 'BARC Technical Excellence Award-2000' on 30.10.2001. Mr Badodkar is heading the 'Control Mechanism Section' of DRHR. Presently, Mr Badodkar is working on the design and development of Drive Mechanisms for AHWR and 'Critical Facility'.*

N.K. Singh

M.K. Mishra

Mr N. K. Singh *and* ***Mr M. K. Mishra*** *of CMS, DRHR, have worked on mechanical design of drive mechanism for TAPP-3&4, test-rigs for qualification of sub-assemblies and they were closely associated with design validation and life cycle testing of prototype on full scale test station.*

N.S. Dalal

C.B. Kothari

Mr N. S. Dalal, *and* ***Mr C. B. Kothari*** *of CMS, DRHR, have worked on the test console for design validation and life cycle testing of drive mechanism for TAPP-3&4, test set-up for qualification of critical components and they were associated for performance and life cycle testing of prototype on full scale test station.*

Mr G. Veda Vyas *of CMS, DRHR, has been associated for life cycle testing of drive mechanism for TAPP-3&4. He is working on developing a model for rod drop performance and dashpot performance for the shut-off rod drive mechanism.*

Folded Tandem Ion Accelerator Facility at BARC

Pitamber Singh
Nuclear Physics Division
Bhabha Atomic Research Centre

Abstract

The Folded Tandem Ion Accelerator (FOTIA) facility has been commissioned recently at BARC. Several beams (^1H, ^7Li, ^{12}C, ^{16}O, ^{19}F) have been accelerated upto a terminal voltage of 3 MV with N_2+CO_2 as insulating gas. The terminal voltage is stabilized within ± 2 kV. The beams are used for elemental analysis using the Rutherford Back Scattering (RBS) technique. After making a few measurements around this terminal voltage, SF_6 will be filled in the accelerator tank in order to raise the terminal voltage to 6 MV. Some of the salient features of the FOTIA facility are discussed here.

Introduction

In the last few decades, low energy accelerators, capable of delivering light and heavy ion beams, have played an important role both in basic and applied sciences particularly in the fields of astrophysics, material science, accelerator mass spectrometry, beam foil spectroscopy, etc.

Although there are a large number of Van-de-Graaff accelerators in different laboratories only a few of them have been converted into folded tandem accelerators [1]. A project [2] was taken up at BARC to nvert the existing 5.5 MV Model CN single stage Van-de-Graaff accelerator, which was in continuous operation since 1962 at the Nuclear Physics Division, into a 6 MV Folded Tandem Ion Accelerator (FOTIA). Due to limited power available in the terminal it was possible to produce and accelerate beams of only H^+ and He^+ ions in the old Van-de-Graaff accelerator at BARC.

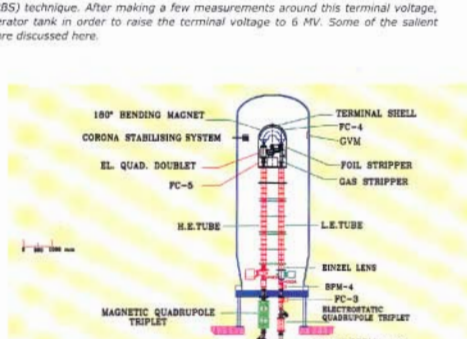

Fig. 1: Schematic diagram of the Folded Tandem Ion Accelerator

However, FOTIA can accelerate heavy ion beams of up to A≈40 and energy up to 60 MeV.

Description of the FOTIA Facility

The layout of the FOTIA (Fig.1) was worked out by optimizing the ion optics parameters [3] despite severe geometrical constraints

due to the utilization of the existing infrastructure of the Van-de-Graaff accelerator. One of the novel features of the ion optics is introduction of an einzel lens at the entry of the low energy tube. With this in operation it will be possible to get good transmission even at very low terminal voltages. This has contributed to the enhancement of dynamic range of its operation. In view of the modification in the beam optics, it was found necessary to raise the high voltage column structure by 1 m to accommodate, at the exit of the high energy accelerating tube, the additional magnetic quadrupole triplet and steerer magnets which are essential for optimum transmission of the beam. A tank raising structure (1m long, 2.5 dia.) has been incorporated in the system. This was really a challenging task as this additional collar had to withstand a load of 18 tons due to pressure vessel, high voltage column section, 180° magnet, alternator, etc. Also, the structure had to be built in two halves as otherwise it was not possible to take it to the accelerator room on the first floor of the Van-de-Graaff building.

Fig. 2: SNICS II ion source

The FOTIA is an accelerator amongst a few of its kind in the world. The construction of FOTIA involved development of technologies of several important components like:

- dipole magnets,
- high voltage generator,
- electrostatic and magnetic focusing lenses
- steering devices,
- vacuum systems,
- SF_6 gas handling system,
- computer control system

In FOTIA, the negative ion beams extracted from the SNICS-II source (Fig.2) are pre-accelerated up to 150 keV. Out of all the charged particles extracted from the ion source the negative ions of the desired mass are selected using a 70°-dipole magnet for injection into the low energy accelerating tube.

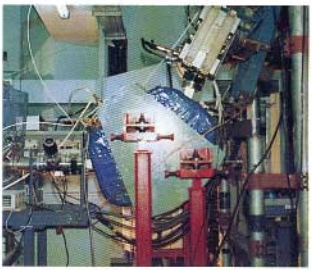

Fig. 3: The 70° pre injector magnet

As can be seen in Fig. 1, three dipole magnets [2] are used in FOTIA and their parameters are given listed in Table 1. The 70°-magnet (Fig.3) is designed for a magnetic field of 14 kG in the pole gap of 4 cm and has a bending radius of 40 cm. It can bend the ions having mass-energy product (ME/q^2) ≤ 15. A magnetic field of 14.5 kG was realised, with field uniformity of ± 0.1%, at a current of 180 Amp.

Several beams were extracted from the ion source and then analysed using the 70°-magnet. Analysed beam currents of several microamperes (H^-(4.5 μA), Li^-(0.5 μA), C^-(5

Table 1: Design parameters of the dipole magnets

Parameter	70^0	180^0	90^0
(A) CORE DETAILS			
Air gap(mm)	40	15	40
Gap width(mm)	100	42	110
Bending radius(mm)	400	305	750
Gap field(KG)	14	14	14
Field uniformity(%)	0.10	0.15	0.10
Pole geometry	ANAC	NORMAL	ANAC
(B) COIL DETAILS			
Material	Copper	Copper	Copper
Conductor	Strip	Strip	Hollow Copper tubes
Size(mm x mm)	0.80x75	0.78x50	12x12
No. of coils	2	2	2
No. of turns per coil	150	75	56
Resistance per coil	85 mΩ	75 mΩ	40 mΩ
Current capacity Inter-turn insulation	200 amp Mylar	120 amp Nomex	500 amp Fiber glass
Max. coil temp	70°	50^0	70°

μA), O^-(24 μA), Si^-(13 μA), Cl^-(11 μA)) were obtained. A typical mass spectrum obtained with Fe_2O_3 cathode sample is shown in Fig. 4.

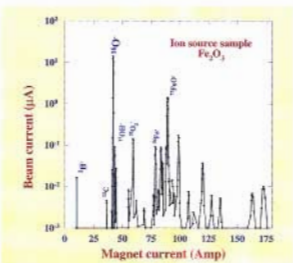

Fig. 4 : Mass spectrum for Fe_2O_3 cathode sample

The beams are injected into the low energy accelerating tube through a 20°-electrostatic deflector. An electrostatic quadrupole triplet and an einzel lens are used to focus and match the beam parameters to the

Fig. 5: The 180^0 – folding magnet located inside the high voltage terminal

acceptance of the low energy tube. The electrons of these accelerated negative ions get stripped off at the stripper and a desired charge state of the positive ions thus produced is selected with the 180° magnet inside the high voltage terminal before being bent into the high energy accelerating tube where they are further accelerated.

The 180°-magnet (Fig.5) (ME/q^2=10, R=30.5 cm) has been tested for its field uniformity, which was found to be ± 0.15%. A magnetic field of 10.2 kG was measured at 100 Amp.

Fig. 6 : The 90° – analyzing magnet

At the exit of the 180° magnet the beam diverges. An electrostatic quadrupole doublet is used to focus the beam before it enters the high-energy tube. The beams accelerated in the high energy accelerating tube are focussed using a magnetic quadrupole triplet (MQT) before being analyzed by the 90°-magnet (Fig.6). The 90°-dipole magnet is designed for a magnetic field of 14 kG and ME/q^2=50 with a radius of curvature of 75 cm. A magnetic field of 15.5 kG was obtained at 500 Amp (Fig.7).

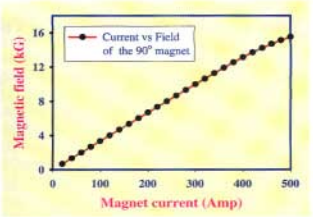

Fig.7 : Magnetic field vs coil current for the 90° magnet

The analysed beam is transported to the scattering chamber through the experimental beam line, which consists of MQT, switching magnet, magnetic steerer [4], beam profile monitors (BPM), Faraday cups (FC), etc. These components (MQT, the magnetic steerers (Fig.8), BPM, Faraday cups) were obtained either from local vendors or designed and fabricated in BARC.

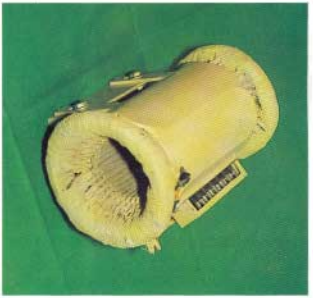

Fig.8 : Magnetic steerer designed and built for FOTIA beam line

In Table 2, final beam energies, ME/q^2 values and relative intensities of different charge states produced at the foil stripper in the terminal are listed. The FOTIA facility has been commissioned recently [5] and all the components (low and high energy beam lines, high voltage column section, charging assembly, SF_6 gas handling and computer

Table 2 : The final beam energies at a terminal voltage of 6 MV for ions with different charge state (q)

Ion	Z	q+	Relative %	E_f(MeV)	ME/q^2	Ion	Z	q+	Relative %	E_f (MeV)	ME/q^2
^{1}H	1	1	100	12	12	^{28}Si	14	5	16	36	40
^{4}He	2	2	100	18	18			6	34	42	33
^{12}C	6	3	12	24	32			7	31	48	27
		4	52	30	23			8	13	54	24
		5	33	36	17	^{32}S	16	6	28	42	37
^{16}O	8	4	24	30	30			7	34	48	31
		5	47	36	23			8	19	54	27
		6	23	42	19	^{37}Cl	17	6	29	42	43
^{24}Mg	12	4		30	45			7	33	48	31
		5	24	36	35			8	18	54	27
		6	39	42	32	^{40}Ca	20	7	31	48	39
		7	25	48	24			8	26	54	34
		8	6	54	20			9	12	60	30

control systems, magnets, electrostatic and magnetic lenses, steerers, scattering chamber, etc.) has been working satisfactorily [6].

Commissioning of the FOTIA Facility

The commissioning of the FOTIA basically involved: a) design, fabrication, installation and testing of its sub-systems, b) high voltage tests, c) beam trials and their characterization, and d) calibration of the 90° analyzing magnet.

High Voltage Tests

The high voltage system of the FOTIA consists of different components like high voltage column section, charging mechanism and measurement & control system.

The high voltage column section consists of six modules (Fig.9); each designed for one million volt. Each module has 4 ceramic insulating posts, which are ceramic to metal bonded with 18 corona gaps connected by equipotential hoops. A pellet chain charging system, made of metallic pellets and nylon links, is used for generating the voltage on the terminal. The electrical power, required in the terminal, for 180°-magnet, ion pump, foil and gas strippers, electrostatic quadrupole doublet, Faraday cup and other electronic components, is generated by the 5 KVA alternator. The maximum vibration amplitude with both Perspex shaft and pellet chain running was found to be less than 30 μ [7] (Fig.10), which was within the safe limit.

Fig. 9 : High Voltage Column section of FOTIA

The high voltage measurement system of the FOTIA uses a generating voltmeter (GVM) mounted on the inside surface of the tank, in front of the high voltage terminal. The high voltage control system uses a corona probe mounted inside the tank opposite to the GVM. The high voltage tests were carried out using N_2+CO_2 mixture as an insulating gas. At a tank pressure of 98 psig, a sustained voltage of 3.4 MV was achieved [8].

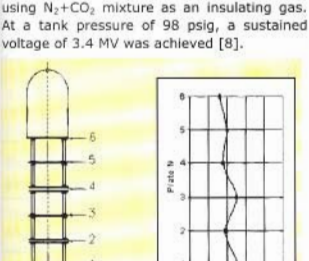

Fig.10 : Vibration amplitude across the column section

In FOTIA, SF_6 will be used as insulating gas. Since hydrocarbon free environment is required inside the accelerator tank oil free equipments are used. The new gas handling system [9] consists of an oil free compressor, a centrifugal blower, a heat exchanger, dust filters, dryers and a vacuum pump etc. The gas handling system, is used mainly: a) to transfer gas from storage tank to accelerator tank and vice versa. b) to evacuate the accelerator tank to a pressure ~0.5 Torr. This maintains purity of gas by minimizing the contamination of the gas by residual air c) to remove moisture and breakdown products by re-circulating gas in a close loop system containing activated alumina dryer, heat exchanger, blower and filters, d) to maintain the temperature, inside the accelerator tank, to its designed value.

The accelerating tubes are subjected to very high voltage gradient of about 2 MV/m, which requires a hydrocarbon free and clean vacuum for smooth operation of the accelerator. A distributed pumping system having eight pumping stations has been used to maintain UHV in the entire accelerator including an experimental beam line and the scattering chamber [10]. The type of the pumps installed in a particular section is based on the gas load in that section (Table 3). The vacuum chamber of the 180° magnet (Fig. 11) has been provided with a separate ion pump, as its cross section (14 mm x 24 mm) is small. The ion source section has a large gas load, which increases substantially whenever samples are changed in the ion source. A turbo-molecular pump, with the speed of 1600 litres/sec, is used to maintain ultra high vacuum in this region. The other sections are pumped by a combination of titanium sublimation and sputter ion pumps or only by sputter ion pumps. A vacuum of 8 x 10^{-9} Torr was achieved in the entire system.

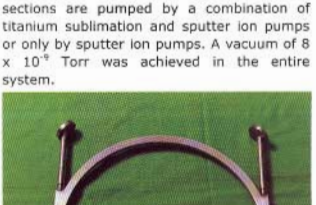

Fig. 11 : Vacuum chamber for the 180° magnet

Voltage stabilization system

In tandem accelerators, the energy of the beam depends on the terminal voltage V_T and charge state q of the ions. The terminal voltage stability therefore determines the energy spread of the beam. A terminal voltage stabilization (TVS) system [11] was designed and developed for the FOTIA facility, and has been used extensively during beam trials. It is a closed loop control system, which involves measurement and monitoring of terminal voltage, beam energy and their stabilization. The present control &

Table 3 : Gas load estimates

Section No.	Name of the section	Main components	Volume (cm^3) & surface area (cm^2)	Gas load (Torr-lit/sec)	Pumping speed (lit/s)
1.	Ion source	Ion source, Acc. Tube, E.S. steerer	47713 **10822**	1.44×10^{-5}	1600
2.	Injection line	BPM, FC, 70° Magnet Chamber, 20° Deflector, E.S. Steerer	51616 **19287**	6.3×10^{-6}	820 *
3.	Low energy accelerating tube	Einzel lens, Acc. Tube , E.S. Steerer, valve	22407 **17194**	1.08×10^{-6}	120
4.	Terminal	Stripper and 180° Magnet Chambers, Pumping unit	9628 **4473**	9.34×10^{-7}	120
5.	High energy accelerating tube	Acc. Tube , Mag. Quad. Triplet , Pumping unit	31455 **20812**	7.5×10^{-6}	120
6.	Analysing magnet	90° Magnet chamber, BPM,FC, Slits, Pumping unit	40834 **18393**	1.0×10^{-6}	1640 **
7.	Experimental Beam line	Scatt.chamber, S/W magnet, Mag. Steerer, M.Q.T.	106306 **50198**	9.5×10^{-6}	3000

* 820 = 700 (TSP) + 120(SIP), ** 1640 = 1400 (TSP) + 120(SIP)
Note : TSP pumps are put on only when they are required.

monitoring system consists of GVM and its amplifier, a slit amplifier and a corona probe drive controller circuit. The TVS system works in two modes namely: a) GVM control mode and b) slit control mode.

The generating voltmeter (GVM) is used to measure the terminal voltage. In GVM control mode, the TVS controller generates an error signal by comparing the terminal voltage reading from the GVM amplifier with the set reference. In FOTIA, 90° magnet is used to analyse the beam and determine its energy, which in turn is used to obtain the terminal voltage V_T. Any change in V_T will reflect on the beam position at the exit of the analyzing magnet. A slit system located just after the analyzing magnet monitors the beam position by measuring the current pick-ups on low energy and high energy slits. In the slit control mode, the TVS compares the low and high energy slit currents and generates an error signal which is used for locking the beam position. The corona probe controller works as a shunt regulator by loading the charging system. In both the cases, corona probe controller uses the error signals for stabilizing the terminal voltage.

The TVS system regulates terminal voltage over a wide range of its operation. The TVS controller also incorporates the facility to monitor various signals like terminal voltage, corona probe current, grid voltage and slit pick-ups. The system was tested both in GVM control mode and slit control mode with a beam current as low as 2 nA and its

performance was satisfactory. The voltage stability was found to be about ± 2 kV.

Control and monitoring system

A PC based system [12] developed in BARC has been used in FOTIA for controlling and monitoring parameters of beam handling components located both at the high voltage and ground potentials. The ion source parameters are controlled using a fibre-optic data telemetry system [13]. The control and monitoring system has a network of PCs with a front-end interface using CAMAC instrumentation and uses QNX real time operating system.

Beam Characterization and Energy Calibration

The first beam (^{12}C) on target was delivered on April 21, 2000. The beam was characterised [5] by measuring the Rutherford Back Scattering (RBS) from the self-supporting targets of ^{197}Au, ^{120}Sn and ^{56}Fe. The targets were mounted inside the 80 cm diameter scattering chamber (Fig.12).

Fig 12 : Scattering chamber used for RBS measurements

The elastically scattered particles were detected using a surface barrier detector mounted at θ_{lab}=160^0. The experimental set up is shown in Fig.13. To calibrate the pulse height of the detector, an alpha source was mounted on one of the target holders.

Using kinematics, the incident energy (E_i) was calculated from the scattered particle energy (E_s) for each of the targets using the following relation:

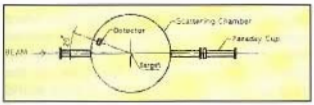

Fig. 13 : Experimental set up used for beam characterization

$$\frac{E_s(\theta)}{E_{in}} = \frac{m_1^2\cos 2\theta + m_2^2 + 2m_1\cos\theta\sqrt{m_2^2(\cos^2\theta - 1) + m_2^2}}{(m_1 + m_2)^2}$$

Here m_1 and m_2 are masses of the projectile and target. The θ is scattering angle in the lab system.

The terminal voltage V_T was calculated from this E_i using the relation $E_i = E_{is} + (q+1)V_T$, where E_{is} is the energy of the beam from the ion source and q is the charge state of the analysed ^{12}C beam. In the present experiment charge state of 4$^+$ was selected. The average terminal voltage calculated using above RBS data, after correcting for energy loss in the dead (dead) layer of the detector and kinematic broadening etc. was found to be 2.54 ±0.020 MV, which was consistent with the generating voltmeter reading of 2.54 MV. Subsequently, stabilization system has been modified and terminal voltage stability has been improved to ± 2 kV [14].

For the magnetic field B (in Tesla), generated by the 90^0 magnet, the energy E (in MeV) of the beam is given by the relation,

$$B = (K/q)\ [\ AE\ \{1 + (E/2Am_uc^2)\}]^{1/2}$$

where A, m_u and q are the mass number, mass of the projectile in amu and the charge state of the particle, respectively. The K-value of the magnet can be obtained once the energy of the beam is known. Both back scattering (BS) and resonance scattering techniques were used to obtain the K-value [15].

In the BS measurements, proton, Lithium, Carbon and Fluorine beams were used. In the case of BS with proton beam, the energy was calibrated by measuring the backscattered protons from Tantalum (^{181}Ta), Niobium (^{93}Nb) and Carbon (^{12}C)

targets. The back scattered protons were measured by a silicon surface barrier detector placed at θ_{lab}=160° using the setup discussed above. In the spectrum of the thick target, center of the falling edge at the highest energy is taken as the scattered energy of BS from the front surface. The incident beam energy (E_{inc}) was calculated from the energy of the scattered ions for each of the targets for different terminal voltages. In these measurements, the terminal voltage was varied between 2.1 - 2.5 MV. The BS of ^{7}Li, ^{12}C and ^{19}F beams (with different charge states) were done from gold targets. The BS spectrum of ^{7}Li from ^{197}Au measured for calibration of the 90° -analyzing magnet is shown in Fig. 14. The alpha peaks from Am-Pu source mounted on one of the target holder positions are also seen in the figure.

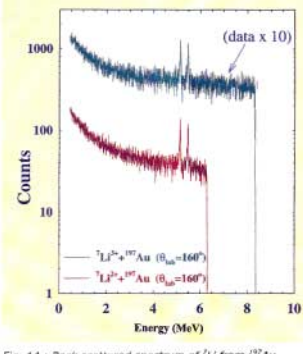

Fig. 14 : Back scattered spectrum of ^{7}Li from ^{197}Au.

In resonance scattering, the elastic scattering cross sections for $^{12}C(p,p)^{12}C$ reaction were measured as a function of incident beam energy. The proton beam energy was varied from 4.2 to 5.0 MeV (Fig.15). From the literature it is known that the energy of the resonance peak, as also obtained from our measurement, corresponds to E_{lab}= 4.408 MeV with a width of 11 keV. After correcting for the energy loss in the carbon target, the incident beam energy was calculated and in turn the "K" value of the magnet was estimated. The "K" values for the 90°-analysing magnet, obtained from both the methods are close to each other and the average is 0.1805 ±0.0002 (Tesla/MeV$^{1/2}$/amu$^{1/2}$).

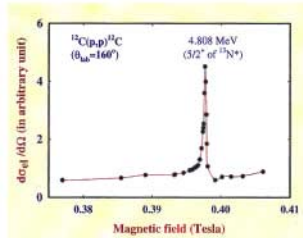

Fig.15 : Excitation function for the $^{12}C(p,p)$ ^{12}C reaction

Safety Issues-Radiation Shielding and Interlocking System

In order to get an idea about expected radiation level around the high voltage terminal of the FOTIA, radiation measurements were made, using proton, carbon and oxygen beams, at various locations including high voltage terminal of the 14 UD pelletron accelerator by simulating FOTIA conditions [16]. The x-ray radiation level was found to be negligible and well below the permissible limit. The radiation level was also very small when beam was stopped on a thick SS stopper mounted in one of the holes of the stripper foils. In both the cases neutron intensity was found to be consistent with the NCRP values. This data was a very useful input to the shielding calculations for the FOTIA project.

Radiations measurements were made both with heavy ion and proton beams upto a terminal voltage of 3 MeV. With heavy ion beams dose rates both for gamma and neutron were negligible. In the case of proton beams the gamma dose rate were very small at all the energies. However, for a

current of 10 nA the neutron dose rate were measured to be 0.06 and 0.8 mR/hr at 2.5 and 3.0 MV terminal voltage, respectively. Therefore interlocking of beam hall door is essential whenever proton beams are accelerated at higher terminal voltages.

A PLC based safety interlocking system has been implemented in FOTIA. This system takes care of different abnormal conditions and generates suitable audio/visual alarms and brings the malfunctioning units to safe shutdown condition. The components related to charging, vacuum systems, SF_6 leakage and radiation, etc have been connected to this system for status display and safety interlocking purpose. The system has been tested and working satisfactorily.

Summary and Conclusions

The folded tandem ion accelerator facility has been commissioned recently. Several sub-systems involving state-of-the-art technologies were developed. Beams from ^{1}H to ^{19}F have been accelerated upto a terminal voltage of 3 MeV. The terminal voltage is stabilized to ± 2 kV. Progressively the terminal voltage will be raised to 6 MV and other beams up to ^{40}Ca will be accelerated. This facility will be widely used for multi-disciplinary research of interest & relevance to BARC. Recently, experiments were done [17], in collaboration with Radiochemistry Division, to investigate the effect of hydrophobicity of membrane matrix on the selectivity towards cations. The membranes were prepared by physical inclusion of hydrophobic cation-exchanger in the matrix formed by polymer chains of cellulose triacetate with a plasticizer. The 4 MeV proton beams were used for depth profiling using Rutherford Back Scattering technique.

In order to carry out experiments in different fields like nuclear physics, astrophysics, atomic physics, AMS, etc, a new hall has been constructed and five beam lines are being set up.

Acknowledgements

I thank Dr Anil Kakodkar, Mr B. Bhattacharjee, Dr S.S. Kapoor, Dr V.C. Sahni and Dr S. Kailas for their keen interest and continuous support to the FOTIA project. I am indebted to all members of the FOTIA team from several Divisions (NPD, APPD, TPPED, ED, CWS, RSMD, CnID, TSD, RED, RSD, A&CED, AFD, etc.) of BARC and CAT, Indore, for their contributions towards development of the FOTIA facility. But for their excellent cooperation and contributions it would not have been possible to set up such a unique facility at BARC.

References

1. H. Naylor, Nucl. Instrum Meth., **63** (1968) 61. P.J.S.B. Barratt, T.R. Brock, G. Doucas, Greenway, A. Henwood, A.R. Holmes, McK Hyder, A.B. Knox, G.M. Parkar and A. Takacs, Nucl. Instru. Meth. **184** (1981) 9;
2. P. Singh, Proc. Int. Conf. on Vacuum Science & Technology & SRS Vacuum Systems, (CAT, Indore), Vol. **1**, 1995, p147-154. P. Singh, Indian J Pure & Appl Phys. **35** (1997) 172.
3. V.A. Hattangadi, P. Singh, N.M. Thakur, S.S. Kerekatte, P. Surendran and M.A. Eswaran, PATPAA-93, Calcutta, 1993, p76. S. Santra and P. Singh, Pramana-J Phys. **59** (2002) 53.
4. S. Santra, P.Singh and S.K. Gupta 4th National Symp. on Phys. and Tech. of Part. Accelerator and their Applications, PATPAA-96, Nov.26-29, 1996, Calcutta.
5. P. Singh, P.V. Bhagwat, S.K. Gupta, S. Santra, M.J. Kansara, A. Agarwal, Rajesh Kumar, E. Shallom, A.K. Gupta, R.V. Patkar, Sapna P, S.P. Sarode, N.B.V. Subrahmanyam, P.J. Raut, S.C. Ojha, B.K. Jain and S.S. Kapoor, Proc DAE Symp. on Nucl. Phys. **B43** (2000) 522.
6. P. Singh, Accelerator Based Research in Basic and Applied Sciences, 2002, Eds. Amit Roy and D.K. Avasthi, Phoenix Publishing House Pvt Ltd., New Delhi; P. Singh, Pramana-J Phys. **57** (2001) 639.
7. P.V. Bhagwat, R.L. Suthar, P. Singh, R. Majumder, S.C.Ojha, A. Agarwal, Rajesh Kumar, A. Rama Rao, P.G. Jose, B.K. Jain, P.H. Ron and S.S. Kapoor DAE Symp. on Nucl. Phys. **B42** 448 (1999).

8. P. Singh, P.V. Bhagwat, S.K. Gupta, M.Y. Vaze, A. Agarwal, Rajesh Kumar, S. Santra, M.J. Kansara, E. Shallom, R.V. Patkar, Sapna P, S.P. Sarode, N.B.V. Subrahmanyam, P.J. Raut, S.C. Ojha, B.K. Jain and S.S. Kapoor, Proc DAE Symp. on Nucl. Phys. **B42** (1999) 366.
9. S.K. Gupta, R.V. Patkar, P. Singh, E. Shallom, A. Agarwal, S. Santra, Rajesh Kumar, S.P. Sarode, P.J. Raut, B.K. Jain, S.V. Gogte, R.R. Patankar, M.G. Andhansare, A.C. Tikku and M.G. Khadilkar, Proc DAE Symp. on Nucl. Phys. B42 (1999) 438.
10. S.K. Gupta, S. Santra, P. Singh, E. Shallom, A. Agarwal and Rajesh Kumar, Bull. Indian Vacuum Society, **3** (2000) 31.
11. M.J. Kansara, Sapna P., N.B.V. Subrahmanyam, J.B. Bhatt and P. Singh Int. Conf. on Heavy Ion Accelerator Tech. (HIAT-2001), Jan. 14-18, 2002, Nuclear Science Centre, New Delhi. (to be published in PRAMANA)
12. M.J. Kansara, Sapna P, N.B.V. Subrahmanyam, M.Y. Vaze, P. Singh, B.K. Jain, T.S. Ananthkrishan, S.K. Singh and M.D. Ghodgaonkar, Proc Int Symp Nucl Phys. **B43** (2000) 524.
13. M.J. Kansara, M.Y. Vaze, N. Sridevi and P. Singh, Indian J Pure & Appl Phys. 35 (1997) 212.
14. P. Singh, S.K. Gupta, , M.J. Kansara, A. Agarwal, S. Santra, Rajesh Kumar, A. Basu, Sapna P, S.P. Sarode, N.B.V. Subrahmanyam, J.P. Bhatt, P.J. Raut, S.S.Pol, P.V. Bhagwat, S. Kailas and B.K. Jain Int. Conf. on Heavy Ion Accelerator Tech. (HIAT-2001), Jan. 14-18, 2002, Nuclear Science Centre, New Delhi. (to be published in PRAMANA)
15. S. Santra, K. Mahata, P. Singh, C.V. Fernandes, Hemlatha M. and S. Kailas, Nucl. Instrum. Meth. A (2002)- in press
16. S.D. Pradhan, A.R.Nayak, Sunil Kumar, P.Singh and S.K. Mehta Rad. Prot. Env. **20**, 17 (1997)
17. R. Tripathi, A.K. Pandey, B.S. Tomar, S.B. Manohar, S. Santra, K. Mahata, P. Singh and S. Kailas, Nucl. Instrum. Meth. (2002)- submitted for publication.

Dr Pitamber Singh was conferred the BARC Technical Excellence Award for the year 2000 for his exemplary contributions to Accelerator Physics and Technology.

About the author ...

Dr Pitamber Singh *joined the Nuclear Physics Division in 1976 after graduating from 19th batch of the BARC Training School. He received his Ph.D. degree in physics from Mumbai University in 1983. Dr Singh spent more than one year at the Max-Planck Institute fuer Kernphysik, Heidelberg, Germany, and has worked in several accelerator labs. In addition to designing and building the first 2 MV Tandem Accelerator at BARC, he has made an outstanding contribution in setting up the 6 MV Folded Tandem Ion Accelerator (FOTIA) facility at BARC. Recently, he has also been selected as a member of the "National Academy of Sciences, India" for his excellent contribution towards indigenous development of the accelerator technology in the country and nuclear reaction studies using heavy ion beams from charged particle accelerators. Presently, he is working on the development of High Intensity Proton Accelerators. Dr Singh is a co-author of about 175 scientific publications. Presently, he is Head of FOTIA Section of the Nuclear Physics Division.*

Ultrafast Dynamics of Charge and Electron Transfer Reactions in Condensed Media

Dipak K. Palit
Radiation Chemistry & Chemical Dynamics Division
Bhabha Atomic Research Centre

Photoinduced charge or electron transfer (PET) reaction is one of the most important photochemical reactions, which are essential for the existence of human civilization. For example, the primary reaction involved in the photosynthesis processes in bacterial reaction centers, is the PET process. It has been well established that in this process electron travels at ultra-high speed along the molecular units – the distance of 17 Å is traveled in about 3 picosecond. The most important fact is that the quantum efficiency of the process is near unity. Hence, it has been a challenging job for the photochemists and biophysicists to understand the mechanism of this process and mimic the system for conversion of solar energy into another usable form. Photo galvanic cells have been considered to be one of the potential devices for harnessing and storing solar energy. The photochemical process involved in this device is PET reaction. However, the best efficiency achieved by any of the man made devices are only about 10%. To understand the limitations of these devices, we need to understand the basic mechanism of the PET reaction, which can be represented schematically as shown in scheme I:

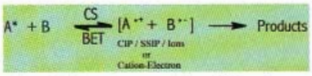

Scheme I: Schematic representation of PET reaction

One of the reactants, A, in the excited state, i.e. A*, reacts with another reactant, B, in the ground state to undergo charge separation reaction to form radical ion species, which may exist as either contact ion-pair (CIP) or solvent separated ion-pair (SSIP) or free ions in homogenous solutions. In heterogeneous media, A*, adsorbed on a suitable kind of surface, such as semiconductor nanoparticle, injects electron into it to form cation radical of A, (A^{+}). The injected electrons are mobile in the semiconductor particle. However the efficiency of the photoinduced charge separation process is reduced if the ion-pairs or the cation-electron pairs recombine to generate back the reactants. This process is known as back electron transfer (BET) reaction. BET is an energy wasting process and responsible for reduction in efficiency of the charge separation or electron transfer process. Hence the main aim of our recent studies on PET processes has been to characterize the BET reaction and find out the methods to eliminate or minimize this process in order to improve the efficiency of the charge separation process. The detailed knowledge of this process will be useful in designing new energy storage devices with increased efficiency.

Among several ways to prevent BET, two of the most attractive ones, which we have studied in our laboratory are:

1. *Photoinduced dissociative electron transfer* (PDET), in which either the donor or the acceptor molecule or both of them undergo dissociation following PET reaction, eliminating the possibility of occurrence of the BET process.
2. *Electron transfer in heterogeneous medium*, in which an excited donor dye molecule, adsorbed on a nanoparticle surface, injects electron into the nanoparticle. Higher efficiency of the PET process depends on fast electron injection

and slow recombination between the cation and the injected electron.

We will discuss briefly about the principle of these methods taking the chemical systems studied in our laboratory as the models.

Recently large size electron donor-acceptor (EDA) molecules have shown promising applications in optical memory devices, optical sensors and optical switches. The applicability of an EDA molecule for a particular purpose depends on how good control one has on the forward and the backward charge transfer reactions. In the case of a memory device, the forward and backward charge transfer reactions can be used for storing in and reading out the data, and in optical switches, for switching on and switching off, respectively. For these purposes, a suitable molecule, in which the donor and the acceptor are widely separated but linked via a long molecular bridge, is designed and synthesized to control both the processes. However, the problems with the optical devices made from such large EDA molecules are evident from the fact that following optical excitation, such a large size molecule in condensed phase (in solid or liquid solution medium) undergoes a numerous number of intra and intermolecular processes, which are associated or competing with the intramolecular charge or electron transfer process. Among them three are the most important ones: vibrational cooling, the solvation of the excited state and the conformational relaxation or isomerization. All of the said processes take place in pico and subpicosecond time domain and can be followed by probing the relaxation dynamics of the electronically excited molecules in condensed phase using ultrafast transient absorption spectroscopic techniques. Information regarding these processes should help in designing better and more efficient devices.

Experimental

Over the years, we have developed the ultrafast transient absorption spectrometers, which have provided us the capability of investigating the characteristics of the transient intermediate species produced in photoinduced chemical processes with pico and femtosecond time resolution. These facilities, which are unique in India till today, has been proved to be work-horses in the study of dynamics of photochemical reactions to unravel the intricacies of the mechanistic details of them. Figure 1 shows the block-diagram of our femtosecond laser kinetic absorption spectrometer, which has been indigenously developed in this laboratory. The working principle of the picosecond absorption spectrometer is the same as that of the femtosecond spectrometer, but the laser system used in the later is a commercially available active-passive mode-locked Nd:YAG laser from Continuum, USA.

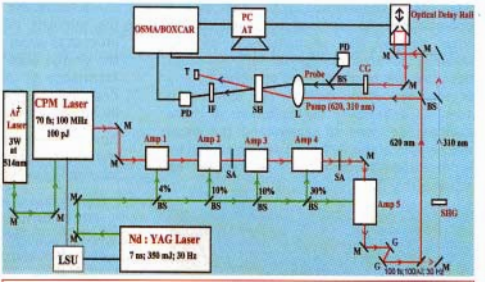

CPM Laser: Colliding pulsed mode-locked dye laser; M Mirror; G : Gratting; BS : Beam Splitter; L : Lens; SH : Sample Holder; SA : Saturable Absorber; CG : Continuum Generation; IF : Interference Filter; T : Beam Block; PD Photo Diode Detector; P : □/4 Plate; LSU : Laser Synchronisation Unit

Fig. 1: Block diagram of the femtoseond laser kinetic absorption spectrometer.

Intramolecular charge transfer process in the excited electronic states of LDS-821 dye

We have chosen LDS-821 dye, also known as styryl 9M dye, as a model EDA molecule to study the effect of bridging group and the surrounding medium in intramolecular charge transfer process by using femto- and picosecond transient absorption / stimulated emission spectroscopic technique. The molecular structure of LDS-821 has been presented in Scheme II.

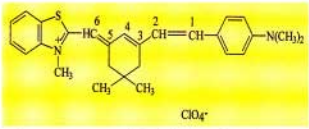

Scheme II: Structure of LDS 821 dye molecule

In LDS-821, a hexamethine hemi-cyanine dye, the dimethylaminophenyl (donor) group is connected to the methylbenzothiazolium (acceptor) group by a π-conguated spacer group consisting of a polymethine chain having three ethylenic unit. However, among these three ethylenic units, two are parts of a rigid cyclohexenyl ring and the other is flexible and hence only the latter is able to undergo torsional motion to take part in trans-cis isomerization process.

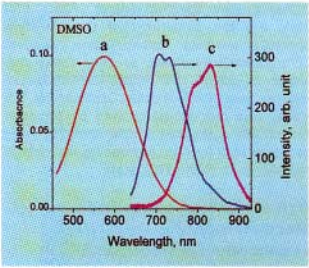

Fig 2 : Steady state spectra of LDS-821 in dimethyl-sulfoxide (DMSO): absorption spectra at 298 K (a) and fluorescence spectra at 298 K (c) and at 77 K (b).

The steady state absorption and fluorescence spectra of LDS-821 in dimethylsulfoxide (DMSO) at room temperature (298 K) and also the emission spectra in solid matrix at 77 K is shown in Figure 2. The emission spectrum recorded at room temperatures is very much red shifted with respect to the one recorded at 77 K. This indicates that the electronic structure of the emitting species at 77 K and 298 K are different. The large Stokes' shift between the maxima of the absorption and emission spectra recorded at 298 K indicates that certainly the Franck-Condon (FC) excited state is not the emitting state at this temperature. The steady state fluorescence maximum also shifts to lower energy region due to increase in solvent polarity.

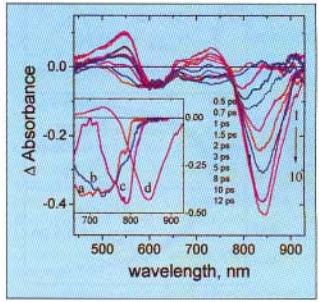

Fig 3: Time resolved transient absorption spectra of LDS-821 in DMSO due to excitation by 620 nm laser pulses of 150 fs duration. Inset shows the evolution of the stimulated emission spectra in 650 - 930 nm region, recorded at 0.5 (a), 0.7 (b), 1 (c) and 12 (d) ps time delays, as they have been normalized to approximately the same intensity at the wavelength maximum of each spectrum.

Figure 3 shows the time resolved transient absorption/stimulated emission spectra obtained due to photolysis of LDS-821 in DMSO in subpicosecond time domain. The negative absorption band appearing in the 500 - 650 nm region is due to ground state bleaching. The lifetime of the bleaching recovery is about 560 ps (not shown in the figure). The transient spectrum (curve 1)

recorded at 0.5 ps after the pump laser pulse, shows a weak stimulated emission band in the 650 - 800 nm region with a maximum at *ca* 700 nm. With increase in time delay, this emission band disappears with a concomitant development of a positive absorption band in the same region as well as another emission band in the red side of the former (i.e. in the region 800 - 900 nm). With increase in time delay the wavelength maximum of this new emission band shifts gradually from ca 800 nm, as it starts developing during *ca* 1 ps delay, to 842 nm at 15 ps, when it is fully grown (curve 10). The temporal dynamics of the transients monitored at 590, 730 and 850 nm have been shown in Figure 4.

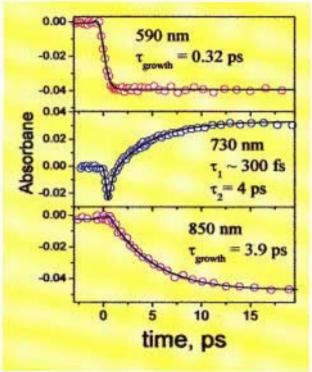

Fig 4: The temporal evolution of the transient absorption/ stimulated emission due to photoexcitation of LDS-821 in DMSO.

The excited state dynamics of LDS-821 have been monitored in a few other solvents. The gross features of the time-resolved transient absorption characteristics are more or less similar in other solvents as those described in case of ACN. We observe the gradual shift of the maximum of the time resolved stimulated emission band (which is popularly known as the dynamic Stokes' shift), only in polar solvents, but not in relatively less polar chloroform solution. Hence, the growth of the emission band, which is accompanied by the dynamics Stokes' shift, in 800 - 850 nm regime, could be assigned to the formation of an intramolecular charge transfer (ICT) state and its simultaneous solvation.

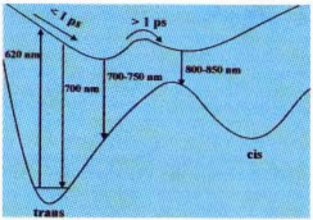

Fig 5 : Potential energy surface depicting the two-state two-mode model for the relaxation of LDS-821 molecule in the excited singlet state.

The time resolved spectra as well as the temporal dynamics of the stimulated emission monitored at different wavelengths (Figures 3 and 4) mainly reveal the features of two-state two-mode kinetic process – local excited (LE) state to the twisted intramolecular charge transfer (TICT) state (Figure 5). For short wavelength detection, e.g. at 730 nm, we observe the S_1 state relaxation in the region close to the FC point. The observation of a short (≤1 ps) rise time as well as very fast spectral evolution in this higher energy spectral regime (700 - 800 nm), are the signatures of the transient species evolving along the skeletal deformation coordinate in the 'valley-like' region to attain the metastable untwisted intermediate conformation, called the LE state. This process is followed by torsoinal motion about the free double bond ($C_1 = C_2$) accompanied by the intramolecular charge transfer to form the TICT state.

Dye sensitized photo-induced electron injection into TiO_2 semiconductor nanoparticle

Interfacial electron transfer between molecular adsorbate and semiconductor nanoparticle is an intense area of research

because of its large number of applications, such as solar energy conversion as well as nanoelectronic devices. Figure 6 shows the schematic representation of electron injection and BET process in dye-sensitized TiO_2 nanoparticle system. In Figure 6, Es/s^+ represents the ground state redox potential value of the dye adsorbed on TiO_2 nanoparticle surface. It lies below both the conduction band edge (E_c) and Fermi level (E_f) of the nanoparticle. But when the dye is excited, the excited state redox potential value, E^*s/s^+, falls within the energy region of the conduction band. Hence, the dye in its excited state can inject electron into the conduction band of the semiconductor nanoparticle. Following injection, if it is not removed from the surface under the influence of a bias voltage applied to the particle, the electron relaxes very fast to the conduction band edge. As the time progresses, the electron relaxes to different trap states (swallow and deep). These electrons trapped in different trap states undergo BET reaction to recombine with the dye molecule reducing the efficiency of the PET process. Our aim has been to understand the effect of electronic coupling between the dye and the semiconductor nanoparticle on the BET process.

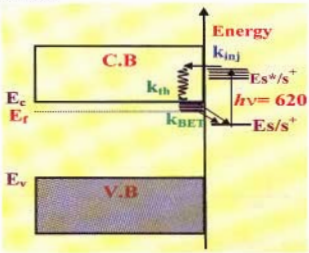

Fig 6: Schematic representation of electron injection and BET processes in dye-sensitized TiO_2 nanoparticle

Recently, TPM dyes, which have good absorption for the solar radiation and good electronic coupling with TiO_2 nanoparticle surface, have been considered as the potential sensitizers for the solar cells. However, the photocurrent efficiency of the cells made by using these TPM dyes were found to be less than 1%. We made an attempt to investigate the photoinduced electron injection process from the excited states of the TPM dyes, to the TiO_2 nanaoparticles by using ultrafast transient absorption spectroscopic technique. The structures of the TPM dyes used here have been presented in Scheme III.

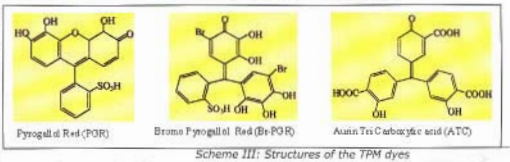

Scheme III: Structures of the TPM dyes

These dyes are known to form association complex with TiO_2 nanoparticle. In the case of pyrogallol dyes the appearance of new absorption band indicates a very strong coupling with TiO_2. Scheme IV shows an illustration of the complexation reaction between the hydroxylated TiO_2 surface and catecol (A) (for PGR and Br-PGR) and (B) salicylate (for ATC) type of ligands.

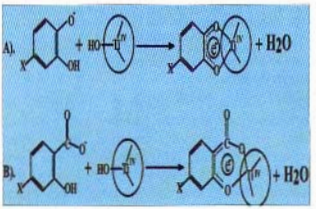

Scheme IV: Complexation between TiO_2 and TPM laser dyes (see text)

Electronic coupling element, H_{ab}, for these dyes have been determined by using Mulliken-Hash equation and in Table 1, these

have been compared with those of N_3 and other dyes, with which the best efficiency for solar energy conversion has been achieved.

$$H_{ab} = \frac{2.06 \times 10^{-2} (\nu_{max} \varepsilon_{max} \Delta\nu_{1/2})^{1/2}}{r_{ab}}$$

Table 1

Dye Molecule	H_{ai}, cm^{-1}
Pyrogallol red (PGR)	6.8×10^{-3}
Bromo-pyrogallol red (Br-PGR)	8.2×10^{-3}
Aurin triboxylic acid (ATC)	4×10^{-2}
Coumarin-343	2×10^{-2}
$Ru(III)L_2(NCS)_2$ (N_3 Dye)	1.3×10^{-2}

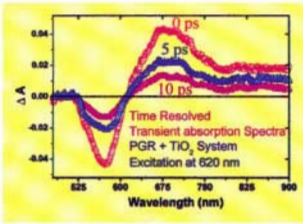

Fig 7: Transient absorption spectra of PGR sensitized TiO_2 nanoparticle in water at 0, 5 and 10 ps after excitation at 620 nm laser pulses of 150 fs duration. The features of each spectrum consists of a bleach at 515 –620 nm and the absorption peak due to the PGR cation radical at 690 nm and a broad absorption band in the spectral region 750 –900 nm due to the injected electron into thesemiconductor particle.

Our studies on ultrafast dynamics of photoinduced electron transfer processes of the three strongly coupled TPM dyes adsorbed on TiO_2 nanoparticle surface have established that electron injection from the excited dye to the nanoparticle takes place faster than 200 femtosecond. Appearance of both the bleaching as well as cation radical absorption are faster than our instrumental response function (Figures 7 and 8). Also both the bleach recovery and cation decay follow similar kind of dynamics, which are

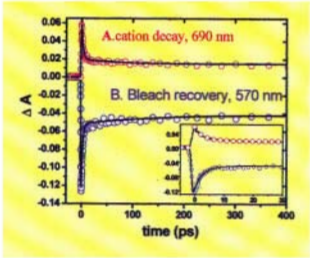

Fig 8 : Cation decay and bleach recovery in PGR-TiO_2 system following photoexcitation by 620 nm laser pulse of 150 fs duration.

nonexponential, in the case of the pyrogallol dyes. These temporal profiles show that more than 70% of bleach has recovered or cation decay has taken place within 10 picosecond time scale. However, in case of ATC sensitized TiO_2 system, in which the coupling of the dye with the semiconductor particle is relatively weaker, the bleach recovery is much slower than those of the pyrogallol dyes (figure 9). Both the bleach recovery and the cation radical decay represent the BET reaction. BET reaction has been seen to be continued up to nanosecond and microsecond time scale. However the BET reaction is much slower for the weakly coupling dye ensuring better efficiency for the charge separation process.

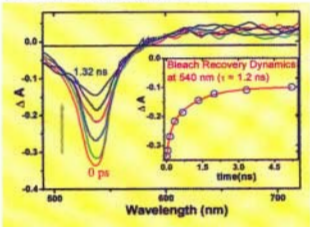

Fig 9 : Transient absorption spectra of ATC sensitized TiO_2 nanoparticle in water at 0, 33, 132, 330, 660 and 1320 ps after photoexcitation. (Inset: the bleach recovery kinetics)

Dynamics of PDET reaction in solution

The occurrence of the thermal and electrochemical dissociative ET (DET) reaction is well documented in the literature. Recently we reported our studies on PDET reaction between phenothiazines and chloroalkanes in solution. Like other DET processes, PDET reaction also has been shown to follow two different mechanisms (Scheme V) :

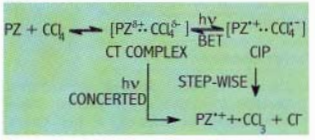

Scheme V: Two different mechanisms for PDET Reaction.

a. *Concerted*: Cleavage of any of the bonds takes place immediately following ET, without involvement of any intermediate – possibility of BET is completely eliminated.
b. *Step-wise*: ET reaction takes place via formation of CIP, which geminately recombines to produce back the reactants.

Obviously if the PDET reaction follows the concerted mechanism, the overall efficiency of the process is increased as compared to that follows the stepwise mechanism. Hence it is an exciting proposal whether a stepwise PDET reaction can be made to follow a concerted path in order to increase the efficiency of the PDET process. From our studies on the mechanism of the PDET reaction between phenothiazines and chloroalkanes using ultrafast absorption spectroscopic technique, we have been able to show that this proposal is feasible in reality and it should be possible to control the reaction mechanism at our will, by tuning or varying the driving force of the reaction (i.e. the free energy change of the reaction, ΔG^0), which can be written by the following equations.

$$\Delta G^0 = E(PZ/PZ^+) - E(CCl_4/CCl_3 + Cl^-) - E_{00} - \frac{e^2}{\varepsilon_s r}$$

$$E(CCl_4/CCl_3 + Cl^-) = E(Cl/Cl^-) - BDFE(CCl_3 - Cl)$$

$E(Pz/Pz^{+})$ is the oxidation potential of the phenothizines (PZ), E_{00} is the energy of the lowest excited singlet state, and $e^2/\varepsilon_s r$ is the columbic energy experienced by the radical ion pair at a transfer distance, r, in a solvent of static dielectric constant, ε_s. $E(Cl/Cl^-)$ and $BDFE(CCl_3\text{-}Cl)$ are the reduction potential of chlorine atom and the bond dissociation free energy of CCl_4, respectively. This equation clearly predicts that the ΔG^0 value of the PDET reaction could be varied in two different ways:

1. *Using different donor – acceptor pairs.* Differently substituted phenothiazine derivatives (PZ), as shown in Table 2, have been used in our studies. Table 2 also shows the values of ΔG^0 for the PZ – CCl_4 pair in acetonitrile solution as calculated using the above equation as well as the mechanism followed by the PDET reaction in the same solvent. Only for the PTH-CCl_4 pair, the PDET reaction follows the step-wise mechanism, but for the other pairs, ΔG^0 values are less negative and concerted mechanism is followed.

2. *Solvent polarity* too can be varied to alter the value of ΔG^0 for a particular pair of reactants. In solvents of higher polarity, ΔG^0 value becomes more negative while the reverse is true for solvents of less polarity. We investigated the PDET reaction for MPTH-CCl_4 pair in DMSO (higher polarity than acetonitrile) and seen to follow step-wise mechanism. On the other hand PTH-CCl_4 pair is seen to follow concerted mechanism in less polar solvent, ethylacetate.

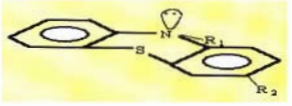

Table 2

PZ	R_1	R_2	$-\Delta G^0$, (eV)	Mechanism
PTH	H	H	2.00	Step-wise
MPTH	CH_3	H	1.92	Concerted
PMZ	$(CH_2)_3N(CH_3)_2$	H	1.85	Concerted
CPZ	$CH_2CH(CH_3)$ $N(CH_3)_2$	Cl	1.78	Concerted

The predominance of one mechanism over the other depending on ΔG^0 value can be explained by the relative position of the potential energy surface (PES) of the reactants and the intermediate (Figure 10). If the minima of these two are vertically close to each other, there is possibility that the reactant PES can cross the same of the intermediate, and in such cases the reaction follows the step-wise mechanism. But if the minimum of the PES of the reactants goes down vertically, reducing the possibility of crossing its PES with that of the intermediate, the reaction follows concerted mechanism, without formation of any intermediate.

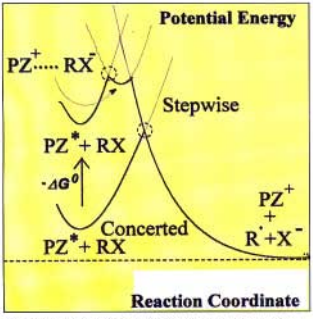

Fig 10 : Potential energy diagram for the passage from step-wise to concerted mechanism as a function of ΔG^0 of the reaction

Conclusion

Our discussion establishes that pico and femtosecond transient absorption spectroscopy is a powerful technique to unravel the mechanistic details of photoinduced charge and electron transfer reactions, both in homogeneous and heterogeneous media. Back electron transfer (BET) reactions are responsible for the reduced efficiency of the man-made energy storage devices, which use the photoinduced electron transfer process. BET reactions need more detailed investigations to improve the efficiency of these devices by eliminating or minimizing the same.

References

1. Dipak K. Palit, *Studies of Ultrafast Reaction Dynamics in the Excited States of Molecules in Solution*, J. Ind. Chem. Soc. 2002 , January Issue (Invited Article).
2. D. K. Palit, A. K. Singh, A. C. Bhasikuttan and J. P. mittal, *Relaxation Dynamics in the Excited States of LDS-821 in Solution*, J. Phys. Chem. A 105 (2001) 6294 - 6304.
3. G. Ramakrishna, H. N. Ghosh, A. K. Singh, D. K. Palit and J. P. Mittal, Dynamics of Back Electron Transfer Processes of Strongly Coupled Triphenylmethane Dyes Adsorbed on TiO_2 Nano-particle Surface as Studied by Fast and Ultrafast Visible Spectroscopy, J. Phys. Chem. B 105 (2001) 12786 - 12796.
4. S. Nath, A. K. Singh, D. K. Palit, A. V. Sapre and J. P. Mittal, Change in Reaction Mechanism with driving force in Photoinduced Dissociative Electron Transfer (PDET) Reaction - A Subpicosecond Transient absorption Study, J. Phys. Chem. A. 105 (2001) 7151.

Acknowledgement

The author is grateful to Dr. J. P. Mittal, Director, Chemistry & Isotope Group, Dr. T. Mukherjee, Head, Radiation Chemistry & Chemical Dynamics Division, and Dr. A. V.

Sapre, Head, Chemical Dynamics Section, for their constant encouragement and support throughout his career. The author also acknowledges the active scientific contributions from his co-workers and co-authors of the papers mentioned in the reference section. Without their help it would not have been possible to write this article.

Dr Dipak Kumar Palit was awarded the "Bronze Medal of 2001" by the Chemical Research Society of India in its Annual Conference held at Pune during February 28 – March 2, 2002. The article is written on the lecture delivered by the author in this conference.

About the author ...

Dr Dipak Kumar Palit *joined the Chemistry Division, BARC, after completion of the one-year orientation course (26th batch) of BARC Training School. After obtaining his Ph. D. degree from Bombay University in 1989, he was awarded "BOYSCAST Fellowship" of DST for his post-doctoral work on ultrafast spectroscopy in the University of Pennsylvania, USA. His current research interest is to study chemical reaction dynamics in condensed phase using ultrafast lasers and accelerators.*

Preparation, Optimization/Characterization and Ion-Exchange Behaviour of V(II) Formulations

J Manjanna and G Venkateswaran
Applied Chemistry Division
Bhabha Atomic Research Centre

Abstract

The low oxidation state metal ion, V^{2+} being a strong reducing agent can be formulated/ complexed with suitable chelating agents to obtain a significant dissolution (reductive) of iron oxides, commonly found on the primary system surfaces (iron base alloys) of water-cooled nuclear reactors. The relative strength of the complexes of V^{2+} (as formate) with different chelating agents, L such as picolinic acid, EDTA and citric acid is studied by measurements of redox potential and UV-Visible spectra. The decay kinetics of the reduction of water by V(II)-picolinate i.e. V^{2+} to V^{3+} conversion under deaerated condition was estimated using redox potential values and decay was found to follow two stages of first order kinetics with a faster initial stage (k_1 = 3.45 x 10^{-3} min^{-1}) and a slower second stage (k_2 = 3.84 x 10^{-4} min^{-1}). The cation and anion exchange resin behaviour of the complexes/ formulations in their different oxidation states with their derived species is reported and the V(III)-picolinate is shown to exist as an anionic species in formate medium. The use of V(II)-EDTA and V(II)-citrate for dissolution has an advantage as their oxidation to V(III) stage at concentrations > 7mM has not resulted in any precipitation/ crystallization unlike in the case of V(II)-picolinate.

Introduction

The chemical decontamination of primary coolant circuit in water-cooled nuclear power reactors involves the dissolution of corrosion films (Ni, Cr-substituted as well as simple iron oxides) accumulated on the structural surfaces[1-6]. The Cr-containing iron oxides are not easily amenable for dissolution in conventional organic acid based formulations like citric acid-EDTA-ascorbic acid (CEA) mixture[5,6]. However, low oxidation state metal ions (LOMI) such as V^{2+} and Cr^{2+} in presence of suitable chelating agents are known to be very strong reducing agents (rapid kinetics) towards the dissolution of such oxide matrices[1,2]. Normally V(II) based LOMI formulations involving V(II)-picolinate is employed for such purposes[1]. Use of V(II) picolinate complex is limited to concentration levels below 7 mM. Above this concentration level, V(III) picolinate (which is generated either during reductive dissolution of corrosion films accumulated on structural surfaces or some times by air oxidation due to system air leaks) precipitates/crystallizes out. The use of EDTA and citric acid as complexing agents can overcome such solubility problems. The electrochemical method of preparing V(II) enables the generation of composition specific formulations, which is an important consideration towards base material compatibility aspects in real system applications. The relative stability of electrochemically prepared V(II)-picolinate, V(II)-EDTA and V(II)-citrate complexes/ formulations as derived from the redox and UV-Visible spectra are reported in this paper. The behaviour of these complexes in their different oxidation states on the conventional ion-exchange resin is studied, and the derived species getting sorbed is reported. The detailed studies on the dissolution of Cr-substituted oxides in these formulations are published elesewhere[5].

Experimental Set Up

Electrochemical Assembly : A flat bottomed glass vessel of 500 mL capacity

was used for preparing V^{2+} (as formate). Fig. 1 shows the electrode compartments and its power supply unit as well as arrangement for cathode/solution potential measurements. The cylindrical Pt gauze was made as anode, and Hg pool served as cathode. A sintered glass disc separated the anode and cathode compartments. A saturated calomel electrode (SCE) was used as reference electrode.

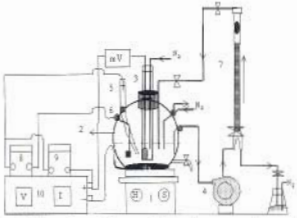

Fig. 1:Electrochemical assembly for the preparation, and on-line estimation of V(II) formate. 1. Magnetic stirrer-cum hot plate; 2. Cathode compartment; 3. Anode compartment; 4. Peristaltic pump; 5. SCE with luggin probe; 6. Pt foil electrode; 7. Assembly for on-line titration of electrolysis product; 8 & 9. Voltammeters for Solution potential and Cathode potential measurement respectively; 10. DC Power supply Unit

Table 1: The optimized parameters for the electrochemical generation of V(II) formate

Catholyte, $NaVO_3$ *pH* 2.8	Anolyte, HCOOH	Cell Current	Cell Voltage	Time (min)
4 mM	2.0 M	80 mA	40 V	60
11 mM	2.6 M			60
22 mM	3.5 M			70
44 mM	4.0 M			90

Electrolysis : The electrolysis was carried out after charging required amounts of catholyte and anolyte. In cathode compartment a known amount of aqueous $NaVO_3$ in formic acid media (*pH* ~2.8) was placed, while in the anode compartment only formic acid of appropriate concentration was taken. Before starting the electrolysis the solutions (both anolyte and catholyte) were kept for deoxygenating ca.~30 min using high purity N_2 gas (scrubbed through V^{2+} trap generated by Zn-amalgum in HCl) and N_2 bubbling was continued throughout the electrolysis. The concentration of formic acid (anolyte), cell-current, cell-voltage and time required for completion of electrolysis (Table 1) to obtain V^{2+} (as $V^{II}(HCOO)_2$) in the concentration range of 4 - 44 mM were optimized/standardized from the initial experiments. The optimization was done by number of initial trial experiments based on the stoichiometric amount of formate ions required as well as the reduction potentials reported in the literature[7] for the reduction of vanadium species.

Estimation of V(II)-formate : The electro-generation of V^{2+} species was confirmed by online redox potential (~ -0.580V v/s. SCE) measurements. During electrolysis, the solution was kept circulating from the vessel through a burette using a peristaltic pump. This arrangement helped in titrating the solution periodically against standard $KMnO_4$ solution to estimate the extent of V^{2+} generation. The oxidation of V^{2+} by permanganate can be represented as,

$$5V^{2+} + 3MnO_4^- + 24H^+ \ (10\%\ H_2SO_4) \rightarrow 5V^{5+} + 3Mn^{2+} + 12H_2O$$

The electrolysis proceeded with the accompanying colour changes viz. yellow, blue, green and purple for V(V), V(IV), V(III) and V(II) respectively during electrolysis.

Estimation free formic acid : The total formic acid content was estimated at the end of the electrolysis by passing the sample through the strong acid cation exchange resin. The eluate was titrated against standard NaOH solution using phenolphthalein indicator. The free formic acid was calculated from the total formic acid by subtracting two times the V^{2+} concentration and the sodium concentration from the initial sodium metavenadate used for the preparation of V^{2+} (Table 2).

Table 2: Composition of V(II) formulations (in mM) containing stoichiometric amount of L for the dissolution of 20 at.% csh/csm*

[V^{2+}-formate] *pH* 3.0±0.3	[Pic] *pH* 4.0±0.3	[EDTA] *pH* 3.6±0.3	[Cit] *pH* 2.6±0.3	[HCOOH]
4	93	31	31	8
11	114	38	38	39
22	147	49	49	43

*equivalent to 22 mM iron and ~5.5 mM Cr (from $Fe_{1.6}Cr_{0.4}O_3$/ $Fe_{2.4}Cr_{0.6}O_4$) in 200 mL formulation (see ref 5).

Formulation/ Complexation of V^{2+} species : After confirmation and estimation of V^{2+} species, the electrolysis was stopped and the Hg (cathode) was removed carefully (through the outlet provided with the flask). The V^{2+}(as formate) thus generated was then made to complex with different chelating agents viz. picolinic acid (H_3Pic), EDTA (disodium salt, Na_2EDTA) and citric acid ($C_6H_8O_7$). The EDTA and citric acid were added directly in to the cell containing V(II) formate. However, the picolinic acid required to complex with V^{2+} was neutralized (in order to provide the ligand in readily complexable form) with NaOH separately in a deaerated aqueous medium before its addition. In all the cases, stochiometrically excess (w.r.t V^{2+}) amounts of chelating agent, L viz. H_3Pic, Na_2EDTA and $C_6H_8O_7$ were added. Table. 3 shows the composition of V(II) based formulations which have been employed in the dissolution studies of Cr-substituted iron oxides[5]. The amount of chelating agent provided in each case is stoichiometrically equivalent to that required for complexation with V^{2+} species as well as Fe and Cr from the oxide ca. 20 metal atom% Cr-substituted hematite/magnetite (as a typical case).

Dissolution behaviour : *Fig.* 2 shows the typical dissolution profiles of Cr-substituted hematite/magnetite in V(II)-EDTA and CEA (citric acid-EDTA-ascorbic acid) formulations. The details of experiment, and the determination of dissolution rate coefficients using general kinetic equation applicable for polydispersed particles are reported[5,8,9]. It is observed that the Cr substitution in hexagonal lattice (α-Fe_2O_3) has hindered the dissolution to a greater extent than that observed when Cr is substituted in cubic lattice (Fe_3O_4). Using CEA, the complete dissolution of simple iron oxides viz., α-Fe_2O_3 and upto 10% Cr-substituted magnetite can be obtained to the reductive mechanism of internally generated (during the course of dissolution) Fe(II)-EDTA. However, when Cr is substituted to the extent of >10 at%, there was no dissolution[8] even on employing higher concentrations of CEA. As shown in Fig.2, vanadous formulation, V(II)-EDTA has resulted higher dissolution when compared to CEA, and there is a higher dissolution in the case of csm. This observation documents the advantage of employing vanadous formulations over conventional formulations like CEA in dissolving Cr-substituted iron oxides encountered on the structural surfaces of water-cooled nuclear reactors.

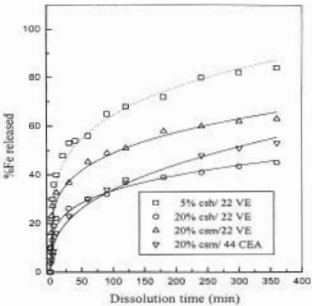

*Fig. 2: Typical dissolution profiles obtained for csh/ csm in VE and CEA formulation. **csh/csm**: Cr-substituted hematite/magnetite; **VE**: V(II)-EDTA formulation, 22 mM; **CEA**: 11 mM citric acid + 44 mM Na_2EDTA + 44 mM ascorbic acid (pH 2.8) mixture.*

Ion-exchange behaviour : During this particular study, the L was added equivalent to the stoichiometric complexation of V^{2+} alone and no extra L (free L) was provided. The V(II)-L (formic acid, picolinic acid, EDTA and citric acid) were passed through strong acid cation and / or anion exchane resin (polystyrene based gel type resin). The resin bed was regenerated (by 5%H_2SO_4 or NaOH) freshly and deoxygenated by circulating deaerated water before passing the V(II)-L. For this purpose, a closed loop was setup from electrolytic cell and resin column with the help of peristaltic pump. Uniform flow rate, 5mL/ min was maintained in each case. The oxidized forms of V(II)-L viz., V(III)/ (IV)/ (V)-L were obtained on controlled air oxidation of V(II)-L for which the conversions were monitored by redox potential measurements.

Results and Discussions

Electrochemical Generation of V^{2+} : The vanadous ion, V^{2+} was prepared as V(II) formate by the electrochemical reduction over the surface of Hg, using deoxygenated aqueous solution containing required amounts of sodium metavanadate ($NaVO_3$) and formic acid at *pH* 2.8. The cell parameters such as current, voltage and duration of electrolysis are shown in Table 1. During electrolysis, the step-wise reduction of VO_2^+ to V^{2+} can be represented[7,10] by the following equations (V versus SHE).

$NaVO_3 \longrightarrow Na^+ + VO_3^-$ on ionization

$VO_3^- + 2H^+ \longleftrightarrow VO_2^+ + H_2O$ chemical process

$VO_2^+ + 2H^+ + e^- \longleftrightarrow VO^{2+} + H_2O$, $E^0 = 1.00V$ ...(1)

VO^{2+} directly goes to V^{2+} irreversibly as

$VO^{2+} + 2H^+ + 2e^- \longrightarrow V^{2+} + H_2O$ ...(2)

Also, V^{2+} thus generated reduces VO^{2+} to V^{2+} easily and in the process gets oxidized to V^{3+} as

$V^{2+} + VO^{2+} + 2H^+ \longrightarrow V^{3+} + V^{2+} + H_2O$ ...(3)

Then V^{3+} from Eq. (3) was reduced to V^{2+} as

$V^{3+} + e^- \longleftrightarrow V^{2+}$, $E^0 = -0.255V$ ...(4)

Due to H^+ consumption during electrolysis, the initial *pH* (2.8) of catholyte was increased slightly to *pH* 3.0 at the end of electrolysis. In anode compartment the decomposition of water resulted in the liberation of O_2 during electrolysis and in order to improve the conductivity of the solution, an appropriate amount of formic acid was placed. Whenever the formic acid was not sufficient (during the initial experiments), a black precipitate of vanadic oxide, which is the hydrolysis product of vanadium was noticed. Monitoring the solution potential on Pt electrode helped in following the reduction process during electrolysis. The yellowish orange VO_2^+ turns to sky blue colour of VO^{2+} which before going to the purplish violet colour of V^{2+} goes through a dark blackish green stage showing the formation of V^{3+} also in the solution according to the Eq. (3). The variation of cathode potential and solution potential during the time of electrolysis in a typical case of 11 mM is shown in Fig. 3.

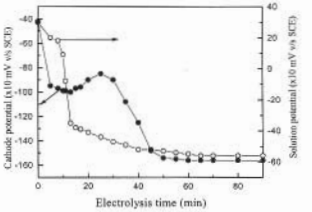

Fig. 3 : Variation of cathode/solution potential with time during the electrogeneration of 11 mM V^{2+} (as formate) from aqueous sodium metavanadate in formic acid buffer (pH 2.8).

The electrolytic generation of V(II)-picolinate and its application in the decontamination of BWR surfaces has been presented previously from our laboratory[10]. During the same study, $E_{1/2}$ was found to be −1.32V (vs. SCE) and the potential corresponding to the limiting diffusion current is −1.4 to −1.6V using DC polarogram. In the present case also a cell of ~40V yielded a cathode potential of −1.55V in the later stage of electrolysis. Also, the V^{2+} could be generated

with the desired conditions in the concentration range of 4 to 44 mM. During the course of electrolysis, the cathode potential (Fig 2) was found to decrease in the first phase (lasting ~ 10 min), there was a slight increases and thereafter it decreased slowly reaching a plateau value of ~ -1.55V. The increase of cathode potential in the mid-way of electrolysis indicates the formation of V^{3+} during the process of reducing VO^{2+} by V^{2+} according to Eq. (2).

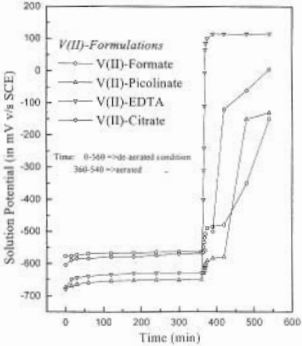

Fig. 4 : Variation of solution potential for V(II)-L as a function of time in de-aerated followed by aerated condition at 353 ± 5 K.

On providing chelating agents, L viz. picolinic acid, EDTA and citric acid into the V(II) formate solution showed a negative shift in solution potential (Fig. 4). This is a clear indication of complex formation between V(II) and L. Relatively more potential shift was observed (Fig. 4, at t = 0) in case of EDTA and picolinic acid when compared to citric acid, indicating their better complexing ability. This observation is in corroboration with the UV-Visible spectra, which showed a blue shift as the ligand was changed successively from formic acid to citric acid to picolinic acid, and to EDTA (Fig. 5). The choice of L was based on the various dissolution studies reported in the literature[1-4].

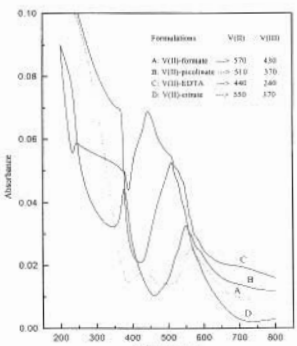

Fig. 5: UV-Visible absorption spectra of V(II) based formulations/ complexes (A, C and D are 4 mM while B is 1 mM).

Stability of V(II)-formulations : Solution potential measurements using a Pt electrode against SCE were employed to assess the stability of V(II)-L (L= picolinic acid, EDTA or citric acid). Vanadous ion is very easily oxidized by exposing the solution to air ($4V^{2+} + O_2 + 4H^+ \rightarrow 4V^{3+} + 2H_2O$). The extent of oxidation was assessed when a typical concentration (ca. 11mM) of the formulation was kept stirred magnetically at 353 ± 5 K for about 6 h under deoxygenated condition using high purity nitrogen gas. Fig. 4 show the variation in the redox potential with time of V(II)-L under deaerated and aerated conditions. The initial negative shift (t = 0) of redox potential upon adding different L to V(II)(as formate) under deaerated conditions was in the order: picolinate ≥ EDTA > citrate > formate showing the chelating ability of the complexes as formate < citrate < -EDTA < picolinate. The V(II)-L (L= picolinate, EDTA and citrate) formulations upon storage under deaerated conditions (Fig. 4) showed a positive potential shift of ~ 25 mV in 6 h duration suggesting the reduction of water by the reaction (V^{2+}-L + $H^+ \rightarrow V^{3+}$-L + ½ H_2) thereby contributing to the oxidation of V(II). Converting the potential values into

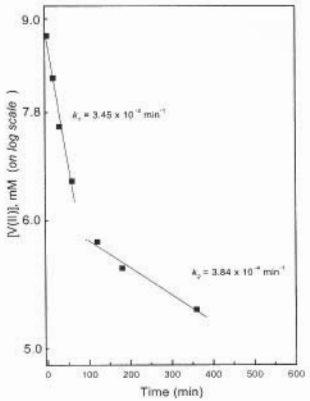

Fig. 6 : Decay kinetic of V(II)-picolinate in water under de-aerated conditions at 353 ± 5 K.

concentrations using the Nernst equation, the decay of [V(II)] with time was computed. Fig. 6 shows the decay kinetics in a typical case of V(II)-picolinate when the solution was kept stirred under deaerated condition at 353±5 K. A two stage first order kinetics with a fast initial stage showing a rate constant k_1 = 3.45 x 10^{-3} min^{-1} and a slow second stage having a k_2 = 3.84 x 10^{-4} min^{-1} is observed. The lower rate constant in the second stage is probably due to V^{3+} build up in solution resisting the further decay of V(II). Since the potential shift observed in case of other two chelating agents is of same magnitude (< 30 mV) the rate constants for their decay are expected to be the same. However, when N_2-bubbling was stopped, all the formulations got oxidized V(III)-L in < 5 min. The further air oxidation leading to V(IV) state took ~ 15 min in case of EDTA and citrate. While picolinate and formate took ~ 90 min and 150 min respectively. This observation is of importance with respect to dissolution of oxides in these formulations as the V(III)-L (EDTA and citrate) can also serve as internally generated reducing agents for further dissolution unlike V(III)-picolinate whose oxidation appears to be kinetically hindered. In no case, V(V) state was reached even after a sufficient exposure to air ~ 6 h.

In the case of V(II)-picolinate when the concentration was >7 mM, the air oxidation over a period of time > 5 h resulted in precipitation as brick-red crystals due to poor solubility of V(III)-picolinate. Although, its effect is insignificant on the dissolution of iron based oxides in a lab scale studies, it will be of serious concern during the large scale application such as reactor system decontamination as it can hinder the dissolution by forming a protective layer (of fine crystals) on the underlying oxide surface at the oxide-solution interface. Also, it may require lot of washings to bring the system to normalcy for operation. In this regard, however the other two formulations, V(II)-EDTA and V(II)-citrate will be of advantageous when it is required to use higher concentration of formulations as they do not pose any such type of precipitation or crystallization ca. in the concentration range of 4 to 44 mM prepared in this study.

UV-Visible spectra : The UV-Visible spectra of pure V(II)-formate showed a λ_{max} at 570nm. When different chelating agents viz. citric acid, picolinic acid and EDTA were added, the maxima shifted to 550, 510 and 440 nm respectively (Fig. 5). The shift in λ_{max} towards blue region suggests the relative strength of complexes in the order as V(II)- formate < citrate < picolinate < EDTA. This is in corroboration with the inferences obtained from initial shift in redox potential measurements (Fig. 4). Fig. 5 shows the absorption maxima values for V(III)-L also since a small fraction (~10%) of V(II)-L got oxidized to V(III) state during spectral measurements. The λ_{max} values of vanadium species at different oxidation states are also shown in Table 3. The reported stability constants[7], log K of V(II)-EDTA and V(II)-picolinate of 12.7 and 12.8 respectively lend support to the conclusion reached in this study from the spectral data are in agreement with the above

observations. Though, the stability constant value of V(II)-citrate is not available, and VO^{2+}-citrate is reported to have a log K of 8.8, from the present study it is expected that citric acid forms relatively weaker complex with V(II).

Ion-exchange behaviour : The decontamination is generally followed by the removal of all the chemical constituents of the decontaminating formulations. Passing the dissolved species (aqueous) through cation and/or anion exchange resin normally does this exercise. The V^{2+} species after reducing the ferric oxides (corrosion products) can go to higher oxidation state of +3 and +4 and some times to even +5 due to the increase in dissolved oxygen content in the system. Hence, the ion exchange behaviour of these complexes of vanadium with citric acid, EDTA and picolinic acid becomes important when spent decontamination solution is treated by synthetic organic ion exchange resin as a part of waste solidification. Thus in this study, all these formulations at different oxidation states of vanadium (higher oxidation states were obtained by air oxidation of V^{2+} formulations) were passed through strong cation and strong anion exchange resin independently. It was found that the anion resin picked up all these species while the V^{2+}, V^{3+} and VO^{2+} excepting VO_2^+-citrate complexes were dissociating on the cation exchanger. The fact that, the V(III)-picolinate which is usually referred as $V(pic)_3$ (neutral complex), gets sorbed on the anion exchanger shows that it is existing as anionic complex in formate medium and may be represented as $[V(pic)_2(HCOO)_2]^-$. Existence of vanadium species in different oxidation states with different chelating agents and their sorption behaviour on the cation/ anion exchanger is shown in Table 4. Thus the ion exchange behaviour of V(II) formulations is highly encouraging for their application in nuclear reactors as a decontamination formulations.

Table 3: Absorption maxima, λ_{max} (in nm) of the vanadous formulations at different oxidation states

Chelating agent	Vanadium species			
	V(II)	V(III)	V(IV)	V(V)
Formic acid	570	430	382	215
Picolinic acid	510	370	361	325
EDTA	440	240	244	232
Citric acid	550	370	242	230

Table 4: Ion-exchange (IX) behaviour of vanadous based formulations and their oxidized forms on polystyrene based strong acid cation and anion exchange resin

o.s	Metal ion species	Likely metal ion species in the complexed form with different chelating agents			IX behaviour	
		Picolinic acid	EDTA	Citric acid	cation	anion
+2	V^{2+}	$[V^{2+}(pic)_3]^-$	$[V^{2+}\text{-EDTA}]^{2-}$	$[V^{2+}\text{-H}_{-1}\text{cit}]^{2-}$	√	√
+3	V^{3+}	$[V^{3+}(pic)_2(HCOO)_2]$	$[V^{3+}\text{-EDTA}]^-$	$[V^{3+}\text{- H}_{-1}\text{cit}]$	√	√
+4	VO^{2+}	$[VO^{2+}(pic)_3]^-$	$[VO^{2+}\text{EDTA}]^{2-}$	$[VO^{2+}\text{-H}_{-1}\text{cit}]^{2-}$	√	√
+5	VO_2^+	$[VO_2^+(pic)_3]^{2-}$	$[VO_2^+\text{EDTA}]^{3-}$	$[VO_2^+\text{-H}_{-1}\text{cit}]^{3-}$	x	√

Here (√) and (x) symbol indicates the removal and non-removal by resin respectively
o.s : oxidation state

Conclusions

The relative complexing ability of chelating agents with V^{2+}(as formate) under deoxygenated condition follows the order can be shown as V(II)-formate < V(II)-citrate < V(II)-picolinate ≡ V(II)-EDTA. Their stability in aqueous medium under deoxygenated condition followed two-stage decay kinetics. The Ion exchange behaviour of the vanadium complexes viz. V(II)-picolinate, V(II)-EDTA and V(II)-citrate and their oxidized species shows that they can be picked up both on anion and cation exchange resin column. The existence of V(III)-picolinate as an anionic species is shown by this study.

Acknowledgement

We wish to thank Dr. N. M. Gupta, Head, Applied Chemistry Division, BARC and Drs. B. S. Sherigara and P. V. Nayak from Kuvempu University for their keen interest and encouragement during this study.

References

1. Swan T, Segal, M G, Williams W J & Pick M E, *EPRI-NP 5522M*, U.S.A, 1987
2. Jonhson Jr A B, Griggs B, Kustas F & Shaw R A, *Water Chemistry of Nuclear Reactor Systems* 2 (BNES, London, U.K), 1980
3. Regazzoni A E & Matijevic E, *Corrosion* 40(5) (1984) 257
4. Segal M G & Sellers R M, *J Chem Soc Faraday Trans* 1, 78 (1982) 1149
5. Manjanna J & Venkateswaran G, *Hydrometallurgy*, 61 (2001) 45.
6. Joseph S, Venkateswaran G & Moorthy P N, *J Nucl Sci Technol*, 36(9) (1999) 798
7. Martell A E & Smith R M, *Critical Stability Tables*, Vol 1-6 (Plenum press, New York), 1975
8. Manjanna J & Venkateswaran G, Sherigara B S & Nayak P V, *Hydrometallurgy*, 60 (2001) 155
9. Manjanna J, Venkateswaran G, Sherigara B S & Nayak P V, *Powerplant Chemistry*, 3(2) (2001) 80
10. Venkateswaran G, Gokhale A S & Moorthy P N, *National Symposium on Electrochemistry in Nuclear Technology*, IGCAR, Kalpakkam, India, 1998

This paper was adjudged as the Best paper presented under Analytical and Environmental Section (AP-23) in XIX Annual Conference of Indian Council of Chemists, held at Kuvempu University, Shimoga (Karnataka) in Dec 2000, and on this occasion Dr J. Manjanna was conferred the 'Young Scientist Award'.

About the authors ...

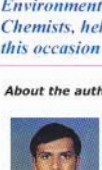

***Dr J. Manjanna**, (M. Sc., Ph.D. - Industrial/ Applied Chemistry, Kuvempu University) was a Jr/ Sr. Research Fellow in Applied Chemistry Division, BARC, under BRNS/DAE Research project (Oct, 1997 to Sept, 2000), which formed part of his Ph.D. work. Currently (from Jan, 2002), he is a Dr. K. S. Krishnan's Research Associate in the same Division. He is a recipient of the 'Young Scientist award' (2000) from the Indian Council of Chemists. His research activities are related to water chemistry of nuclear reactor systems. He is involved in the preparation, characterization and dissolution kinetics of corrosion products (oxides, powders/ scales) in reductive/complexing formulations. Presently, he has some 10 journal publications to his credit.*

***Dr G. Venkateswaran**, (M. Sc. Madras University, Ph.D. Physical chemistry, University of Mumbai) is currently heading the Reactor System Studies Section of Applied Chemistry Division. He joined BARC after graduating in Chemistry from 14th batch of Training School. He has over 30 years of research experience in the field of water chemistry in nuclear reactor systems. His research interests include studies on the chemical decontamination of nuclear reactors, oxide dissolution, metal-ion passivation of reactor system structural surfaces, fuel performance evaluation and ion-exchange behaviour of suspended and dissolved species, etc. Recently (2000) he led the team in successfully carrying out the decontamination of clean-up system of TAPS and now he is preparing for full system decontamination of the same unit. He has over 110 publications to his credit, which include journals, conference/symposia papers, and BARC reports.*

Transport of Metal Ions across a Supported Liquid Membrane (SLM) using Dimethyl Dibutyl Tetradecyl -1, 3-Malonamide (DMDBTDMA) as the Carrier

S.Sriram and V.K. Manchanda
Radiochemistry Division
Bhabha Atomic Research Centre

Abstract

Effect of various strippants on Am transport across a SLM using DMDBTDMA was investigated and a mixture of 0.4M Formic acid, 0.4M Hydrazine hydrate and 0.1M DTPA was found to result in the largest transport rate. The transport rate of various other metal ions studied was U(VI) > Pu(IV) > Am(III) > Eu(III) > Sr(II). Cs(I) showed no transport. High concentration of U in the feed was found to retard the transport of Am.

Introduction

Pentalkyl malonamides are promising as extractants for a host of tri, tetra and hexavalent actinides [1]. Their extraction efficacy, complete incinerability and innocuous nature of radiolytic and chemical degradation products have made this class of extractants promising for the partitioning of actinides from high level waste [2]. Liquid membrane based separation is a technique which deserves special attention because of its great potential for the separation of radionuclides using exotic carriers particularly from dilute waste solutions [3]. The influence of various chemical conditions and diffusion parameters affecting Am transport using DMDBTDMA as carrier has been reported previously by our group [4]. The present investigations deal with the effect of various strippants on the transport rate of Am(III) from 3.0 M nitric acid medium using DMDBTDMA in n-dodecane as the carrier. Transport of various other metal ions viz. Pu(IV), U(VI), Eu(III), Sr(II) and Cs(I) has also been studied. Transport of Am(III) in the presence of macro amounts of U in the feed as well as from lean simulated waste solution was also investigated

Experimental

DMDBTDMA was synthesised and purified in our laboratory by an earlier reported procedure [1]. PP membrane with an average pore size of 0.57 μm and porosity of 75% was used through out the study. Effective membrane area was found to 3.68 cm^2. The supported liquid membane studies were carried out using a pyrex glass cell consisting of two compartments viz. the feed side of 25mL separated by a strip side of 10 mL capacity. Solutions in both compartments were stirred continuously at a stirring rate of 700 r.p.m. Permeability coefficient (P) of metal ion was computed by the following relation: $\ln (C_t/C_o) = -(A/V)P \times t$ where V is the volume of the feed phase (in mL), A is the effective membrane area (in cm^2), C_t and C_o are the concentrations of metal ion in the feed compartment at time 't'(in secs) and at the beginning of the experiment respectively. Metal ion concentration in the various phases determined by radiometric assay was found to be reproducible within ± 5% of the stated values.

Results and Discussion

It has been observed previously that with solvating extractants as carriers, nitric acid is also transported along with the metal ion thereby causing a decrease in the strippant efficiency [5]. Table 1 shows the effect of various strippants on the transport of Am(III). The strippant mixture used in the present studies is a mixture of weak acid

Table 1: Effect of strippant on the transport of Am (III)

(Feed : ^{241}Am in 3.0 M HNO_3 ; Carrier: 0.6 M DMDBTDMA in n-dodecane)

Strippant*	Permeability coefficient of Am (cm/sec) x 10^4
0.1 M DTPA	2.48
0.1 M Citric acid	2.38
0.1 M Oxalic acid	2.17
0.1 M Ascorbic acid	0.60

- In addition to the complexing agent all the strippants contained 0.4M Formic acid and 0.4M Hydrazine hydrate

(formic acid), a weak base (hydrazine hydrate) and a complexing agent. The buffering action of the weak acid and weak base helps in maintaining the acid concentration in the strippant side to the levels at which the complexing agent can strip the metal ions effectively. The initial pH of the stripping mixture was ~8 which was reduced to around ~4 and ~0.5 after a run of 8 and 24 hours respectively.

The stripping mixture involving diethylene triamine pentaacetic acid (DTPA) showed maximum Am permeability which could be attributed to the higher stability constant of the complex formed with Am as compared to other complexing agents. An additional experiment with 0.5M sodium citrate as strippant showed P_{Am} = 1.34 x 10^{-4} cm/sec.

Table 2: Permeability coefficients for different metal ions from 3.0 M nitric acid medium

(Carrier : 0.6 M DMDBTDMA in n-dodecane; Strippant : 0.4 M hydrazine hydrate + 0.4 M Formic acid + 0.1 M DTPA)

Metal ions	Permeability coefficient (cm/sec) x 10^5
U(VI)	1.90
Pu(IV)	1.45
Am(III)	2.48 x 10^{-1}
Eu(III)	1.23 x 10^{-1}
Sr(II)	0.6 x 10^{-2}

Table 2 shows that under similar experimental conditions, the permeability coefficient varied in the order U(VI) > Pu(IV) > Am(III) > Eu(III) > Sr(II). Cs(I) showed no transport during the entire period of the experiment (8 hours). The lower transport of Pu as compared to U appears to be due to its poorer stripping in view of the slow reduction of Pu(IV) to Pu(III) as reported earlier [6].

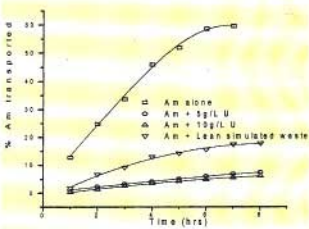

Fig.1 : Transport of Am from 3.0 M nitric acid in the presence of uranium and lean simulated waste solution. Carrier concentration : 0.6 MDMDBTDMA in n-dodecane Strippant : 0.4 M hydrazine hydrate + 0.4 M formic acid + 0.1 M DTPA

Since high level waste (HLW) solutions invariably have a large uranium content, transport of ^{241}Am was studied from 3.0 M nitric acid solution in the presence of uranium (Fig.1). It is seen from the figure that the transport of americium slows down in the presence of uranium due to the co-transport of latter ion. To enhance the transport rate of americium using the liquid membrane technique, it is therefore necessary to separate uranium from the HLW. This could be achieved by equilibrating the simulated HLW thrice with fresh 30% TBP. Transport of Am was carried out with lean simulted HLW (concentration of

U ~ 10ppm) and a maximum transport of ~ 18 % was achieved in 8 hours. It is desirable to explore the strippants with larger buffering capacity which ensure relatively higher equilibrium pH on strippant side.

References

1. G.R.Mahajan, D.R.Prabhu, K.Manchanda and L.P.Badekha, *Waste Management*, **18**, 125 (1998).
2. C.Cuilledier, C.Musikas, P.Hoel, L.Nigond and X.Vitart, *Sep. Sci. Technol.* **26(9)**, 1229 (1991).
3. P.R.Danesi, R.Chiarizia, P.Rickert, and E.P.Horwitz, *Solv.Ext. Ion.Exch.* **3**, 111 (1985).
4. S.Sriram, P.K.Mohapatra, A.K.Pandey, V.K.Manchanda and L.P.Badekha, *J.Memb.Sci.* **177**, 163 (2000)
5. P.R.Danesi, C.Cianetti and E.P.Horwitz, *Solv.Ext. Ion Exch.* **1(2)**, 299 (1983).
6. A.Ramanujam, P.S.Dhami, V.Gopalakrishnan, N.L.Dudwadkar, R.R.Chitnis and J.N.Mathur, *Sep. Sci. and Technol.* **34(8)**, 1717 (1999).

This paper won the Best Paper award at NUCAR-2001 held at University of Pune, Pune

About the authors ...

Dr S. Sriram *obtained his M.Sc. (Analytical Chemistry) from University of Mumbai in 1996 and joined Radiochemistry Division, BARC, as a Ph.D. student. He was awarded the Ph.D. degree in 2001 for his thesis entitled, "Separation Chemistry of Actinides and Fission Products". Dr Sriram won many prizes for his presented papers at National Conferences / Symposia. He was selected for the DAE Krishnan Fellowship for Post-Doctoral studies at BARC. Presently, he is a Post-Doctoral Research Fellow at the McMaster University, Hamilton, Canada. His research areas of interest include separation chemistry particularly with membranes. Dr. Sriram has more than 25 papers to his credit.*

Dr V. K. Manchanda *joined the Radiochemistry Division, BARC, in 1969 after graduating from Delhi University and from the 12th batch of the BARC Training School. He was awarded Ph.D. by Mumbai University in 1975 and carried out Post-Doctoral work at UTEP, Texas, U.S.A. as Fulbright Scholar (1985-87). His research interests include thermodynamics and kinetics of complexes of macrocyclic ligands with lanthanides and actinides, physico-chemical studies on actinide complexes, design and synthesis of novel extractants for actinides and chemical quality control of Pu based fuels. A research Guide in Chemistry for M.Sc. and Ph.D. recognized by University of Mumbai, Dr Manchanda currently heads the Actinide Chemistry Section, Radiochemistry Division. Dr Manchanda has over 250 publications to his credit.*

Remotely Operated Non-Destructive Surface Sampling Techniques for Assessment of Residual Service Life

Kundan Kumar and B.B. Rupani
Reactor Engineering Division
Bhabha Atomic Research Centre

Introduction

Surface Sampling Techniques remove the samples from a parent material or component either by cutting, sectioning, trepanning, scraping or scratching etc. These samples can be subjected to destructive or non-destructive examinations for determination of the physical or chemical properties of the component. A non-destructive method of extraction of such samples from an operating component is quite useful. A very small portion of material sample is removed from a component such that the integrity of the component is not affected and the component is still useful for further service. If such non-destructive surface sampling technique is extended to be used for obtaining *in situ* samples remotely from an operating component, which is directly inaccessible, it will be very useful for assessment of residual service life of the component. Reactor Engineering Division, BARC has developed some such non-destructive, remotely operated, *in situ*, surface sampling techniques, e.g. as Sliver Sample Scraping Technique, Boat Sampling Technique and Cast Impression Technique. The paper highlights briefly the description of the techniques, type of samples and the use of the samples for generation of useful data for determination of health status of any operating component.

Sliver Sample Scraping Technique

A remotely operable Sliver Sample Scraping Tool, shown in Fig. 1, has been developed

Fig. 1: Sliver Sample Scraping Tool

for taking sliver samples from the bore of a tube. This technique is useful for obtaining statistically significant number of samples without damaging the integrity of the tube, *in situ*, i.e. without removing it from the service. The sample of thickness about 100 microns is obtained by this technique, as shown in Fig. 2. The sampling is done in two tandem steps, with the help of two tool bits, one followed by another, Front tool-bit removes the outer surface of the bore of the tube, which may contain oxide layer or foreign particles, while rear tool-bit obtains actual metal sample from the underneath, by following the same path.

Fig. 2 : Typical silver samples

This technique ensures that the tube (parent material) is reusable after scraping operation and the operation does not lead to loss of integrity and reduction in its residual service life. The scraped region on tube, Fig. 3, does not lead to an ultrasonic indication, which can be interpreted as flaw, i.e. the contour of the scraped region merges smoothly with internal profile of the tube. Tool bits follow the profile of the bore of the tube, in order to

eliminate the effect of dimensional deviations and geometrical tolerances of the tube such as ovality, change in diameter due to radial creep, straightness and variation in wall thickness etc.

Fig.3: Multiple scraped locations inside a tube

The dimension and weight of the sample is dependent on the requirement of analysis purpose and available margin in the parent material. Determining factor of the dimension of the sample is such that it should be sufficient for carrying out required destructive as well as non-destructive examination of the samples and it is free from unwanted contamination.

The sliver sample can be analysed for the following purposes:

- Chemical composition
- Qualitative material strength, based on cutting force
- Surface condition based on oxide layer thickness
- Ductility based on coiling and number of pieces in one sliver operation

Boat Sampling Technique

Boat Sampling Technique (BST) has been developed for obtaining thick metal samples remotely from the surface of an operating component, *in situ*. By this technique a sample (1mm to 3mm thick, adjustable) is obtained without plastic deformation or thermal degradation of the base material of the components for metallurgical analysis. The shape and size of the metal sample depends upon the shape of the cutter and the surface geometry of the base material.

Boat Sampling technique is remotely operable, non-destructive surface sampling technique, which does not lead to loss of integrity and reduction in residual service life of the operating component. The contour of the scooped region merges smoothly with the surface profile of the base material. so that the contour should not lead to an ultrasonic indication which can be interpreted as flaw.

Fig. 4 : Boat Sampling Module

The dimension and volume of the boat sample is determined by analysis requirements, such that it should be sufficient for carrying out required destructive as well as non-destructive examination of the samples. The technique incorporates a Sampling Module, Fig. 4, which consists of a cutter, feeding system,

driving system, depth control mechanisms. The cutter feed rate and cutter feed position are operated through a Control Unit.

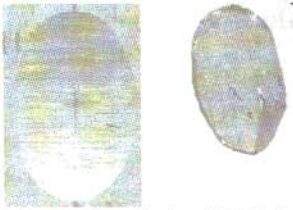

Fig. 5: Contour of scooped region and a Boat Sample

A sample, Fig. 5, removed from a flat surface is elliptical in plan view and of boat shaped in front view. The depth of the depression left in the base material is equivalent to the sample thickness plus the kerf width. Kerf width would depend upon the thickness of cutter and operating asymmetries. A typical sample is removed in about one to two hours.

The sample would remain in the cutter shell or in the housing of the sampling module. The sample has to be picked up remotely. During Sampling operation, along with the boat sample, fine mesh type of powder is generated due to grinding action. The boat samples are collected by gravitation mode, while the metal dust is partially collected into system and partially into cutter shell.

Non-destructive extraction of samples can be used for direct evaluation of material condition, as follows:

- Chemical Composition,
- Collection and analysis of surface deposits
- Fracture Toughness and Mechanical properties by Small Punch Test technique
- Microhardness evaluation
- Physical characteristics, such as crack, scratch, wall thinning etc,
- Other degrading mechanisms :
  - Corrosion
  - hydrogen damage,
  - thermal ageing
- Metallurgical evaluation of samples for determination of the following:
  - Microstructure
  - Etch test for detecting presence of sensitisation
  - Electrochemical Potentiokinetic Reactivation (EPR) technique to estimate extent of sensitisation
  - Texture and grain size

Cast Impression Technique

A technique has been developed for remotely obtaining a replica of the profile from an operating component. A device, Figure 6,

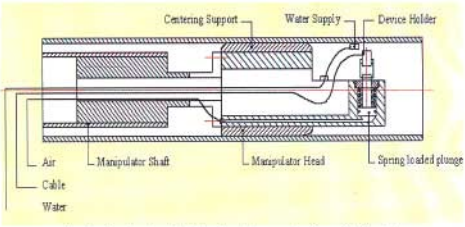

Fig. 6 : Device for obtaining Cast Impression from ID of a tube

has been developed for operating remotely for obtaining cast impression from inner diameter of any operating component, *in situ*. However, replica can be taken directly for accessible component. The replica is analysed for study the profilometry, which can give information regarding the following:

- Surface condition
- Surface finish
- Depth
- Profile of surface
- Existence of any notch or Crack
- Local wall thinning
- Corrosion defects
- Scratch mark

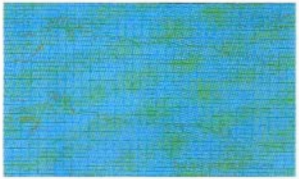

Fig. 7 : Typical magnified profiles of scraped regions on inside diameter, obtained by manual cast impression technique. This gives depth of scraped region and pattern of smoothness.

Conclusion

The Sliver Sample Scraping Technique, Boat Sampling Technique and Cast Impression Technique are usable as remotely operated surface sampling techniques for determination of residual service life of an operating component without affecting the integrity of the component.

The present version of SSST is being used for obtaining samples from a pressure tube of 83mm bore at various Pressurised Heavy Water Reactors (PHWR), in India, however, the technique can be extended for taking samples from any size of tube as per the requirement and available margin, by slightly modifying the design of the gripping systems and sample collection devices.

The BST has been developed for taking larger samples upto 4 grams for metallurgical evaluation purpose, however, the technique can be extended for getting even larger samples, if required. The current version of BST is proposed to be utilised for taking samples from core shroud of Boiling Water Reactor in near future.

The cast impression technique is being regularly used as dimensional inspection of rolled joint grooves and other similar applications for profilometry studies.

This paper was adjudged as the Best Paper at the seminar on "Role of NDE in Residual Life Assessment & Plant Life Extension", held at Lonavala during December 7-9, 2001 and organised by Indian Society of NDT(ISNT), Mumbai.

About the authors ....

Mr Kundan Kumar *is actively working on design and development of various techniques required for residual life assessment and life extension of Coolant Channels of Indian Pressurised Heavy Water Reactors and Core Shroud of Tarapur Atomic Power Station.*

Mr B.B. Rupani *has taken a leading role in the design and development of various innovative tools, systems and techniques required for in service inspection, repair, life-extension and replacement of coolant channels of Indian Pressurised Heavy Water Reactors.*

Simulation of Pressurised Heavy Water Reactor Data Using Artificial Neural Network for Reactor Status / Transient Identification

P.V. Varde and R. Chowdhury
Reactor Operations Division
Bhabha Atomic Research Centre

and

Gopika Vinod, A.K. Babar and H.S. Kushwaha
Reactor Safety Division
Bhabha Atomic Research Centre

Abstract

This paper presents the work carried out on the development of a prototype ANN model for safety status monitoring for Pressurised Heavy Water Reactor. ANN has been trained for 13 plant conditions. Presented here is the highlights of the basic approach adopted for the development and training of ANN. Simulation studies were carried out by performing series of recall tests using near real-time conditions. Recall tests results show that the system was able to identify the plant state with reasonable accuracy.

Introduction

When a transient / disturbance occurs in a plant, sensor outputs or instrument readings deviate from those during a steady state and constitute a different symptom pattern which represents the identification code for a particular reactor condition. The fact that each reactor condition has an unique symptom pattern, provides a basis for identifying plant status monitoring.

Using above characteristic of the transients a Prototype Artificial Neural Network (ANN) has been developed for reactor safety status monitoring for a Pressurised Heavy Water Reactor. Accordingly, relevant data pertaining to Madras Atomic Power Station (MAPS) were collected and compiled for ANN training & simulation.

This paper describes, in brief, the simulation work carried out on MAPS data using ANN and presents the results of this simulation. Also, based on the experience gained during this simulation, this work identifies the added features desired / expected from the General Purpose Neural Network being developed in collaboration with Indian Institute of Technology, Kanpur.

ANN Model

The ANN model has been formulated for reactor status monitoring using the characteristics of reactor transients as mentioned above. For this study the model has been implemented using a feedforward multi layer neural network with an input layer, an output layer and one hidden layer. The input nodes which receives the input from the plant are connected through the hidden layer nodes to the output which finally gives the ANN output. As shown in Fig. 1, the implemented model consists of 29 nodes in the input layer (which include digital as well as normalized analog signals), 28 nodes in hidden layer and 13 nodes for identifying plant conditions in the out put layers.

Preparation Of Training Patterns

ANN was configured keeping in view the type and number of input data sets available for MAPS, the characteristics of the problem and

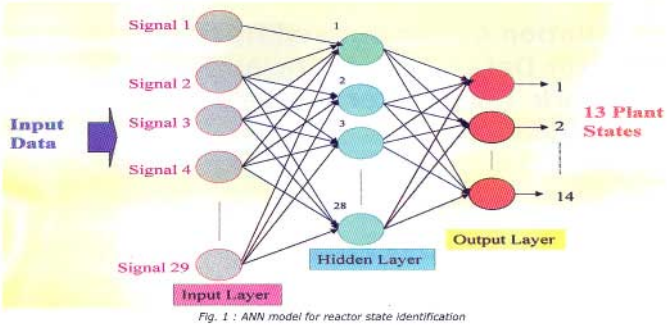

Fig. 1 : ANN model for reactor state identification

Table 1: MAPS input data used for ANN simulation

S. No.	Parameter Description	Instrument Range	Unit
1.	PHT Storage Tank Level	0 to 170	cm
2.	PHT Pressure	0 to 120	Kg/cm^2
3.	North FM Vault Pressure	-0.5 to 10	gm/cm^2
4.	North FM Vault Temperature	0 to 70	$^\circ$C
5.	Boiler Room Pressure	-25 to 25	gm/cm^2
6.	Boiler Room Temperature	0 to 100	$^\circ$C
7.	Calandria Vault Level	0 to 500	mm
8.	Calandria Level	0 to 100	%
9.	Calandria Vault Pressure	0 to 350	gm/cm^2
10.	Boiler 1 Level	0 to 125	cm
11.	Boiler 2 Level	0 to 125	cm
12.	Boiler 3 Level	0 to 125	cm
13.	Boiler 4 Level	0 to 125	cm
14.	Boiler 5 Level	0 to 125	cm
15.	Boiler 6 Level	0 to 125	cm
16.	Boiler 7 Level	0 to 125	cm
17.	Boiler 8 Level	0 to 125	cm
18.	North FM Vault Activity	1 to 100	R/hr
19.	South FM Vault Activity	0 to 100	R/hr
20.	South FM Vault Pressure	-0.5 to 10	Kg/cm^2
21.	South FM Vault Temperature	0 to 70	$^\circ$C
22.	Steam Activity (No on-line measurement)	0 to 0.5	
23.	Dump Tank Pressure	1 to 2	Kg/cm^2
24.	Dump Sump Level	0 to 160	mm
25.	Moderator Sump Level	0 to 75	cm
26.	North Delayed Neutron Room Temperature	0 to 100	$^\circ$C
27.	South Delayed Neutron Room Temperature	0 to 100	$^\circ$C
28.	PHT Temperature	0 to 320	$^\circ$C
29.	Process Water Activity	0 to 4096	Digital

North Boiler Level = Average of level of Boilers 1,2,3 & 4
South Boiler Level = Average of levels of Boilers 5,6,7 & 8

Table 2: MAPS data - Input template for ANN training and simulation

Para Vector	1	2	3	4	5	6	7	8	9	10	11	12	13	14
1.	.705	.725	.01	.743	.36	.55	0	.9859	0	.52	.52	.52	.52	.52
2.	0	0	.047	0	.5	0	0	0	0	0	0	0	0	0
3.	.56	.285	.74	.922	.36	.7	0	0.98	0	.52	.52	.52	.52	.52
4.	.56	.33	.01	.74	.36	.7	.328	.986	.427	.52	.52	.52	.52	.52
5.	.6117	.6825	.665	.9224	.6338	.7	0	.9859	0	.52	0.52	.52	.52	.52
6.	.6117	.7156	.0104	.743	.36	.55	0	.9859	0	.52	.52	.52	.52	.52
7.	6455	.67375	.0104	.7428	.5074	.7686	0	.9859	0	.29912	.299	.299	.299	.52
8.	.6455	.67375	.0104	.742	.36	.55	0	.9859	0	.29912	.299	.299	.299	.299
9.	.70589	.725	.1047	.7428	.36	.55	0	.9859	0	.52	.52	.52	.52	.52
10.	.6411	.667	.0104	.7428	.54	.55	0	.9859	0	.52	.52	.52	.52	.52
11.	.6117	.594	.01047	.7428	.36	.55	0	.9859	0	.52	.52	.52	.52	.52
12.	.6117	.5933	.0104	.7428	.36	.55	0	.9859	0	.52	.52	.52	.52	.52
13.	.5294	.625	.0104	.7428	.36	.55	0	.9859	0	.576	.312	.312	.312	.36

Para Vector	15	16	17	18	19	20	21	22	23	24	25	26	27	28	29
1.	.52	.52	.52	0	.001	0	.7428	.002	.68	1	0	.25	.25	.89	0
2.	0	0	0	0	0	0.0470	0	0	0	0	0	00	0	0	0
3.	.52	.52	.52	0	.01	0	.002	.002	.68	1	0	.25	.25	.89	1
4.	.52	.52	.52	0	.01	0	.002	.002	.68	1	0	.25	.25	.89	4
5.	.52	.52	.52	0	.01	0	.002	.002	.68	1	0	.25	.25	.89	0
6.	.52	.52	.52	0	.01	0	.002	.002	.68	1	0	.25	.25	.89	0
7.	.52	.52	.52	0	.01	0	.002	.002	.68	1	0	.25	.25	.89	4096
8.	.299	.299	.299	0	.01	0	.002	.002	.68	1	0	.25	.25	.89	0
9.	.52	.52	.52	0	.01	0	.002	.002	.68	.0456	.0285	.25	.25	.89	128
10.	.52	.52	.52	0	.01	0	.002	.002	.68	1	0	.25	.25	.89	2
11.	.52	.52	.52	0	.105	.6828	.002	.002	.68	1	0	.25	.25	.89	256
12.	.52	.52	.52	0	.001	0	.002	.002	.68		0	.7008	.25	.89	32
13.	.36	.36	.36	0	.01	0	.002	.002	.68	1	0	.25	.25	.89	4096

Table 3: Reactor status identification code

1	Normal	1.0 0.0 0.0 0.0 0.0 0.0 0.0 0.0 0.0 0.0 0.0 0.0 0.0 0.0
2	Not Critical	0.0 1.0 0.0 0.0 0.0 0.0 0.0 0.0 0.0 0.0 0.0 0.0 0.0 0.0
3	Medium LOCA	0.0 0.0 1.0 0.0 0.0 0.0 0.0 0.0 0.0 0.0 0.0 0.0 0.0 0.0
4	Single Pr. Tube Fail	0.0 0.0 0.0 1.0 0.0 0.0 0.0 0.0 0.0 0.0 0.0 0.0 0.0 0.0
5	Break in FMV	0.0 0.0 0.0 0.0 1.0 0.0 0.0 0.0 0.0 0.0 0.0 0.0 0.0 0.0
6	Heavy Water Leak	0.0 0.0 0.0 0.0 0.0 1.0 0.0 0.0 0.0 0.0 0.0 0.0 0.0 0.0
7	Steam line brk inside Cont.	0.0 0.0 0.0 0.0 0.0 0.0 1.0 0.0 0.0 0.0 0.0 0.0 0.0 0.0
8	SDV Stuck Open	0.0 0.0 0.0 0.0 0.0 0.0 0.0 1.0 0.0 0.0 0.0 0.0 0.0 0.0
9	Leak in Moderator Room	0.0 0.0 0.0 0.0 0.0 0.0 0.0 0.0 1.0 0.0 0.0 0.0 0.0 0.0
10	Break in Boiler Room	0.0 0.0 0.0 0.0 0.0 0.0 0.0 0.0 0.0 1.0 0.0 0.0 0.0 0.0
11	End Fitting Failure	0.0 0.0 0.0 0.0 0.0 0.0 0.0 0.0 0.0 0.0 1.0 0.0 0.0 0.0
12	Leak in North Delayed Nt Rm	0.0 0.0 0.0 0.0 0.0 0.0 0.0 0.0 0.0 0.0 0.0 1.0 0.0 0.0
13	Steam Gen Tube Rupture	0.0 0.0 0.0 0.0 0.0 0.0 0.0 0.0 0.0 0.0 0.0 0.0 1.0 0.0

the results expected from this simulation. All the 29 input parameters as shown in Table 1 are analog parameters normalized between 0 to 1. The '0' value corresponds to the '0' of the analog scale and '1' corresponds to the full-scale value on the instrument. For example, for the parameter no. 1, 'PHT Storage Tank Level' the instrument scale shows Min. Value as 0 cm and Max. value as 170 cm. On the normalised scale the '0' cm corresponds to normalized '0' and 170 cm corresponds to normalized 1.0. Using these

normalised values 13 input vectors were formed as shown in Table 2. The number of nodes in the input training pattern were kept as 42, 29 nodes for the given input parameters and remaining 13 nodes as spare nodes for future expansion of the input layer. These 13 spare nodes were assigned a value of '0'.

To begin with it was decided that the ANN training will be carried out based on the available 13 sets of data. Accordingly, for each of the 13 given conditions of the reactor a reactor status identification matrix of 13 X 13 was formed as shown in Table 3.

ANN Training Procedure

The most successful learning algorithm devised for feedforward architecture is known as the back propagation network (BPN) algorithm [1]. The BPN learning algorithm seeks to find weights such that given an input pattern from the training set of pairs of input / output patterns, the neural network will produce the corresponding output of the training set [2]. When supplied with previously 'unseen' input, the ANN tries to generalise the characteristics and produces the output close to the nearest match. The networks response is based on its ability to learn through the learning algorithm. The fundamental relationship between the input and output pairs form the training set(s). The BPN algorithm attempts to minimise the overall root mean square (rms) error between the desired and actual output values for all the output nodes over all the input patterns by iteratively adjusting the weights.

ANN Training & Simulation

Convergence of a BPN algorithm to a large extent influenced by the selection of training coefficient η, momentum coefficient α, and number of nodes in the hidden layer [3]. The training was carried out in batch modes by carrying out parametric studies, i.e. by varying the value of one parameter while keeping other two constant. The learning rate η, momentum coefficient α, and number of nodes in the hidden layer were varied one by one such that a particular combination of η, α and number of nodes in the hidden layer allows the efficient convergence of the rms error to a given criteria of rms error of < 0.001. For this training the convergence was achieved using $\eta = 0.5$ and $\alpha = 0.2$ with 28 nodes in the hidden layer. Given below is the final configuration of the ANN:

Table 4: Final ANN configuration for MAPS data simulation

Number of Layers	3
Number of hidden layer	1
Number of nodes in the input layer	29
Number of nodes in the hidden layer	28
Number of nodes in the Output layer	14
Optimum value of learning rate, η	0.5
Optimum value of Momentum Coefficient, α	0.2
Maximum average error	0.001
Maximum individual error	0.0001
Number of iterations for convergence	1,13,400
CPU Time required for training the ANN	5.2 hrs

Simulation of MAPS data - recall test with complete data set (File name: mapsm1.inp)

```
nn

Enter Training Rate [Default=0.800000]: 0.5
Enter Momentum Coefficient
[Default=0.700000]: 0.2
Specify data file :mapsm1.inp
File contains 55 columns.
No. of parameters : 42
No. of input vectors : 13
No. of neurons in hidden layer? [Default=28]
Return
Read weights from file "mapsm1.wht" (y/n)?
y ( 'n' for new training)
Continue in debug mode? (y/n)n
Train_network function called
Train Further ? (y/n)n
Open input file (y/n)?y
Input File name ?mapsm1.inp
Open output file (y/n)?y
Output File name ?mapsm1.out
```

Note: The underlined text is an input from the computer terminal

Fig 2: A session with ANN simulation

Figure 2 shows the final session with the ANN for training and subsequent recall test performed on the network. As can be seen above, the convergence of rms error to a value of 0.001305 took ~ 5.2 hrs. This simulation work was carried out on *Land Mark III* computer in Unix environment at Computer Division of BARC.

Table 5 : Results of first recall test with complete data set for 13 conditions

Reactor State -1 : Normal
Recall Vector : 0.994567 0.000079 0.000000 0.000161 0.001693 0.005577 0.000003 0.001505 0.000878 0.001541 0.000054 0.000614 0.000000 0.000000
Transient 1 identified with 0.002225 rms error

Reactor State -2 : Not Critical
Recall Vector : 0.000000 0.997928 0.000004 0.000001 0.000970 0.000578 0.000000 0.001053 0.000150 0.000000 0.001268 0.000000 0.000000 0.001096
Transient 2 identified with 0.000824 rms error

Reactor State -3: Medium LOCA
Recall Vector : 0.000000 0.000073 0.997372 0.001319 0.001853 0.000000 0.000557 0.000000 0.001036 0.000214 0.000399 0.000977 0.000000 0.001349
Transient 3 identified with 0.001084 rms error

Reactor State 4: Single Pressure Tube Failure
Recall Vector : 0.000000 0.000006 0.000956 0.997460 0.000000 0.000210 0.000369 0.000000 0.000085 0.001215 0.000342 0.001336 0.000099 0.001156
Transient 4 identified with 0.000936 rms error

Reactor State 5 : Break in Fuelling Machine Vault
Recall Vector : 0.000067 0.001197 0.001455 0.000151 0.997133 0.000773 0.000491 0.000655 0.000117 0.000025 0.000000 0.000006 0.000000 0.000002
Transient 5 identified with 0.000967 rms error

Reactor State 6: Heavy Water Leak
Recall Vector : 0.004913 0.000184 0.000000 0.000727 0.001310 0.994169 0.000000 0.001585 0.000041 0.000044 0.000084 0.000308 0.000000 0.000000
Transient 6 identified with 0.002122 rms error

Reactor State 7 : Steam Line Break Inside Containment
Recall Vector : 0.000014 0.000021 0.000037 0.000268 0.000020 0.000000 0.996984 0.001405 0.000420 0.001676 0.000003 0.000069 0.001498 0.000004
Transient 7 identified with 0.001082 rms error

Reactor State 8: SDV Stuck Open
Recall Vector : 0.001556 0.001081 0.000000 0.000002 0.000335 0.000004 0.001535 0.997246 0.000004 0.000000 0.000001 0.000019 0.001223 0.000001
Transient 8 identified with 0.001040 rms error

Reactor State 9: Leak in Moderator Room
Recall Vector : 0.001045 0.000411 0.001084 0.000060 0.000003 0.000000 0.000304 0.000000 0.997812 0.000638 0.000447 0.000453 0.000020 0.000000
Transient 9 identified with 0.000762 rms error

Reactor State 10: Break in Boiler Room
Recall Vector : 0.001535 0.000004 0.000370 0.001619 0.000002 0.000000 0.002005 0.000000 0.001651 0.996774 0.001498 0.001252 0.001731 0.000000
Transient 10 identified with 0.001441 rms error

Reactor State 11: End Fitting Failure
Recall Vector : 0.000000 0.001607 0.000681 0.000119 0.000000 0.000066 0.000000 0.000000 0.000759 0.001201 0.997436 0.001179 0.001078 0.000199
Transient 11 identified with 0.001009 rms error

Reactor State 12: Leak in North Delayed Neutron Room
Recall Vector : 0.000000 0.000000 0.000819 0.000884 0.000000 0.000001 0.000020 0.000000 0.000691 0.001501 0.001427 0.997314 0.000816 0.000087
Transient 12 identified with 0.001004 rms error

Reactor State 13: Steam Generator Tube Rupture
Recall Vector : 0.000000 0.000020 0.000001 0.000502 0.000000 0.000000 0.001660 0.001037 0.000024 0.000351 0.000863 0.000924 0.996788 0.001834
Transient 13 identified with 0.001180 rms error

Recall Tests on ANN

Having completed training of the ANN successfully, the next stage was to perform the recall tests on the network. The recall tests are carried out by presenting the trained as well as 'unseen' or 'new patterns' to the network. The network response is seen as to whether it is capable of giving the intended results. ANN is capable of training itself, if presented with an altogether new pattern. Since for this simulation only 13 patterns were available the recall tests were carried out on these 13 plant conditions. Table 5 presents the results of the recall tests performed on the network. It can be seen that ANN was able to identify all the 13 conditions successfully and the rms error was max. 0.002225 for Reactor State no. 1 and min. of 0.000824 for Reactor State no. 2. It is pertinent that further testing of ANN should be carried out using new or unseen patterns. It will be worthwhile here to mention that Dhruva simulation was carried out using many unseen patterns, including the patterns with 20 % error, two unlearned patterns, pattern with sensor failure data, patterns with fuzzy data, etc, and the ANN was tested capable and performed as intended [4]. For MAPS data simulation more data will be obtained so that Neural Network can be made more robust.

The Features Expected from General Purpose Neural Network

Based on the experience gained during above simulation work and keeping in view the limitations of ANN, specifications have been prepared towards incorporating some features in the General Purpose Neural Network which are specific to this types of problem. For instance, the above simulation was carried out in off-line mode with well-defined patterns fed to the ANN for corresponding reactor conditions. Nevertheless, this type of tool will be more effective if the training is carried out by simulating, if not in real-time, at least in near real-time conditions. Keeping in view above observations it is desired that the General Purpose Neural Network, along with the earlier specified features, should offer following added features:

i) Provision of 'leaf-nodes' for processing 2-out-of-3 trip and alarm conditions.
ii) Flexibility for varying number of nodes at input as well as at the output layer.
iii) The network is expected to process digital as well as analog inputs. Keeping in view the characteristics of these two types of inputs, provision should exist for processing above two types of inputs at the input nodes of the network including automatic normalization of the input values.
iv) User friendly interface for connecting corresponding input signals to the identified nodes in the ANN.
v) Facility for varying the 'scanning' and 'sampling' time of the plant's inputs.
vi) User friendly output window for presenting the results of the network. This includes keeping2 provision for displaying the advise generated by the network specific to a given reactor condition.
vii) Provision for transferring the control from network to a rule based expert system so that after the network identifies the reactor state, detailed plant diagnostics can be performed even at sub-system and component level.

Finally, the overall structure of the network should be such that it can cater to the on-line data analysis requirements also. It will be worthwhile to mention here that some of the above requirements, viz, item nos. i, ii and v in the above list, are already implemented on general purpose neural network and work on implementation of remaining requirements is in progress.

References

1. Rich E., Knight,K., "Artificial Intelligence", Tata-Mcgraw-Hill, New Delhi (1992).
2. Uhrig, R.E., *Potential Application of Neural Networks to the operation of Nuclear Power Plants,* Nuclear Safety, **32**, 68 (1992).
3. Ragheb, M. and Campas, T., *Nuclear Power Plants Transients Patterns*

Recognition Using a Neural Network Methodology, Trans America Nuclear Society, **62**, 129 (1990).

4. Varde, P.V., *An Integrated Approach for Research Reactor Operations and Fault Diagnosis Through Connectionist Framework and PSA Based Knowledge Based System*, Ph.D. Thesis, Indian Institute Of Technology, Bombay, 1996.

This paper has been adjudged as one of the Best papers in the technical sessions of International Conference on Quality, Reliability and Control (ICQRC-2001) held at Mumbai during December 26-28, 2001

About the authors ...

Dr P.V. Varde : *After graduating as Mechanical Engineer, Dr Varde joined Reactor Group, BARC in 1983 (27th batch of Training School). He was associated with the operations of Dhruva reactor as Shift Engineer from 1985 to 1995. In 1996, he completed his Ph.D. in the area of "Research Reactor Operational Safety & Reliability" from the Dept. of Reliability Engineering, Indian Institute of Technology, Bombay. At present, he is involved in carrying out Probabilistic Safety Assessment of Research Reactors at BARC. He has carried out extensive research and developmental work in the area of application of Artificial Intelligence tools, like Artificial Neural Network and Knowledge Based Systems for the development of PSA based operator support systems for nuclear plant operations and fault diagnosis. He has also served as M.Tech. and Ph.D. thesis examiner at IIT, Bombay, and referee for Int. Journal of Reliability Engineering and System Safety. Based on his research and development work, he has published a number of papers at national and international levels.*

Mr R. Chowdhury : *Mr R. Chowdhury joined Cirus reactor operations in the year 1968 and worked as Senior Operations Engineer and later as ROD Engineer till 1981. Thereafter, he was associated with the electrical systems design group of Dhruva reactor. From 1984, he was involved in the commissioning of Dhruva as Assistant Reactor Superintendent. He was later Reactor Superintendent for Dhruva for about eight years. He is presently the Head of the Reactor Operations Division and is responsible for the three research reactors at Trombay. He is also associated with safety review of a number of other plants in various capacities including that of Chairman, Kaiga Atomic Power Units 1 & 2 and Rajasthan Units 3 & 4, Safety Committee appointed by Atomic Energy Regulatory Board.*

Ms Gopika Vinod : *Ms Gopika Vinod joined BARC from 37th batch of Training School. She has been actively involved in Risk Analysis of Nuclear Power Plants and Research Reactors. She has worked in areas like Risk Informed In-Service Inspection, Reliability Database development, Probabilistic Fire Risk Analysis, Reliability based Operator Support Systems for Indian Nuclear Power Plants.*

Mr A. K. Babar *: Mr A. K. Babar joined BARC from 10th batch of Training School. He has been involved in various disciplines of reliability engineering and reactor safety studies for more than 25 years and is currently engaged in conducting PSA studies of PHWRs, Research Reactors and PFBR. He has contributed significantly as Group Leader of the team towards PSA study of NAPP and Kaiga Generating station. He is presently the Head of Probabilistic Safety Assessment of Reactor Safety Division.*

Mr H. S. Kushwaha *: Mr H.S. Kushwaha joined BARC from 14th batch of Training School. He played a key role in the in-house development of finite element codes in the area of structural mechanics, heat transfer and fluid mechanics. He has done M.Tech in Mechanical Engineering from IIT, Kanpur, in 1978. He has participated in a number of International round robin exercises in the field of fatigue, fracture mechanics, nonlinear analysis of steel and concrete containment and seismic analysis of reinforced concrete. He has also been associated with failure analysis, life estimation and extension studies, Leak-Before-Break studies, seismic reassessment of existing nuclear power plants and structural reliability of pressure vessel and piping components. He is presently the Head of Reactor Safety Division.*

Removal of Ru along with Cs & Sr from the Low Level Radioactive Liquid Waste of Reprocessing Plant by Chemical Treatment Method

S.G. Kore, Vinod Prasad, U.S.Singh, R.G.Yeotikar, Ajai Mishra and S.S. Ali
Waste Management Facilities
BARC complex, Tarapur

Abstract

Low level radioactive waste (LLW) having Cs & Sr activity is decontaminated by chemical co-precipitation method at LWTP Tarapur. Chemicals like copper sulphate, potassium ferrocyanide, ferric nitrate, barium chloride and sodium sulphate are being used for above work. However, this method does not offer any decontamination for ruthenium due to its complex nature. For removal of ruthenium, separate treatment schematic is required which should take care of other fission products like Cs & Sr also. A combined chemical treatment method has been evolved for removal of ruthenium along with Cs & Sr. This method offers advantages of single step due to its combined nature, better decontamination factor (DF) for all the radionuclides, reduction in sludge volume, reduction of man rem exposure etc. This method has been successfully adopted on the plant scale at LWTP, Tarapur.

Introduction

Existing low level liquid waste treatment plant, Tarapur (LWTP) is decontaminating the low level radioactive liquid waste (LLW) having Cs and Sr activity which was generated during spent fuel reprocessing. Intermediate Level Waste (ILW) is also generated at the reprocessing plant. The treatment process for ILW, adopts decontamination with respect to α (alpha) by hydroxide precipitation of actinides and use of resorcinol formaldehyde (RF) resin for decontamination with respect to $\beta\gamma$ (Beta, Gamma) activity at Waste Immobilisation Plant (WIP), Tarapur. Treatment of ILW by above methods offers very good decontamination factor (DF) for radio nuclides like $Cs^{134+137}$, Sr^{90} and actinides(1). This method does not offer any DF for ruthenium due to its complex multiple valency nature. The effluent generated after ion exchange treatment at WIP is LLW. The LLW is transferred to LWTP for further processing before discharge to the environment. This waste contains mainly $Cs^{134+137}$ & Sr^{90} apart from Ru^{106}.

At LWTP, LLW is decontaminated by chemical co-precipitation method using $CuSO_4$, $K_4Fe(CN)_6$, $BaCl_2$, Na_2SO_4 and Fe $(NO_3)_3$ at pH 8-8.5. Apart from Cs & Sr, the above LLW coming from WIP contains Ru. Efforts have been made to formulate and evaluate the chemical co-precipitation technique for treatment of such type of waste and adaptation of this technique on the plant scale. The treatment for Ru should be carried out at low pH 2-2.5, in presence of reducing agent such as sodium sulphite. Chemicals like $FeSO_4$, $CuSO_4$, $K_4Fe(CN)_6$, $BaCl_2$ and Na_2SO_4 are added, mixed and pH is raised to 8-8.5. The precipitation of Ferrous-Ferro cyanide under reducing conditions (2) along with formation of ferrous hydroxide at pH 8 – 8.5 does effect the removal of Ru. In this case oxidation of ferrous to ferric should be prevented. The method includes receipt of waste, pH adjustment– if required, addition

of required chemicals, final pH adjustment, overnight settling, removal and discharge of decant and cementation of chemical sludge.

Experimental

Waste analysis

The complete Chemical & Radiochemical analysis of LLW was carried out from batch to batch. The range of various components is given in Table-1. The concentration of radionuclides vary because of performance of RF column & dilution of waste during transfer.

Lab scale studies

Laboratory scale Jar tests were carried out for decontamination of waste with respect to Cs, Sr and Ru. The Jar tests were performed sequentially by three different ways.

a) Treatment for Cs+Sr, followed by Ru : The above alkaline waste was subjected to chemical treatment after adjusting pH to 8 – 8.5 with concentrated nitric acid. 500 ml. of waste was taken in five beakers and chemicals for removal of Cs and Sr were added in required concentrations. Final pH was then adjusted to 8 – 8.5 and kept overnight for settling and then the decant was analysed for isotopic constituents. Decant of this treated waste was then subjected to chemical treatment for removal of Ru. The pH was reduced to 2- 2.5 by using concentrated nitric acid and then reducing agent like Na_2SO_3(Sodium Sulphite) was added and stirred for 15 minutes. Then Ferrous Sulphate solution (prepared in 0.2 N H_2SO_4) was added. Final pH was adjusted to 8 – 8.5 by using NaOH solution. Dark green precipitate of ferrous hydroxide was obtained. The same was kept overnight for settling and then analysed for isotopic constituents. All the chemicals used were of AR grade. The average results of five batches are given in Table-2. The details of concentrations of chemicals are given in Table-3.

b) Treatment for Ru followed by Cs+Sr : The treatment as above was reversed i.e. chemicals for Ru treatment were added first at low pH 2-2.5. Final pH was adjusted to 8 – 8.5 by adding NaOH solution. It was analysed for isotopic constituents. Decant was then subjected to chemical treatment at pH 8 – 8.5 by adding respective chemicals for removal of Cs+Sr. After second step treatment, analysis was carried out for individual isotopes. Average results of five batches are given in Table-4.

c) Combined Chemical treatment : Fresh 1 ltr. of LLW was taken in five beakers. Reducing agent like Na_2SO_3 was added after adjusting pH 2-2.5 by using concentrated HNO_3 solution. The solution was stirred for 15-20 minutes and then subjected to combined chemical treatment for the removal of Cs, Sr and Ru together, by adding all chemicals sequentially. Final pH was adjusted to 8 – 8.5 and allowed for overnight settling. It was then analysed for isotopic constituents. Since removal of Ru requires reducing agent like Na_2SO_3 , ferric nitrate is not added during the combined treatment. Instead of that, ferrous sulphate was added which acts as coagulating agent after hydrolysis. Average results of five batches are given in Table-5.

Plant scale studies

Since the laboratory scale experiment has indicated the feasibility of two steps combined chemical treatment for decontamination of LLW with respect to Cs+Sr and Ru, plant scale treatment has been carried out on $4m^3$ scale of LLW. The waste was taken in SS tank , pH was brought down to 2 - 2.5 by addition of nitric acid. Sodium sulphite, 0.01 M (1260 ppm.) was added as reducing agent. The solution was homogenised by purging air for about 30 minutes. After purging, all chemicals were added as per Table-3. The sequence of addition was ferrous sulphate, copper sulphate, potassium ferrocyanide, barium chloride and sodium sulphate. Thereafter the pH was adjusted to 8-8.5 by addition of alkali and allowed for over night for settling. The decant was removed, analysed and discharged. Data for few operations are given in Table-6.

Table-1 : Analysis of LLW

	Chemical Analysis	
Total Solids	20 – 25 % as Sodium Nitrate	
pH	12 – 12.5	
	Radiochemical Analysis	
	μ Ci/ml.	kBq/lit.
Gross Beta	$(2.5 - 3.6) \times 10^{-2}$	925.0-1332
Cs^{137}	$(5.1 - 6.2) \times 10^{-3}$	188.7-229.4
Ru^{106}	$(4.0 - 4.5) \times 10^{-3}$	148.0-166.5
Sr^{90}	$(2.4 - 3.2) \times 10^{-4}$	08.88-11.84

Table -2 : Treatment for Cs+Sr, followed by Ru

	Cs+Sr Treatment			Ru Treatment		
Analysis	Activity after Treatment			Activity after Treatment		
pH	8 – 8.5			8 – 8.5		
	Radiochemical Analysis					
	μ Ci/ml.	kBq/lit.	DF*	μ Ci/ml.	kBq/lit.	DF*
Gross β	$(1.0-1.5)\times10^{-2}$	370-555	2-3	$(1.2-1.6)\times10^{-3}$	44.4-59.2	19-26
Cs^{137}	$(2.1-2.5)\times10^{-4}$	7.77-9.25	23-27	$(2.0-2.5)\times10^{-4}$	7-9.25	23-28
Ru^{106}	$(4.0-4.5)\times10^{-3}$	148-168.5	1	$(3.2-3.5)\times10^{-4}$	11.84-12.95	12-13
Sr^{90}	$(1.2-2.3)\times10^{-4}$	4.45-8.51	2-4	$(1.1-2.2)\times10^{-4}$	4.07-8.14	2-4

Note : * DF is with respect to initial activity.

Table -3 : Concentration details of co-precipitating chemicals

Chemicals	Reactive ion	Concentration in ppm.
$CuSO_4$	Cu^{+2}	40- 60
$K_4 Fe(CN)_6$	$Fe(CN)_6^{-4}$	60-90
$BaCl_2$	Ba^{+2}	200-250
Na_2SO_4	SO_4^{-2}	500-1000
$Fe(NO_3)_3$	Fe^{+3}	25-50
$FeSO_4$	Fe^{+2}	600-900
Na_2SO_3	Reducing agent	1260

Table -4 : Treatment for Ru followed by Cs+Sr

	Ru Treatment			Cs+Sr Treatment		
Analysis	Activity after Treatment			Activity after Treatment		
pH	8 – 8.5			8 – 8.5		
	Radiochemical Analysis					
	μ Ci/ml.	kBq/lit.	DF*	μ Ci/ml.	kBq/lit.	DF*
Gross β	$(5.7-8.9)\times10^{-3}$	210.9-329	3-5	$(1.3-1.8)\times10^{-3}$	48.1-66.6	17-23
Cs^{137}	$(4.8-6.0)\times10^{-3}$	177.6-222	1	$(3.0-3.8)\times10^{-4}$	11.1-14.06	15-19
Ru^{106}	$(3.1-4.1)\times10^{-4}$	11.47-15.17	10-13	$(3.1-4.2)\times10^{-4}$	11.47-15.54	10-13
Sr^{90}	$(2.3-3.1)\times10^{-4}$	8.51-11.47	1	$(1.2-2.3)\times10^{-4}$	4.44-8.51	2-4

Note : * DF is with respect to initial activity.

Table -5 : Combined chemical treatment

	Combined Treatment		
Analysis	Activity after Treatment		DF*
pH	8 – 8.5		
	Radiochemical Analysis		
	μ Ci/ml.	kBq/lit.	
Gross β	$(0.95 - 1.1)x10^{-3}$	35.15-40.7	28-33
Cs^{137}	$(1.8 - 2.1) \times 10^{-4}$	6.66-7.77	27-31
Ru^{106}	$(2.2 - 2.9)x\ 10^{-4}$	8.14-10.73	15-19
Sr^{90}	$(1.0 - 2.1) \times 10^{-4}$	3.7-7.77	2-5

Note : * DF is with respect to initial activity.

Table -6 : Analysis of samples generated during plant scale treatment

Analysis	Initial Activity		After Combined treatment		DF
pH	12.5-13.0		8-8.5		
	μ Ci/ml.	kBq/lit.	μ Ci/ml.	kBq/lit.	
Gross β	$(1.68–2.63)x10^{-2}$	621.6-973.1	$(1.17-3.10)x10^{-3}$	43.29-114.7	8–14
Cs^{137}	$(0.63–1.75)x10^{-2}$	233.1-647.5	$(0.23-1.31)x10^{-3}$	9.51-48.47	13–27
Ru^{106}	$(1.46–3.89)x10^{-3}$	54.02-143.93	$(4.63-3.24)x10^{-4}$	17.13-11.99	3–12
Sr^{90}	$(4.80- 5.20) \times 10^{-4}$	17.76-19.24	$(1.51-2.30)x10^{-4}$	5.59-8.51	2–3

Result and Discussion

1. The co-precipitation methods such as treatment for Cs+Sr followed by Ruthenium and Ruthenium followed by Cs+Sr offers very good DF for Cs, Sr and Ru. The final DF with respect to initial activity, obtained by both the methods, were found comparable. Hence any of the treatment method can be followed.

2. Laboratory scale Jar tests have indicated the possibility of two step combined chemical treatment. In first step, the presence of reducing agent like sodium sulphite in acidic medium, at pH 2-2.5, sodium sulphite, reduces the valencies of Ru and also prevents oxidation of ferrous ions to ferric. Hence addition of the reducing agent in acidic medium is essential. In second step, combined chemical treatment by addition of all chemicals sequentially and thereafter adjusting pH to 8-8.5 offers better DF for Ru, Cs and Sr. The activity is confined to chemical sludge so obtained and the volume reduction factor is around 100.

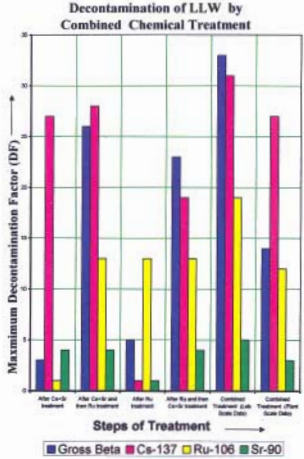

3. Based on the laboratory scale results, the two step combined chemical treatment method has been adopted successfully on the plant scale and nearly 1.5 lakh liters of waste have been treated at LWTP(T). The sludge has been conditioned in to the cement vermiculite matrix at solid waste management facility. The combined chemical treatment has offered advantages like i) Substantial reduction of processing time ii) Reduction of sludge volume iii) Avoid of multiple steps and cross contamination. iv) Reduction of a Man-rem exposure, etc.

References

1. Kulkarni Y., Samanta S.K., Bakare S.Y., Kanwar Raj and Kumra M.S., "Process for treatment of intermediate level radioactive waste based on radio nuclide separation," Proc: Waste Management Symposia- 96 (WM-96), Tuscon Community Centre, Tuscon, Arizona, USA, Feb 25-29, 1996.
2. Mead, F.C. USAEC Document, WASH 275, 231, 1954

This paper was adjudged as the Best paper in the Twelfth Annual Conference of Indian Nuclear Society (INSAC-2001) held during October 10-12, 2001 at Centre for Advanced Technology, Indore.

About the authors ...

Mr S.G. Kore *(M.Sc.- Chemistry, from Mumbai University), joined Waste Management Facilities, Tarapur, in 1986. He is associated with process control laboratory of Waste Management Facilities, Tarapur. He is involved in leaching study of various cement waste products, process development for removal of radionulcies by chemical treatment, evaluation of flocculating agent, etc. He has also carried out experiments with reverse osmosis technique using TFCP membrane for the decontamination of radionuclides present in LLW at Tarapur.*

Mr Vinod Prasad *joined Waste Management Division, BARC, Tarapur, in 1982 after graduation in science from Garhwal University, Srinagar. His main area of assignment includes removal of radionuclides from Low Level Radioactive Liquid Waste by chemical treatment. He has also carried out a number of studies on the separation of Ru-106 by Zn- Charcoal adsorption column and membrane process ultrafiltration.*

Mr U. S. Singh *(B.Sc. from Gorakhpur University), joined Waste Management Facilities, BARC, Tarapur, in 1973. Since then, he is associated with treatment and conditioning of Low Level Radioactive Waste generated at TAPS and Reprocessing plant, PREFRE. He is actively involved in the finalisation of composition of cement waste matrix for conditioning of various waste streams (chemical sludge, ILW, filter sludge, etc.) His field of interest includes leaching of various cement waste products, chemical treatment of LLW, evaluation of flocculating agent, etc. and adaptation of these technique on the plant scale. He is also involved in surveillance programme of near surface disposal facility which is used for disposal of solid waste by monitoring various borewells. He has 5 publications to his credit.*

Mr R.G. Yeotikar *(M.Sc.- Chem., M.Tech.- Chemical Technology from Nagpur University), joined Waste Management Division, BARC, after graduation from 20th batch of BARC Training School. Presently, he is Superintendent, Laboratories, Waste Management Facilities, Tarapur. He is responsible for carrying out various development activities for management of all types of nuclear waste and their possible adaptation on plant scale in addition to normal analytical support to the plant. His main field of work includes development of methods such as chemical treatment of low level waste, conditioning of intermediate level waste in cement matrix and vitrification of high level radioactive liquid wastes. His main contribution also includes development and regular adaptation of various methods for evaluation of chemical durability and other properties of waste products. He was a member of Co-ordinated Research Program of International Atomic Energy Agency. He is having about 45 publications to his credit.*

Mr Ajai Mishra *B.Sc. (Engg.) Mechanical from Agra University, joined Waste Management Division, BARC in 1979 after graduating from 22nd batch of Training School, BARC. He is overall responsible for construction, operation and maintenance of various Rad Waste Management Facilities at BARC Complex Tarapur. He is also involved in a number of development studies related to treatment of Low Level Radioactive Liquid Waste and conditioning into cement matrix and final adaptation on the plant scale. His field of work also includes safe management of various of types of solid waste from various DAE sites at Tarapur, in near surface disposal facility and its surveillance. He has also participated as consultant and expert at Vienna in IAEA Technical Committees.*

Mr S.S.Ali *graduated in Chemical Engineering from Osmania University in 1970. After working with a heavy chemical industry, he joined BARC in March 1973. From 1973 to 1997 May, he has worked at Rajasthan Atomic Power Plant as In-Charge of Effluent Management unit. He was responsible for safe management of radioactive waste at RAPS and planning & augmentation of Waste Management Facilities including Construction, Commissioning & subsequent operation of Solar Evaporation Facility at RAPS. He has generated and compiled the data on waste management requirement of a 220 MW (e) PHWR. He has participated in Project Design review of Waste Management Plants like NAPP, KGS, RAPP-3&4.*

End Plug Welding Of PFBR Fuel Tubes with a 2.5 kW CW CO_2 Laser

Rakesh Kaul, P. Ganesh, M.O. Ittoop and A. K. Nath
Centre for Advanced Technology, Indore –452 013

Aniruddha Kumar, R. B. Bhatt and Arun Kumar
Advanced Fuel Fabrication Facility, BARC, Tarapur –401 504

Introduction

A titanium-stabilized fully austenitic alloy D9 (a 15Cr-15Ni-2 Mo stainless steel), because of its superior resistance to irradiation-induced swelling and higher creep strength under irradiation, has been selected for fuel-clad and wrapper applications in 500 MWe Prototype Fast Breeder Reactor (PFBR). Fuel clad tube of PFBR is a 6.6 mm outer diameter tube (wall thickness = 0.45 mm) made of alloy D9. The two ends of fuel clad tube are encapsulated by welding with end plugs made of AISI 316M stainless steel (Fig. 1).

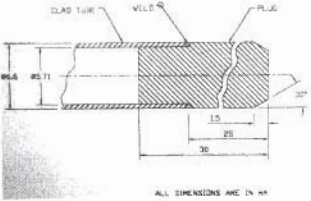

Fig.1 : Details of end plug of PFBR fuel pin

Table 1 presents chemical compositions of the materials of construction of clad tube and end plug, respectively. An accepted weld should have complete fusion of fuel clad tube/plug interface and should be free from defects like porosity, inclusions and cracks. End plug welding process has been qualified using Pulsed Gas Tungsten Arc Welding (PGTAW) and this method has been adopted to weld the end plugs. The objective of the present study is to explore technical feasibility of using high power continuous wave (CW) CO_2 laser for making consistently good quality end welds of PFBR fuel pin. Being a non-contact process, laser welding does not generate active wastes in the form of used electrodes and defects like tungsten inclusions are completely eliminated. Moreover, it will also simplify glove box operation as it obviates electrode replacement, arc gap adjustment etc. Since no information is currently available on laser weldability of alloy D9, it was essential to carry out detailed investigation in this regard.

Table-1 : Chemical compositions of clad tube & end plug (in wt%) Clad tube

Clad tube

C	Cr	Ni	Mn	Si	Mo	P	S	Ti	Fe
0.04	14.53	14.25	1.5	0.59	2.07	0.053	0.005	0.23	Bal.

End Plug

C	Cr	Ni	Mn	Si	Mo	P	S	Fe
0.04	17.2	10.19	1.45	0.58	2.19	0.053	0.015	Bal.

Background

Solidification cracking is one of the major problems associated with austenitic stainless steel welding. The reason for solidification cracking is attributed to the formation of low melting point eutectic phases at the grain boundaries of solidifying weld metal which

facilitates intergranular cracking under the influence of welding induced thermal stresses[1]. The crack sensitivity of a particular weld metal is largely determined by its primary mode of solidification. Austenitic stainless steel welds, depending upon their chemical composition, can solidify with primary phase being either ferrite or austenite. Primary ferrite solidified welds are more crack resistant than primary austenite solidified welds[2].

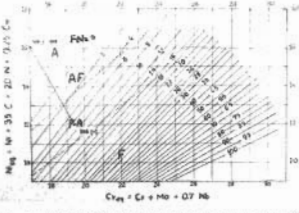

Fig. 2 : WRC 1992 diagram with positions of alloy D9 (fuel clad tube) and AISI 316M stainless steel (end plug)

Figure 2 presents positions of clad tube and end plug materials on WRC-1992 diagram[3]. Alloy D9 (Cr_{eq} = 17 & Ni_{eq} = 16) solidifies with completely austenite mode (with FN=0) under GTAW conditions. Completely austenitic mode of solidification along with presence of titanium (segregates in interdendritic regions and forms carbides and carbosulphides) makes this alloy particularly susceptible to solidification cracking during welding[4]. On the other hand, FA mode of solidification is predicted (with FN=9) for AISI 316M stainless steel (Cr_{eq} = 19.4 and Ni_{eq}= 12). The composition of the fusion zone on the tie line connecting points corresponding to alloy D9 and AISI 316M stainless steel is determined by the degree of dilution of clad tube and end plug. For achieving desirable FA mode of solidification, the dilution from clad tube should not exceed 28%.

Experimental

An indigenously developed 2.5 kW CW CO_2 laser system was used for laser welding. It involved irradiating joint of the rotating tubular specimens with a focused laser beam. Argon was used as the shield gas during welding.

Results & Discussion

Initial welding (laser power = 900W & welding speed =10-20 rpm) produced welds with almost complete penetration and with primary austenite mode of solidification. One of these welds was associated with a centre-line crack (Fig.3). The welds also carried craters at weld termination sites (Fig.4). Subsequent laser welds were made with higher heat input (laser power = 2 kW; welding speed = 12-36 rpm). Use of higher heat input aimed at enhancing solidification cracking resistance of laser welds through achieving greater fusion of underlying end plug material (with higher Cr_{eq}/Ni_{eq} ratio) which serves to shift primary mode of solidification towards ferrite side. No defects (except crater at weld termination site) were noticed in the resultant welds. The welds still exhibited primary austenite mode of solidification. Table-2 presents dimensions of laser welds made with different parameters.

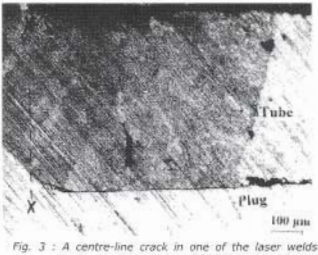

Fig. 3 : A centre-line crack in one of the laser welds made at laser power = 900W & welding speed = 20 rpm

Next set of experiments involved welding with focused laser beam displaced towards end plug side (displacement = 0.1-0.35 mm). As laser beam was progressively displaced towards end plug side, the fraction of the fusion zone representing primary ferrite mode of solidification increased at the cost of that

Fig. 4 : A crater at weld termination site.kdjfdkjfdf

associated with primary austenite mode of solidification. Area fraction measurement revealed that the ferrite solidified region of the fusion zone increased from 4-5 % (with laser beam at clad tube/end plug interface) to 95-96% when laser beam was displaced by 0.35 mm from fuel clad tube/end plug interface towards plug side (Table-3). This transition in primary mode of solidification from austenite to ferrite side with progressive displacement of laser beam towards end plug side represents greater degree of solidification cracking resistance. The maximum distance to which laser beam could be safely displaced without endangering proper fusion of fuel clad tube/end plug interface is about 0.25 mm

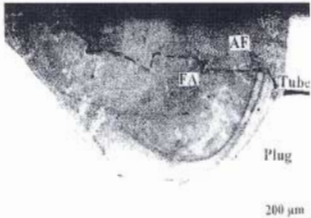

Fig.5 : Cross - section of a sound end plug weld made at laser power 2 kW and welding speed=25 rpm. Laser beam wasdisplaced by 0.25mm from fuel clad tube / end plug interface.

Abrupt switching off of laser power at the end of welding is responsible for the development of poorly filled crater[4]. Ramping of laser power during welding was successful in

Table -2: Dimensions of laser welds

Laser Power (Watts)	Welding Speed (rpm)	Weld width (mm)	Weld penetration (mm)
900	10-20	1-1.1	0.45-0.50
1500	12	1.52-1.59	0.8-1.1
1500	25	1.45-1.5	0.51-0.58
2000	25	1.53-1.6	0.83-1
2000	36	1.4-1.5	0.5-0.63

eliminating crater and associated defects. Ramping schedule adopted was: slope-up time = 0.5 sec, followed by normal welding laser power (2 kW) for 6 seconds (for rpm = 25) and a slope-down time of 1 sec. During welding, laser beam was displaced by 0.25 mm from clad tube/end plug interface towards plug side. Figure 5 presents photomicrograph of a sound weld with largely ferrite mode of solidification.

Table –3 : Results of area fraction measurement on laser welds (Laser Power=2 kW; welding speed = 25 rpm)

Position of laser beam from fuel clad tube/plug interface	Area of the fusion zone with primary ferrite mode of solidification	Area of the fusion zone with primary austenite mode of solidification
At the interface	4-5 % of the fusion zone	95-96 % of the fusion zone
0.1 mm towards end plug side	13-28 % of the fusion zone	72-87 % of the fusion zone
0.25 mm towards end plug side	70-82 % of the fusion zone	18-30 % of the fusion zone
0.35 mm towards end plug side	95-96 % of the fusion zone	4-5 % of the fusion zone

Conclusion

The present study demonstrates that sound end welds of PFBR fuel tube with crack resistant microstructure can be obtained by

optimizing laser welding parameters, proper positioning of laser beam and ramping of laser power during welding.

References

1. Kou S., Welding Metallurgy, 1987, John Wiley and Sons Inc., p.211.
2. Dixon, B. F, Control of Magnetic Permeability & Solidification Cracking in Welded Nonmagnetic Steel. Welding Jr, 68(5), 1989, pp. 171s -180s.
3. Kotecki D.J.& Siewert T.A, WRC-1992 Constitution Diagram for Stainless Steel Weld Metals: A Modification of the WRC-1988 Diagram, Welding Jr, 71(5),1992, pp. 171s-178s.
4. Shankar V., Gill, T. P. S., Terrance A.L. E, Mannan S. L., & Sunderesan S, Relation between Microstructure, Com- position and Hot Cracking in Ti-Stabilized Austenitic Stain- less Steel Weldments, Metall-. urgical and Materials Trans: 31A, 2000, pp. 3109-3122.
5. Dickerson P.B., Weld Disconti- nuities - Causes & Cures, . Welding Jr. 77(6), 1998, pp. 37-42.

This paper received the Second Best paper award at the Symposium INSAC 2001 held at Centre for Advanced Technology, Indore

About the authors ...

Mr Rakesh Kaul *received his B.E (Metallurgy) degree from University of Roorkee in 1986. After graduating from BARC Training School, Mumbai, he joined IGCAR, Kalpakkam, in 1987. In IGCAR, he worked on the commissioning of post irradiation examination facilities and failure analysis of engineering components. In 1995, he joined Centre for Advanced Technology, Indore. Since then, he is engaged in laser material processing. He is the recipient of Metallography contest awards in 1989 and 1991, IT Mirchandani and NUCOR awards from Indian Institute of Welding, II best presentation award from Gramya Research Analysis Institute, Vadodara, and II best paper award from Indian Nuclear Society for paper presented in INSAC-2001.*

Mr P. Ganesh *obtained his Master's degree in Metallurgical Engineering from IIT, Kharagpur in 1997. In the same year he joined Centre for Advanced Technology, Indore. Since then he has been working on laser material processing.*

Mr M.O. Ittoop *obtained his diploma in Electronics Engineering from Govt. Polytechnic, Palghat, Kerala, in 1991. He joined Centre for Advanced Technology, Indore, in 1993. Since then, he has been working on the development of micro-controller based embedded systems and programmable power supplies for high power lasers.*

Dr A.K. Nath *received his B.Sc (Physics) Honours degree from Patna University in 1970. After graduating from BARC Training School, Mumbai, he joined Laser Section of BARC, Mumbai in 1972. Since then, he has worked extensively on various aspects of high power continuous wave and pulsed TEA carbon dioxide lasers and material processing applications. He received his Ph.D degree from Mumbai University in 1982 for his theoretical and experimental studies on multi-rotational behavior of TEA CO_2 lasers. From 1982-1984, he was with the University of Alberta, Canada, as a post-doctoral research fellow and worked on the development of multikilowatt CW CO_2 lasers. Since 1986, he is with Centre for Advanced Technology, Indore, where he heads the Industrial CO_2 laser section, and is engaged in the development of high power CO_2 lasers and their industrial applications.*

Mr Aniruddha Kumar *obtained his Master's degree in Physics from Burdwan University in 1990. In AFFF, BARC, he has been working on the development of different welding processes & techniques required for nuclear fuel fabrication of power reactors. His other research interest includes CO_2 lasers both pulsed and continuous. He has actively participated in the development of helium less operation of TEA CO_2 lasers. He is currently working towards his Ph.D on the topic entitled, "Development & characterization of a single mode long pulse TEA CO_2 laser".*

Mr R.B.Bhatt *graduated in Metallurgical Engineering from Regional Engineering College,Jaipur, in 1988 and acquired M.Tech degree in the field of Metal - joining from IIT,Madras in 1991. He belongs to 33rd batch of BARC Training School. He joined AFFF, BARC, Tarapur in 1990. Since then he is associated with development and fabrication of different types of MOX fuel elements. His main areas of interest are welding techniques and systems for nuclear fuel fabrication and welding metallurgy of stainless steels. He is a life member of Indian Institute of Welding.*

Mr Arun Kumar *is a Metallurgical Engineer from BIT Sindri, Ranchi University. After graduating from 16th batch of BARC Training School, he joined Radio Metallurgy Division, BARC, in 1973. In RMD, he worked for the development of Plutonium bearing oxide fuels for thermal & fast reactors. In the year 1987, he joined Advanced Fuel Fabrication Facility and is presently working as Superintendent, Fuel Manufacture. He worked for the development and fabrication of BWR MOX assemblies for TAPS. He is presently engaged in the development of fabrication flow sheet for manufacture of PFBR and PHWR MOX fuel pins. He along with his associates have developed and inducted pulsed TIG welding technique in fuel pin end plug welding. In collaboration with CAT, Indore, he is working for the development and induction of laser welding technique for fuel pin end plug welding, which will be suitable for remote fabrication of fuel elements.*

Development of a Repetitive Widely Tunable Single Mode TEA CO_2 Laser, its Application on NH_3 Laser and Related Studies

J. Padma Nilaya
Laser and Plasma Technology Division
Bhabha Atomic Research Centre

The importance of a carbon dioxide laser operating repetitively on a single longitudinal mode (SLM) either on one or multiple transitions in selective photochemical studies is well recognised. Further, the generation of coherent radiation at longer wavelengths with a carbon dioxide laser as the pump source plays a significant role in these studies. In this dissertation four important features of the pump laser, which, among others, enhance the efficiency of both the above-mentioned processes, are addressed. They are a) the single frequency operation of the pump laser, b) the wide tunability of the emission frequency of the pump laser with respect to the absorption feature of the molecule of interest, c) the capability of the pump laser to simultaneously operate on more than one frequency and d) its repetitive operation capability. In addition, the operation of molecular lasers (in particular NH_3 laser) optically pumped by CO_2 laser providing coherent radiation in the longer wavelength region also forms an important part of this thesis.

In an isotopic mixture of molecules, selective excitation and an eventual dissociation of one of the species leading to the separation of isotopes is possible if the frequency of the pump laser matches with the absorption feature of the molecule. The efficiency of such selective multi photon dissociation processes depends strongly on the proximity of the emission frequency of the pump to the absorption centre of the isotopic species of interest. Chance coincidence of these two is extremely remote. The operation of the pump on single longitudinal widely detunable mode, therefore, is preferred.

The popular methods of obtaining SLM operation viz., the hybrid or the injection locking configurations, offer limited detunability of the lasing mode, as the lasing bandwidth, governed by the broadening in the low-pressure section, is small. In the method reported in this thesis, on the other hand, a judicious combination of the free spectral range (FSR) of the cavity and the positioning of the loss line allowed only one mode to experience net gain resulting in SLM operation with a detunability an order of magnitude more than that obtainable by the conventional methods. Under certain operating conditions of this laser, emission of two pulses that originate from the intra-pulse temperature induced change of the refractive index, was observed[1, 2]. A cavity mode when appropriately located with respect to the centre of transition can be pushed out of lasing due to this effect. Following this as the temperature equilibrates the mode is pulled back in to the gain domain causing thereby the emission of the second pulse. The laser should therefore be operated outside this double pulsing window for its use in multiphoton dissociation experiments or as a pump for other molecular lasers. Remarkable stretching of the pulse from this mini laser was also observed under conditions for which oscillation on a higher order transverse mode followed that on the TEM_{00} mode with partial temporal overlap between the two[3]. Judicious combination of spatial and spectral

control helped realise such an oscillation condition.

The vibrational energy levels of a molecule get gradually closer due to anharmonicity with increasing vibrational energy of the molecule making its absorption line centre red shifted with respect to the initially resonant incident pump laser frequency. The capability of a CO_2 laser to operate simultaneously on a number of rotational vibrational transitions greatly simplifies such selective multi-photon excitation processes and results in higher dissociation yield, better selectivity, reduction in the threshold fluence etc.

A CO_2 laser normally lases on a single transition possessing the highest gain, as the rotational thermalisation time is much shorter as compared to the duration of the laser pulse. Simultaneous oscillation on a number of lines can be obtained if the gain to loss ratio can be made nearly the same on all these transitions. Selection of a set of transitions on which simultaneous lasing can occur is generally not possible by the existing techniques. The judicious imposition of longitudinal mode control onto a resonator cavity, the Q value of which increased with decreasing wavelength in the 11-9 micron region, made possible the simultaneous oscillation on all the four branches from a low pressure cw CO_2 laser[4]. This low power multiline photon distribution was subsequently amplified in a high-pressure section in the hybrid configuration[5]. Tailoring the Q value of the cavity can, in principle, generate any desired combination of lasing lines. Injection locking on a weak gain line was achieved in a non-dispersive TEA CO_2 laser cavity with moderate seed photon power[6]. The success of this technique owed primarily to the utilisation of a slave cavity with large FSR such that tuning its cavity length to some specific values actually offsets the large gain difference between a strong and a weak line. This work gives rise to the prospect of amplification of a low power multiline distribution of photons in a non-dispersive slave cavity. In course of this work, the important role played by spatial hole burning effect in determining the emission characteristics of a laser was elegantly brought out in an experiment where the spatial hole filling rate was varied by two orders of magnitude by utilising slow and fast axial flow CO_2 laser systems[7].

To access the absorption features of molecules with no possible overlap with the emission frequencies of CO_2 laser, pumping a suitable molecular medium with the CO_2 laser emission can be an attractive method of generating new coherent sources at longer wavelengths. A number of difficulties are encountered in the operation of an optically pumped molecular laser (OPML). Efficient coupling of the pump radiation into the OPML medium while maintaining, at the same time, high Q of the OPML cavity is far from simple. The instabilities caused in the pump laser as the unabsorbed pump retraces its path back into it renders it unsuitable for many experiments. A novel cavity configuration where most of these problems could be eliminated to a satisfactory level has been conceived and the performance of this versatile cavity has been demonstrated in the pulsed operation of an NH_3 laser pumped by a TEA CO_2 laser[8]. To be noted here that the performance of the optically pumped molecular laser would also benefit by the detunable SLM repetitive operation capability of the pump laser.

Apart from the suitable emission characteristics, the other important attribute of a pump laser that decides the efficiency and yield of selective photo-excitation processes is its repetitive operation capability. Spark gaps, by virtue of their operation in arc mode, are unsuitable for repetitive applications and are normally replaced by thyratrons[9]. By rotating a suitably configured dielectric plate between the electrodes of an ordinary spark gap, it was possible to enhance the repetition rate capability of a spark gap[10]. The unique geometry of this device was exploited to obtain large number of advantages[11-13] otherwise not possible by the conventional command resonant charging scheme. In course of this work it was found that for fast discharges, which normally is the case with

TE lasers, the recovery of a switch is independent of the energy transferred through it[14].

References

1. Observation of double pulsing in a single mode TEA CO_2 laser caused by the effect of mode pulling and pushing, J. P. Nilaya and D. J. Biswas, BARC News letter, **189**, 90 (1999).
2. Observation of intra-pulse thermal effect induced double pulsing in a single mode TEA CO_2 laser, J. P. Nilaya and D. J. Biswas, J. Phys D:Appl Phys **34,** 78 (2001).
3. Pulse stretching due partial temporal overlap of two modes in a TEA CO_2 laser, J. P. Nilaya and D. J. Biswas, Rev Sci Instrum **71**, 579 (2000).
4. Four branch oscillation from a dual polarisation cavity CO_2 laser, D. J. Biswas, J. P. Nilaya, and U. K. Chatterjee, Appl Phys B **57**, 227 (1993).
5. Dual band multiline lasing from hybrid CO_2 lasers, D. J. Biswas, J. P. Nilaya, and U. K. chatterjee, Opt Quantum Electron **29**, 501 (1997).
6. Evidence of injection locking in a non dispersive slave CO_2 laser, J. P. Nilaya and D. J. Biswas, Opt Engg **37**, 1080 (1998).
7. Effect of longitudinal flow velocity on the emission spectrum of CO_2 laser, D. J. Biswas, J. P. Nilaya, S. K. Sehgal, and U. K. chatterjee, J Appl phys **76,** 1340 (1994).
8. A versatile cavity for optically pumped molecular lasers, J. P. Nilaya and D. J. Biswas, Rev Sci Instrum **72**, 1343 (2001).
9. D. J. Biswas and J. P. Nilaya, Review Article, Prog. Quantum Electron **26,** pp 1-63 (2002).
10. High repetition rate operation of a rotating dielectric spark gap, J. P. Nilaya, D. J. Biswas, B. S. Narayan, and U. K. Chatterjee, Rev Sci Instrum **65**, 3590 (1994).
11. Latch proof operation of a switch of a high repetition rate laser with D-C Resonant charging, D. J. Biswas, J. P. Nilaya, and U. K. chatterjee, Rev Sci Instrum **66**, 4813 (1995).
12. A single switch as driver of two high repetition rate lasers,D.J. Biswas, J. P. Nilaya, and U. K. Chatterjee, Opt Engg **36**, 588 (1997).
13. Diode less operation of a resonantly charged TE laser pulser, D. J. Biswas, J. P. Nilaya, Rev Sci Instrum **72**, 2505(2001).
14. On the recovery of a spark gap in a fast discharge circuit, D. J. Biswas, J. P. Nilaya, and U. K. Chatterjee Rev Sci Instrum **69**, 4242 (1998).

Dr (Ms) J. Padma Nilaya received the "Indian Laser Association Best Ph.D. Thesis Award" for her thesis presented at the National Laser Symposium, CAT, Indore, 2001

About the author ...

***Dr (Ms) J. Padma Nilaya** received her M.Sc. (physics) degree from Nagpur University in 1991 and joined the erstwhile MDRS, BARC in 1992 after successfully graduating from the 35th batch of the BARC Training School. She is the recipient of University gold medals for securing first position in the B.Sc and M.Sc examinations. She received the Young Physicists Colloquium award of Indian Physical Society in 1999. Her research interest includes generation of coherent mid-infrared sources and their application to isotope separation. She has obtained her Ph. D from the University of Mumbai in 2002.*

Heavy Ion Induced Fusion-Fission Reactions

L. M. Pant
Nuclear Physics Division
Bhabha Atomic Research Centre

Nuclear fission is a process whereby a heavy nucleus splits into two fragments of comparable mass. One of the main characteristics of the fission process is, therefore, the mass distribution of the fission fragments. From the early days, it was established that in the low energy fission of the actinide nuclei, the fragment mass distribution is highly asymmetric, and this was attributed to the influence of the doubly closed shell in the heavy fragment mass region. With the advent of heavy ion accelerators, it has been possible to study the fission process in detail by populating compound nuclei over large excitation energies and angular momenta by various entrance channels using heavy ion reactions. As the excitation energy of the fissioning nucleus is increased, the mass distribution becomes more symmetric due to washing out of the shell effects at high excitation energies [1].

Another important aspect in the study of the fusion-fission reactions is the fission-fragment angular distributions, which have also been investigated in great detail in the recent years [2]. The interest in this field has been renewed with the observation that the fragment angular distributions in many target projectile systems show anomalous features when they are compared to the standard saddle point statistical model (SSPSM) calculations [3].

The SSPSM model accounts well for the fragment angular distributions in the light ion induced fission reactions however, anomalous angular distributions have been reported mainly for heavy ion reactions using actinide target nuclei and are attributed to be due to an admixture of non-equilibrated fission events such as *pre-equilibrium fission, fast fission* and *quasi-fission* along with the normal compound nuclear fission events. Mass distributions following such an admixture would be expected to be broader than those for normal fission because non compound fission reactions are expected to have more asymmetric component arising due to incomplete equilibration in mass degree of freedom. The onset of such non-equilibrated fission events is governed by the dynamics of the fusion and fission processes in the heavy ion reactions.

The dynamics of the fusion-fission reactions can also be explored by studying the pre-scission neutron multiplicities in the fission reactions. It is observed that in a large number of heavy ion induced fusion-fission reactions, the pre-scission neutron multiplicities are also anomalously larger than that predicted by the SSPSM calculations [4]. The excess of pre-scission neutron multiplicity is now attributed to be due to a time delay in the fission process arising due to dynamical effects in the fission process.

In the present work, we have addressed different dynamical aspects in the study of heavy ion induced fusion-fission reactions through mass-energy correlations, mass dependent variation of fission fragment anisotropy and measurements of pre-scission neutron multiplicities. We have measured the mass and kinetic energy distributions of fission fragments using ^{16}O and ^{19}F projectiles on ^{209}Bi target at energies around the Coulomb barrier for fusion. In the second part of the measurements, we have studied the fission fragment angular anisotropies as a function of fragment mass in two

target-projectile systems namely $^{11}B+^{237}Np$ and $^{16}O+^{209}Bi$ having different entrance channel mass asymmetries and lying on either side of the Bussinaro Gallone critical mass asymmetry, α_{BG}. Finally, the pre-scission neutron multiplicity measurements have been carried out in the $^{19}F+^{209}Bi$ reaction, which have provided new information on the fission time delay in this system resulting due to the dynamics and energy damping in the fission process. The experiments were carried out using heavy ion projectiles from the 14MV BARC-TIFR Pelletron Accelerator Facility at Mumbai.

The design and development of the Large Area Position Sensitive Ionization Chamber (LAPSIC) [5], formed the main cornerstone for carrying out the fission coincidence measurements described in this work. Fig. 1 shows LAPSIC in the Pelletron Beam Hall. This detector is used for simultaneous measurement of energy, mass, charge and angle of emission of the reaction products. It consists of two identical gas chambers having a common cathode. Each half has a four-element anode section for particle identification and a θ-grid to measure the angle of the particle. The detector is normally operated with P10 gas in flow mode. The detector subtends a solid angle of ~ 40 mSr at the target. The entrance window at 121 cm from the target center makes it suitable for time of flight measurements of the reaction products. The signals from the θ-grid are read out via the delay line method.

Fig.1 : LAPSIS in the Pelletron Beam Hall

Mass Energy Correlations in $^{16}O+^{209}Bi$ and $^{19}F+^{209}Bi$ Reactions

The mass and kinetic energy distributions of the fission fragments are decided during the transition from saddle to scission stages in the fission process and therefore can reveal important information about the reaction mechanisms involved in the fusion-fission dynamics in heavy ion induced reactions. Studies of mass and energy correlations were carried out for the ^{16}O and $^{19}F+^{209}Bi$ systems over a wide range of excitation energies (E^*=30-50 MeV) [6].

The experiment was carried out using a 60 μm silicon surface barrier detector and the LAPSIC, kept at the fission folding angle to detect the complementary fragments. Experimental arrangement was similar to that as shown in Fig. 5. The solid state detector was kept at 70° with an angular opening of ± 3° and the LAPSIC was kept at a mean angle of 90° with an acceptance angle of ± 9.8° on either side of the beam for detecting the coincident events. The peak of the folding angle was well covered for both the systems with this angular acceptance. The ^{16}O and ^{19}F beam energies were varied to cover both below and above barrier energy regions for the respective systems.

The pulse heights from the two detectors were converted into the post-scission kinetic energies of the two fragments by an event by event iterative analysis. The center of mass energies of the fragments were derived after kinematic trans-formation assuming full momentum transfer to the compound nucleus. These energies were further corrected for neutron evaporation effects to obtain the pre-neutron emission masses by using the mass and momentum conservation relations.

Fig. 2 shows the variance, σ_A^2 of the fragment mass distributions as a function of the bombarding energy. The

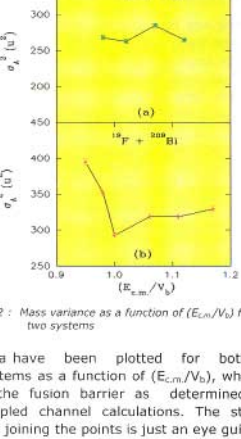

Fig.2 : Mass variance as a function of $(E_{c.m}/V_b)$ for the two systems

data have been plotted for both the systems as a function of $(E_{c.m}/V_b)$, where V_b is the fusion barrier as determined by coupled channel calculations. The straight line joining the points is just an eye guide.

It is seen that in case of the $^{16}O+^{209}Bi$ system, the variance of the mass distribution, σ_A^2 remains nearly flat with variation in $(E_{c.m}/V_b)$, whereas for the $^{19}F+^{209}Bi$ system, σ_A^2 initially has a slow decrease with decrease in the bombarding energy upto the barrier energy, and then rises sharply at below barrier energies. The experimentally observed values for σ_A^2 at above barrier energies match well with the available systematics for the compound nuclei populated close to the present systems [7,8].

It has also been observed in the recent experiments [9,10], that there is a clear evidence for a transition from double humped to single humped mass distributions in low energy fission around A_{CN} = 226. Systems with A_{CN} < 226 end up in predominantly single humped distributions, whereas systems with A_{CN} > 226 predominantly show double humped distributions when fissioning with low excitation energies. The two systems, $^{16}O+^{209}Bi$ and $^{19}F+^{209}Bi$ investigated in the present work are just below and above this limit respectively. A contribution of asymmetric fission in the heavier system could lead to the increased width of the mass distributions in the low energy region. Brosa's random neck rupture formalism also predicts the strong influence of mass asymmetric modes which affects the mass widths. There is a spherical shell corresponding to N=82 and Z=82 (standard I) and the deformed shell for N=88 and Z=60-64 (standard II). The N=88 shell drives the mass distribution in the Th-Pa zone while the two shells compete with each other in the U-Pu zone. The varying influence of spherical and deformed shells in these mass regions gives rise to differences in the mass-energy correlations observed in these two systems.

Mass Dependence of Fission Fragment Anisotropies in $^{11}B+^{237}Np$ and $^{16}O+^{209}Bi$ Systems

Fission fragment angular distributions have been used to provide important information on the fission process. The fission fragment mass distribution is expected to be largely determined closer to the scission point and is influenced by the dynamics during the saddle to scission transition stage [11]. In order to understand the dynamics of the fission process, particularly that of the saddle to scission transition, it is of interest to study the correlation between the angular distribution of fission fragments and the fission fragment masses. In the SSPSM formalism, the angular anisotropy of fission fragments can be approximated by:

$$A \sim 1 + (\langle I^2 \rangle / 4K_0^2)$$

where A is the angular anisotropy, $\langle I^2 \rangle$ is the mean square value of the angular momentum distribution and K_0^2 is the variance of the K distribution at the saddle point. In this work [12] we report the results for $^{11}B+^{237}Np$ and $^{16}O+^{209}Bi$ for which the mass asymmetry parameter α lie on either side of the Businaro Gallone critical mass asymmetry α_{BG} [13]. The mass asymmetry parameter is given as:

$\alpha = [(A_T - A_P)/ (A_T + A_P)]$

where A_T and A_P are target and projectile mass numbers. Measurements were carried out on mass, energy correlations of fission fragments for the systems of $^{11}B+^{237}Np$ at E_{lab} = 76 MeV and $^{16}O+^{209}Bi$ at E_{lab} = 100 MeV at forward and perpendicular angles of emission with respect to the beam direction.

The measured fragment anisotropies averaged over all fragment masses matched well for both the systems with the calculations of the standard saddle point statistical model (SSPSM). The variations of the angular anisotropy and total kinetic energy of the fission fragments were studied as a function of the mass of the fragment pair. A self supporting ^{209}Bi target of 420μg/cm^2 thickness and a ^{237}Np target of 220μg/cm^2 thickness coated over a nickel backing (114μg/cm^2) were used in the experiment. Energies of the two complementary fission fragments were measured to determine the fragment mass distributions at forward and perpendicular angles to the beam direction.

Fig. 3 shows the variation of angular anisotropy with fragment mass for $^{11}B+^{237}Np$ and $^{16}O+^{232}Th$ systems. The data for $^{16}O+^{232}Th$ system have been taken from ref.[14], where the measurements have been done by radiochemical methods, and hence only a few selected masses have been measured in that experiment. Both the systems populate to the same compound nucleus, ^{248}Cf.

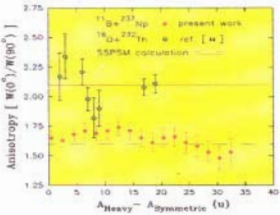

Fig.3 : Mass dependent anisotropy for two systems populating the same compound nucleus (^{248}Cf), but lying on either side of α_{BG}.

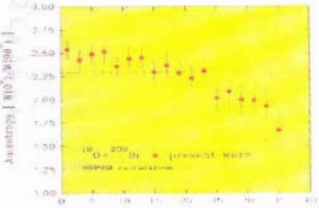

Fig.4 : Mass dependent anisotropy for the system with $\alpha < \alpha_{BG}$.

$^{11}B+^{237}Np$ system correspond to the entrance channel mass asymmetry, $\alpha > \alpha_{BG}$, whereas for $^{16}O+^{232}Th$, $\alpha < \alpha_{BG}$. The mass averaged anisotropy expected from SSPSM calculations is shown by the dashed line.

It is seen that for $^{11}B+^{237}Np$ system the fragment anisotropy does not vary significantly with mass, whereas for $^{16}O+^{232}Th$ system the fragment anisotropy for symmetric split is much larger as compared to asymmetric split. Fig.4 shows the variation of angular anisotropy with fragment mass for $^{16}O+^{209}Bi$ system. This system also corresponds to $\alpha < \alpha_{BG}$. The calculations of SSPSM are shown by the dashed line.

It is seen that for this system although mass averaged anisotropy agrees with the SSPSM calculation, the anisotropy for symmetric mass split is larger as compared to asymmetric split. This feature is qualitatively similiar to that observed for $^{16}O+^{232}Th$. Larger observed anisotropy for certain fragment mass divisions than that given by the SSPSM calculations can be interpreted as due to either larger $<I^2>$ or smaller value of K_0^2 for these masses. For the present systems the l_{max} values are in the range of 25ħ to 28ħ, over which the fission barrier is not expected to vary significantly with angular momentum. Moreover, the mass dependence of pre-scission neutron multiplicities is not sufficient to explain the required change in K_0^2 as a function of mass for the $^{16}O+^{232}Th$ and $^{16}O+^{209}Bi$ reactions.

The present results may be a manifestation of entrance channel effect while going from ^{11}B to ^{16}O projectiles in the two systems, in terms of α being greater or smaller than α_{BG}. For the systems for which $\alpha > \alpha_{BG}$ the results are consistent with the assumption that the fragment angular distribution is decided at the saddle point during the fission process and is not affected by the mass division which is decided at a later stage during the transition from saddle to scission. However for systems with $\alpha < \alpha_{BG}$, larger anisotropies for symmetric fragments as compared to asymmetric fragments may indicate that the dynamical paths followed by the fragments of different mass asymmetries are different.

Neutron Multiplicity Measurements in ^{228}U Compound System

Measurements of pre-scission neutron multiplicities in heavy ion induced fusion-fission reactions provide useful information on fission dynamics and the effects of nuclear viscosity on the fission process [15].

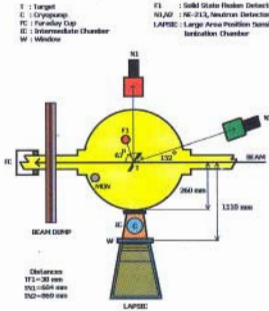

Fig.5 : Schematic of the experimental set-up for measurement of mass dependence of neutron multiplicity

To investigate further the fragment mass dependence of neutron multiplicities in heavy ion induced reactions, we have measured the fragment-neutron angular correlations for emission along and perpendicular to the fission direction for $^{19}F+^{209}Bi$ system at 108 MeV projectile energy. As shown in Fig. 5, a silicon surface barrier detector (F1) and the LAPSIC were used to detect the complementary fission fragments. The neutrons were detected by two (6inch ϕ × 5inch thick) NE-213 neutron detectors placed at 90° and 152° with respect to the beam direction to detect coincident neutrons along and perpendicular to the fragment direction. By measuring the fragment-neutron angular correlations at ~ 0° and ~ 90°, one can deduce the average pre-scission and post-scission neutron multiplicities in the fission process.

The pulse shape discrimination property of the NE-213 detectors was used to differentiate neutrons from the gamma rays. The efficiencies of neutron detectors were determined from Monte-Carlo simulations. Pre-scaled singles fission events were also recorded to obtain neutron multiplicity per fission. The neutron energy was determined from the measured time of flight. The neutron energy spectra were obtained after correcting for the neutron detection efficiency for each neutron detector. The parameters for pre-scission and post-scission components are derived by carrying out moving source fits to the observed neutron energy spectra.

It is assumed that pre-scission neutrons are emitted from a source moving with a center of mass velocity of the compound system.

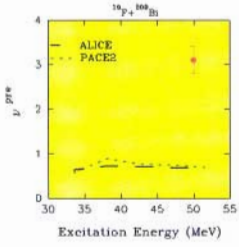

Fig. 6 : Experimentally observed pre-scission neutron multiplicity as compared to that predicted from statistical models

The emission of the post-scission neutrons is from the two fully accelerated fragments. In both cases, emission from the rest frame of the emitting system is assumed to be isotropic. From the fitted values of ν^{pre} and ν^{post}, the total neutron multiplicity was derived as:

$$\nu^{total} = \nu^{pre} + 2\times(\nu^{post})$$

which is found to be 4.06 for the present system. Fig. 6 shows the value of ν^{pre} (filled circle) measured in this work alongwith the results of ALICE (solid line) and PACE2 (dots) calculations using a level density parameter equal to $A_{cn}/10$ MeV^{-1}, as a function of the excitation energy of the ^{228}U compound system. It is seen from Fig. 6 that the measured values are much higher than the statistical model calculations. Therefore considerable number of neutrons are emitted in the fission process over and above those expected from the statistical phase space considerations.

This result implies that there is large amount of time delay involved in the fission process in this reaction. The excess number of pre-scission neutrons, $\nu^{pre(excess)}$ can be related to the total dynamical time available in the fusion-fission process and is expressed as:

$$\nu^{pre\ (excess)} = \nu^{pre\ (measured)} - \nu^{pre\ (calculated)}$$

where $\nu^{pre\ (calculated)}$ is the value predicted by the statistical model. The dynamical fission times $\tau_{fission}$ of the fissioning system can be deduced from the number of excess neutrons, $\nu^{pre}_{(excess)}$. Thus a given ν^{pre} can be mapped directly to the time since formation of the nucleus. The $\tau_{fission}$ value as deduced from this analysis is found to be $120(\pm10)\times10^{-21}$ seconds for ^{228}U system, corresponding to a level density parameter $a_n = A/10$ MeV^{-1} and $a_n = a_f$. This time scale is in broad agreement with the earlier systematics for the fusion-fission time scales [16] for systems having similar excitation energies and fissility. We detected the two fragments (M1 and M2) in coincidence in F1 and LAPSIC and also looked for its effects on the measured neutron multiplicities. For the symmetric split, mass window was selected from 104u to 124u i.e. ± 10 mass units with respect to symmetric mass split at 114u, for the ^{228}U compound system, whereas for the asymmetric mass splits the mass window extended from 125u to 145u. Fig. 7 shows the neutron energy spectra along with the fits for the pre-scission and post-scission

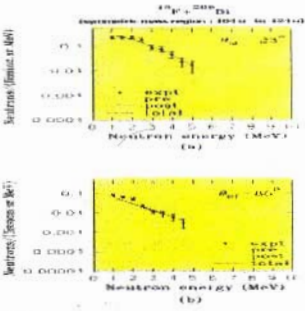

Fig. 7 : Neutron multiplicities for symmetric mass split in ^{228}U

Table 1

Neutrons in coincidence with	ν^{pre} (error)	$2\times\nu^{post}$ (error)	ν^{total} (error)	T^{pre} (MeV)	T^{post} (MeV)
Fission singles in F1	3.11±0.30	1.84±0.12	4.95±0.32	0.90	0.63
M1-M2 dependence (symmetric region) (104 u to 124 u)	2.83±0.25	1.58±0.11	4.41±0.27	1.00	0.56
M1-M2 dependence (asymmetric region) (125u to 145u)	3.31±0.31	2.24±0.15	5.55±0.34	0.58	1.35

components for ^{228}U compound system for symmetric split region. The values for ν^{pre}, ν^{post}, T^{pre} and T^{post} are listed in Table 1 for both the integral and mass dependent measurements. For the mass dependent measurements we find that ν^{pre} is enhanced for asymmetric splits as compared to symmetric splits and this is attributed to the variations in the fragment mass distributions at different stages in multiple chance fission at medium excitation energies [17].

Conclusions

In conclusion, the present work concerns the investigations of the dynamics of heavy ion induced fusion-fission reactions through mass-energy correlations of fission fragments, mass dependence of fission fragment anisotropy and also the studies on the pre-scission neutron multiplicities in the fission reactions. The shell effects seem to play an important role in deciding the mass widths in case $^{19}F+^{209}Bi$ reaction at below barrier energies. In the $^{11}B+^{237}Np(\alpha>\alpha_{BG})$ reaction, the fragment anisotropy is seen to be nearly independent of the fragment mass whereas for the $^{16}O+^{209}Bi(\alpha<\alpha_{BG})$ system, the anisotropy is seen to decrease with increasing fragment mass asymmetry. The results are discussed on the basis of the statistical model of fragment angular distributions and mass division in the fission process. Pre-scission neutron multiplicities have been measured for the first time in the fission of ^{228}U compound system and the results suggest that there is large dynamical delay $[\sim 120(\pm 10)\times 10^{-21}$ seconds] in the fission process in this system. The enhanced values of neutron multiplicity for asymmetric splits as compared to symmetric splits is suggestive of the existence of multiple chance fission at medium excitation energies. The present experiments carried out with various target-projectile systems have provided important results from the point of understanding the various dynamical models of the fusion-fission process.

Acknowledgements

I am thankful to Dr. R.K.Choudhury for his continuous guidance and motivation for this work. I am also grateful to all the collaborators in this work for their kind help and support.

References

1. R. K. Choudhury, A. Saxena, V. S. Ramamurthy, D. M. Nadkarni and S. S. Kapoor, Nucl. Phys. A**463** 597 (1987).
2. A.Bohr in *Proceedings of the Second United Nations International Conference on Peaceful Uses of Atomic Energy, Geneva, 1958* (United Nations, New York, 1958) vol.15 p 398.
3. V. S. Ramamurthy, S. S. Kapoor, R. K. Choudhury, A. Saxena, D. M. Nadkarni, A. K. Mohanty, B. K. Nayak, S. V. S. Sastry, S. Kailas, A. Chatterjee, P. Singh and A. Navin, Phys. Rev. Lett. **65**, 25 (1990).
4. A.Saxena, A.Chatterjee, R.K.Choudhury, S.S.Kapoor and D.M.Nadkarni, Phys. Rev. C**49**, 932 (1994).
5. L. M. Pant, D. C. Biswas, B. V. Dinesh, R. G. Thomas, A. Saxena, Y.S.Sawant and R.K. Choudhury. Communicated to NIMA (2001).
6. L. M. Pant, A. Saxena, R. K. Choudhury and D. M. Nadkarni. Phys. Rev. C**54** 2037 (1996).
7. D. J. Hinde, H. Ogata, M. Tanaka, T. Shimoda, N. Takahashi, A. Sinohara, S. Wakamatsu, K. Katori and H. Okamura, Phys. Rev. C**39** 2268 (1989).
8. M. G. Itkis, Yu. Ts. Oganessian, G. G. Chubarian, V. S. Salamatin, A. Ya. Rusanov and V. N. Okolovich, (*Proceedings of the XV EPS Conference on Low Energy Nuclear Dynamics (LEND-95)*, St. Petersburg, Russia, 1995, edited by Yu. Ts. Oganessian (World Scientific, Singapore 1995) p177.
9. I. V. Pokrovsky, M. G. Itkis, J. M. Itkis, N. A. Kondratiev, E. M. Kozulin, E. V. Prokhorova, V. S. Salamatin, V. V. Pashkevich, S.I. Mulgin, A. Ya. Rusanov, S. V. Zhdanov, G. G. Chubarian, B. J. Hurst, R. P. Schmitt, C. Agodi, G. Bellia, L. Calabretta, K. Lukashin, C.Maiolino, A. Kelic, G. Rudolf, L. Stuttge and F. Hanappe, Phys. Rev. C**62** 014615 (2000).

10. K.-H. Schmidt, A. R. Junghans, J. Benlliure, C. Böckstiegel, H. -G. Clerc, A. Grewe, A. Heinz, A. V. Ignatyuk, M. de Jong, G. A. Kudyaev, J. Müller, M. Pfützner, and S. Steinhäuzer, Nucl. Phys. A**630** 208c (1998).
11. R.Freifelder, M.Prakash and J.M.Alexender, Phys. Rep. {\bf 133}, 315(1986)
12. L. M. Pant, R. K. Choudhury, Alok Saxena and D. C. Biswas. Eur. Phys. J. A **11**(1) 47-58 (2001).
13. M.Abe, KEK Report No.86-26, KEK, TH-28.1986
14. B. John, A. Nijasure, S. K. Kataria, A. Goswami, B. S. Tomar, A. V. R. Reddy and S. B. Manohar, Phys. Rev. C**51**, 165 (1995).
15. J. O. Newton. Pramana **33** 175 (1989).
16. D. J. Hinde, H. Ogata, M. Tanaka, T. Shimoda, N. Takahashi, A. Shinohara, S. Wakamatsu, K. Katori and H. Okamura, Phys. Rev. C**39** 2268 (1989).
17. L. M. Pant, Alok Saxena, R. G. Thomas, D. C. Biswas and R. K. Choudhury Communicated to Eur. Phys. J. A (2002).

Dr L.M.Pant's thesis work on "Heavy-ion induced fusion-fission reactions" was awarded the best thesis presentation in the 46th DAE-BRNS Symposium on Nuclear Physics held at Saha Institute of Nuclear Physics, Kolkata during December 26-30, 2001.

About the author ...

Dr L.M.Pant *(M.Sc. - Physics, Lucknow University) graduated from the 31st batch of the BARC Training School and joined Nuclear Research Laboratory at Srinagar (Kashmir) in 1988. Since 1990, he is working in the Nuclear Physics Division in various experimental activities using the Pelletron Accelerator Facility. He obtained his Ph.D. degree from Mumbai University in 2001. His research interests include studying the dynamical aspects of heavy-ion induced fusion-fission reactions. He has made significant contributions in the mass-energy correlations and neutron multiplicity measurements of fission fragments. He has participated in an experiment at LNL, Legnaro, Italy, using the neutron ball facility for studying the fission dynamics in the synthesis of Super Heavy Elements (SHE). His primary contributions are in the design and development of position sensitive ionization chambers and liquid scintillators.*

Solvent Effects on the Reaction of Organohaloperoxyl Radical with Bovine Serum Albumin: A Pulse Radiolytic Study

Ravi Joshi and T. Mukherjee
Radiation Chemistry & Chemical Dynamics Division
Bhabha Atomic Research Center

Abstract

The oxidation reactions of the bovine serum albumin (BSA), a carrier protein, with organohaloperoxyl radicals in aqueous-glycerol solution have been studied at higher viscosity, pH and different solvent polarities using the pulse radiolysis technique. In this medium of higher viscosity (7.7 cP), unlike in dilute aqueous solution (~0.9cP), electron transfer from tyrosine to tryptophan radical has been clearly observed to takes place. The oxidation of BSA, tryptophan and tyrosine in this medium has been compared with that taking place in dilute aqueous solutions. The kinetics of oxidation of BSA have been found to be affected by viscosity, pH and polarity of the medium.

Introduction

The radiation-induced modification, damage, protein-protein and protein-DNA cross-linking is a subject of interest to radiation chemists, biologists and clinicians. The redox reaction kinetics of various proteins and enzymes in dilute aqueous solutions have been well reported [2] but the reactions, which take place in cellular environment, are expected to be different compared to those in a dilute aqueous solution. This is of significance due to the fact that biological systems have high viscosity and self-assembly, which increases efficiency of the biological processes. It is recognized that charge migration can facilitate transport of radical-centre away from the initial site. Thus the harmful cross-links can be formed at amino acids far away from the site where the primary reaction occurs. The effects of solvent polarity and viscosity on the free radical induced oxidation reactions of proteins with free radicals, though very important, have not been reported. The difficulty in studying oxidation reaction in viscous medium arises because of the high concentration of solutes necessary for increasing the viscosity of the medium. The kinetics and mechanism of reduction reaction of BSA are known to be affected by solvent properties [3,4].

Experimental

Pulse radiolysis of the solutions has been performed by 7 MeV electron pulses of 500 nano-seconds duration using the linear electron accelerator in RC &CD Division, BARC. The energy deposition by high-energy electrons, ionizing radiation, produces transient species in micro-molar concentration in the medium. Appropriate chemical system is used to convert these transient species into another specific transient species to study the desired chemical reaction. The primary species produced upon radiolysis of water are:

$$H_2O \xrightarrow{\text{7 MeV electrons}} e_{aq}^-, H^{\cdot}, {}^{\cdot}OH \ldots \quad (1)$$

The solutes were present in a medium containing glycerol (45 wt%), 2-propanol (3 M), phosphate buffer (2×10^{-3} mol dm^{-3}) and CCl_4 (4×10^{-2} mol dm^{-3}). The viscosity of this medium has been measured to be 7.7 cp with Analytical Viscometer AV-250 (DjScientific) and Ostwald viscometer. The dielectric constant of this medium (ca. 63.66) is lower than that of pure water (78.5). The dielectric constant of the medium has been calculated by taking the algebraic sum of the dielectric constant of a component multiplied with its mole fraction. Glycerol was added to increase the viscosity

9933of the medium and 2-propanol was used to dissolve CCl_4. Glycerol and 2-propanol scavenge H and OH radicals to produce species un-reactive in the time scale of observation. The reactions, which take place, are:

$$H / OH + CH_3CHOHCH_3/glycerol \longrightarrow H_2/H_2O + CH_3C\,OHCH_3/glycerol \quad (2)$$

$$Cl_4 + e_{aq}^- \longrightarrow Cl^- + CCl_3^\cdot$$

$$CCl_3^\cdot + O_2 \longrightarrow CCl_3O_2^\cdot \quad (3)$$

$$CCl_3O_2^\cdot + S \longrightarrow CCl_3O_2^- + S^+ \quad (4)$$

The transients were then followed by kinetic spectrophotometry from nano-seconds to milli-seconds in the wavelength range of 200-800 nm. The measurements were done at 26 °C. The error in the measurement of rate constants is ± 10 %. Trichloromethyl-peroxyl radical ($CCl_3O_2^\cdot$) is an organo-haloperoxyl radical which causes one-electron oxidation of the solute along with addition and is used to study solvent effects on the reaction of peroxyl radicals with organic solutes [5]. Charged species are produced in the reaction 4 from uncharged species and so the reaction also depends on the polarity of the medium.

Results and Discussion

Effect of viscosity

Transient absorption spectrum obtained from the reaction of BSA with $CCl_3O_2^\cdot$ at pH 6.8 in this medium shows (Fig. 1) simultaneous decay of 460 nm absorption and growth of 410 nm absorption (inset of Fig. 1) after the first step of formation of absorption at these two positions (scheme 1 & 2). This suggests some radical transformation, which has not been reported earlier in dilute aqueous solutions.

Transient absorption spectrum recorded for the amino acids, tryptophan, tyrosine and disulfide links, more prone to reaction with $CCl_3O_2^\cdot$, suggest that the transient absorption at 410 and 460 nm is due to tyrosine ($TyrO^\cdot$) and tryptophan ($Trp^\cdot$) radicals, respectively. In this medium Trp radical has been found to have transient absorption maximum at 460 nm instead of

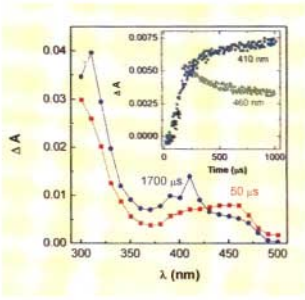

Fig. 1

510 nm peak observed in dilute aqueous solutions. However, 460 nm transient absorption decayed at a rate of $8.8 \times 10^3\ s^{-1}$ (first order) and second step of growth of absorption at 410 nm has been found to be $1.0 \times 10^3\ s^{-1}$. Similar transient absorption spectrum has been observed in the reaction of BSA with $CHCl_2O_2^\cdot$ at pH 6.8 in this medium confirming that the transient absorptions are due to reaction with organo-haloperoxyl radical only. The measured reaction rate constants with $CHCl_2O_2^\cdot$ radical (σ =5.88) are little lower (Table 1) than that with $CCl_3O_2^\cdot$ (σ = 5.88), in agreement with the reduced Taft parameter (σ). The antioxidant effect of ascorbate in scavenging protein radical has also been observed in this medium with $k = 2.4 \times 10^6\ dm^3\ mol^{-1}\ s^{-1}$.

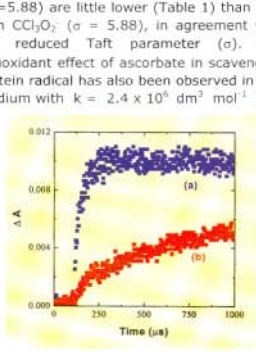

Fig. 2

Second step formation of tyrosine radical reduces to even lower rate at 90% v/v glycerol and pH 6.8 (Fig. 2b). Such radical transformation is reported for lysozyme (a protein) in dilute aqueous solution but has not been observed in the present medium. This suggests even some conformational changes of protein in this medium.

The rate constants for the reactions studied are given in table 1.

Table 1 : Rate constants for the reaction of different solutes with $CCl_3O_2^{\cdot}$ radical

Solute	PH	λ (nm)	k_f ($dm^3mol^{-1}s^{-1}$) x 10^{-8}	
			Water	45 wt % glycerol
Tryptophan	6.8	460	---	2.25
	6.8	520	0.85	0.39
Tyrosine	10.0	410	0.71	0.54
DMDS	6.8	380	42.0	35.0
BSA	6.8	400	4.8	3.3
	6.8	460	5.7	3.2
	6.8	510	13.0	8.6
BSA + $CHCl_2O_2^{\cdot}$	6.8	400	---	1.1
	6.8	460	---	3.1

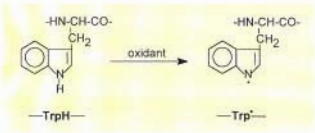

Scheme 1 : Formation of tryptophan radical

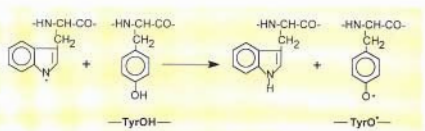

Scheme 2 : Radical transformation from tryptophan to tyrosine

The rate constants have not been found to reduce in proportion to increase in viscosity. This suggests that diffusion affects the rate constants but is not the only factor in these reactions.

Effect of pH

Transient absorption spectrum obtained from the reaction of BSA with $CCl_3O_2^{\cdot}$ in this medium at pH 10 also shows (Fig. 3) simultaneous decay of 460 nm absorption and growth of 410 nm absorption. This suggests that radical transformation takes place even at pH 10. It has been found that even at pH 10 reaction rate constants decrease with increase in viscosity of the medium but are still higher than that at pH 6.8 (see table 1). The decay rate of 460 nm absorption ($Trp^{\cdot}$) has been found to be the same at pH 6.8 and 10 suggesting that it is due to the same process of charge transfer from tyrosine to $Trp^{\cdot}$

Higher value of ΔA at 410 nm with increase in pH is in accordance with the fact that the basic form of any radical has higher molar extiction coefficient than that of the acidic form. According to the reactivities of the amino acids tryptophan and tyrosine with $CCl_3O_2^{\cdot}$ radical in this medium, at neutral pH almost 100 % of the $CCl_3O_2^{\cdot}$ radical should react with tryptophan and even at pH 10 almost 30 % of the radicals should react with tryptophan in the first step followed by the radical transformation.

Effect of Polarity

The reaction of BSA with $CCl_3O_2^{\cdot}$ at pH 6.8 has been studied at different solvent polarity to study the effect of polarity exclusively (Table 2). The reaction rate constants for the formation of both tryptophan and tyrosine radicals decrease with decrease in dielectric constant (ε) of the medium.

Table 2 : Rate constants ($k \times 10^{-8} dm^3 mol^{-1} s^{-1}$) for the oxidation of BSA with $CCl_3O_2^-$ in different solvents

Solvent*	ε	at 410 nm	at 460nm
2-propanol (20 % v/v))	75.20	4.8	5.7
tert-butanol (25 % v/v)	74.57	3.0	5.0
tert-butanol (40 % v/v)	71.05	2.0	1.8
tert-butanol (50 % v/v)	67.89	1.1	1.1
glycerol (45 wt%)+ 2-propanol (30 % v/v)	63.66	3.3	3.2

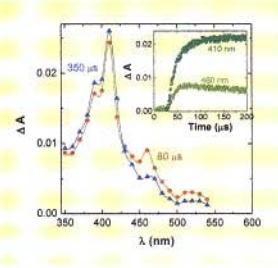

Fig. 3

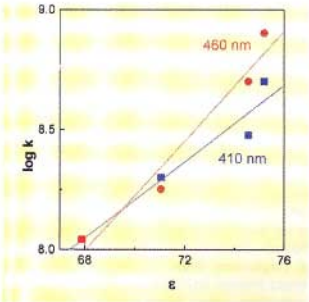

Fig. 4

This is in accordance with the fact that reduction in polarity reduces the rate of formation of charged species (see eqn. 4). The logarithms of reaction rate constants at 410 and 460 nm, in this medium, have been found to vary linearly with the dielectric constant of the medium (Fig. 4). However, the rate constants for the aqueous-glycerol solution having even lower dielectric constant have not reduced to further lower values but are higher (see table 2). This suggests that reduction in polarity reduces the rate constants for the reaction of BSA with $CCl_3O_2^-$ but this is not a major factor.

Conclusions

The reaction of BSA with $CCl_3O_2^-$ radical in aqueous-glycerol and 50 % (v/v) tert-butanol shows a clear charge transfer from tyrosine to the tryptophan radical unlike in dilute aqueous solution. $Trp^{\cdot}$ radical has transient absorption maximum at 460 nm unlike in dilute aqueous solution at 510 nm. The rate constants for the reaction of BSA with $CCl_3O_2^-$ measured at 410 and 460 nm and at pH 6.8 in this medium follow the equation:

$$\text{Log } k = A + B.\varepsilon + C / \eta.$$

The rate constants for the formation of tryptophan and tyrosine radical of BSA decrease with decrease in polarity and increase in viscosity (η) of the medium. It can be said that charge transfer takes place in physiological environments in those reactions, which is not observed in dilute

aqueous solutions. This study suggests that not only kinetic and/or thermodynamic parameters but also three-dimensional structure of the protein molecule affecting the proximity of the donor-acceptor pair is also a governing parameter in charge transfer.

References

1. Ravi Joshi and T. Mukherjee, Charge transfer between tryptophan and tyrosine in casein: a pulse radiolysis study, Biophys. Chem. 96 (2002) 15-19.
2. G. V. Buxton, C. L. Greenstock, W. P. Helman and A. B. Ross, Critical Review of rate constants for reactions of hydrated electrons, hydrogen atoms and hydroxyl radicals ($^{\cdot}OH/O^{\cdot-}$) in aqueous solution, J. Phys. Chem. Ref. Data 17 (1988) 513-886.
3. Ravi Joshi, S. Adhikari, C. Gopinathan and P. O'Neill, Reduction reactions of bovine serum albumin and lysozyme by $CO_2^{\cdot-}$ radical in polyvinyl alcohol solution: a pulse radiolysis study, Radiat. Phys. Chem. 53 (1998) 171-176.
4. Ravi Joshi, S. Adhikari and C. Gopinathan, Pulse radiolytic reduction study of bovine serum albumin and lysozyme in quaternary microemulsion, Res. Chem. Intermed. 25 (1999) 393-401.
5. P. Neta, R. E. Huie, P. Maruthamuthu and S. Steenken, Solvent effects in the reactions of peroxyl radicals with organic reductants. Evidence for proton transfer mediated electron transfer, J. Phys. Chem. 93 (1989) 7654-7659.

This paper received the "Association of Kineticist Award, 2001" in Physical Chemistry section at 38th Annual Convention of Chemists held at J. N. V. University, Jodhpur in December 2001.

About the author ....

*After obtaining M. Sc. in Physical Chemistry from MLS University, Udaipur, in 1993, **Ravi Joshi** joined Chemistry Division, BARC, in 1995, through BARC Training School Course (38th batch). Ravi Joshi has submitted his Ph. D. thesis on "Free radical characteristics and reactions of some biomolecules in aqueous and microheterogeneous media" (Guide: Dr. T. Mukherjee). His current research interests include free radical reactions of biomolecules, natural products, drugs and solvent effects on free radical reactions.*

Separation and Recovery of Pu From a Mixture Containing Macroconcentration of Th

L.B. Kumbhare, P.K. Mohapatra and V.K. Manchanda
Radiochemistry Division
Bhabha Atomic Research Centre

Abstract

A two-stage ion-exchange separation method was developed for the quantitative separation of Pu from macro quantity of Th from nitric acid medium. The first step involves quantitative sorption of plutonium from the mixture while about 90% of Th could be washed in 6 column volumes. The plutonium, which was eluted using 0.5M HNO_3 + 0.2M hydrazinium nitrate + 0.2M hydroxyl ammonium nitrate, and the residual (10%) Th was subsequently loaded onto a cation exchange column in a second step. The Pu was easily washed with 2M HNO_3 (in ~ 8 column volumes) containing 0.2M hydrazinium nitrate + 0.2M hydroxyl ammonium nitrate. The final elution of thorium from the cation exchange column was achieved using 6 column volumes of 1M α-hydroxy isobutyric acid. The recovery of both plutonium and thorium were found to be > 99% and > 98% respectively.

Introduction

Due to limited uranium deposits and vast thorium reserves in our country, thorium based fuels are being proposed for the next generation of power reactors. Advanced Heavy Water Reactor (AHWR) employing ThO_2 with 4% PuO_2 as the fuel is at an advanced stage of design. It is desirable to develop separation processes for the recovery of Pu and Th from the fabrication scrap solution of the proposed AHWR fuel containing 200 g/L Th, 8 g/L Pu, 4 M HNO_3, 0.1M $Al(NO_3)_3$ and 0.01M HF.

The ion exchange and the solvent extraction methods are being studied in our laboratory for Pu- Th separation. In the solvent extraction route, the tail end purification is proposed to be done by an ion exchange method. The difference in the complexing ability of Pu(III) and Th(IV) in HNO_3 medium has been utilized for Pu/Th separation through cation exchanger [1]. An independent separation method based on a two-stage ion exchange method (anion exchanger followed by cation exchanger) is used in the present study. The present paper deals with a sequential anion-exchange/ cation-exchange method developed for the recovery of Pu and Th from HNO_3 medium. The oxidation state of Pu was maintained as 4+ during anion exchange resin loading and as 3+ during elution from anion exchanger and during cation exchange resin loading/ elution.

Experimental

Batch distribution experiments

Batch experiments were carried out using both cation exchange as well as anion exchange resins (about 100-200 mgs) by equilibrating with 2 ml of acid solution containing tracer (Pu-239 / Th-234) for 1 hr in a thermostat bath at 25± 0.5° C. The K_d values for Th (IV) and Pu (III) as a function of acid concentrations were determined by the following formula.

$$K_d = \frac{(C_0 - C)/ W}{C/ V}$$

where, C_0 = Initial concentration of metal ion, C = Total concentration of metal ion after equilibration; W = Weight of resin taken in gm, V = Volume of the aqueous phase in ml.

Column experiments

Studies with an anion exchange column: Column studies using an anion exchange column (2.8 gm of resin, 70 cm x 1 cm) were carried out with various synthetic solutions viz. Pu(III) alone (μg/ml), Th(IV) alone (200 mg/ml), and a mixture containing macro Th (200mg/ml) and Pu (in μg/ml) at 2M HNO_3. These experiments were later scaled up to a synthetic mixture containing 200 mg/mL of Th and 8mg/mL of Pu.

Studies with an cation exchange column: Cation exchange studies using a column (0.8gm of resin, 10 cm x 0.4 cm) were carried out for synthetic solutions containing 8 mg/mL of Pu in 2M HNO_3 + 0.2M hydroxyl ammonium nitrate + 0.2M hydrazinium nitrate along with varying amounts of Th (8 mg/ml to 200 mg/mL). The fraction containing entire Pu along with residual Th along with HN and HAN was adjusted to 2M HNO_3 by adding few ml of concentrated HNO_3. This solution was passed over preconditioned column containing 0.8 gm of cation exchanger Biorad AGW 50x4 (50-100 mesh). Subsequently Pu was recovered by washing and Th was eluted by α-HIBA.

Results and discussion

Batch experiments

The batch distribution studies with the anion exchange resin were carried out in a wide range of acidity (1 - 8M HNO_3). As shown in Table 1, the K_d values for Th(IV) and Pu (IV) increased with the aqueous acidity and for all acidities, K_d values for Pu(IV) were higher than those for Th. This is due to the presence of predominating Pu anionic species compared to that of Th under identical conditions [2]. Separation factor values were found to be nearly constant at lower acidities and increased thereafter. Due to the possibility of easy washing of Th at lower acidity, the column experiments were carried out at 3M HNO_3.

For the cation exchanger, the batch distribution studies were carried out in the acid concentration range of 0.5M - 5M HNO_3. As shown in Table 2, the high separation factors (Th / Pu) of ~ 28 and 60 were

Table 1: Uptake of Pu(IV) and Th(IV) by Dowex 1x4 (50 – 100 mesh) as a function of acid concentration

$[H^+]$	HNO_3	
	$K_{d,Pu}$	$K_{d,Th}$
1	58	3.1
2	117	5.3
3	200	8.9
4	420	18
5	450	57
6	450	107
7	770	190
8	4010	206

Table 2: Uptake of Th(IV) and Pu(III) by cation exchanger Biorad 50× 8 (50-100 mesh) as a function of HNO_3 concentration in the presence of 0.2M HAN and 0.2M HN

$[HNO_3]$, M	$K_{d,Pu(III)}$	$K_{d,Th(IV)}$	S.F. $= K_{d,Th(IV)} / K_{d,Pu(III)}$
0.5	109.5	>1000	>9
1	36.4	1000	28
2	10.3	604	59
3	4.4	119	27
4	2.4	43.7	18
5	1.4	24.8	18

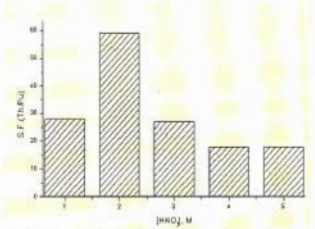

Fig.1 : Separation factors (Th/Pu), in cation exchanger as a function of acidity

obtained at 1M and 2M HNO_3 respectively. This could be attributed to two factors, competition with increasing protons and depletion of cationic metal ion species as acid concentration increased. Over the entire acidity range (0.5-5M), $K_{d,Pu(III)}$ was lower than $K_{d,Th(IV)}$. In the acidity range 0.5-1M, K_d for both the metal ions were higher which

demanded large column volume for elution of both the ions whereas in 3-5M acid range, K_d values for both the metal ions were found to be too low to be held onto the column. 2M HNO_3 was thus the optimum acidity as $K_{d,Pu(III)}$ is very low (~10) and $K_{d,Th(IV)}$ is sufficiently high (~600) with the separation factor of ~ 60 (Fig. 1).

Column experiments

In view of the low Th(IV) K_d value, high Pu(IV) K_d value and high separation factor (Pu / Th), it was decided to carry out the column studies using the anion exchanger at 3M nitric acid. On the other hand, the low K_d value of Pu(III) and high K_d value of Th(IV) in cation exchange resins prompted us to carry out the experiments at 2M nitric acid. The sorption of Th and Pu were studied individually as well as with a synthetic mixture conforming to the proposed AHWR scrap composition. The loading of both Th and Pu onto the anion exchange column (2.8 gm of resin, 70 cm x 1 cm) was carried out from 3M HNO_3. While Th could be washed away from the column with 3M HNO_3 itself, it was required to reduce Pu to Pu^{3+} using 0.2M Hydrazinium nitrate + 0.2M hydroxyl ammonium nitrate in 0.5 M HNO_3.

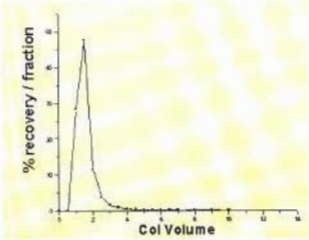

Fig. 2: Pu elution with 0.4M HNO_3+0.3M HAN+0.3M HN

Based on these principles, the separation of Pu-Th from synthetic solution containing 205 mg/ml of Th and 8.1 mg/ml of Pu was carried out in two stages. First stage involving anion exchange at 3M HNO_3, Pu was adsorbed strongly whereas Th was adsorbed very weakly. About 90% of Th was washed out in 7-8 column volumes leaving entire Pu and residual Th in the column. Both the metal ions eluted quantitatively with 0.4M HNO_3 + 0.3 M HN and HAN in 6 column volumes (Fig. 2). This stage helped to deplete the bulk of Th thereby avoiding a large column capacity and large volume of the eluent required in the second stage of cation exchange. Eluted portion from first stage was adjusted at 2M HNO_3 containing about 0.2 M HN + 0.2M HAN and loaded onto the cation exchange column (0.8gm of resin, 10 cm x 0.4 cm). Pu was recovered quantitatively by washing with 8 column volumes followed by Th elution in 6 column volumes (Fig. 3) using 1M α-HIBA at pH 4.0. Thus, the cation exchanger method facilitated the removal of Pu in the trivalent state from residual Th.

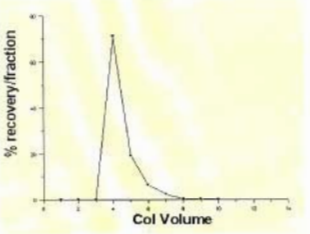

Fig.3 : The elution by 1M HIBA at pH=4 (loading solution Th)

This way the overall Pu recovery was > 99% while > 98% Th could be recovered when the recovered Th were combined from both the anion exchanger as well as cation exchanger columns. This two-stage column chromatographic separation method can be used for the separation of Pu and Th from the AHWR fuel scrap in nitric acid medium.

Conclusion

Pu-Th could be efficiently separated from stripped solution by cation exchange method at the loading conditions of 2M nitric acid containing 0.2M of hydroxyl ammonium

nitrate as reducing agent and 0.2M of hydrazinium nitrate as holding reductant. 1M α-HIBA was found to be an efficient eluting reagent for thorium and had no interference in the oxalate precipitation. Quantitative recovery of Pu from the synthetic solution containing 200g/L of Th and 8g/L of Pu was successfully achieved through two stage process where anion exchange was followed by cation exchange.

References

1. J. J. Katz, G. T. Seaborg, and L. R. Morss, The chemistry of the actinide elements, second edition, Chapman and Hall, New york, (1986) p.p.550-561
2. Plutonium Ion Exchange Process, TID 7607 (1960)

This paper received the Best Poster award at the 20th Annual Council of Chemists held at Mysore University, Mysore, during October 2001

About the authors ...

Mr L. B. Kumbhare *joined Radiochemistry Division, BARC, in 1998 after obtaining his M.Sc. (Chemistry) from Nagpur University and after successfully graduating from the 41st batch of the B.A.R.C. Training School. His main area of research is actinide partitioning using branched mono amides and diamides. Mr. Kumbhare has carried out syntheses of several such reagents. His research interest also includes ion exchange separation of actinides.*

Dr P. K. Mohapatra *joined the Radiochemistry Division, BARC in 1987 after completing his M.Sc. in Inorganic Chemistry from Utkal University and graduating from the 30th batch of the BARC Training School. He was awarded Ph.D. by Mumbai University in 1994. Dr Mohapatra carried out post-doctoral research work at University of Liege, Belgium under BOYSCAST Fellowship, DST (1998 - 1999) and University of Mainz, Germany, under Humboldt Fellowship (1999 - 2000) on 'MRI contrast agents' and 'Chemistry of super heavy elements', respectively. His research interests include the chemistry of macrocyclic compounds and separation studies of actinides and fission products using novel extractants. Dr Mohapatra has to his credit over 100 publications in international journals and conferences.*

Dr V. K. Manchanda *joined the Radiochemistry Division, BARC, in 1969 after graduating from Delhi University and from the 12th batch of the BARC Training School. He was awarded Ph.D. by Mumbai University in 1975 and carried out Post-Doctoral work at UTEP, Texas, U.S.A. as Fulbright Scholar (1985-87). His research interests include thermodynamics and kinetics of complexes of macrocyclic ligands with lanthanides and actinides, physico-chemical studies on actinide complexes, design and synthesis of novel extractants for actinides and chemical quality control of Pu based fuels. A recognised Guide in Chemistry for M.Sc. and Ph.D. by University of Mumbai, Dr Manchanda currently Heads the Actinide Chemistry Section, Radiochemistry Division. Dr. Manchanda has over 250 publications to his credit.*

Pilot Plant Experience of Recovery of Rare, Natural Protactinium from the Insoluble Muck: Installation and Operation

S. Sethi, P. Anupama and L.M. Gantayet
Laser & Plasma Technology Division
Bhabha Atomic Research Centre

and

M. P. Bellary
Chemical Engineering Division
Bhabha Atomic Research Centre

Abstract

The concentration of the protactinium-231, one of the rarest elements on the earth ranges from 0.2ppb to 0.9ppb in the uranium bearing ores in India. The maximum concentration of ^{231}Pa in one of the streams of the plant processing these ores is 5-6.5 ppb, i.e. the insoluble muck of monazite processing plant of IRE, Alwaye. A pilot plant has been established for the recovery of ^{231}Pa from this stream. The recovery of ^{231}Pa from a ppb level in the low radioactive source requires extreme care in every aspect of the process scale-up, plant operation, material balance, effluent control and safety considerations. In this paper we discuss different experiences of the scale-up and operation of the protactinium recovery plant.

Introduction

^{231}Pa is a recurring nuclide in the Thorium Fuel Cycle, and hence studies related to its behavior at various stages, is important to the future nuclear program in India.

Naturally occurring protactinium (^{231}Pa) is one of the rarest elements in the earth crust, and can be found only in the uranium bearing ore. As its half-life is 32,400years compared to its parent ^{235}U half-life of $3x10^{8}$y, the ratio of protactinium to U is $0.34x10^{-6}$, in the undisturbed geological formations [Palshinn et al.]. In the Indian ores the concentration of protactinium is around 0.2ppb (parts per billion) in Jaduguda ore and 0.9ppb in Monazite sand.

In the uranium ore processing plants this element gets fractionated unevenly into various streams. Rigorous prospecting for protactinium in all the streams of the ore processing plants showed that the richest source of protactinium is the waste insoluble muck at 5-6.5 ppb (dry basis) of the monazite processing plant at IRE, Aluva [Anupama et al. 2001 (a)]. As the waste insoluble muck is an exit stream from the IRE Aluva plant, it could be processed for recovery of ^{231}Pa without disturbing the plant operations.

Brief Description of the Process

A process has been developed for recovery of protactinium from insoluble muck in the bench scale [Anupama et al. 2001 (b)]. The process is based on selective leaching of protactinium from the muck with oxalic acid. The muck contains large quantity of free HCl (30% moisture of 2N HCl strength) and soluble chloride salts of rare earths and thorium, which are readily hydrolyzed at higher pH. Therefore, these have to be carefully removed by HCl wash and then by water wash. Finally, the free HCl acid content in the muck should be reduced to below 0.1N for effective complexing of ^{231}Pa by oxalic acid. This step in the process is called pretreatment.

The pretreated muck is then leached with oxalic acid to bring the protactinium from the insoluble muck to liquid oxalic acid in the form of an oxalate complex. Along with protactinium, other ions as zirconium, niobium, uranium, iron, which form oxalate complexes are also dissolved. The bulk of rare earths and thorium do not dissolve because of low solubility product of their oxalate salts. The dry basis concentration of protactinium in the oxalic acid leachate increases to around 350 ppb. This step in the process is called the leaching step. The protactinium can be recovered from the oxalic acid leachate either by co-precipitation or by ion-chromatography. After careful study of these two options the path of ion-chromatography has been selected.

Ion chromatography on the anionic exchange resin being more selective, the separation factor between protactinium and the co-ions is higher. In this step, the oxalate form of resin is first converted into chloride form. The conversion should be carried out with the least loss of protactinium, as it is known that the K_d factor for protactinium in the mixed oxalic acid and hydrochloric acid medium is lower. After the chloride conversion, zirconium is first eluted with 6N HCl, and then protactinium is eluted with a mixture of 8N HCl and 0.2N HF. Finally, the bed is stripped of uranium and iron ions by 0.2N HCl. The trace fluoride ions are removed by complexing with 0.1N $AlCl_3$. The process steps of the ion chromatography, developed in the laboratory are described by Verma et al. [Verma et al.,2001(a)]. The eluate is precipitated using sodium hydroxide and protactinium concentration now is 10-15 ppm (dry basis). This process was proven in the lab-scale and in 500gm-bench scale. The process flow diagram developed and implemented in the pilot plant is given in Figure 1.

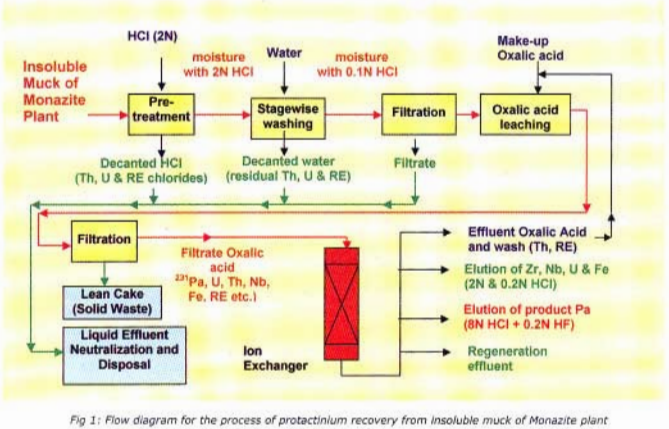

Fig 1: Flow diagram for the process of protactinium recovery from insoluble muck of Monazite plant

Plant Design Considerations

Radioactive solid handling

The ground monazite comes in the average size of 5μm. Handling of these sub micron size particles in large tonnage, and separating the liquid and solid with negligible carryover of solid posed a challenge. Manual handling of slurry, cake and solutions could expose the workers to radioactivity dose and at the same time high degree of sophisticated automation was not warranted for a campaign type of operation. This was taken care of in the proper equipment selection and suitable plant layout. A perspective view of the plant is given in Figure 2.

The plant layout was so designed that gravity flow of the materials was possible to a large extent. Filtration equipment, where normally filter press is used, involves prolonged manual handling of radioactive solids. Drum filters would be too expensive. So a vacuum Nutsche filter was selected.

Effluent control

Reducing radioactive effluent was one of the prime considerations in the plant. For creating vacuum, the normally preferred water-ring pump was again avoided, as it would generate large quantity of low active cooling water effluent spread over a large area of piping, and cooling tower basin. Hence a rotary piston pump, which has a high tolerance to air and moisture, was selected. A suitable trap at the inlet trapped and removed moisture and a homemade mist filter, made of high performance distillation packing removed the oil vapour from the exhaust air. All the other liquid effluent is neutralized in a rubber lined tank. The slurry is assessed for radioactivity and then sent to waste management division, for disposal as per procedure.

Fig.2 : Perspective view of ^{231}Pa recovery plant

Ion exchange equipment

As the ratio of the loading and eluate cycles was 10:1, one ion exchange column with more plumbing for operational flexibility was preferred to two standard ion exchange columns. Pre-concentration being one of the prime objectives in the ion exchange resin, the free board volume over the resin was reduced drastically compared to the conventional ones, so as to allow only for resin shrinkage in oxalate form and expansion of the bed, in chloride and hydroxide form. The design considerations for ion exchange separation are summarised in Table 1.

Table 1: Design Considerations for Ion Chromatography Column

Design Parameters

Loading to Elution batch ratio	10-11 batch Leaching/Elution
Resin Bed Height (GS 300)	1.2 to 1.5 m
Resin Bed Diameter	385 mm
Loading, Washing & Elution Rates	6.0 $m^3/m^2/h$.
Turbidity of Feed solution	< 3 NTU (using micro filter 10, 1.0 & 0.5μm)
Compatible MOC	PP lines FRP (to withstand 4 kg pressure)

Other Considerations

- Single column due to large Loading to Elution batch ratio
- Resin expansion and shrinkage volumes
- Minimal Free board volume
- Compact distributor

Purity of reagents

DM water was used at all stages of the Ion Chromatography. Similarly, the HCl used had to be pure. Instead of purchasing analytical grade HCl at prohibitive cost, HCl was purified in the pilot plant, economically in a ~13litre FFIP (supplied by M/s. Ion Exchange India Ltd.) resin bed in a FRP column. The technical grade HCl from the storage tank was decanted into the resin bed at a controlled flowrate and the purified HCl collected in carbuoys or process tanks. The fumes of HCl were contained by using covered equipment, and covering all openings with wet PP cloth.

Materials of construction

Protactinium is readily hydrolyzed and known to stick to the equipment walls. It would be very difficult to recover 3mg of protactinium from 1Te quantity of solid, and from $4m^3$ of liquid unless the material of construction and the flow medium transporting protactinium are carefully selected. The agitated tanks were made of polypropylene lined FRP, as was the ion-exchange column [both manufactured by M/s Plastochem Fabrication, Trombay, Mumbai-88]. The Nutsche filter was made of FRP [manufactured by M/s Plastochem Fabrication, Trombay, Mumbai-88], with the wetted surface coated with polyvinyl-ester for higher resistance against strong acid mixtures. For liquid transfer, reinforced polythene hoses were used. Teflon lined diaphragm valves with polypropylene body were used. The ball valves did not withstand the wear due to the abrasive fine solids. Polypropylene cloth of nominal pore size was selected as filter medium. For easier filtration, cellulose acetate was used as filter aid wherever a carrier was necessary to remove very small quantities of valuable solid from the liquid. The filter aid was evaluated in the laboratory and was found not to adsorb protactinium-hydroxide. It was found suitable and was used. Polypropylene pumps [manufactured by M/s Antico Ltd., Mumbai] with teflon gland packing or ceramic mechanical shaft seal could handle the acids of the plant with ease.

The stirrers for 2N HCl were rubber-lined, whereas for oxalic acid, SS stirrer with PVC taping was sufficient to withstand one year long operation. Air agitation though

preferred for not breaking the flocs, could not be used to avoid the radioactive aerosols in the environment.

Measurements

Magnetic float in Teflon rotameter was used for the measurement of the flow in the Ion exchange column. At all the stages, tanks were volume calibrated with water and painted. Calibrated volume measurement with stopwatch gave an accurate measure of flow at all stages. Hydrometer and pH papers were extensively used to measure the specific gravity of the liquid and the pH respectively.

Quality control

The strength of the decanted HCl and water washes was determined by titration in the plant by the operator. Suitable procedures were devised in the lab to take care of rare earths chlorides and thorium chloride, while titrating for free HCl. The strength of oxalic acid was determined by titration with $KMnO_4$ in presence sulphuric acid.

Process Implementation in the Plant

Pretreatment

500gm scale tests in the lab, revealed that, thorough mixing is necessary after loosening of the cake. The time taken for dissolution of soluble salts is minimal. At times, the reduction in weight after dissolution was as high as 30%, which was attributed to the higher content of soluble salts due to continued attack by the free acid in the moisture. The main considerations in the scale-up of the step were solid-liquid separation and dilution of the acid in every wash stage. The vacuum filtration with 5μm particle size solid slurry was slow. It was then decided to resort to sedimentation, and sludge dewatering, which can be enhanced by using polyelectrolyte flocculant. Several flocculants were tried for the 2N slurry and 852 Rishabh (852R) [obtained from M/s. Rishabh Metals and Chemicals Ltd., Mumbai-20] was found suitable for use at 80ppm dosage. The flocculant was prepared at 0.2% concentration, for better mixing. The concentration of 80ppm was optimum to give hard flocs, which remained stable during subsequent water washes.

The stirrer used was selected for multipurpose use of the $0.8m^3$ capacity tank [Figure 3]. A small propeller placed at an inclined angle served the purpose of providing minimum shear in the bulk of the fluid and thorough mixing within 45 sec. The conical bottom of the tank was given a slope of 30°, to facilitate easy removal of the sludge.

Fig.3 : Agitation tank used for ^{231}Pa recoveryplant

For decantation, an adjustable height strainer was provided. The decantation rate could be controlled to avoid re-agitation of the sludge. Up to 80% of the liquid added could be decanted, which reduced the requirement of dilution, and consequently the total volume of the effluent.

Filtration of pretreated sludge

The Nutsche filter is mainly used for the filtration of the decanted volume. A layer of coarse solids is first formed, to act like filter aid for deep bed filtration for the nearly clear decant.

The sludge is lowered onto the Nutsche filter for final dewatering and drying (when it cracks). Based on the lab scale data a 1.2m diameter Nutsche with an available ΔP of 460 to 600 mm Hg was found suitable. The cake is removed manually using wooden ladles into polythene-lined drums to store for the next step of operation. The vacuum is created by 100m^3/h rotary piston pumps [manufactured by M/s H. K. Industries, Kalina, Mumbai-98] with an ultimate vacuum of 1 mbar [Figure 4]. The first vacuum trap was an expansion tank, where the moisture condenses, and is drained periodically. The pump exhaust trap is also periodically drained to remove oil-water emulsion. The oil consumption was two litres per 100 hours of operation.

Fig.4 : Vacuum station used for ^{231}Pa recovery plant

Leaching

600 litres of 1M oxalic acid is prepared in the tank. 150 kg of weighed cake is lowered while stirring is on. The stirring time is around $2^1/_2$ hrs. At the end of the extraction cycle the solids are flocculated for better filtration characteristics. 40 ppm of 852R is the optimum concentration of flocculant. The filtration arrangement is similar to the pretreatment step. Here a wash is given with 0.5N oxalic acid to recover the leachate from the cake. The volume of oxalic acid used is the same as the pore volume of the cake.

Loading of ion exchange column

The clarity of the oxalic acid is very important as oxides of zirconium, niobium and iron can adsorb protactinium after the oxalic acid is washed out in the column. Moreover, the column can get silted. The turbidity was measured by nebulometer and found to be 9 NTU. A micro filter of around 10μm, followed by 1.0μm & 0.5μm cartridge was used for the oxalic acid loading step, which reduced the turbidity below 3 NTU.

The loading rate determined at the lab was 6.0 m^3/m^2/h. The column was designed to have 1.2m to 1.5m bed height (lab bed height was around 0.8m) and a volume for holding 10-11 batches of leachate solution. The effluent oxalic acid was quite clear. Initially, in the first bed volume, the oxalic acid strength dropped from 2N to 1.1N, because of the conversion of the ion exchange resin from chloride form to oxalate form. The effluent oxalic acid was held in an intermediate tank and returned for leaching after adjusting the concentration to 2N. In the normal batches the oxalic acid strength reduces to around 1.6N because of its reaction with rare earths and thorium in the pre-treated cake.

Demineralised Water (DM) water wash

The oxalic acid is washed to 0.05N by 3 bed volumes (BV) of demineralised water wash. There is no loss of protactinium in this step.

HCl conversion

Initially 8N HCl and 7N HCl was used for the conversion of the bed. During the operation once due to pump failure, the HCl remained in the column, leading to standing of HCl-oxalic mixture in the column. This led to substantial loss (12% loss of protactinium) from the column. The 7N HCl wash is followed by 6N wash to remove zirconium. During this step a small quantity of protactinium is lost. Niobium is also eluted along with zirconium. The details of the elution steps are discussed by Verma et al. [2001 (b)].

Elution

For elution of protactinium 8N HCl & 0.2N HF eluent was passed through the column at a very slow rate of 1.0 $m^3/m^2/h$, in order to reduce the tailing and the consumption of high molarity acid. Lower consumption of eluate means, less requirement of NaOH for neutralisation. 2.5 BV of eluate was considered adequate. The last 0.5 BV of eluate containing lower quantity of Pa was recycled as the first BV of eluent for the next stage. A typical elution curve for the plant column is shown in Figure 5.

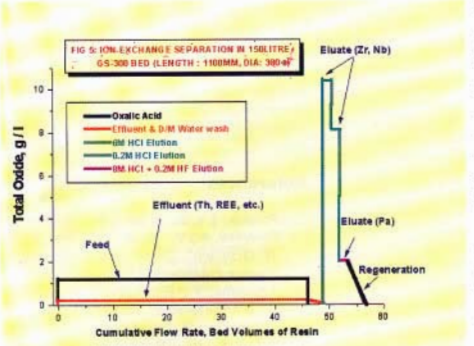

Fig.5 : Ion-exchange separation in 150 litre GS-300 bed (length : 1100 mm, dia : 380Φ)

There was always 5-10% loss in the Ion exchange steps. However, since the gel resin contained negligible quantity of hydrolyzed protactinium, it is expected that this quantity of protactinium would be adhering to the walls of the pipes and equipment.

Neutralisation

The eluent is neutralised, and filtered. The hydroxide containing 16ppm of protactinium was washed with demineralised water and then dissolved in 25litre of 2N oxalic acid for the next stage of Ion chromatography in the same column.

Radiological and Other Safety Procedures

The contact radiation field in the raw muck barrels (150kg) is typically 15mR/h (milli roentgen per hour). The process tanks gave a contact radiation field of 1mR/h. The effluent slurry had an alpha activity of 50-60 Bq/ml. Although these fields are low, the prescribed radiation safety rules were complied with. The workers in the plant wore TLD badges. After a few monthly assessments of the badges, which showed nil dosage, the badges were then counted every quarter. Annual dose received by each worker was also assessed and the records were maintained.

The process vessel walls, the floor and structures of the plant were cleaned everyday to remove slurry splashes, which on standing could give avoidable surface activity. Personnel safety gears, such as, facemasks, PVC gloves, aprons, safety shoes were mandatory for any work in the plant. The operators were provided rigorous training to maintain high safety standards.

Table 2: Production Figures (15 September 2000 – 18 December 2001)

Batch size	Pretreatment	200kg insoluble muck
	Leaching	150kg insoluble muck
No. of batches	Pretreated	~90 (200kg batch) at BARC 2 (3 Te batch) at IRE Alwaye
	Leaching	~130 batches
	Elution	13 batches (10 batch leaching/ batch Elution)
Total Quantity Processed	Insoluble Muck 22 Te	231Pa Obtained 35 mg

Summary

The plant was operated for 70 hours a week on the average. The production figures are given in Table 2. For the first time a material available in 5 ppb in the source has been extracted on this scale. The process of oxalic acid leaching and ion-chromatography has not so far been used elsewhere for protactinium recovery. The methodology followed for operation, quality control, and book keeping of product in every stream, is useful to any team trying to separate and purify valuable and rare minerals. Systematic establishment of the procedures, in close collaboration with the chemistry laboratory, has helped in maintaining efficiency and consistency. Effective radioactive effluent management procedure could be established. Conscious effort by the entire team resulted in nil incident safety record. The spin-off processes resulting from the pilot plant experiences are mineralisation of the monazite processing plant [Sethi et al. 2001], and decontamination of zirconium/ niobium from other elements when it is recycled from the nuclear reactor [Gantayet et al. 2001].

Acknowledgements

The authors acknowledge the contribution of Ms. Manisha Gupta, Mr Dileep Kumar and Mr K. K. Mishra, LPTD, BARC, for the help in the fabrication and testing of some of the components/equipment of the pilot plant and M/s. IRE Ltd. for the supply of the insoluble muck.

References

1. Palshin, E.; S., Myasoedov, B. F.; and Davydov, A., V., "Analytical Chemistry of Protactinium", Chapter IV, Ann-Humprey Science Publishers, 1970.
2. Anupama, P.; Gantayet, L. M.; Verma, R.; Parthasarathy, R.; Anil Kumar, S.; Dingankar, M. V.; Ghosh, S. K.; and Patra, R. N., "Prospecting for natural ^{231}Pa in India" BARC Report No. BARC-2001/E/020, 2001(a).

3. Anupama P.; Verma, R.; Parthasarathy, R.; Gantayet, L. M.; Anil Kumar, S.; Sethi, S.; Gupta, Manisha; Sadhukhan, S.; Bellary, M. P. and Patra R. N., "Development of a Process for Recovery and Pre-concentration of Protactinium-231: From the Waste Insoluble Muck of the Indian Rare Earth Plant by selective Leaching and Co-precipitation on Carrier", pp 60, Technical Abstracts, CHEMCON-2001.
4. Verma, R.; Anupama P.; Bellary, M. P. and Gantayet, L. M., "Development of a process for separation of protactinium from REE, Thorium, and other metal ions by ion chromatography", SPAREI-2001, August 17-19, Munnar, Kerala, 2001(a).
5. Verma, R.; Gantayet, L. M; Anupama P.; Sethi, S. and Bellary, M. P., "Development of a High Selectivity process for separation of Protactinium-231 from rare earths, thorium, uranium and other metal ions by Ion Chromatography and its implementation in the Protactinium recovery plant", pp 42, Technical Abstracts, CHEMCON-2001.
6. Sethi, S.; Anupama P.; Gantayet, L. M and Nair V. R., "Process for Washing and Mineralisation of the insoluble muck of Rare-earth plant for easy disposal- Some studies and implementation at Plant scale", SPAREI-2001, August 17-19, Munnar, Kerala, 2001.
7. Gantayet, L. M.; Verma, R.; Anupama P.; Sethi, S.; Sudersanan, M.; Sahoo, K. C. and Venugopal V., "Development of a process for removal of actinides and other impurities from recycled zirconium", INS-2001, October, 10-12, at CAT, Indore, 2001.

This paper was adjudged as the First Best paper in the oral presentation in the technical main session "Industrial Process" at CHEMCON-2001 symposium held at Central Leather Research Institute, Chennai, during December 19-22, 2001

About the authors ...

Mr Sanjay Sethi *joined Laser & Plasma Technology Division, BARC through 36th batch of BARC Training School in 1992. He completed his B.E. (Chemical Engineering) in 1992 from Panjab University, Chandigarh and M. Tech. (Chemical Engineering) in 2000 from IIT, Bombay. His fields of interest include heat transfer in molten metals, computational fluid dynamics, process development, vacuum technology and photochemical reactors.*

Ms P. Anupama *graduated from the 38th batch of Training school (Chemical Engineering) and joined the Laser & Plasma Technology Division. She is working on the development of processes for separation and recovery of nuclear elements, processes related to laser based separation, and experimental heat transfer studies in concentrated energy systems.*

Dr L. M. Gantayet *graduated from the 15th batch of Training School as Homi Bhabha Awardee in Chemical Engineering. He has specialised in the development of difficult separation processes such as isotope separation processes, Laser based chemical processes, gas dynamics, pressure diffusion and ion exchange based separation related to the nuclear fuel cycle. His other areas of expertise are technology development, process innovation and synthesis, modeling and simulation of separation process plants, and safety and accident analysis of plants.*

Mr M. P. Bellary *joined Chemical Engineering Division, BARC in 1974, after completing graduation in chemistry. Since then he is associated with process development for the recovery of nuclear material, such as thorium, lithium and uranium. His fields of interest are chemical analysis, solvent extraction and ion exchange processes.*

Development of a High Selectivity Process for Separation of Protactinium - 231 from Rare Earths, Thorium, Uranium and Other Metal Ions by Ion Chromatography and its Implementation in the Protactinium Recovery Plant

R. Verma
Analytical Chemistry Division
Bhabha Atomic Research Centre

L.M. Gantayet, P. Anupama and S. Sethi
Laser & Plasma Technology Division
Bhabha Atomic Research Centre

and

M. P. Bellary
Chemical Engineering Division
Bhabha Atomic Research Centre

Abstract

^{231}Pa is available at a concentration of around 350ppb (parts per billion) in the oxalic acid leachate of the protactinium recovery plant. An ion exchange process has been developed for purification of protactinium from iron, uranium, zirconium, niobium and other co-ions by ion exchange. An anionic exchange resin GS-300 (M/s. IEL Ltd.) has been used for the trials. The ion exchange process was developed in different stages: laboratory scale with 0.01-0.03dm^3 resin bed, industrial bench scale with 0.375dm^3 resin bed and implemented in the plant using a bed of 125-150dm^3 GS-300 resin bed. ^{95}Zr, ^{95}Nb, ^{233}Pa tracers were used to determine the movement of these ions in the bed. ^{231}Pa at a concentration of around 10ppm could be obtained by this process. The ion -exchange process development and its implementation in the plant are discussed in this paper.

Introduction

^{231}Pa, one of the rarest elements is of interest to the thorium fuel cycle studies of the Indian Nuclear power program. ^{231}Pa occurs at 5-6.5 parts per billion (ppb) concentration in the waste insoluble muck of the Monazite Processing Plant of Indian Rare Earths at Aluva. A process for recovery of protactinium from the insoluble muck by selective leaching by oxalic acid, to arrive at a concentration of around 350ppb is reported by Anupama et al., 2001.

Further purification of protactinium from iron, uranium, zirconium, niobium, thorium, titanium and rare earths was proposed to be done by the high selectivity ion exchange (I-X) process. Earlier workers have used I-X process to purify protactinium in high molarity HCl using strong anion exchange resin Dowex 1X8 [Collins et al., 1962, Krauss et al., 1958, Kluge et al., 1980, Palshin et al., 1970]. The present process is based on the oxalic acid leachate, which contains around 350ppb protactinium. The ion exchange process was developed in 3 stages, namely, lab scale trials using bed volumes of 0.01-0.03dm^3, industrial bench scale trials using a bed volume of 0.4dm^3 with column height of 750mm, and finally in the plant using a bed of 125-150dm^3. The typical anlysis of oxalic acid leachate and the

TABLE 1(a) DISTRIBUTION COEFFICIENT (K_d) IN OXALIC ACID & 6N HCl

Element	K_d in oxalic acid	K_d in 6N HCl
Pa	$> 10^5$	50
Zr	$> 10^4$	5
Nb	$> 10^4$	20
U	$> 10^4$	200
Fe	$> 10^4$	5000
Th	low	no adsorption
REE	low	no adsorption

TABLE 1(b) TYPICAL ANALYSIS OF OXALIC ACID LEACHATE

Element	*Concentration (mg/litre)*
Zr	668
Fe	86
Nb	52
U	42.3
Ti	54
Al	10.9
Cr	5.4

Average total oxide in feed: 2.5gpl

Resin: GS-300, (M/s IEL Ltd.) anion exchanger equivalent to Dowex 1X8

DATA OBTAINED

Process step	Medium
Loading	Oxalic acid / HCl
Selective elution of Zr, Nb	6N / 7N HCl
Elution of Pa	9N HCl + 0.2N HCl / HCl + oxalic mixture
Stripping	0.2N HCl / DM water
Regeneration	DM water

Physico-chemical data

- Swelling, shrinkage in various mediums
- Buoyancy effects with reagents

Three stages of development

Scale	Resin bed volume
Lab scale	0.01-0.03dm^3
Industrial bench scale	0.4dm^3, 75cm height
Plant	125-150dm^3, 1.5m ht. column

Fig.1 : Purification by ion exchange elution chromatography

distribution coefficient of the various elements in oxalic acid and 6N HCl are presented in Tables 1(a) and 1(b).

Experimental Work

Laboratory scale trials

The Indian resin GS-300 (manufactured by M/s. Ion Exchange India Ltd.) was chosen for trials, after establishing the equivalence with Dowex 1X8. The lab scale trials were conducted to obtain preliminary data on (a) maximum loading capacity for protactinium, and conditions for (b) selective elution of zirconium, niobium, (c) elution of protactinium, (d) stripping, (e) regeneration of the bed etc. The physico-chemical data such as, swelling and shrinkage in various mediums, buoyancy effect with reagents

were also determined. For protactinium elution, several eluants were tried: hydrochloric acid and dilute hydrofluoric acid mixture, hydrochloric and oxalic acid mixture at different normalities. Lesser number of bed volumes was required for elution of protactinium with HCl and HF mixture. 9N HCl and 0.2N HF mixture was used as eluant for protactinium in all the subsequent experiments. The details of these experiments have been reported by Verma et al., 2001. A summary of the data obtained in the lab scale trials and the stages of development are given in Figure 1.

Industrial bench scale trials

The industrial bench scale column was a glass column of 25mm diameter, 750mm length containing 0.375dm^3 GS-300 resin (0.3 - 1.0mm size range). The oxalic leachant from the plant was used as feed and the process data for the following six steps of the ion exchange process were obtained. The integrated flow in terms of bed volumes was used as a parameter to designate each step of operation. The schematic of the industrial bench scale column is presented in Figure 2.

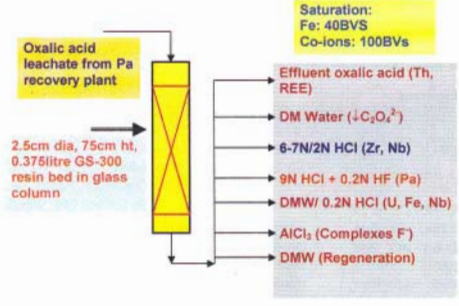

Fig. 2: Schematic of industrial bench scale ion-exchange column

1. Breakthrough with respect to ^{231}Pa: The feed oxalic acid contained 350ppb of protactinium in the form of an anionic complex. The major fractions of anionic complexes were those of iron, zirconium, niobium, uranium etc. present to the extent of 2-3gpl (measured in terms of precipitated and calcined oxides). The saturation with respect to protactinium was reached in 100 bed volumes (BVs) [Verma et al., 2001]. The bed was saturated with respect to iron in around 40 bed volumes. For the experiments of the subsequent steps, 40 BVs of the feed oxalic acid was loaded.
2. Washing of the bed: To prevent the loss of protactinium, a demineralised water wash was introduced before elution of zirconium with hydrochloric acid. This step diluted the oxalic acid and reduced the loss of ^{231}Pa in the subsequent step.
3. Selective elution of zirconium and loss of ^{231}Pa: The selective elution of zirconium with 6-7N HCl was based on relatively low K_d (distribution coefficient) factor of zirconium. As K_d of protactinium is also lower, the loss could be reduced by faster elution velocity. It is also known from lab trials that a mixture of oxalic and hydrochloric acid reduced the K_d for protactinium further. Therefore, maintaining rate of flow for the first BV of 6-7N HCl was very important. The movement of protactinium, zirconium, and niobium was determined by using ^{233}Pa, ^{95}Zr, and ^{95}Nb tracers respectively. Uranium and iron were determined by chemical analysis. The elution data presented in Table 2 shows that a large proportion of Nb is also eluted with Zr.
4. Elution of protactinium: The elution of ^{231}Pa was done with 8N HCl and 0.2N NH_4F. In the earlier runs, 9N HCl and 0.2N HF was used, but as this solution made the resin slightly buoyant, 8N HCl instead of 9N HCl was used in this run. Solid NH_4F was used instead of

Table 2:Elution of Zr and Nb with 6N HCl from GS-300 ion exchange resin bed

- Resin bed volume: ~375ml = 1 bed volume (BV)
- Feed is plant oxalic acid leachate = 40BVs
- Demineralised water wash: 2 BVs
- Elution with 6N HCl - 10 BVs
- Tracers used: ^{95}Zr, ^{95}Nb, ^{233}Pa

BVs of 6N HCl eluate collected	Cumulative % collected Zr	Nb	Pa
0.5	0	0	0
1.0	25.1	14.47	4.35
1.5	38.86	28.42	6.67
2.0	48.79	38.19	7.59
2.5	55.92	45.21	8.32
3.0	61.32	50.44	8.93
3.5	65.68	54.43	9.54
4.0	69.24	57.81	10.12
4.5	72.40	60.39	10.58
5.0	75.46	62.40	11.04
6.0	97.30	71.40	12.99
7.0	98.91	73.16	13.29
8.0	102.98	75.48	13.74

Table 3: Elution of Protactinium with 8N HCl and 0.2N HF from GS-300 ion exchange resin bed

Resin bed volume: ~375ml = 1 bed volume (BV)
Demineralised water wash: 2 BVs
Elution of Pa with 8N HCl + 0.2N NH_4F: 5 BVs

BVs of eluate collected	Cumulative % collected Nb	Pa
0.5	0.12	1.38
1.0	0.35	33.40
1.5	2.66	55.74
2.0	2.70	66.80
2.5	5.17	72.75
3.0	7.18	76.28
3.5	8.67	78.24
4.0	9.80	79.37
4.5	9.96	80.52

HF, as it was easier and safer to handle. The elution had to be at a low velocity ($2m^3/m^2/hr$) to avoid tailing at the later stages of elution. The reduction in the reagent could be achieved by flow rate control. The elution data presented in Table 3 shows that part of the remaining niobium also gets eluted with protactinium.

5. Stripping of the resin: The lab scale trials showed that 0.2N HCl could remove the remaining co-ions such as uranium and iron. The stripping with 0.2N HCl was efficient and not much influenced by flow rates.
6. Regeneration of the resin: The F^- needs to be complexed with sufficient quantity of $AlCl_3$ for re-adsorption of protactinium. One bed volume of 0.1N $AlCl_3$.wash is given, after washing the bed with sufficient amount of demineralised water.

Plant Scale Implementation

Based on the industrial bench scale data, the process was scaled up to 125-150L-resin bed. A 380mm diameter, 1500mm tall polypropylene lined FRP column was designed and fabricated [Sethi et al., 2001]. The process was implemented in this column with a 125-150L GS-300 resin bed. The ion chromatography column used in the industrial bench scale experiment and the full-scale column in the plant are presented in Figure 3.

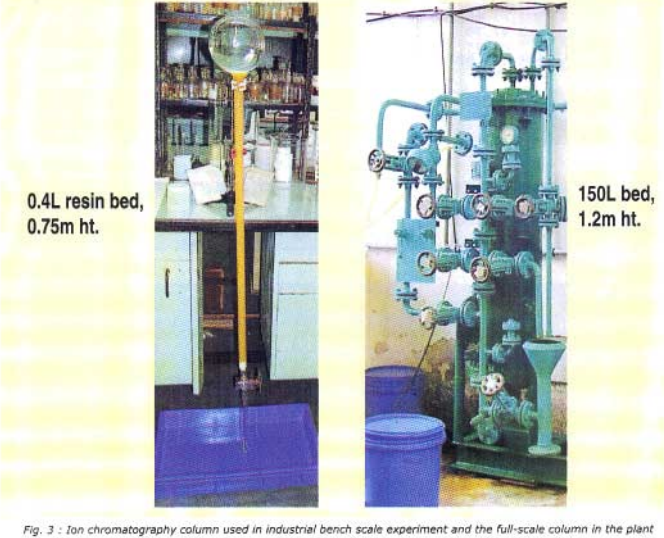

Fig. 3 : Ion chromatography column used in industrial bench scale experiment and the full-scale column in the plant

1. Loading: 40BVs of feed oxalic acid solution is loaded into the column at around 6.3m^3/m^2/hour.
2. Recycle of effluent: The oxalic acid effluent, which is free from the anionic complexes of Pa, Zr, Nb, U, Fe, etc., is adjusted to 2N strength and recycled to the leaching section of the plant for protactinium leaching from pre-treated insoluble muck.
3. Washing of bed: 3BVs of demineralised water wash is given at around 12.6m^3/m^2/hour to reduce the oxalic acid concentration. During the demineralised water wash, the oxalic acid concentration was measured to determine the axial mixing/dispersion of the liquid, which is passed through the bed. The data is presented in Table 4. Although the free pore volume in the bed is only 40%, it took nearly three bed volumes (150L bed) to reduce the concentration of oxalic acid in the effluent from 1.6N to 0.07N.

Table 4: Axial mixing studies in the Plant column

1. Column Dimensions: 380mm diameter, 1500mm length
2. Resin bed volume: ~150litre = 1 bed volume (BV)
3. Demineralised water wash: 3 BVs

Bed volumes of effluent collected	*Concentration of $C_2O_4^{2-}$ (N)*
0.0	1.60
0.5	1.59
1.0	0.98
1.5	0.39
2.0	0.12
2.5	0.10
3.0	0.07

4. Selective elution of zirconium, niobium and stripping of the bed: 2N, 6N, 7N, 8N HCl eluant was used in different batches for selective elution of zirconium, niobium and other co-ions. The eluate solutions were collected in fractions and the total oxide was determined in the fractions by hydroxide precipitation and calcination of hydroxide. The oxide content was used as a parameter to rate the effectiveness of the eluate in removing impurities. 2N HCl could convert the resin bed to Cl^- form and elute most of the co-ions with least loss of protactinium. Further, the stripping step of 0.2N HCl was scheduled before the elution of protactinium to remove niobium and other co-ions. The 0.2N HCl solution was recycled till it was saturated with co-ions. This reduced the consumption of acid. This procedure did not reduce the impurity content of protactinium in the eluate, but reduced the loss of protactinium in the 2N HCl step.
5. Selective elution of ^{231}Pa: It could be done with less than 2BVs of 8N HCl and 0.2N HF mixture. As HF was readily available, it was used instead of NH_4F. The ^{231}Pa concentration in the first BV of eluate is low. The subsequent 1.5BVs of eluate eluted around 90-92% of the protactinium. This eluate contained ^{231}Pa at around 4-15ppm dry basis concentration with major impurities of zirconium and niobium.
6. Neutralisation of eluate: The eluate is neutralised with sodium hydroxide, the precipitate is filtered, washed with demineralised water and redissolved in a smaller volume of 2N oxalic acid for the next stage of purification using the same resin bed.

Summary

A new process for purification of ^{231}Pa from rare earths, thorium, zirconium, niobium, uranium, iron by ion chromatography in oxalic acid medium has been developed and successfully implemented in a pilot plant scale. The GS-300 anion exchange resin is quite suitable for this process. The purification of protactinium with respect to other dissolved co-ions is possible with 2N HCl, which saved considerable amount of reagents. However, if zirconium has to be collected separately the 6N HCl wash will be required. As a spin-off, a process for purifying zirconium was also established [Gantayet et al., 2001].

Further work is aimed at establishing the stability of the resin on long-term operation,

and improving separation factors by using larger column lengths, and optimum flow rates.

Acknowledgements

The authors acknowledge Mr Anil Kumar and Ms Narayani, Radiation Safety and Systems Division (RSSD), BARC, for counting the samples by gamma spectrometry. The authors thank Head, Laser & Plasma Technology Division, Head, Analytical Chemistry Division, Head, Chemical Engineering Division and Head, RSSD, BARC, for supporting this work.

References

1. Anupama P., R. Verma, R. Parthasarathy, L.M. Gantayet, S. Anil Kumar, S. Sethi, Manisha Gupta, S. Sadhukhan, M. P. Bellary, R. N. Patra, "Development of a Process for Recovery and Pre-concentration of Protactinium-231: From the Waste Insoluble Muck of the Indian Rare Earth Plant by selective Leaching and Co-precipitation on Carrier", pp60, Technical Abstracts, CHEMCON-2001.
2. Collins, D., A., Hillary, J., J., Nairn, J., S. and Phillips, G., M., "The development and application of a process for the recovery of over 100g of Protactinium-231 from a uranium refinery waste material", Journal of Inorganic Nuclear Chemistry, 24, pp 441-459, 1962.
3. K. A. Krauss and F. Nelson, Oak Ridge Laboratory, "Anion Exchange Studies of Fission Products", Symposium on Ion Exchange and Chromatography in Anal. Chemistry, ASTM No. 195, Philadelphia, 1958.
4. Kluge and K. H. Lieser, "Separation of Thorium, Protactinium and Uranium by Ion Exchange and Extraction", Radiochimica acta 27, 161-171, 1980
5. L. M. Gantayet, R. Verma, Anupama P., S. Sethi, M. Sudersanan, K. C. Sahoo, V. Venugopal, "Development of a process for removal of actinides and other impurities from recycled zirconium", INS-2001, October, 10-12, at CAT, Indore.
6. Palshin, E., S., Myasoedov, B. F., and Davydov, A., V., "Analytical Chemistry of Protactinium", Ann-Humprey Science Publishers, 1970.
7. R. Verma, Anupama P., M. P. Bellary, and L. M. Gantayet, "Development of a process for separation of protactinium from rare-earth elements, thorium and other metal ions by ion chromatography", SPAREI-2001, August 17-19, Munnar, Kerala.
8. S. Sethi, Anupama P., L. M. Gantayet and M. P. Bellary, "Pilot Plant experience of protactinium recovery from the insoluble muck: Installation and Operation ", pp 42, Technical Abstracts, CHEMCON-2001.

This paper was adjudged as the Second Best paper in the poster presentation of poster-main session"Industrial Process," at CHEMCON-2001 symposium held at Central Leather Research Institute, Chennai, during December 19-22, 2001

About the authors ...

Dr Rakesh Verma *graduated from BARC Training School (Chemistry) in 1983 and joined the Analytical Chemistry Division. He is working in the field of activation analysis.*

Dr L. M. Gantayet *graduated from the 15th batch of Training School as Homi Bhabha Awardee in Chemical Engineering. He has specialised in the development of difficult separation processes such as isotope separation processes, laser based chemical processes, gas dynamics, pressure diffusion and ion exchange based separation related to the nuclear fuel cycle. His other areas of expertise are technology development, process innovation and synthesis, modeling and simulation of separation process plants, and safety and accident analysis of plants.*

Ms P. Anupama *graduated from the 38th batch of Training school (Chemical Engineering) and joined the Laser & Plasma Technology Division. She is working on the development of processes for separation and recovery of nuclear elements, processes related to laser based separation, and experimental heat transfer studies in concentrated energy systems.*

Mr Sanjay Sethi *joined Laser & Plasma Technology Division, BARC through 36th batch of BARC Training School in 1992. He completed his B.E. (Chemical Engineering) in 1992 from Panjab University, Chandigarh and M. Tech. (Chemical Engineering) in 2000 from IIT, Bombay. His fields of interest include heat transfer in molten metals, computational fluid dynamics, process development, vacuum technology and photochemical reactors.*

Mr M. P. Bellary *joined Chemical Engineering Division, BARC in 1974, after completing graduation in chemistry. Since then he is associated with process development for the recovery of nuclear material, such as thorium, lithium and uranium. His fields of interest are chemical analysis, solvent extraction and ion exchange processes.*

Indigenously Developed LiF : Mg, Cu, P Thermoluminescent Phosphor for Radiation Dosimetric Applications

S.S. Shinde, B.S.Dhabekar and B.C.Bhatt
Radiological Physics and Advisory Division
Bhabha Atomic Research Centre

Abstract

A highly sensitive and tissue equivalent LiF:Mg,Cu,P Thermoluminescent (TL) phosphor in powder form has been developed. The TL sensitivity of this phosphor is about 1.5 times that of Harshaw-Bicron LiF:Mg,Cu,P (TLD-100 H) by peak height measurements. It gives TL emission band around 370 nm. Its dose -vs -TL response is linear up to 10 Gy. Reusability study shows that its sensitivity does not decrease even after 10 cycles of reuse. Annealing temperature was found to affect the glow curve shape and sensitivity.

Introduction

Nakajima et al (1978) reported for the first time in 1978, the preparation of LiF:Mg,Cu,P, a highly sensitive and nearly tissue equivalent TL phosphor. Thereafter many workers (Wu et al 1984, Wang Shoushan 1988, Azorin et al 1989, Horowitz et al 1990, Kolotilin et al 1993, Zha et al 1993) prepared this phosphor in their laboratories following different procedures and studied in detail its characteristics. It is worth noting that unlike $CaSO_4$:Dy (Yamashita et al 1968, 1971, Ayyangar et al 1974, Azorin 1984), none of the laboratories reported to have used the same preparation procedure. By manipulation of dopant concentration Horowitz and Horowitz (1992) could achieve the TL sensitivity about 35 times as compared to that of TLD-100. Wang Shoushan (1988) has also studied extensively the effect of concentrations of Mg, Cu, P on the sensitivity and glow curve structure of LiF:Mg,Cu,P and concluded that Mg and P concentration influences the height and width of 220 °C glow peak whereas concentration of Cu influences not only 220 °C and 250 °C peak but also the intensity of 110 °C peak. As per their investigation, the optimum concentration was found to be 0.2 mol % MgF_2, 0.0046 mol % CuF_2 and 1.90 mol % $(NH_4)H_2PO_4$. Patil and Moharil (1995) showed that LiF:Mg,Cu,P could be made using simple procedure which did not involve a use of nitrogen atmosphere.

In the present paper, the preparation procedure and characteristics of LiF:Mg,Cu,P TL phosphor prepared indigenously in BARC are described and compared with that of TLD100-H.

Materials and Methods

Commercially available LR grade LiF was purified by vacuum distillation method (Muralidhar Rao 1974). Appropriate quantities of purified LiF and dopants Mg, Cu and P in the form of MgF_2, $CuCl_2.2H_2O$ and $(NH_4)H_2PO_4$ respectively were mixed thoroughly. The mixture was melted in a platinum crucible at 960 °C in a furnace for fifteen minutes and then cooled rapidly to room temperature. The polycrystalline phosphor thus obtained was ground to powder (74-210 microns). Several such batches were prepared by varying the dopant concentrations. The batch having highest TL output was chosen to study its sensitivity and other TL characteristics in comparison with Harshaw TLD -100H.

A locally made TL reader having EMI 9524B photomultiplier (S-11 response) as a detector was used for taking the TL measurements,. Glow curves were recorded

using linear heating rate of 10°C/s. For optimisation of annealing temperature, virgin phosphor samples were annealed at various temperatures in the range 240°C-320°C for 10 minutes. Peak height of 210°C glow peak was recorded after a test dose of 0.1 Gy. For gamma dose - vs -TL response, phosphor samples from the same batch were irradiated with Co - 60 gamma rays from 0.01 to 10^4 Gy.

Reusability studies were carried out for 10 cycles of reuse by adopting two different procedures:

Procedure # 1

All the 10 samples (30 mg each) were first annealed at 280°C for 10 minutes, irradiated to a test gamma dose (0.01Gy) and then readout by holding the temperature at 280°C for 10 seconds. After reading all the samples, one of the samples was removed from the process and marked as "cycle 1". This was repeated for ten cycles.

Procedure #2

The above process was repeated except that instead of pre-annealing at 280°C for 10 minutes, pre-annealing was done at 240°C for 10 minutes and the samples were also readout holding the temperature at 240°C for 10 seconds.

TL emission spectra were recorded on an indigenously made TL emission spectrometer using a locally made monochromator (CEL India). 1 nm slit was used for recording the TL emission spectra.

Results

During preparation of LiF:Mg,Cu, P, only freshly distilled LiF powder was used as it observed that it gave better reproducibility.

Glow curve

Figure 1 shows the glow curves of virgin LiF:Mg,Cu,P (BARC) phosphor prepared in this laboratory and Harshaw TLD 100-H after a test gamma dose of 0.1 Gy. Both the phosphors have similar glow curves with main dosimetric peak at about 210°C. Out of various batches prepared by varying

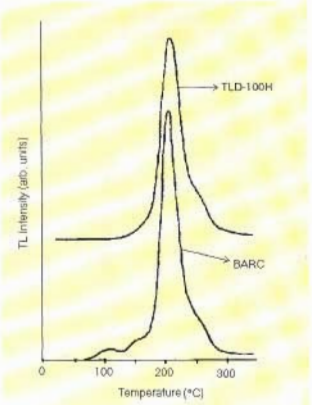

Fig. 1 : TL glow curves of virgin LiF:Mg,Cu,P phosphor powder

concentrations of Mg, Cu and P, the batch of LiF prepared by doping 0.4 mol % Mg, 0.002 mol % Cu and 0.85 mol % P was found to give highest TL sensitivity which was about 1.5 times (peak height) as compared to TLD 100-H.

Effect of annealing treatment

Figure 2 shows the glow curves of LiF:Mg,Cu,P (BARC) taken after various pre-irradiation annealing treatments. In general four glow peaks at about 120, 165, 210 and 275°C are seen. It can be seen that, as the annealing temperature is increased from 230 to 320°C, 165°C glow peak decreases whereas 210°C glow peak height increases up to pre-annealing temperature of 280°C and beyond this temperature, it again decreases. The effect of annealing treatment on the TL sensitive (210°C peak height) of LiF:Mg,Cu,P (BARC) and TLD 100H is shown in Figure 3. It can be seen that 280°C for 10 min annealing treatment increases the TL sensitivity of LiF: Mg, Cu, P (BARC) phosphor by about 1.25 times as compared to 240°C, 10 min annealing treatment, whereas in the

case of TLD-100H, annealing treatment 240°C, 10 min gives maximum TL sensitivity.

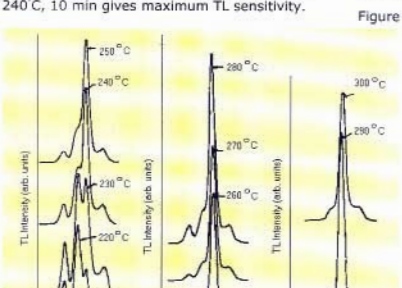

Fig. 2 : TL glow curves of LiF:Mg,Cu,P (BARC) annealed at various temperatures

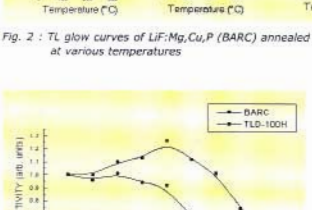

Fig. 3 : Effect of annealing temperature on LiF:Mg,Cu,P (BARC) and TLD100-H

Effect of phosphorus doping

Figure 4 shows the variation of TL sensitivity of LiF:(Mg 0.4 mol % ,Cu 0.002 mol %, P) with various phosphorus concentration. The TL sensitivity increases with phosphorus concentration. It was observed that the TL sensitivity is a step function of P concentration. This result agrees with the observation made by Bilski et al 1996.

Gamma Dose vs. TL Response

Figure 5. shows the gamma dose -vs-TL response of LiF:Mg,Cu,P (BARC) and TLD-100H. Both phosphors show linear response up to 10 Gy. Beyond this, the dose response becomes sub-linear and saturates above 10^3 Gy.

Reusability

No loss the in sensitivity was observed after 10 cycles of reuse if reusability procedure #2 is adopted. However, 25% loss of sensitivity was observed in case f reusability procedure #1. It was observed that, although, 280°C,10 minutes annealing treatment gave maximum TL sensitivity, it was not very useful for reuse of the phosphor. Pre-irradiation annealing treatment at 240°C for 10 min give better reusability.

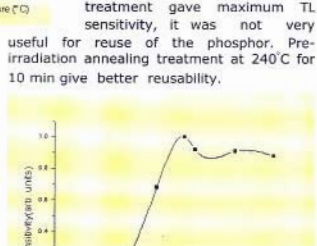

Fig. 4 : Variation of TL sensitivity with Phosphorus concentration in LiF (Mg0.4,Cu 0.002 mol%, P(x))

Emission spectrum

The figure 5 shows an emission spectrum of LiF: Mg,Cu,P (BARC) taken at 200°C temperature. The spectrum shows a broad TL emission band around 370 nm which corresponds to Cu^+ emission as reported by Patil and Moharil (1995).

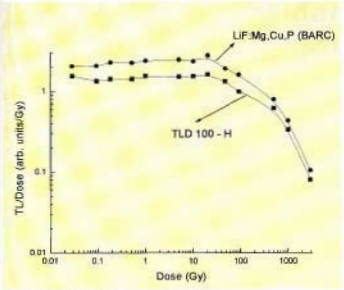

Fig. 5 : Dose vs TL response curves of LiF:Mg,Cu,P

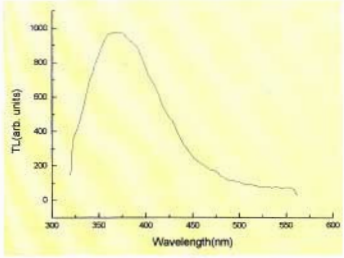

Fig. 6 : TL emission spectra of LiF:Mg,Cu,P (BARC)

Discussion

Although the role of Mg in LiF:Mg,Cu,P to provide trapping centres for electrons is well established, there is no consensus about the roles of Cu and P. For example, McKeever (1991) states that neither Cu nor Mg are directly involved in the emission process since in the material doped with only Cu, the wavelength of emission is very different from those samples which contain P. He also argued that since it is necessary to have large quantities of P in order to obtain the brightest material, it can be assumed that the TL is emitted from Mg / P phases. Mahajna et al (1995) claimed that P takes role of Ti in LiF:Mg,Cu,P. Bos et al (1996) proposed the dual role of P, which is involved in the trapping of charge carriers (although the role of Mg is more dominant). It also acts as luminescent centre. Bilski et al (1996) proposed that P is luminescent centre while Cu induces some competitive processes, which reduce the formation of higher order complexes of Mg related defects. According to them, Cu doesn't involve directly in the TL process. On the contrary, the work of Patil and Moharil (1995) shows that Cu^+ is acting as a luminescent centre. They proposed that radiation creates excess electron colour centres and defects associated with trapped interstitial halogen atoms. During heating, the halogen atoms are released from interstitial position and they recombine with electrons. The energy of recombination is efficiently transferred to nearby Cu^+ ion, which acts as luminescent centre. But the above-proposed model doesn't discuss the role of phosphorus.

As the gamma vs. TL dose response curve (fig. 5) is linear up to 10 Gy, this phosphor can be used for personnel monitoring and radiation dosimetry up to a dose level of 10 Gy.

Conclusions

1. TL sensitivity of LiF:Mg,Cu,P phosphor is highly dependent on the preparation procedure and specially on age and purity of LiF powder,
2. Although the best annealing treatment of 280°C, 10 minutes to LiF:Mg,Cu,P phosphor prepared in this laboratory was found to give highest sensitivity as against 240°C,10 minutes, for TLD-100 H and GR-200, however, pre-annealing treatment at 240°C,10 min was found to best suited for reusability of the phosphor.
3. Presence of phosphorus helps in incorporation of more copper into the lattice which has been found to be responsible for increasing the sensitivity of LiF:Mg,Cu,P phosphor.
4. Indigenously developed nearly tissue equivalent LiF:Mg,Cu,P phosphor can be

used for personnel and environmental monitoring and in medical physics applications.

References

1. Ayyangar K, Lakshmanan A R, Bhuwan Chandra and Ramadas K 1974 Phy. Med. Biol **19** 665.
2. Azorin J, Gonzalez G, Gutierrez A, Salvi R 1984 Health Phys **46** 269.
3. Azorin J, Gtierrez A, Gouzales P 1989 Technical Reort A-87-08 ININ-Mexico.
4. Bilski P, Budzanowski M and Olko P 1996 Rad. Prot. Dosim. **65** 195.
5. Bos A J J, Meijvogel, Bilski P, Olko P 1996 Rad. Prot. Dosim. **65** 199.
6. Horowitz A and Horowitz Y S 1990 Rad. Prot. Dosim. **33** 267.
7. Horowitz A and Horowitz Y S 1992 Rad. Prot. Dosim. **40** 265.
8. Kolotilin V V, Hokhrekov V I, Tarasova L M and Zakhriapin S B 1993 Nucl. Track. Radiation Process **21** 1169.
9. Mahajna S, Yossian D and Horowitz Y S 1995 Rad. Effects and Def. in Solids **136** 181.
10. McKeever S W S 1991 J. Phys. D: Appl. Phys. **24** 988.
11. Muralidhar Rao S and Bhide G K 1974 Indian J Pure and Appl. Phys. **12** 358.
12. Nakajima T, Murayama Y, Matwazawa T and Koyano A 1978, Nucl. Instrum. Methods **157** 155-162.
13. Patil R R and Moharil S V 1995 J. Phys.: Condens Matter **7** 9925.
14. Wang Shoushan, 1988 Radiat. Prot. Dosim. **25** 133.
15. Wu DA-Ke, Sun Fu-Yin and Dai Hong-Chen 1984 Health Phys. **46**, 1063.
16. Yamashita T, Nada N, Onishi and Kitamura S 1968 Proc.2nd Int on Lum. Dos. T. N. Gatlin bung 4 and also in 1971 Health Phys. Vol; **21** 295.
17. Zha Z, Wang S, Shen W, Jhu J and Cai G 1993 Radiat. Prot. Dosim. **47** 111.

This paper was adjudged as Best Paper (poster session) in the International Conference on 'Radiation Protection Measurements and Dosimetry : Current Practices and Future Trends (IARP-IC-2K1)' held at Mumbai during February 20-23, 2001

About the authors ...

Dr S.S. Shinde *joined BARC in March 1969 in the Directorate of Radiation Protection after obtaining M.Sc. (Physics) from Nagpur University. He obtained Ph.D. (Physics) from Mumbai University in 1994. He has initially worked on neutron dosimetry and threshold detector. He has worked on development of new TL materials for personnel monitoring and studied their TL characteristics for their use in personnel and environment monitoring. He developed highly sensitive TL materials such as $BaSO_4:Eu,P$, $BaSO_4:Eu,Na$, $CaSO4:Dy,P$. Also developed $LiF:Mg,Cu,P$, $Li_3PO_4:Mg,Cu$ phosphors for their use in personnel monitoring. He has more than 65 publications in national/international journals. He was superannuated in October 2001.*

Mr Bhushan Dhabekar *completed his M.Sc. in Physics from Nagpur University. He joined Radiological Physics and Advisory Division, BARC, through Training School (41st batch). His fields of interest are in the development and characterisation of new dosimetric materials for their use in personnel and environment monitoring and in medical physics, TL defect centres characterisation using TL, optical absorption, fluorescence and ESR techniques.*

Dr B.C. Bhatt *joined BARC in the year 1969 after graduating from 12th batch (Physics Course) of BARC Training School. He obtained his Ph.D. degree in Physics in 1982 from the University of Mumbai. He has more than 30 years of experience in the field of thermoluminescence dosimetry, personnel monitoring, medical dosimetry and radiation safety. He is a member of Standing Committee of Radiotherapy Development Programme, DGHS, Ministry of Health. He is also a member of various BARC and AERB committees dealing with radiological safety. He was Visiting Professor to Department of Physics, University of Sao Paulo, Brazil, during 1999. Presently he is Head, Radiological Physics and Advisory Division. He has more than 230 publications to his credit. He is guide for M.Sc. and Ph.D. in Physics for University of Mumbai.*

Differential Antioxidant Effects of Plumbagin in Rat Tissues

Jai C. Tilak and T.P.A. Devasagayam
Cell Biology Division
Bhabha Atomic Research Centre

Meenal Banerjee
School of Life Sciences, Devi Ahilya Vishva Vidhyalaya
Indore – 452 017

S. Adhikari
Radiation Chemistry and Chemical Dynamics Division
Bhabha Atomic Research Centre

and

G.J. Chintalwar and S. Chattopadhyay
Bio-organic Division
Bhabha Atomic Research Centre

Abstract

Oxidative stress has been implicated in the etiology of a number of human ailments. Hence, antioxidants, especially derived from natural sources and capable of protecting against damage induced by reactive oxygen species (ROS) may have potential applications in prevention and/or cure of the disease. Indian medicinal plants provide a rich source of these potentially useful compounds. Plumbago zeylanica (known as 'chitrak') and its constituents are credited with potential therapeutic properties including antiatherogenic, cardiotonic, hepatoprotective and neuroprotective properties. Plumbagin (2-methyl-5-hydroxy, 1:4 naphthoquinone), isolated from the root of this plant was considered as the active ingredient. To examine the possible antioxidant activity of plumbagin in relation to its reported beneficial properties, its ability to protect against oxidative damage in mitochondria from rat tissues was studied, by incorporating it in mitochondria during isolation. Mitochondria from rat liver, brain and heart were exposed to ROS generated by ascorbate-Fe^{2+}, H_2O_2-Fe^{2+} and the peroxyl radical generator, 2,2'-Azobis(2-methylpropionamide) dihydrochloride (AAPH). The parameters of damage assessed were products of lipid peroxidation, loss of mitochondrial enzymes and protein oxidation. Our results indicate that plumbagin, gave protection to different extents in the tissues examined. This differential ability can be ascribed to the presence of various amounts of substrates for oxidative reactions and antioxidants/prooxidants in these tissue preparations. The possible mechanisms involved were examined by pulse radiolysis. Upon exposure to radiation-derived hydroxyl radical there was formation of plumbagin radical, with absorption at 390 nm. The formation kinetics of this radical reveal a fairly high rate constant of plumbagin with hydroxyl radical in the range of 2 x10^9 M^{-1} s^{-1}. In conclusion, our studies reveal that the membrane protective properties of plumbagin, in mitochondria, may be related to its radical scavenging abilities and that this antioxidant ability, may at least in part, explain its potential therapeutic properties.

Introduction

Enhanced generation of reactive oxygen/ nitrogen species (ROS/RNS) and the ensuing phenomenon in the form of oxidative stress have been implicated in the etiology of a large number of human ailments including the major forms such as cardiovascular diseases, neurodegenerative diseases and cancer (Sies, 1996; Thomas and Kalyanaraman, 1997; Payne, Bernstein et al., 1999). Antioxidants due to their ability to neutralize the toxic free radicals or damage induced by them have potential applications in the prevention and/or therapy of human ailments (Sies, 1996; Rao and Agarwal, 2000; Cuzzocrea, Riley et al., 2001). Natural compounds especially derived from dietary sources or medicinal plants and having antioxidant abilities may have the dual benefits of dietary component/therapeutic agent as well as that of neutralizing the reactive species (Mantle, Lennard et al., 2000; McDermott, 2000). India has a rich

heritage of possessing ancient systems of medicine for treating illnesses in the form of *'Ayurveda'*, *'Siddha'* and *'Unani'*. These have identified a large number of plants with potential therapeutic efficacies (Lele, 1999; Tripathi, 2000; Okamoto and Hino, 2000; Lele, 2001).

Among these medicinal plants, *Plumbago zeylanica* (*Chitrak*) has been credited with therapeutic properties to treat several diseases (Kirtikar and Basu, 1984; Thakur, Puri et al., 1989; Sharma, Singh et al., 1991a; Oyedapo, 1996). These include digestive diseases such as dysentry, rubefaciency in rheumatism, lumbago, paralytic affections, leucoderma, piles, bronchitis, anemia, liver diseases, obesity, anasarca, dyspepsia and leprosy. The plant preparations are also being used for the treatment of arthritis, epilepsy, hysteria and other diseases connected with the nervous system besides for bacterial, microbial and helminth infections. It has also been useful in increasing appetite. In combination with other plants it also has been used in antihepatotoxic herbal formulations. Moreover, it brings about regression of atheroma and hinders plaque formation. The major portion of the plant used for therapeutic applications is the root. An herbal preparation "yogaraj guggal", derived from the root, is being used in the treatment of arthritis, rheumatism and related diseases.

The root contains several bioactive chemical constituents which include plumbagin, 3-chloroplumbagin, droserone, chitranone, zeylanone, isozeylonone, plumbazeylone, coumarin, elliptinone, triterpenoids, β-sitosterol, maritinone, 2-methylnaphthazarin and anthroquinones (Gunaherath, Gunatilaka et al., 1988; Dinda and Saha, 1989; Thakur, Puri et al., 1989; Dinda, Hajra et al., 1997; Gupta, Siddiqui et al., 2000). Plumbagin is a naphthoquinone and is a major component constituting about 0.03 % of dry weight of the roots and is considered as the active ingredient responsible for therapeutic effects (Gupta, Verma et al., 1993). Besides it has a strong germicidal action. In small doses it stimulates muscular tissue of heart, intestines and uterus. It has a stimulant action on nervous system and possesses cardiotonic, hypolipidaemic, wound healing, antiatherosclerotic, anticoagulant, antifungal, antibacterial, antitumor, antimutagenic and antifertility properties (Premakumari, Rathinam et al., 1977; Kirtikar, Basu et al., 1984; Bhargava, 1986; Itoigawa, Takeya et al., 1991; Sharma, Gusain et al., 1991b; Durga, Sridhar et al., 1992; Sugie, Okamoto et al., 1998). The mechanisms of action of plumbagin, however, are not fully understood. The detailed studies on its possible antioxidant properties also have not been carried out. The present study attempts to fulfill this lacuna.

Various ROS, generated *in vivo* by endogenous systems, can significantly alter subcellular components and induce different forms of oxidative damage. Among the subcellular organelles mitochondria are among the crucial ones that are highly susceptible for oxidative damage (Salet and Moreno, 1990; Munday, Sriratana et al., 1996). Both lipids and proteins are susceptible to ROS induced damage. The protection afforded by antioxidants differs in tissues like brain, liver and heart, depending on their composition (Pushpendran, Subramanian et al., 1998). These tissues also have implications in the medicinal properties credited to plumbagin. Hence, in this study we have examined the *in vitro* oxidative damage to mitochondria isolated from rat liver, brain and heart induced by different endogenous model systems such as ascorbate-Fe^{2+}, peroxyl radicals and hydroxyl radical besides the protection afforded by plumbagin. To examine possible mechanisms involved we have studied the reaction of plumbagin with hydroxyl radical by pulse radiolysis.

Materials and Methods

Materials

1,2,4-Aminonaphtholsulphonic acid (ANSA), adenosine triphosphate, ammonium molybdate, ascorbic acid, dichlorophenol indophenol, dinitrophenyl hydrazine, ethylene diamine tetraacetic acid (EDTA),

ferrous sulphate, guanidine hydrochloride, perchloric acid, phenazine methosulphate, sodium cyanide, succinate, 2-thiobarbituric acid and trichloroacetic acid were purchased from Sigma Chemical Co., U.S.A. 2.2'-Azobis (2-amidinopropane) dihydrochloride (AAPH) (=2.2'-Azobis(2-methylpropionamidine) dihydrochloride) was from Aldrich Chemical Co., U.S.A. Tetraethoxypropane was used as the standard for estimating malonaldehyde equivalents. Other chemicals used in our studies were of the highest quality commercially available from local suppliers.

Methods

Isolation of plumbagin from roots of P. zeylanica

380 gms of fresh roots of *P. zeylanica* were extracted (Soxhlet) with petroleum ether three times at 60 to 80 °C. All the extracts were mixed and evaporated by rotavapor. The concentrate was dissolved in minimum amount of distilled petroleum ether and the crystalline compound with a yield of 0.03% was obtained. The purity of this preparation was checked by thin layer chromatography (TLC) and gas liquid chromatography (GLC).

Isolation of mitochondrial fraction

Three months old female Wistar rats (weighing about 250 ± 20 g) were used for the preparation of mitochondria (Kamat, Boloor et al., 2000). In brief, rat liver, brain and hearts were excised, homogenized in 0.25 M sucrose containing 1 mM EDTA. The homogenate was centrifuged at 3000 x g for 10 min to remove cell debris and the nuclear fraction. The resultant supernatant was centrifuged at 10,000 x g for 10 min to sediment mitochondria. This pellet was washed thrice with 0.15 M Tris-HCl buffer, pH 7.4, to remove sucrose. Protein was estimated and pellets were suspended in the above buffer at the concentration of 10 mg protein/ml. For incorporating plumbagin, it was dissolved in ethanol at a concentration of 10 mM, added to the mitochondrial pellet before the last washing, homogenized for 1 min at low speed and then the pellet was sedimented by centrifugation. The concentration of plumbagin in mitochondria was calculated by its selective absorption at 267 nm after sonication of mitochondria to release the compound incorporated inside this organelle.

Exposure of mitochondria to agents for inducing oxidative stress

Oxidative damage was induced by ascorbate-Fe^{2+}-system as described previously (Kamat and Devasagayam, 1996). The procedure for ascorbate-Fe^{2+} induced lipid peroxidation was that of Hammer and Wills (1978) as modified by Devasagayam (1986). The incubation mixture (0.5 ml) contained: (i) 700 µl of basic medium (0.15 mM Tris-HCl, pH-7.4), (ii) 100 µl of $FeSO_4$ in 0.1 N HCl (final concentration 50 µM), (iii) 100 µl ascorbic acid (final concentration of 0.4 mM) and (iv) 100 µl of mitochondrial sample. Incubations were carried out at 37 °C in a shaker-water bath. After the incubations, pink coloured thiobarbituric acid reactive substances (TBARS) formed were estimated at 532 nm spectrophotometrically as malonaldehyde equivalents after accounting for appropriate blanks. Malonaldehyde standard was prepared by the acid hydrolysis of tetraethoxypropane. Peroxyl radical induced lipid peroxidation was examined using AAPH by incubation at 37 °C (Kamat & Devasagayam, 1995). Oxidative damage in mitochondria was also induced using hydroxyl radicals, generated by H_2O_2-Fe^{2+} system by using 150 µM H_2O_2 and 150 µM Fe^{2+} (final concentrations) in HEPES buffer, pH 7.4.

Biochemical assays

The total ATPase activity (Quigley and Gotterer, 1969) and succinate dehydrogenase activity (Caplan and Greenwalt, 1968) were estimated by standard methods. Succinate dehydrogenase activity was expressed as units and one unit is defined as one µmole of dichlorophenol indophenol reduced/min/mg protein (Sajan, Satav et al. 1995). Protein oxidation products were estimated as protein carbonyls (Palamanda and Kehrer, 1992). Appropriate sample blanks were taken to

ensure that plumbagin does not interfere with the assay methods. Statistical analysis of the data was done using Student's 't' test.

Determination of rate constant by pulse radiolysis studies

To study the reaction of plumbagin with $^{\cdot}OH$, pulse radiolysis technique was employed. 7 MeV electrons from linear accelerator of pulse widths 50 ns were used and the transients were detected by kinetic spectrophotometry. Typical maximum doses with 50 ns pulses were 15 Gy (Das and Priyadarsini, 1994). The dosimetry was performed with air saturated 0.01 mol dm^{-3} KSCN solution with a $G\epsilon$ (500 nm) value of 2.23 x 10^{-4} M^2J^{-1} for $(SCN)_2^{\cdot-}$ transient species. The kinetic spectrophotometric detection system covered the wavelength range from 280 to 800 nm. Cells with optical path length of 1 cm were used for these measurements. For pulse radiolysis measurements the absorbed dose was kept to a minimum to avoid decomposition of the test compound and the samples were changed after every pulse to minimize losses due to sample decomposition. The reactions of plumbagin (1 x 10^{-4} mol dm^{-3}, pH 6.7) with $^{\cdot}OH$ were carried out using N_2O-saturated aqueous solution where e^-_{aq} is quantitatively converted to $^{\cdot}OH$ ($N_2O + e^-_{aq} \rightarrow {}^{\cdot}OH + OH^- + N_2$). The bimolecular rate constants were calculated by plotting pseudo first order rate of formation of the transient against the concerned solute concentration. The uncertainty in the measurement in bimolecular rate constant is ± 10%.

Results

Fig. 1a presents data on the comparative potentials of the three different tissues, brain, liver and heart to ascorbate-Fe^{2+} induced lipid peroxidation. The lipid peroxidation in the brain was much higher than other tissues (almost 3 times than liver and 10 times that of heart, at 10 min of incubation). The increase in lipid peroxidation as a function of time also started very early in the brain. The lipid peroxidation induced by AAPH and H_2O_2-Fe^{2+} was quite low as compared to that induced

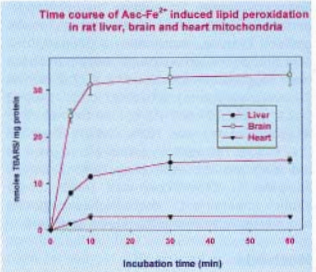

Fig. 1a : Ascorbate-Fe^{2+} induced lipid peroxidation in mitochondria isolated from rat brain, liver and heart. Mitochondria (0.5 mg protein/ml) were exposed to ascorbate-Fe^{2+} system for various incubation times at 37 °C. The formation of TBARS was estimated. The values are ± S.E.M. from 4 experiments

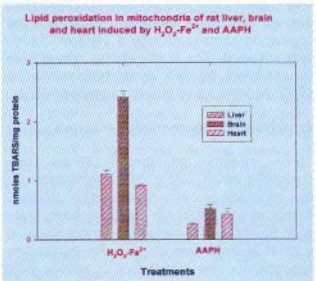

Fig. 1b : H_2O_2-Fe^{2+} and AAPH induced lipid peroxidation in mitochondria isolated from rat brain, liver and heart. Mitochondria (0.5 mg protein/ml) were exposed to H_2O_2-Fe^{2+} or 2,2'-Azobis(2-methyl-propionamide) dihydrochloride (AAPH) systems for 60 min at 37 °C. The formation of TBARS was estimated. The values are ± S.E.M. from 4 experiments

by ascorbate-Fe^{2+} (Fig. 1b). Heart showed relatively high potential for peroxidation with AAPH, almost similar to that of brain. With H_2O_2-Fe^{2+} induced lipid peroxidation also, maximum damage was seen in brain while the extent of damage in liver and heart were

much less and almost similar. The differential susceptibilities of the three tissues can be due to varied composition of substrate for lipid peroxidation as well as the relative amounts of different antioxidants.

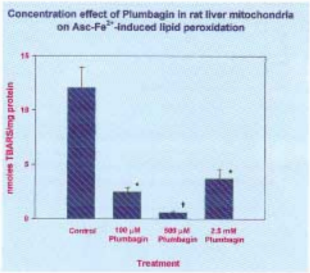

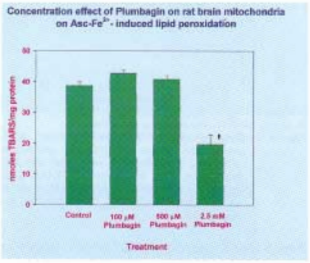

*Fig. 2 : Concentration dependent effect of plumbagin on ascorbate-Fe^{2+} induced lipid peroxidation in mitochondria from rat liver (Fig. 2a) and brain (Fig. 2b). Mitochondria (0.5 mg protein/ml) were exposed to ascorbate-Fe^{2+} system at 37 °C for 60 min, with and without various concentrations of plumbagin. The formation of TBARS was estimated. The values are ± S.E.M. from 4 experiments. * P< 0.01 and ' P< 0.001, as compared to respective controls*

The effects of plumbagin, added in ethanol, on lipid peroxidation in rat liver and brain mitochondria are shown in Fig. 2. In liver, addition of plumbagin showed a concentration dependent inhibition of lipid peroxidation (Fig. 2a). The inhibition amounted to 79.44 % with 100 µM, 95.27 % with 500 µM and 69.23 % with 2.5 mM. In brain, the pattern of alteration was different (Fig. 2b). With 100 and 500 µM there were enhancements of lipid peroxidation by 10.43 % and 5.42 % respectively. At a higher concentration of 2.5 mM, on the other hand, it showed inhibition of lipid peroxidation (49.26 %).

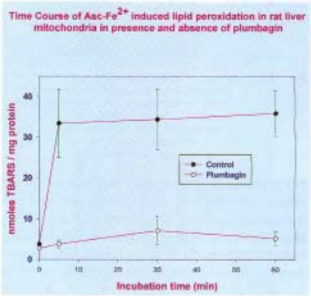

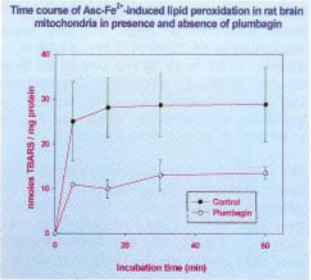

*Fig. 3 : Time course of ascorbate-Fe^{2+} induced lipid peroxidation in from rat liver (Fig. 3a) and brain (Fig. 3b) mitochondria with and without plumbagin incorporated during isolation. The concentration of plumbagin in rat liver mitochondria was 156 µM and in brain 138 µM. The formation of TBARS was estimated. The values are ± S.E.M. from 4 experiments. * P< 0.01 as compared to respective controls*

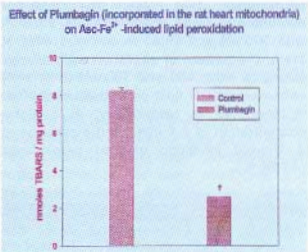

Fig. 3c : Effect of plumbagin on ascorbate-Fe^{2+} induced lipid peroxidation in from rat heart mitochondria incorporated during isolation. The formation of TBARS was estimated. The values are ± S.E.M. from 4 experiments. 'P< 0.001 as compared to respective controls

Fig 3 shows the extent of inhibition observed when plumbagin was incorporated into mitochondria from the three tissues during their isolation. The inhibition observed in rat liver mitochondria (Fig. 3a) with 156 μM was very prominent and amounted to 96.35 % at 5 min (P<0.01), 85.58 % at 30 min (P<0.01), and 91.97 % (P<0.01) at 60 min. The inhibition by plumbagin (138 μM) in brain mitochondria (Fig. 3b) was lower amounting to 56.32 % at 5 min, 64.68 % at 15 min, 54.65 % at 30 min and 53.20 % at 60 min. In heart mitochondria (Fig. 3c) too the incorporated plumbagin showed a significant inhibition (P<0.001), amounting to 68.7 % at 60 min of incubation.

The effects of incorporated plumbagin on lipid peroxidation induced by H_2O_2-Fe^{2+} in different tissues are shown in Fig 4. In both liver and brain (Fig 4a and Fig 4b), plumbagin did not show any significant effect over the entire incubation period of 60 min. However, in rat heart mitochondria, plumbagin incorporation showed significant inhibition of lipid peroxidation. Similar inhibition by plumbagin incorporation was also seen with AAPH-induced lipid peroxidation in heart but not in other tissues (Table 1). In liver, however, there was no significant effect.

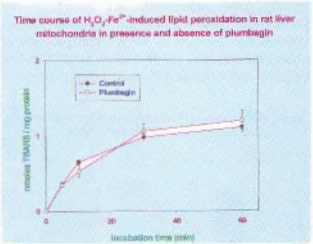

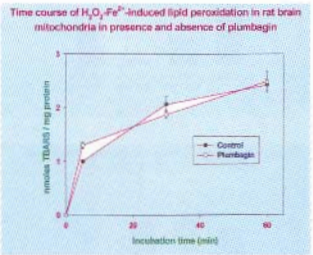

Fig. 4 : Time course of H_2O_2-Fe^{2+} induced lipid peroxidation in rat liver (Fig. 4a) and brain (Fig. 4b) mitochondria with and without plumbagin. The formation of TBARS was estimated. The values are ± S.E.M. from 4 experiments. 'P< 0.001 as compared to respective controls

Figs.5 and 6 show the effect of plumbagin on the levels of two mitochondrial enzymes namely ATPase and succinate dehydrogenase (SDH). Plumbagin did not influence the levels of total ATPase altered by both ascorbate-Fe^{2+} and H_2O_2-Fe^{2+} in rat liver mitochondria (Fig 5a & 5b). The effect of plumbagin on AAPH induced oxidative damage of SDH is shown in Fig 6a and Fig 6b. Since ascorbate interfered with SDH assay, we could not ascertain the effect of plumbagin incorporation on ascorbate-Fe^{2+} induced damage to SDH. In both liver and brain mitochondria, plumbagin was able to significantly protect SDH against oxidative damage.

Table 1 : Effect of 'incorporated plumbagin' on AAPH-induced lipid peroxidation in rat liver and heart mitochondria.

Tissues	nmoles TBARS/mg protein			
	Control		Plumbagin	
	0 min	60 min	0 min	60 min
Liver	0	0.26 ± 0.02	0	0.26 ± 0.02
Heart	0	0.43 ± 0.02	0	0

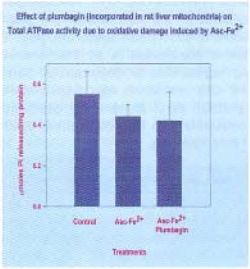

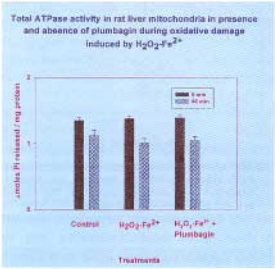

*Fig. 5: Effect of incorporated plumbagin on ascorbate-Fe^{2+} induced (Fig. 5a) and H_2O_2-Fe^{2+} induced (Fig. 5b) oxidative damage on ATPase in rat liver mitochondria. The values are ± S.E.M. from 4 experiments. *P< 0.001 as compared to respective controls.*

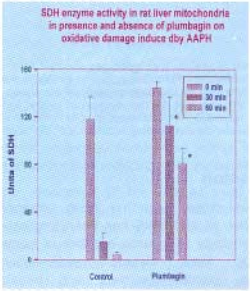

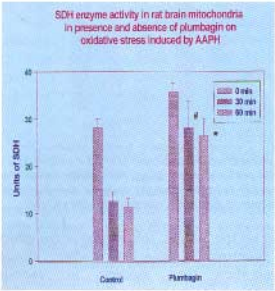

*Fig. 6 : Effect of incorporated plumbagin on AAPH induced oxidative damage on succinate dehydrogenase in mitochondria of rat liver (Fig. 6a) and brain (Fig. 6b). The values are ± S.E.M. from 4 experiments. # P < 0.05, * P< 0.01 and *P< 0.001 as compared to respective controls*

Effect of plumbagin on protein oxidation induced by ascorbate-Fe^{2+} in liver and brain is shown in Fig 7. The ascorbate-Fe^{2+} system induced significant protein oxidation in both rat liver and brain mitochondria. Plumbagin showed a significant protection in liver (56.19 % at 60 min, P<0.01).

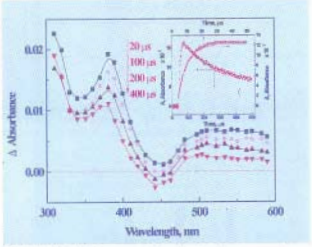

Fig. 7 : Effect of incorporated plumbagin on ascorbate-Fe^{2+} induced oxidative damage on protein oxidation in rat liver mitochondria. The values are ± S.E.M. from 4 experiments.
** P< 0.01 as compared to respective controls*

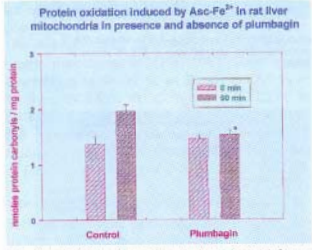

Fig. 8 : Transient absorption spectra obtained from a N_2O-saturated aqueous solution of pH 6.7 containing 1 x 10^{-4} mol dm^{-3} plumbagin. Inset: Absorbance versus time plot for (a) formation and (b) decay of the plumbagin radical formed during the reaction with ·OH radical

Based on the results, the antioxidative effect of plumbagin, especially after tissue incorporation was evident in various biological test systems. Considering that Fenton systems (both ascorbate-Fe^{2+} and H_2O_2-Fe^{2+}) generally operate via the intermediary of hydroxyl radical, its reaction with plumbagin was also examined using pulse radiolysis technique.

Reaction of plumbagin with ·OH derived from radiation pulses yielded a plumbagin radical (PbZ radical) (Fig. 8). The time course of such radical formation is shown in Inset of Fig. 8. The radical formation increased rapidly upto 20 µs after which it got stabilized. The decay of PbZ radical started after about 100 µs and continued upto 500 µs to reach approximately half the absorbance (Inset of Fig. 8). The absorption characteristics of the PbZ radical are shown as a transient absorption spectrum (Fig. 8). The peak of absorption is at 390 nm with bleaching region due to depletion of parent at around 450 nm. Such absorbance of PbZ radical plotted as a function of plumbagin gave a relatively high rate constant of 2.03 x 10^9 dm^3 mol^{-1} s^{-1} (Fig. 9).

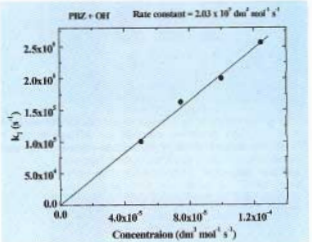

Fig. 9 : Plot of pseudo-first order rate constant for the formation of plumbagin radical (measured at 380 nm) for the determination of bimolecular rate constant for the reaction of radical with plumbagin. The bimolecular rate constant as found by this method is 2.03 x 10^9 dm^3 mol^{-1} s^{-1}

Discussion

Oxidative stress resulting from enhanced generation of ROS/RNS has been implicated in the etiology of a large number of human ailments. hese include cardiovascular ailments, neural disorders and hepato-toxicities induced by various toxicities (Sies, 1996; Thomas and Kalyanaraman, 1997). Mechanisms of damage linking oxidative

stress to disease involve undesirable alterations to lipid and protein components of membranous organelles (Sies, 1996; Cuzzocera, Riley et al., 2001). Among the subcellular organelles, mitochondria are considered as important (major) targets of oxidative damage being responsible for reduced cellular functions in the form of energy generation or responsible for cell death (Raha and Robinson, 2000). Oxidative damage to mitochondria adversely affects specific carriers for succinate, citrate and oxaloacetate, as a result their intracellular levels are reduced (Salet and Moreno, 1990). Membrane lipids, due to the presence of polyunsaturated fatty acids, are highly prone to oxidative damage induced by various oxidants. In our studies we have used mitochondria from rat liver, brain and heart whose damage may be linked to the diseases for which *Plumbago zeylanica* has been suggested as a cure.

P. zeylanica has been credited with various therapeutic properties. Some of these pertain to diseases of the nervous, cardiovascular and gastrointestinal systems as well as for hepatotoxicities. Plumbagin from *P. zeylanica* has been suggested as the 'active ingredient' in medications and herbal preparations (Gupta, Verma et al., 1993). To examine possible mechanisms of action, we have studied the ability of plumbagin to prevent oxidative damage in mitochondria isolated from these tissues. The three endogenously relevant systems are ascorbate-Fe^{2+} that generates $^{\cdot}OH$ radical-like species, H_2O_2- Fe^{2+} that yields $^{\cdot}OH$ and AAPH that releases peroxyl radical ($ROO^{\cdot}$) on incubation at the physiological temperature of 37 °C (Kamat, Boloor et al., 2000). The above three systems also differ in their mechanisms in inducing lipid peroxidation.

The responses of the tissues used namely brain, liver and heart to the above mentioned oxidant-generating systems significantly differ. Brain is rich in polyunsaturated fatty acids that are substrates for peroxidation. Liver and heart contain lesser amounts of these components. The amounts of endogenous antioxidants like glutathione, vitamins C and E as well as antioxidant enzymes also are different in these tissues (Pushpendran, Subramanian et al, 1998). The differential response of the three tissues to oxidants as well as the extent of inhibitions with plumbagin can be attributed to these factors.

Lipid peroxidation in tissues is controlled by the interaction of several factors. These include (i) availability of substrates for peroxidation in the form of unsaturated fatty acids mainly present in phospholipids, (ii) inducers of peroxidation such as ascorbate, Fe^{2+}, compounds which can convert Fe^{3+} to Fe^{2+}, oxygen, initiators of free radical reactions and functioning of the electron transport chain which serve as sources of reactive species, (iii) antioxidant defense in the form of glutathione, α-tocopherol, superoxide dismutase, carotenoids, substances chelating Fe^{2+}, substances reducing lipid hydroperoxide, a GSH dependent labile factor and glutathione peroxidase system etc., and (iv) the physical properties of the membrane lipid such as fluidity and surface charge and the location of the polyunsaturated fatty acid in the membrane. Our earlier studies showed that the tissues examined (brain, liver and heart) significantly differ from each other in their susceptibility to undergo lipid peroxidation when oxidative damage is induced *in vitro* (Devasagayam, 1983; Pushpendran, Subramanian et al., 1998). Among these tissues brain is extremely susceptible to oxidative damage due to high levels of unsaturated fatty acids and the increased capacity of oxygen consumption (Kamat and Devasagayam, 1999).

Plumbagin protects against oxidative damage in majority of our experiments. The inhibition is observed with lipid peroxidation, protein oxidation as well as against inactivation of succinate dehydrogenase. The protective effect, however, was not seen with ATPase. Among the three systems used to induce oxidative damage, protection was observed against oxidative damage induced by ascorbate-Fe^{2+} and AAPH, and not against H_2O_2- Fe^{2+}. This can probably be attributed to inability of plumbagin to neutralise either H_2O_2 or Fe^{2+} or both in this system.

Incorporation of plumbagin into mitochondria also was more effective than external addition to mitochondria. This may possibly be due to better uptake and presence of plumbagin at the site of ROS generation inside mitochondria. The extent of inhibition observed is relatively less as compared to other antioxidants like α-tocopherol, tocotreinols or curcumin (Nesaretnam, Devasagayam et al., 1993; Kamat and Devasagayam, 1995; Sreejayan, Rao et al., 1997; Devasagayam, Kamat et al., 2001). Hence it may indicate that *P. zeylanica* may also contain other components with better antioxidant activities.

Though in our experiments plumbagin has not been used in whole cell systems, whole organs or animal levels many studies using such systems have indicated the beneficial effects of plumbagin. For instance it has immunomodulatory effects as assessed by macrophage functions in BALB/c mice (Kamal and Rao, 1995), and anticancer effects in different systems such as Ehrlich ascites tumors and sarcoma 180 in mice (Singh and Udupa, 1997; Naresh, Udupa et al., 1996, Devi, Solomon et al., 1999), lymphocytic leukemia in mice (Krishnaswamy and Purushothaman, 1980), Dalton's ascites lymphoma in mice (Kavimani, Ilango et al., 1996), methylcholanthrene induced fibrosarcoma in rats (Krishnaswamy and Purushothaman, 1980) and azoxymethane induced intestinal carcinogenesis in rats (Sugie, Okamoto et al. 1998). Similar in vivo studies for checking the antioxidant activity of plumbagin using various indicators of oxidative damage can yield rich dividends.

In certain systems plumbagin has been observed to have prooxidant effects due to its redox cycling. This is observed mainly in biological systems lacking superoxide dismutase (SOD) as in the case of anaerobic bacteria. This also has been postulated to account for its antimicrobial activity (Archibald and Fridovich, 1981; Diguiseppi and Fridovich, 1982). In aerobic systems, however, such an effect was not observed.

The possible reason for the observed antioxidant effect of plumbagin can be due to radical scavenging as observed by pulse radiolysis. In our studies we have shown that reaction of radiation derived radicals lead to the formation of plumbagin radical that is fairly stable. The radical is probably a phenoxyl type of radical. The characteristic absorption peak at 430 nm is buried into the bleaching spectrum due to the depletion of the parent. But the broad absorption around 500 nm due to the said radical is evident. The decay of the radical as measured at 390 nm was found to be of mixed order. The spectral as well as kinetic characteristics of the radical, matches well with the known phenoxyl radical. Hence the mechanistic pathway for the free radical scavenging property of plumbagin is via the formation of phenoxyl radical.

In conclusion, our studies show that plumbagin, isolated from *P. zeylanica* exhibit antioxidant effects in the form of membrane protective properties in mitochondria from three different rat tissues, liver, brain and heart. The extent of inhibition observed differs in these tissues. The observed antioxidant effects of plumbagin can be explained based on its ability to scavenge ·OH, as is seen in our pulse radiolysis experiments. The antioxidant ability of plumbagin, considered as the active ingredient of *P. zeylanica*, may at least, in part, explain observed therapeutic properties of this medicinal plant.

Acknowledgements

The authors wish to thank Dr K.B. Sainis, Head, Cell Biology Division, for his encouragement and helpful suggestions as well as Mr D.V. Kathole for his excellent technical assistance. They also wish to thank Dr Gnanadhass Devasahayam, Professor, Government Siddha Medical College, Tirunelveli, Tamil Nadu, for his helpful suggestions regarding *P. zeylonica* and emphasizing the importance of this medicinal plant in Indian systems of medicine, which prompted the authors to take up this work.

References

1. Archibald, F.S. and Fridovich, I. (1981). Manganese, superoxide dismutase, and oxygen tolerance in some lactic acid bacteria. J. Bacteriol. 146: 928-936.
2. Bhargava, S.K. (1986). Effect of testosterone replacement therapy on quantitative spermatogenesis following plumbagin treatment in immature rats. Acta. Eur. Fertil. 17: 217-219.
3. Caplan, A.I. and Greenawalt, J.W. (1968). The effect of osmotic lysis on the oxidative phosphorylation and compartmentation of rat liver mitochondria. J. Cell Biol. 36: 15-31.
4. Cuzzocrea, S., Riley, D.P., Caputi, A.P. and Salvemini, D. (2001). Antioxidant therapy: a new pharmacological approach in shock, inflammation, and ischemia/reperfusion injury. Pharmacol. Rev. 53: 135-159.
5. Devasagayam, T.P.A., Pushpendran, C.K. and Eapen, J. (1983). Differences in lipid peroxidation in rat liver rough and smooth microsomes. Biochim. Biophys. Acta. 750: 91-97.
6. Devasagayam, T.P.A. (1986). Lipid peroxidation in rat uterus. Biochim. Biophys. Acta. 876: 507-514.
7. Devasagayam, T.P.A., Kamat, J.P. and Sreejayan N. (2001). Antioxidant action of curcumin. In: *Microneutrients and Health. : Molecular Biology Mechanism*. Edited by Nesaretnam K. and Packer L.. AOCS Press, Champaign, IL, USA, pp.42-59.
8. Devi, U., Solomon, F.E. and Sharada, A.C (1999). Plumbagin, A plant naphthoquinone with antitumor and radiomodifying properties. Pharmaceutic. Biol. 37: 231-236.
9. Diguiseppi, J. and Fridovich, I. (1982). Oxygen toxicity in *Streptococcus sanguis*. The relative importance of superoxide and hydroxyl radicals. J. Biol. Chem. 257: 4046-4051.
10. Dinda, B. and Saha, S. (1989). A new binaphthoquinone from *Plumbago zeylanica* Linn. Indian J. Chem. Section B- Org. Chem. Including Med. Chem. 28: 984-986.
11. Dinda, B., Hajra, A.K. and Chel, G. (1997). Naphthoquinones of *Plumbago* species - A Review. J. Indian Chem. Soc. 74: 974-979.
12. Durga, R., Sridhar, P. and Polasa, H. (1992). Antimutagenic activity of plumbagin in Ames *Salmonella typhimurium* test. Indian J. Med. Res. 96: 143-145.
13. Gunaherath, G.M.K.B., Gunatilaka, A.A.L. and Thomson, R.H. (1988). Studies on medicinal and related plants of Sri Lanka: Part 18. Structure of a new naphthoquinone from *Plumbago zeylanica*. J. Chem. Soc. Perkin Transac. 10: 407-410.
14. Gupta, M.M., Verma, R.K., Uniyal, G.C. and Jain, S.P. (1993). Determination of plumbagin by normal phase high performance liquid chromatography. J. Chromat. 637: 209-212.
15. Gupta, A., Siddiqui, I.R., Singh, J., 2000. A new anthraquinone glycoside from the roots of *Plumbago zeylanica*. Indian J. Chem. 39 B, 796-798.
16. Hammer, C.T., Wills, E.D., 1978. The role of lipid components of the diet in the regulation of fatty acid composition of the rat liver endoplasmic reticulum and lipid peroxidation. Biochem. J. 174, 385-393.
17. Itoigawa, M., Takeya, K., Furukawa, H., 1991. Cardiotonic action of plumbagin on guinea-pig papillary muscle. Planta Med. 57, 317-319.
18. Kamat, J.P., Devasagayam, T.P.A., 1995. Tocotrienol from palm oil as potent inhibitors of lipid peroxidation and protein oxidation in rat brain mitochondria. Neurosci. Lett. 195, 179-182.
19. Kamat, J.P., Devasagayam, T.P.A., 1996. Methylene blue plus light induced lipid peroxidation in rat liver microsomes: inhibition by nicotinamide (vitamin B3) and other antioxidants. Chem.-Biol. Interact. 99, 1-16.
20. Kamat, J.P., Devasagayam, T.P.A., 1999. Nicotinamide (vitamin B3) as an effective antioxidant against oxidative damage in rat brain mitochondria. Redox Report. 4, 179-184

21. Kamat, J.P., Boloor, K.K., Devasagayam, T.P.A., 2000. Chlorophyllin as an effective antioxidant against membrane damage in vitro and ex vivo. Biochim. Biophys. Acta. 1487, 113-127.
22. Kirtikar, K.R., Basu, B.D., (Eds) 1984. Indian Medicinal Plants, Vol – I & II, Publishers Blatter, E., Cauis, J.R. and Mhaskar, K.S., Basu, L.M., Allahabad, India.
23. Lele, R.D., 1999. Ayurveda (ancient Indian system of medicine) and modern molecular medicine. J. Assoc. Physicians. India. 47, 625-628.
24. Lele, R.D., 2001. Ayurveda and modern medicine. Bharatiya Vidya Bhavan, Mumbai.
25. Mantle, D., Lennard, T.W., Pickering, A.T., 2000. Therapeutic applications of medicinal plants in the treatment of breast cancer: a review of their pharmacology, efficacy and tolerability. Adverse Drug React. Toxicol. Rev. 19, 223-240.
26. McDermott, J.H., 2000. Antioxidant nutrients: current dietary recommendations and research update. J. Am. Pharm. Assoc. 40, 785-799.
27. Munday, A.D., Sriratana, A., Hill, J.S., Kahl, S.B., Nagley, P., 1996. Mitochondria are the functional intracellular target for a photosensitizing boronated porphyrin. Biochim. Biophys. Acta. 1311, 1-4.
28. Nesaretnam, K., Devasagayam, T.P.A., Singh, B.B., Basiron, Y., 1993. Influence of palm oil or its tocotrienol-rich fraction on the lipid peroxidation potential of rat liver mitochondria and microsomes. Biochem. Mol. Biol. Internatl. 30, 159-167.
29. Okamoto, T., Hino, O., 2000. Drug development with hints from traditional Indian *Ayurveda* medicine: hepatitis and rheumatoid as an example. Int. J. Mol. Med. 6, 613-615.
30. Oyedapo, O.O., 1996. Studies on bioactivity of the root extract of *Plumbago zeylanica*. Int. J. Pharm. 34, 365-369.
31. Palamanda, J.R. and Kehrer, J.P., 1992. Inhibition of protein carbonyl formation and lipid peroxidation by glutathione in rat liver microsomes. Arch. Biochem. Biophys. 293: 103-109.
32. Payne, C.M., Bernstein, C., Bernstein, H., Gerner, E.W., Garewal, H., 1999. Reactive nitrogen species in colon carcinogenesis. Antioxid. Redox Signal. 1, 449-467.
33. Premakumari, P., Rathinam, K., Santhakumari, G., 1977. Antifertility activity of plumbagin. Indian J. Med. Res. 65, 829-838.
34. Pushpendran, C.K., Subramanian, M., Devasagayam, T.P.A., Singh, B.B., 1998. Study on lipid peroxidation potential in different tissues induced by ascorbate-Fe^{2+}: Possible factors involved in their differential susceptibility. Mol. Cell. Biochem. 178, 197-202.
35. Quigley, J.P. and Gottere, G.S., 1969. Distribution of (Na^+-K^+)-stimulated ATPase activity in rat intestinal mucosa. Biochim. Biophys. Acta. 173, 456-468.
36. Raha, S., Robinson, B.H., 2000. Mitochondria, oxygen free radicals, disease and ageing. Trend. Biotechnol. 25, 502-508.
37. Rao, A.V., Agarwal, S., 2000. Role of antioxidant lycopene in cancer and heart disease. J. Am. Coll. Nutr. 19, 563-569.
38. Sajan, M.P., Satav, J.G., Bhattacharya, R.K. 1995. Activity of some respiratory enzymes and cytochrome contents in rat hepatic mitochondria following aflatoxin B_1 administration. Toxicol. Lett. 80, 55-60.
39. Salet, C., Moreno, G., 1990. New trends in pathobiology. Photosensitisation of mitochondria. Molecular and cellular aspects. J. Photochem. Photobiol. B Biol. 5, 133-150.
40. Sharma, A., Singh, R.T., Sehgal, V., Handa, S.S., 1991a. Antihepatotoxic activity of some plants used in herbal formulations. Fitoterapia. 62, 131-138.
41. Sharma, I., Gusain, D., Devi,P.U., 1991b. Hypolipidaemic and antiatherosclerotic effects of plumbagin in rabbits. Indian J. Physiol. Pharmacol. 35, 10-14.

42. Sies, H., 1996. Antioxidants in Disease, Mechanisms and Therapy. Academic Press, New York.
43. Sreejayan N., Rao, M.N.A., Priyadarsini, K.I., Devasagayam, T.P.A., 1997. Inhibition of radiation induced lipid peroxidation by curcumin. Int. J. Pharm. 151, 127-130.
44. Sugie, S., Okamoto, K., Rahman, K.M., Tanaka, T., Kawai, K., Yamahara, J., Mori, H., 1998. Inhibitory effect of plumbagin and juglone on azoxymethane-induced intestinal carcinogenesis in rats. Cancer lett. 127, 177-183.
45. Thakur, R.S., Puri, H.S. and Husain, A., 1989. Major Medicinal Plants of India., Central Institute of Medicinal and Aromatic Plants, Lucknow, India.
46. Thomas, C.E., Kalyanaraman, B., 1997. Oxygen Radicals and the Disease Process. Harwood Academic Publishers, The Netherlands.
47. Tripathi, Y.B., 2000. Molecular approach to ayurveda. Indian J. Exp. Biol. 38, 409-414.

This paper won the Best Poster award at the International Conference on "Natural Antioxidants and Free Radicals in Human Health & Radiation Biology (NFHR-2001)" held at Mumbai during July 21-24, 2001.

About the authors ...

Ms Jai C. Tilak *has received her M. Sc. degree in Life Sciences (specialization Biotechnology) from Ruia College, Mumbai, in 2000. She was a topper during her Graduation and Post Graduation from the same college. At present, she is a DAE fellow attached with Cell Biology Division, BARC, pursuing her Ph.D. on a subject entitled, "Studies on the antioxidant effects and other beneficial properties of some Indian medicinal plants".*

Dr T.P.A. Devasagayam *joined BARC in 1975 through BARC Training School in Biology and Radiobiology. At present, he is with Cell Biology Division, BARC. He is deeply involved in research related to Human Health and Radiation Biology. He has done his Post Doctoral work at the University of Dusseldorf, Germany, and at Wagne State University, USA. He holds the post of Honorary Secretary General of SFRR-India and also EMSI-India.*

Ms Meenal Banerjee *received her M.Sc. degree in Microbiology from School of Life Sciences, Devi Ahilya Vishva Vidyalaya, Indore, in 2001. Recently she has joined NCCS, Pune, for her Ph.D. Degree.*

Dr S. Adhikari *received his M. Sc. degree from the Visva-Bharati University, Shantiniketan, in 1989. He graduated from the BARC Training School in 1991 and started his research career in the then Chemistry Division. He obtained his Ph.D. Degree from the University of Mumbai in 2000. In 1999, he worked as a guest scientist in the University of Leipzig, Germany. He is the recipient of the prestigious IUPAC award for young chemist for the year 2001. His recent research interests include Radiation Chemistry in micro-heterogeneous systems and Antioxidants.*

Dr G. I. Chintalwar *joined the Bio-Organic Division in 1967. His work pertains to natural product chemistry and application of radioactive tracer technique for biosynthetic studies of secondary metabolites. His major contributions in these areas are the isolation of various antitumour/ anticancer compounds, natural immunomodulators and radioprotectants. He has also developed a new phytoformulation for application in sericulture.*

Dr S. Chattopadhyay *joined the Bio-Organic Division in 1981 after graduating from the 24th batch of Training School as a chemistry trainee. Presently, he is Head, Bio-Organic Division, BARC. His research interests include asymmetric synthesis, supra-molecular chemistry and chemical biology.*

Molecular Evidence that the Indian Population of *Colletotrichum graminicola* (sorghum anthracnose) is Hypervariable

J. Latha, Apratim Chakrabarti, Prasun K. Mukherjee and R.P. Thakur
Nuclear Agriculture and Biotechnology Division
Bhabha Atomic Research Centre

Abstract

Colletotrichum graminicola is a serious pathogen of sorghum in many parts of the world. Morphological and pathogenic diversity among sorghum isolates of C. graminicola in India is well established. In order to assess the extent of variability and the distribution of the population, we studied the genetic variability of several sorghum isolates of this fungus isolated from India. Initially, 18 isolates collected from Maharashtra and Andhra Pradesh were subjected to RAPD (random amplified polymorphic DNA) analysis, and 11 sub-groups were established. Even, isolates from the same leaf lesion were found to differ from each other in the RAPD profile. Subsequently, we used a more robust PCR-based technique in order to avoid the drawbacks inherent in the RAPD system, e.g., the reproducibility. In the second assay, we amplified the ribosomal DNA intergenic spacer (IGS) region of 20 isolates collected from 5 states of India. The isolates could be sub-grouped into 6 groups based on the size of the amplicon. IGS fragments from the same size group were further analysed by restriction digestion with various enzymes. Two of the restriction enzymes (KpnI and PstI) could further differentiate between the isolates of the same IGS-size groups. Using this technique, we could classify the 20 isolates to 12 sub-groups. These evidences suggest that the Indian polulation of C. graminicola is hypervariable.

Introduction

Sorghum anthracnose, caused by *Colletotrichum graminicola* (Ces.) Wilson, is a destructive disease responsible for as high as 50% loss in grain yield (Ali and Warren, 1992). *Colletotrichum graminicola* is a highly variable pathogen. It is well recognized that pathogenic variability poses difficulty in development and deployment of effective host resistance, which is a dependable and economic means of disease management. In India, several sorghum hybrids with multiple disease resistance are cultivated commercially. A rapid and reproducible tool for characterizing the pathogen genotypes would help researchers to follow the shift in genetic make-up of the pathogen population and thus providing a dynamic picture of the interactions between the host and pathogen genotypes. This would, in turn, help devising strategies for management of this disease. Genetic variability in this fungus is widely studied by using molecular tools like RFLP and RAPD. Restriction analysis of the intergenic spacer region of the rDNA repeats has been useful for variability studies in some fungi like *Fusarium oxysporum* (Appel and Gordon, 1995; Chakrabarti et al. 2001) and *Pyrenophora graminea* (Pecchia et al., 1998). Once optimized (primer sequences and enzyme combinations), this technique combines the advantage of both PCR (simplicity and speed) and RFLP (reproducibility).

Materials and Methods

The *C. graminicola* isolates were collected from six provinces of India where sorghum is cultivated widely. Monoconidial isolates were grown in potato dextrose medium and DNA isolated according to Mukherjee (1999). For RAPD analysis, six random primers from kit A of Operon Technologies, Inc. (OPA- 1, 2, 5, 9, 10 and 15) were used. These primers were selected after a primary screening of all the 20 primers from kit A. For amplification, 50ng of DNA, 0.2mM primer, 0.1mM each dNTPs and 1.0U Taq polymerase (Genei)

were used. The denaturation temperature was 94°C for 1 min and extension temperature 72°C for 2 min. An annealing temp. of 37°C (for 1 min), which is used normally for RAPD was used except for primers OPA1, 2, 9, 15 which have higher thermodynamic Tm, 40°C was used. This modification improved the results by eliminating the non-specific and non-reproducible bands. The amplified products were size separated on 1.5% agarose gel, stained with ethidium bromide and photographed using a polaroid camera. The bands were scored as 1 (if present) or (0 if absent), data analyzed using TreeconW software and a phylogenetic tree constructed. For amplification of the IGS region, primer pair CLN12 (CTGAACGCCTCTAAGTCAG) and CNS1 (GAGACAAGCATATGACTACTG) designed by Appel and Gordon (1995) for *F. oxysporum* were used. Amplification was done at 56°C and separated on 1% agarose gel. Based on the variation in the size of the IGS region, the isolates were first grouped into different size groups and isolates from each size group were analyzed separately for restriction pattern. Initially, eight restriction endonucleases (*Bam*HI, *Eco*RI, *Hind*III, *Pst*I, *Kpn*I, *Sac*I, *Sal*I and *Xho*I), all hexa-base cutters, were used to study the number of sites in the *C. graminicola* isolates from a single group. Based on this result, *Kpn*I and *Pst*I were selected for studies with other groups.

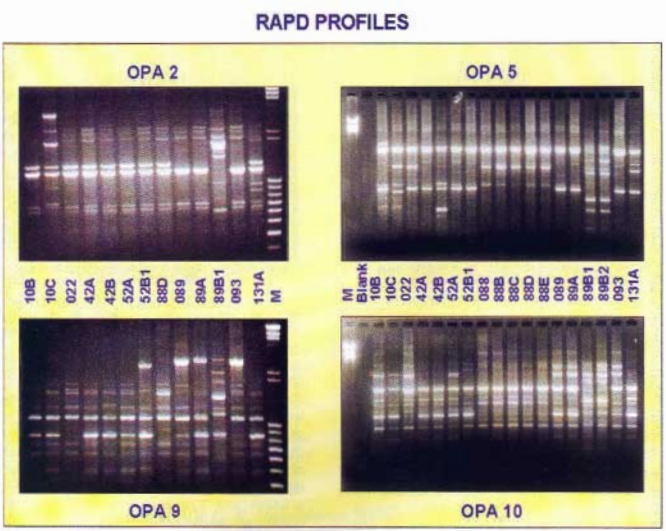

Fig. 1: RAPD profile of Colletotrichum graminicola with primers OPA – 2, 5, 9 & 10

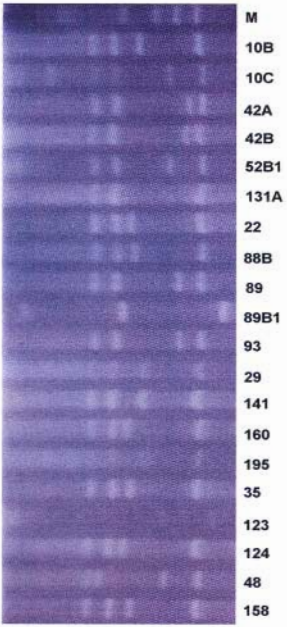

Fig. 2 : Size polymorphism in the PCR- amplified intergenic spacer (IGS) regions of Colletotrichum graminicola isolates

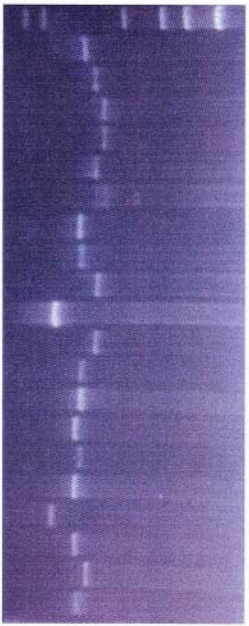

Fig. 3 : Restriction pattern (KpnI) in the amplified IGS regions of different size groups of Colletotrichum graminicola. M denotes molecular weight marker

Results and discussion

Of the eighteen isolates from different localities/single lesions, the isolates 88, 88B, 88C, 88D & 88E (all from a single lesion) were exactly the same with respect to the RAPD profile with the six primers tested. The same was true for 89B1 and 89B2; though 89B1/B2 differed considerably from 89 and 89A (all derived from single lesion). All the isolates (except the two groups mentioned above) were different from each other, even though some originated from the same lesion (Fig. 1). By and large, two major clusters were formed: 89B1/89B2 as one & the rest as one. There was no effect of place of isolation, rather two isolates from two different provinces (eg. 42A from Andhra pradesh and 52A from Maharashtra) were closer to each other than two isolates originating from even the same lesion (e.g.: 42A and 42B). RAPD analysis of *C.*

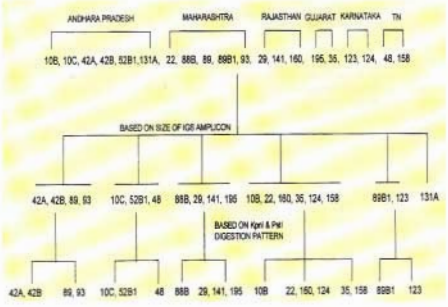

Fig. 4 : Grouping of Colletotrichum graminicola isolates based on origin & IGS polymorphism

gramimnicola isolates indicated that sorghum isolates of *C. graminicola* from India are hyper-variable with distinct genetic variations.

PCR amplification of the IGS region with the primer pair CLN12 and CNS1 yielded single band (except for the isolate 131A, where a doublet could be seen) of 2.5-3.5 kb (Fig. 2). Based on the size and number of amplicons, the 20 isolates could be grouped into six groups (group1: 10C, 52B1, 48; group 2: 42A, 42B, 89, 93; group 3: 88, 29, 141, 195; group 4: 10B, 22, 160, 35, 124, 158; group 5: 89B1, 123; group 6: 131A). Analysis of the isolates from group 1 using 8 restriction enzymes revealed no site for *Bam*HI, *Eco*RI, *Hind*III, *Sac*I, *Sal*I and *Xho*I in the IGS region. *Pst*I had single site and *Kpn*I had three sites, thus yielding four fragments upon digestion of the amplified IGS region. Based on the restriction pattern with *Kpn*I or *Pst*I, isolates 10C and 52B1 could be differentiated from 48. Isolates from the other groups were then analyzed using *Kpn*I and *Pst*I. Based on the polymorphism with respect to these sites in the IGS region, 42A and 42B could be differentiated from 89 and 93; 88 from 29, 141 and 195; and 89B1 from 123 and, the isolates in group 4 could be sub-grouped into three clusters: 10B, 22/160/124, and 35/158. Based on these observations, it was decided that *Kpn*I digestion of the amplified IGS region is a good indicator of genetic polymorphism in *C. graminicola*. We, therefore, digested the IGS region for all the 20 isolates with *Kpn*I and the digestion pattern revealed that this could be used as a sound fingerprinting technique for this pathogen (Fig. 3).

References

1. Ali MEK and Warren HL (1992) Anthracnose of sorghum. Pages 203-208 *In* Sorghum and millet diseases: a second world review (de Milliano WAJ, Frederiksen RA and Bengston GD eds). Patancheru, India: International Crops Resesrch Institute for the Semi-Arid Tropics.
2. Appel DJ and Gordon TR (1995) Phytopathology 84: 786-791.
3. Chakrabarti A, Mukherjee PK, Sherkhane PD, Bhagwat AS and Murthy NBK (2001) Current Science 80: 571-575.
4. Mukherjee, P.K., *As-Pac. J. Mol. Biol. Biotechnol.* 1999, **7**, 95-96
5. Pecchia S, Mercatelli E and Vannacci G (1998) FEMS Microbiology Letters 166: 21- 27.

This paper received "Dr G. R. Damodaran Memorial Award" for the Best Paper at the National Seminar on "Microbial Technology", held at G. R. Damodaran College of Science, Coimbatore, during June 1-2, 2001

About the authors ...

Ms J. Latha, *M.Sc (Biotechnology), is from the 42nd batch of BARC Training School. She is the recipient of the "Homi Bhabha Award" for Biology-Radiobiology discipline in her batch, and is working in the Plant Pathology and Pesticide Residues Section of Nuclear Agriculture and Biotechnology Division (NABTD).*

Dr P. K. Mukherjee. *M.Sc (Agriculture), completed his Ph.D. as a Krishnan DAE research fellow. He is working in the Plant Pathology and Pesticide Residues Section of Nuclear Agriculture and Biotechnology Division (NABTD), on the biocontrol mechanisms of plant diseases. He was awarded the "Pran Vohra Award" for agriural sciences during 1998-1999 by the Indian Science Congress Association.*

Mr Apratim Chakrabarti, M.Sc., is from 41st batch of BARC Training School. He won the Homi Bhabha Award for Biology-Radiobiology Discipline in his batch. He worked in the Plant Cell Culture Technology Section of Nuclear Agriculture and Biotechnology Division.

Radionuclide Biosorption by Bacterial Biomass

Pinaki Sar and S. F. D'Souza
Nuclear Agriculture and Biotechnology Division
Bhabha Atomic Research Centre

Abstract

Bacterial isolates from uncontaminated garden soil were found to be good biosorbents of radionuclides. Among the strains, a copper resistant Pseudomonas was identified as a potent accumulator of uranium (VI) and thorium (IV). Radionuclide (U) accumulation by the bacterium was found insensitive to culture age (lag, log and stationary) so also in presence of carbon/energy source (glucose) and metabolic inhibitor (sodium azide), suggesting it as passive biosorptive uptake. Bacterial cells grown in peptone rich enriched medium or in synthetic minimal medium showed no significant difference in U accumulation at lower U concentration (100 mg l^{-1}). However, at higher concentration range (1000 mg l^{-1}) minimal medium grown cells showed a significantly high metal loading. Such biosorptive uranium and thorium uptake capacity of the bacterium was characterized using metabolically inactivated lyophilized biomass. Radionuclide binding by the test bacterium was rapid, achieving >90% within 1-10 minutes of contact and the equilibrium was attained within two to four hours. Initial solution pH significantly affected U and Th sorption with its optimum at pH 5.0 for U and pH 4.0 for Th. Equilibrium isotherms for both the metals indicate a high affinity, efficient and high capacity uranium and thorium biosorption with the maximum loading of 541 mg U g^{-1} dry wt. or 430 mg Th g^{-1} dry wt. Experimental sorption data showing good conformity to Langmuir model suggests a monolayered metal binding. Sorption in presence of several interfering cations and anions indicates a specific U and Th binding by the Pseudomonas with significant antagonism offered only by the iron (III). Studies are going on to decipher the bacterial radionuclide binding mechanism using various physico-chemical approaches and to exploit its potential in continuous removal /recovery system.

Introduction

Radionuclide and heavy metal pollution by various industrial activities is of significant environmental concern (Barkay and Schaefer, 2001; D'Souza, 1999a; D'Souza et al 2001a; D'Souza, 2002a). Microbial bioremediation of such toxic compounds are increasingly being considered as a potential alternative with high capacity and efficient metal removal from diluted effluent with almost no secondary waste generation. (Taxier *et al.* 1999 and Lloyd and Macaskie 2000). Although considerable studies are made on microbial removal of heavy metals, radionuclides in this regard remained little explored. Among the several microbial processes that determine the environmental fate of metallic toxicants viz. reductive or enzymatic precipitation, solubilization, etc., biosorptive accumulation of heavy metals and radionuclides is of recent interest (Gadd 2000, Hu *et al.* 1996, Dhami *et al* 1998, Sar *et al* 1999, Sar and D'Souza 2001 a, b). Bioremediation of radionuclides, heavy metals and organic waste has been a major recent activity in the authours laboratory (D'Souza, 1999a; Bhainsa and D'Souza 1999; Joshi and D'Souza, 1999; Sar and D'Souza 2001a,b ; Bhainsa and D'Souza, 2001a,b; Sar *et al*, 2001a,b; Sangurdekar *et al* 2001, Melo and D'Souza, 2001; D'Souza, *et al*, 2001a,b; Kazy, *et al*, 2001; Shanmugam *et al*, 2001; Sar and D'Souza 2002; Kazy *et al* 2002; Panchapakesan *et al*,2002; Irani *et al*, 2002). Compared to the conventional treatment methods, these biomass based systems are more acceptable in being cost effective, with high efficiency of detoxification of even very dilute effluents and minimizing the disposable sludge volume. It also offers the flexibility for developing non-destructive desorption techniques for biomass regeneration and/or quantitative metal recovery.

Metal accumulation by microorganisms is either of energy driven active bioaccumulation or metabolism independent passive biosorption. The latter process of microbial metal removal by purely physico- chemical processes seems more appropriate for bioremediation with cation sequestration mainly regulated by the characteristics of the microorganism, the targeted metal and the solution microenvironment. Since, it is the chemical composition of the cell wall and other surface materials responsible for cation sequestration, cell viability or other metabolic activities that do not interfere with such characteristics effectively have no impact on biosorption. In some cases, pregrowth conditions, particularly, the growth medium ingredients also show significant influence on biosorptive metal uptake.

Although, biosorptive uptake of several heavy metals is well documented, such studies on radionuclide sorption are relatively less. Particularly, with respect to uranium, a variety of living and non-living biosorbents composed of fungi and bacteria have been reported to bind the cation considerably, whereas reports on thorium sorption are not impressive. Previous studies on microbial metal sorption by our group have identified the strains of *Pseudomonas* as a potent accumulator of metals and radionuclides (Sar *et al* 1998, Sar *et al* 1999, Kazy *et al.* 1999, Sar *et al.* 2001a, Sar and D'Souza 2001a, Sar and D'Souza 2002, Kazy *et al* 2002). The present study was undertaken to evaluate the uranium (VI) and thorium (IV) biosorption capacity of a *Pseudomonas* soil isolate. Equilibrium sorption behavior of the lyophilized biomass was characterized employing the Freundlich and Langmuir adsorption isotherm models. The effect of solution pH on the chemistry of binding sites of both biosorbent types and also the metallic species in solution was assessed. Effect of bacterial culture age and presence of energy sources or metabolic inhibitor on uranium uptake was also studied. In view of a multimetallic composition of realistic waste, U and Th sorption in presence of other interfering cations and anions was investigated.

Materials and Methods

Microorganism, growth medium and culture conditions

Pseudomonas sp., a garden isolate was grown and maintained in Tris-minimal medium (Kazy *et al.*. 1999). Mid exponential phase cells were collected by centrifugation (12000 × g, 30 min), washed thoroughly with distilled water, dried and used for biosorption experiments.

Uranium and thorium biosorption experiments

All biosorption experiments were done using dry *Pseudomonas* biomass. Nitrate salts of Uranium and Thorium was used ($UO_2(NO_3)_2$, 6 H_2O or Th $(NO_3)_2$, 5 H_2O, Merck, Germany). Other experimental details were same as described previously (Sar and D'Souza 2001, Sar and D'Souza 2002). Dissolved uranium and thorium was determined either by the Arsenazo III method or by inductively coupled plasma atomic spectrometry (ICP-AES).

The biosorption equilibrium uptake (q, mg metal g^{-1} biomass dry wt.) for each sample was calculated according to the mass balance on metal ion expressed as :

$$q = V(C_0 - C_e) / M \qquad (1)$$

Where V is the sample volume (l), C_0, the initial metal ion concentration (mg l^{-1}), C_e, the equilibrium or final metal concentration (mg l^{-1}) and M, the biomass dry weight (g). Adsorption isotherm data were also fitted to the classical Freundlich and Langmuir isotherm equations (De Rome and Gadd 1987).

The linearized form of isotherm equations used are :

$$\text{Freundlich Equation : } \text{Log } q = \text{Log } k + 1/n \text{ Log } C_e \qquad (2)$$

Where q is the equilibrium metal uptake capacity and C_e, the residual metal concentration at equilibrium. The constant 'k'

is a measure of adsorption capacity and '1/n', the intensity of adsorption.

Langmuir Equation : $1/q = 1/q_{max}\, b \times 1/C_e + 1/q_{max}$ (3)

The constant 'q_{max}' represents the maximum specific metal uptake and 'b' the ratio of the adsorption/desorption rates related to energy of adsorption through Arrhenius equation.

Time course of metal biosorption

For sorption kinetic studies, bacterial biomass (0.5 mg ml^{-1}) was mixed with uranium or thorium solution (100 mg l^{-1}), samples withdrawn at timed intervals were centrifuged and dissolved U/Th was estimated.

Effect of pH on biosorption

The effect of solution pH on U and Th sorption was studied by adjusting the initial pH of the contact solution (100 mg Th l^{-1}) over the range pH 2.0-8.0. For pH adjustment, 1.0 M NaOH or 1.0 M HNO_3 was used.

Interference of cations and anions on uranium and thorium biosorption

Uranium and thorium sorption in simultaneous presence of other interfering ions was tested in bimetallic combinations, by adding equimolar concentrations of uranium or thorium (430 µM Th or 420 µM U; equivalent to 100 mg U or Th l^{-1}) and test cation or anion. Details are same as described earlier (Sar and D'Souza 2001a, Sar and D'Souza 2002)

Results and Discussion

Selection of uranium accumulating strain

Initial study on selecting a good uranium accumulating strain was done using four soil isolates, three belonging to *Pseudomonas* sp and one to *Bacillus coagulans*. All these bacterial strains were selected based on their superior metal tolerance capacity. A *Pseudomonas* sp. 2 which showed optimal biosorption was selected for further study on biosorption of uranium (VI) and thorium (IV).

Effect of growth medium, culture age, energy source and metabolic inhibitor on uranium biosorption

Metal and radionuclide biosorption by microbes is strongly influenced by the nature, availability and arrangements of various cellular binding ligands sequestering cationic metallic species. Among the others factors, growth medium ingredients are often found to regulate the synthesis of these metal binding moieties. In the present study *Pseudomonas* cells were pre-grown in synthetic minimal- and peptone containing enriched- medium and their U sorption was compared. At low uranium concentration (100 mg l^{-1}), comparable metal sorption was observed by both enriched (63 mg g^{-1} dry wt.) and minimal (60 mg g^{-1} dry wt.) medium grown cells. However, improved (1.9-fold) uranium loading was found for minimal medium grown cells (245 mg g^{-1} dry wt.) at higher uranium concentration (1000 mg l^{-1}). Although Chang *et al.* 1995 reported a significant enhancement of copper adsorption by growing the culture in peptone containing medium, the present data corroborate very well with U sorption by *P. aeruginosa* CSU strain (Hu *et al.* 1996). The latter investigators also showed an improved uranium sorption following the use of synthetic defined medium instead of nutrient broth.

To elucidate the role of bacterial culture age on uranium sorption, cells collected before, during and after mid exponential growth phase was compared for their U accumulation capacity. Although in certain case (Friis and Myers-Keith, 1986) culture age has shown a strong effect on bacterial metal uptake, the present *Pseudomonas* biomass did not show any significant difference in metal loading for the cells of different growth phase.

Metal accumulation by bacteria could be a metabolism –dependent active uptake or an –independent passive biosorption. In the present investigation, such energy

dependency of U uptake by *Pseudomonas* biomass was tested by adding glucose (as carbon/energy source) or sodium azide (as metabolic inhibitor) in uranium uptake solution. Metal removal was also compared using live, lyophilized and autoclaved cells. Noticeably, no significant difference in U removal was observed, suggesting the metabolic independency of the test biomass in sequestering uranium.

Time course of uranium and thorium sorption

The kinetics of uranium and thorium sorption by lyophilized *Pseudomonas* biomass is shown in Fig 1. For both the radionuclides, the test biomass exhibited a rapid cation uptake with more than 90% of equilibrium was reached within one (for Th) or ten (for U) minutes and the process saturates after 2 (for U) or 4 (for Th) hours. The rapid cation uptake has been suggested as being essential for any good biosorbent as it allows short solution-sorbent contact time and would result in the use of much shallower contact beds of sorbent materials in column application (Tsezos and Volesky 1982, Volesky 1990, Andres *et al.* 1993, Hu *et al.* 1996).

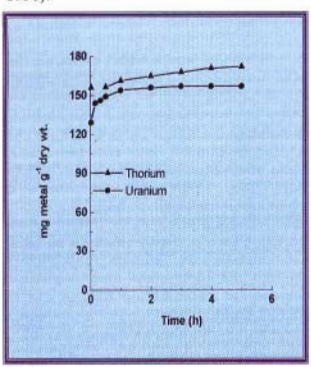

Fig 1 : Time course of U (•) and Th (▲) sorption (100 mg l^{-1}) by Pseudomonas biomass

Effect of pH on uranium and thorium biosorption

Initial solution pH is the most critical parameter for metal sorption as it influences both the bacterial surface chemistry as well as the solution chemistry of soluble metal ions. Uranium and thorium sorption by lyophilized *Pseudomonas* biomass was studied at a range of pH 2-8 and pH 2-6, respectively. As shown in Fig 2, initial solution pH significantly affected the equilibrium U and Th loading capacity. Over the range tested, extreme acid condition (pH 2.0) did not favour sorption of both the cations. As the pH increased, sorption of U and Th also increased and the maximum loading for thorium and uranium was attained at pH 4.0 and pH 5.0, respectively.

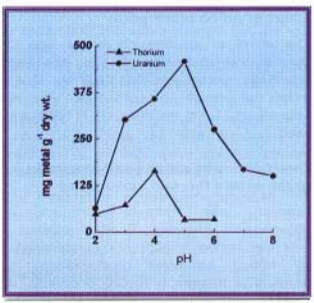

Fig 2 : Effect of pH on U (•) and Th (▲) sorption (100 mg l^{-1}) by Pseudomonas biomass

An increase in pH beyond the optimum caused decline in sorption of respective cations. The reduced sorption at low pH could be attributed to (i) the hydrolysis of biomass metal binding groups resulting in an increased competition by H_3O^+, and (ii) the increased solubility and consequent reduced adsorptivity of thorium ions (Beas and Mesmer 1976). Furthermore, compared to the Th^{4+} and $Th(OH)_2^{2+}$ ions formed at low pH that have been identified as a poor sorbate (Tsezos and Volesky, 1982), the higher uptake at pH 4.0 could be correlated

to the predominance of $[Th_2(OH)_2]^{6+}$ and other polymerized species possessing a greater binding affinity thus facilitating faster and enhanced metal sorption (Gadd and White 1989). For uranium, the observed trend with regard to pH may be explained by an increasing binding affinity of monovalent uranyl species (UO_2OH^+, $(UO_2)_3(OH)_5^+$) formed at higher pH (pH 4.0-5.0) over the divalent (UO_2^{2+}) at low pH (pH 2.0).

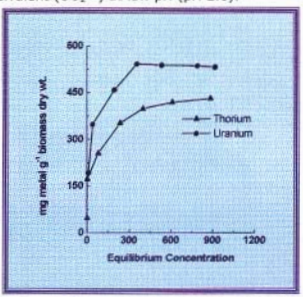

Fig 3 : U (•) and Th (▪) sorption isotherm for Pseudomonas biomass

Biosorption Isotherm

The biosorptive U and Th uptake by *Pseudomonas* biomass was quantitatively evaluated by equilibrium sorption isotherms over a concentration range of 0-1200 mg l^{-1} (Fig 3). Representative isotherm curves for both the cations exhibited very efficient metal binding even at low residual concentration and a high saturation loading at equilibrium. The maximum sorption values obtained are 541 mg uranium g^{-1} dry wt. and 430 mg thorium g^{-1} dry wt. at equilibrium concentration of 359 mg U l^{-1} and 885 mg Th l^{-1}, respectively. Such impressive U and Th binding by the test biomass significantly surpasses the economic threshold level (15% dry wt. basis) for practically usable biosorbents and so also the previous values on Th [*R. arrhizus* (185 mg g^{-1} dry wt.) (Tsezos & Volesky 1981) or *P. chrysogenum* (388 mg g^{-1} dry wt.) (Gadd & White 1989)] and U [*R.. arrhizus* and *Penicillium chrysogenum* (both 180 mg g^{-1}) (Tsezos & Volesky 1981) *P. aeruginosa* CSU (110 mg g^{-1}) (Hu *et al.* 1996), and *M. smegmatis* (44.5 mg g^{-1}) (Andreas *et al.* 1993)] uptake

Table 1 : Freundlich and Langmuir constants for uranium and thorium sorption by *Pseudomonas* biomass

		Uranium	Thorium
Freundlich	k	199.00	159.20
	1/n	0.206	0.176
	r	0.931	0.973
Langmuir	qmax	555.5	476.19
	B	0.0027	0.0009
	r	0.997	0.998

The relationship between equilibrium metal uptake capacity (q) and residual metal ion concentration (Ce) was further described using the model equation of Freundlich and Langmuir. Although linearized sorption isotherm for both the metals showed a reasonably good fit to both the models, the maximum correlation coefficient (r) was obtained with Langmuir equation. Values of respective sorption constants and correlation coefficients (r) are presented in Table 1. The better fitting of Langmuir model suggest a monolayerd U and Th binding on to the biomass with homogeneous surface energy and no interaction between sorbed metals (Langmuir 1918). The asymptotic maximum adsorption capacity as predicted by the Langmuir constant 'qmax' gives a very high value for U and Th while a desirable high affinity of the biomass for test metals are evident from the low values of other constant 'b'.

Effect of interfering ions on uranium and thorium biosorption

Uranium and thorium sorption by *Pseudomonas* biomass was studied in presence of equimolar amount of several competing ions (Table 2). Selection of such ions are based on their likely occurrence in realistic effluent interfering biosorption of U and Th. Among the series of cations tested, a significant antagonism in U sorption was

Table 2 : Effect of interfering ions on U and Th biosorption by *Pseudomonas*

	Percentage of sorption	
	Uranium	Thorium
Control (only U or Th)	100	100
Cations :		
Na^+	100	100
Ag^{2+}	98	84*
K^+	98	86*
Ca^{2+}	98	100
Pb^{2+}	98	100
Cd^{2+}	96	100
Cu^{2+}	78*	83*
Al^{3+}	82*	85*
Fe^{2+}	45*	57*
Fe^{3+}	20*	60*
Th^{4+}	37*	-
UO_2^{2+}	-	92
Anions :		
Cl^-	100	100
PO_4^{2-}	100	-
SO_4^{2-}	100	100
CO_3^{2-}	74*	100

*Initial U/Th concentration 100 mg dm^{-3}, pH 3.5, biomass 0.5 mg cm^{-3}.

offered only by thorium (IV), iron (II and III), aluminium (III) and copper (II) while metals like cadmium (II), lead (II) silver (II) and anions like chloride, phosphate and sulphate had no effect. The order of inhibition to uranium binding by the cations was $Fe^{3+} > Th^{4+} > Fe^{2+} > Cu^{2+} > Al^{2+}$. Iron (III), the cation considered as the most potent competitor of uranium in binding biosorptive sites (Hu *et al.* 1996), also caused a severe decline (80 %) in U loading. Such inhibition to U sorption by Fe^{3+}, is a common phenomenon e.g. *P. aeruginosa* CSU (Hu *et al.* 1996), *R.. arrhizus* and *S. levoris* (Byerley *et al.* 1987). Although Al^{3+} and Ag^{2+} have also been found to inhibit U adsorption by *P. aeruginosa* CSU and *R. arrhizus,* the present *Pseudomonas* biomass remained insensitive with respect to Ag^{2+}, while Al^{3+} was significantly antagonistic. Noticeably, in case of thorium, except iron (III), no other test cation showed an inhibition more than 20%. Th sorption was insensitive to the presence of Na^+, Ca^{2+}, Cd^{2+}, Pb^{2+}, CO_3^{2-}, SO_4^{2-} and Cl^-, while the order of inhibition by other cations is $UO_2^{2+} < Co^{2+} < Ni^{2+} < Al^{3+} < Ag^{2+} < Cu^{2+}$. The observed insignificant interference (only 8% inhibition) of U on thorium binding can be attributed to a higher oxidation state of Th along with additional bonding parameters (Andres *et al.*. 1993). Although, uranium and thorium biosorption by the present biomass was fairly efficient in the presence of a range of cations, the role of Fe (III) in inhibiting U and Th binding imposes serious limitations in wastewater treatment by this biosorbent. Ideally, iron should be removed by pH adjustment or other methods prior to biosorption.

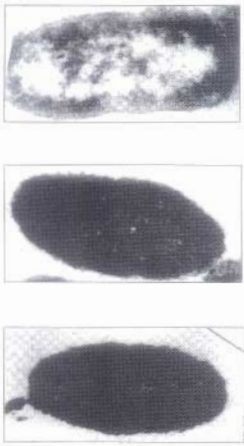

Fig 4 : Transmission electron micrograph of control cell (a), after uranium accumulation (b) and after thorium accumulation (c)

Mechanism of biosorption and use of immobilized microbes in continuous column reactors

Some studies have been undertaken to study the mechanism of biosorption. Transmission electron microscopy of metal loaded cells

revealed an intracellular metal sequestration (Fig.4) with X-ray diffraction pattern ascertaining their phosphide nature. IR spectroscopy and NMR data suggests the role of cellular phosphoryl groups in radionuclide binding. For continuous use in a column the biomass was immobilized using various techniques (D'Souza 1999b; D'Souza 2001b; D'Souza 2002b) including entrapment in radiation polymerized acrylamide beads (Fig. 5). Scanning electron micrograph of immobilized bacterial biomass (Fig.6) indicated no cellular damage/ distortion during the immobilization process. The biomass could be used for repeated sorption -desorption cycles in continuous column operation. More than 90% of biomass bound U and Th was recovered through elution using carbonates.

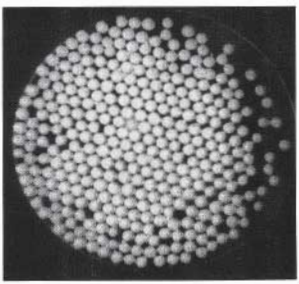

Fig 5: Immobilized Pseudomonas cells as bio beads

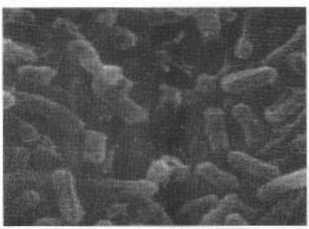

Fig 6 : Scanning electron microscopy of immobilized Pseudomonas cells

Conclusion

The overall study using the *Pseudomonas* strain suggests the present biomass as a potential candidate for developing biosorbent for uranium and thorium removal for wastewater remediation, however, a prior reduction of iron content is necessary. A clear insight on the biomass U and Th binding mechanism(s) and other technological parameters (currently underway) will substantially improve its feasibility in process application.

Acknowledgements

The authors thank Dr (Ms) A. M. Samuel, Director, Bio-Medical Group, BARC, for her keen interest in this work. Special thanks are also given to Director, CIRCOT, Mumbai, Dr T Das, AIIMS, New Delhi and Mr. K.N. Harindran, UED, BARC for extending their technical help in SEM, TEM and ICP analyses, respectively. Pinaki Sar acknowledges the financial assistance made by Board of Research in Nuclear Sciences, Department of Atomic Energy, Govt. of India, in the form of K.S. Krishnan post doctoral fellowship.

Reference

1. Andres Y, MacCordick H J and Hubert J C (1993) Adsorption of several actinide (Th, U) and lanthanide (La, Eu, Yb) ions by *Mycobacterium smegmatis*. *Appl Microbiol Biotechnol* 39 : 413-417.
2. Barkay T, Schaefer J (2001) Metal and radionuclide bioremediation : issues, considerations and potentials. *Curr Opinion Microbiol.* 4 : 318-323.
3. Beas C F Jr and Mesmer R E (1976) *Hydrolysis of cations.* Wiley, New York.
4. Bhainsa K C and D'Souza S F (1999) Biosorption of uranium (VI) by *Aspergillus fumigatus*. *Biotechnol Tech* 13: 695-699.
5. Bhainsa K C. and D'Souza S F (2001a) Biosorption of Radionuclides and Heavy Metals by Fungal Biomass. in *'Industry and Environment'*, R. K. Trivedi, Ed., Global Science Publications, Aligarh, India. pp. 149-155.

6. Bhainsa K C and D'Souza S F (2001b) Uranium (VI) biosorption by dried roots of *Eichhornia crassipes* (water hyacinth). *J. Environ. Sci. Health-A*, 36, 1621-1631.
7. Byerley JJ, Scharer JM, Charles AM (1987) Uranium (VI) biosorption from process solutions. Chem. Eng. J. 36 : B49-B59.
8. Chang D, Fukushi K and Ghosh S (1991) Stimulation of activated sludge culture for enhanced heavy metal removal. Water Environ Res. 67 : 822-827.
9. Dhami P S, Kannan R, Gopalakrishnan V, Ramanujam A, Salvi N, Udupa S R (1998) Sorption of plutonium, americium and fission products from reprocessing effluents using Rhizopus arrhizus. Biotechnol. Lett. 20 : 869-872.
10. D'Souza S F (1999a) Bioremediation of heavy metal and radionuclide waste. Indian Association of Nuclear Chemists and Allied Scientists Bulletin, (IANCAS Bulletin) 15: 46-54.
11. D'Souza S F (1999b) Immobilized enzymes in bioprocess. *Current Sci.* 77, 69-79.
12. D'Souza S F, Melo J S, Bhainsa K C, Sar P and Kazy S (2001a) Bioremediation of heavy metal and radionuclide waste: an overview. Proceedings of the 'International Conference on *'Industrial Pollution and control Technologies'* (ICIPACT-2001)' , JNTU., Hyderabad, pp.102-111.
13. D'Souza S F, Gupte A and Panchapakesan S (2001b) Removal of chromium (VI) by the yeast *Kluyveromyces fragilis* grown on whey. Proceedings of the 'International Conference on *'Industrial Pollution and control Technologies'* (ICIPACT-2001) , JNTU, Hyderabad, pp. 604-608.
14. D'Souza S F (2001) Microbial Biosensors. *Biosensors Bioelectronics* 16:337-353.
15. D'Souza S F (2002a): Low cost biotechnological approaches for environmental management of heavy metal waste. Proceedings of the All India Convention on *'Cost Effective Biotechnology in Modern Waste Water Management'* ational Centre for Technical Development, Mumbai, Hotel Centaur, Mumbai, pp. E1-E7.
16. D'Souza S F (2002b) Trends in immobilized enzyme and cell technology. *Indian J. Biotechnol* (in press).
17. Friis N and Myers-Keith P (1986) Biosorption of uranium and lead by *Streptomyces longwoodensis. Biotechnol Bioeng* 28 : 21-28.
18. Gadd G M (2000) Bioremediation potential of microbial mechanisms of metal mobilization and immobilization. *Curr Opin Biotechnol* 11 : 271-279.
19. Gadd M, White C (1989) Uptake and intracellular compartmentation of thorium in *Saccharomyces cerevisiae. Environ Pollution* 61 :187-197.
20. Hu M Z C, Norman J M, Faison B D and Reeves M (1996) Biosorption of uranium by *Pseudomonas aeruginosa* strain CSU: characterization and comparison studies. *Biotechnol Bioeng* 51 : 237-247.
21. Irani S H, Kohli S S, Patwardan A W, Melo J S and D'Souza S F (2002) Phenol degradation in the rotating biological contactor: Effect of parameters on performance and mathematical model. *J. Chem. Tech. Biotechnol* (in press).
22. Joshi N T and D'Souza S F (1999) Immobilization of activated sludge for the degradation of phenol. *J. Environ. Sci. Health-A*, 34, 1689-1700.
23. Kazy S K, Sar P, Asthana R K and Singh S P (1999) Copper uptake and its compartmentalization in *Pseudomonas aeruginosa* strains : chemical nature of cellular metal. *World J Microbiol Biotechnol* 15 : 599- 605.
24. Kazy S K, Sar P, D'Souza S F, Sen A.K, and Singh S P (2001) Extracellular polysaccharides of *Psuedomonas aeruginosa* strains; effect of heavy metal on its production and chemical composition. Proceedings of the 'International Conference on *'Industrial Pollution and control Technologies* (ICIPACT-2001)', JNTU, Hyderabad, pp. 657-661.
25. Kazy S K. Sar P, Sen A.K, Singh S P and D'Souza S.F (2002) Extracellular polysaccharides of a copper-sensitive and a copper-resistant *Psuedomonas*

aeruginosa strains: synthesis, chemical nature and copper binding. *World J. Microbiol Biotechnol* 18 : 583-588.

26. Langmuir I (1918) The adsorption of gases on plane surfaces of glass, mica, and platinum. *J. Amer. Chem. Soc.* 40 : 1361-1403.
27. Lloyd J R, Macaskie L E (2000) Bioremediation of radionuclide-containing wastewaters. In : Lovely DR, eds, *Environmental Microbe-Metal Interactions.* Washington DC : American Society of Microbiology, pp. 277-327
28. Melo J S and D'Souza S F (2001) Biosorption of uranium and thorium by agro based biomass. Proceedings of Tenth National Symposium on *'Environment'* BARC Mumbai, pp. 293-296.
29. Panchapakesan, S, Melo, J S, Bhainsa, K C and D'Souza, S F (2002) Glucose dependent accumulation of cadmium by a metal tolerant yeast. In *'Applications of biotechnology for clean environment and energy'.* (G. Bali Ed) Oxford Publications, pp. 199-212.
30. Sangurdekar P R, Melo J S and D'Souza S F (2001) Biosorption of radioactive cobalt and cesium using mucilaginous seeds. Proceedings of Tenth National Symposium on *'Environment'* BARC Mumbai, pp. 298-299.
31. Sar P, Kazy S K, Asthana R K and Singh S P (1998) Nickel uptake by *Pseudomonas aeruginosa* : Role of modifying factors. *Current Microbiology* 37: 306-311.
32. Sar P, Kazy S K, Asthana R K and Singh S P (1999) Metal adsorption and desorption by lyophilized *Pseudomonas aeruginosa." Int. Biodeterior. Biodegr.* 44 : 101-110.
33. Sar P and D'Souza S F (2001a) Biosorptive uranium uptake by a *Pseudomonas* strain: characterization and equilibrium studies. *J. Chem. Tech. Biotechnol* 76: 1286-1294.
34. Sar P and D'Souza S F (2001b) Radionuclide biosorption by bacterial biomass . Proceedings of the 'International Conference on *'Industrial Pollution and control Technologies'* (ICIPACT-2001)', JNTU, Hyderabad, pp. 651-656.
35. Sar P, Kazy S K and Singh S P (2001a) Intracellular nickel accumulation by *Pseudomonas aeruginosa* and its chemical nature, *Lett. Appl. Microbiol.* 32: 257-261.
36. Sar P, Kazy S, Singh S P and D'Souza S F (2001b) : Radionuclides and heavy metal biosorption by *Pseudomonas* biomass. Proceedings of Tenth National Symposium on *'Environment'* BARC Mumbai, pp. 218-222.
37. Sar P and D'Souza S.F (2002) Biosorption of thorium (IV) by a *Pseudomonas* strain. *Biotechnol Lett*, 24: 239-243.
38. Shanmugam K, Subrahmanyam S, Tarakad S V, Kodandapani N and D'Souza S F (2001) 2,4-toluene diamines – Their carcinogenicity, biodegradation, analytical techniques and an approach towards development of biosensors. *Analytical Sciences* (Japan) 17: 1369-1374
39. Tsezos M and Volesky B (1981) Biosorption of uranium and thorium, *Biotechnol Bioeng* 23 : 583-604.
40. Tsezos M, Volesky B (1982) The mechanism of thorium biosorption by *Rhizopus arrhizus. Biotechnol. Bioeng* 24: 955-969.
41. Volesky B (1990) *Biosorption of heavy metals*, ed by Volesky B, CRC Press, Boca Raton, FL, pp 7-44.

This paper received the Best Presentation award at the International Conference on 'Industrial Pollution and Control Technologies(ICIPACT-2001)', held at Jawaharlal Nehru Technological University, Hyderabad, during December 7-10, 2001

About the authors ...

Dr Pinaki Sar *obtained his Ph.D. in Botany for this thesis, "Investigation on Pseudomonas aeruginosa as bioaccumulator of nickel" from Banaras Hindu University. He was the recipient of Dr K.S. Krishnan Research Associate, 2nd batch and worked in the area of radionuclide bioremediation at BARC. Currently, he is a faculty member at the Birla Institute of Technology and Science. He has to his credit seven papers in internationally reputed journals and five papers in international and national conference proceedings. His field of research interest is on metal/radionuclide and organic pollutant bioremediation.*

Dr S.F. D'Souza *graduated from the 15th batch of the Training School (Biology & Radiobiology) and is currently the Head of the Nuclear Agriculture and Biotechnology Division of BARC. His major research interest has been in the field of Enzyme and Microbial Biotechnology with special reference to immobilized cells for use in bioprocessing, biosensors and bioremediation. He has to his credit over 150 scientific papers and invited reviews in reputed International/National journals/books. He is a member/expert at National Scientific committees; member of the editorial board of scientific journals and has been invited to deliver talks/key note lectures, chair scientific sessions at various scientific forums. He has also contributed significantly to science education as an invited resource person at National workshops and short term courses as well as UGC Refresher courses, as an invited guest faculty member, as a Ph.D., M.Sc. examiner (Univ/IIT) and as a member of the board of studies and research advisory committees and has guided a number of students for Ph.D. and M.Sc. He was presented the prestigious AMI-Louis Pasteur award (2001) for his significant contributions to the field of Microbiology and has been honoured as a Fellow of the National Academy of Science (1993), Fellow of the Association of Food Scientists & Technologists (1999) and Fellow of the Maharashtra Academy of Science (2001).*

Molecular Characterization of ex-type Strains of *Trichoderma* spp. from two Indian Type Culture Collections

J. Latha and Prasun K. Mukherjee
Nuclear Agriculture and Biotechnology Division
Bhabha Atomic Research Centre

Abstract

Species in the genus Trichoderma are important as commercial source of several enzymes and as biofungicides/growth-promoters. Correct identification of species/ isolates is important not only because several traits are species-specific, but also because two of the species are opportunistic pathogens on immuno-suppressed patients. We have examined two isolates each of six species of Trichoderma collected from MTCC, Chandigarh, and ITCC, New Delhi, using RAPD and rDNA polymorphism analysis. A set of four random primers were used for characterization of twelve isolates of Trichoderma spp., and the cluster analysis showed that the isolates, except T. hamatum isolates, were different from each other, and there were some overlapping with regard to species identification. Analysis of the ITS1-5.8S-ITS2 region of the rDNA showed that the approximate size of the region was 600 bp and size variation was observed. One of the T. viride isolates showed two amplicons against single band in all the other isolates. Restriction analysis of the amplified ITS1-5.8S-ITS2 region showed inter- and intra-specific polymorphism. One of the T. koningii isolates was exactly the same as T. hamatum isolates in RAPD and rDNA polymorphism. The results indicate the need for re-examination and re-classification of Trichoderma spp. strains deposited in Indian culture collections.

Introduction

Species in the fungal genus *Trichoderma* (Ascomycetes, Hypocreales) are of great economic importance as sources of enzymes, antibiotics, as plant growth promoters, xenobiotic degraders, and most importantly, as commercial biofungicides (Mukherjee, 1999). Two species (*T. longibrachiatum* and *T. citrinoviride*) are also known to be opportunistic pathogens on immuno-suppressed patients (Kuhls *et al*, 1999). Until recently, *Trichoderma* spp. were being identified based on morphological data like cultural characteristics, structure of conidiophores/ conidia, etc. (Rifai, M.A., 1969; Bissett, J., 1984, 1991a, 1991b, 1991c, 1992). However, subsequent molecular analysis of several strains, including some ex-type strains revealed that classification based on morphological data have been, to a great extent, erroneous resulting in re-classification of several isolates and species (Meyer et al. 1994; Rehner et al. 1994; Kuhls *et al*. 1996, 1997; Bulat *et al*. 1998; Castle et al. 1998; Kindermann *et al*. 1998; Lieckfeldt *et al*. 1999; Hermosa *et al*. 2000). For example, three Indian isolates of *Trichoderma,* that are deposited at Microbial Type Culture Collection, Chandigarh, as *T. harzianum*, were examined by Hermosa *et al*. 2000. Two of them were found to be *T. inhamatum*, and one was classified as *T. longibrachiatum*, using molecular tools. Correct identification of *Trichoderma* spp. is important both from commercial point of view (as several traits are species-specific), and from safety point of view. This is particularly important for the type cultures as these are used by several workers and are taken as authentic samples. We therefore examined some representative isolates of this commercially important fungal genus using two PCR-based techniques *viz.* RAPD- Random Amplification of Polymorphic DNA, and restriction analysis of the amplified ITS1-5.8S-ITS2 region of the nuclear ribosomal DNA.

Materials and Methods

Two isolates each of six species of *Trichoderma* (*T. virens*, *T. pseudokoningii*, *T. hamatum*, *T. harzianum*, *T. viride* and *T.*

koningii) were procured from either Indian Type Culture Collection (ITCC), New Delhi, or the Microbial Type Culture Collection (MTCC), Chandigarh (Table 1). The isolates were grown in potato dextrose broth at ambient temperature and total genomic DNA extracted as described earlier (Mukherjee, P. K. 1999). For all the PCR amplifications, 50 ng of DNA, 0.5 U of Taq DNA polymerase (Bangalore Genei) and 0.1 mM each of the dNTPs were used. Amplifications were performed in 25 µl reaction volume in an Eppendorf Mastercycler Personal thermal cycler. For RAPD, amplifications were performed with 5 random decamers from Operon Technologies kit A (OPA1-CAGGCCCTTC, OPA2- TGCCGAGCTG, OPA3-AGTCAGCCAC, OPA4-AATCGGGCTG, OPA9-CGGTAACGCC) at 37°C annealing (1'), 94°C denaturation (1') and 72°C extension (2') - 35 cycles. Amplification products were size separated in 2 % agarose gel, visualized after staining with ethidium bromide and photographed with a UVP polaroid camera. The isolates were clustered using TreeconW programme based on binary score for the presence (1) or absence (0) of a band. For amplification of the ITS1-5.8S-ITS2 region, the primer pair ITS1 (TCTGTAGGTGAACCTGCGG) - ITS4 (TCCTCCGCTTATTGATATGC) was used (White *et al.* 1990). To optimize the annealing temperature, amplifications were performed at 56°C, 58°C and 59°C. For restriction analysis, 20 µl of the amplification-product (amplified at 59°C annealing) was digested with 5 units of restriction enzymes (all from Bangalore Genei) for 2 hours and size separated in 2 % agarose gel, stained and photographed as described above.

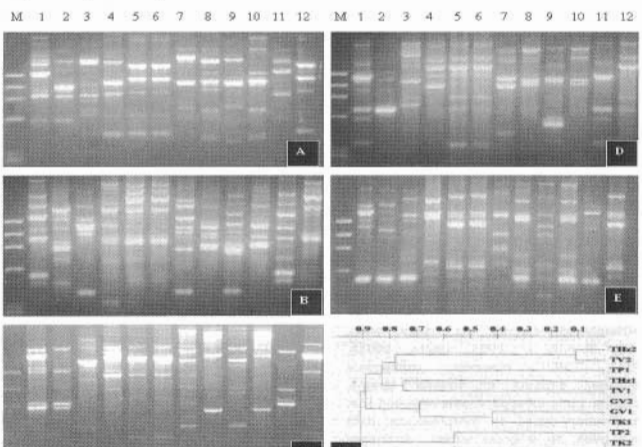

Fig 1 : RAPD analysis of the Trichoderma isolates based on OPA1 (A), OPA2 (B), OPA3 (C), OPA4 (D) and OPA9 (E). Lanes 1= T. virens 1, 2=T. virens 2, 3= T. pseudokoningii 1, 4= T. pseudokoningii 2, 5= T. hamatum 1, 6= T. hamatum 2, 7= T. harzianum 1, 8= T. harzianum 2, 9= T. viride 1, 10= T. viride 2, 11= T. koningii 1, 12= T. koningii 2. M= Molecular weight marker. The cluster analysis (F) was done based on a total of 205 polymorphic bands

Results and Discussion

RAPD analysis based on 5 random primers (selected out of 10 primers after an initial screening) revealed a great deal of intra- and inter-specific variability amongst *Trichoderma* isolates examined except for the two *T. hamatum* isolates that were exactly identical (Fig. 1). Surprisingly, one *T. koningii* isolate (TK2) was also exactly identical to both the *T. hamatum* isolates. The RAPD fingerprinting data (Fig. 1) clearly indicate that there is mixing-up as far as species identification is concerned. For example, *T. harzianum* isolate no. 1 clusters with *T. viride* isolate no. 1, while *T. harzianum* isolate no. 2 clusters with *T. viride* isolate no. 2. Similarly, *T. virens* isolate no. 1 is more close to *T. koningii* isolate no. 1, than to *T. virens* isolate no. 2, while *T. pseudokoningii* isolate no. 2 is more close to *T. hamatum* isolates, than to *T. pseudokoningii* isolate no. 1. Since RAPD is often considered to be less reliable than RFLP data, we also analyzed the RFLP in the amplified ITS1-5.8S-ITS2 region. An annealing temperature of 59°C was found to be suitable for the amplification of ITS1-5.8S-ITS2 region from all the isolates with good product yield and minimum non-specific amplifications. The product size was approximately 600 bp, and there was size variation across the isolates (Fig. 2). At all the three annealing temperatures, we could see two bands only with the *T. viride* isolate no. 1. Digestion of this product with five tetra-base cutters (*Mbo*I, *Hae*III, *Taq*I, *Sau*3AI, *Msp*I) revealed polymorphism in the ITS1-5.8S-ITS2 region (Fig 2). All the isolates could be grouped into broadly four groups (Table 2), which again showed the overlapping in species identification of these strains, e.g., *T. pseudokoningii* isolate no. 2, and *T. koningii* isolate no. 2 grouped with *T. hamatum* isolates.

The present analysis questions the identity of *Trichoderma* isolates maintained in two of the Indian type culture collections. This is not surprising given the fact that these were identified using morphological data, which, as a taxonomic tool for *Trichoderma* spp., has been confusing. It is therefore, proposed

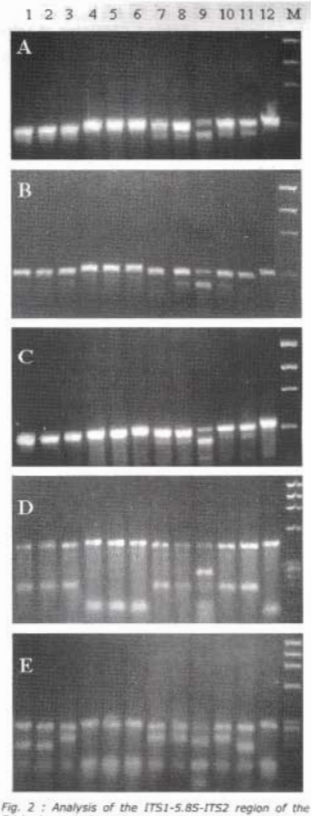

Fig. 2 : Analysis of the ITS1-5.8S-ITS2 region of the Trichoderma isolates (Lanes 1= T. virens 1, 2=T. virens 2, 3= T. pseudokoningii 1, 4= T. pseudokoningii 2, 5= T. hamatum 1, 6= T. hamatum 2, 7= T. harzianum 1, 8= T. harzianum 2, 9= T. viride 1, 10= T. viride 2, 11= T. koningii 1, 12= T. koningii 2. M= Molecular weight marker). A= amplification at 56 C, B= amplification at 58 C, C= amplification at 59 C, D= digestion of the ITS1-5.8S-ITS2 region with HaeIII, E= digestion of the ITS1-5.8S-ITS2 region with MspI.

Table 1 : Isolates of *Trichoderma* spp. used in this study

Species	Isolate Designation	Catalogue no.	Isolated from/Locality*
T. virens	GV1 GV2	MTCC 794 ITCC 4177	Soil/ Pantnagar Mango/Lucknow
T. pseudokoningii	TP1 TP2	MTCC 3011 MTCC 2049	Ginger/Mumbai -/-**
T. hamatum	TH1 TH2	ITCC 2084 ITCC 3380	Soil/South India Mushroom/Hisar
T. harzianum	THz1 THz2	ITCC 4532 MTCC792	Peas/Palampur Soil/Pantnagar
T. viride	TV1 TV2	ITCC 2109 MTCC 793	-/Assam Soil/Pantnagar
T. koningii	TK1 TK2	ITCC 4303 ITCC 2170	-/Solan Soil/Assam

**As mentioned in the catalogue; **Information not available*
MTCC- Microbial Type Culture Collection, Chandigarh; ITCC- Indian Type Culture Collection, New Delhi.

Table 2 : Grouping of *Trichoderma* isolates based on restriction analysis of the ITS1-5.8S-ITS2 region

***Mbo*I/*Hae*III**	***Taq*I/*Sau*3AI**	***Msp*I**
GV1, GV2, TP1, THz1, THz2, TK1, TV2	GV1, GV2, TP1	GV1, GV2, TK1
	THz1, THz2, TK1, TV2	THz1, THz2, TP1,TV2
TP2, TH1, TH2, TK2	TP2, TH1, TH2, TK2	TP2, TH1, TH2, TK2
TV1	TV1	TV1

that all the isolates of *Trichoderma* spp. deposited in Indian type culture collections be re-identified using now available molecular tools (e.g., sequencing of the part of rDNA), in order to effectively utilize these fungi of immense agricultural, bio-technological and industrial importance.

References

1. Mukherjee, P.K., In: *Current Trends in Life Sciences- Agromicrobes* (Ed. Jha, M.N.), 1999, 261-280.
2. Kuhls, K., Lieckfeldt, E., Borner, T. and Gueho, E., *Medic. Mycol.*, 1999, **37**, 25-33.
3. Rifai, M.A., *Mycol. Pap.*, 1969, **116**, 1-56.
4. Bissett, J., *Can. J. Bot.*, 1984, **62**, 924-931.
5. Bissett, J., *Can. J. Bot.*, 1991a, **69**, 2357-2372.
6. Bissett, J., *Can. J. Bot.*, 1991b, **69**, 2373-2417.
7. Bissett, J., *Can. J. Bot.*, 1991c, **69**, 2418-2420.
8. Bissett, J., *Can. J. Bot.*, 1992, **70**, 639-641.
9. Meyer, W., Lieckfeldt, E., Morawetz, R., BÖrner, T. and Kubicek, C.P., *Mycol. Helvet.*, 1994, **6**, 160-171.
10. Rehner, S.A. and Samuels, G.J. 1994, *Mycol. Res.*, 1994, **98**, 625-634.
11. Kuhls, K., Lieckfeldt, E., BÖrner, T., and Samuels, G.J., *Fung. Genet. Biol.*, 1996, **20**, 105-114.
12. Kuhls, K., Lieckfeldt, E., Samuels, G.J., Kubicek, C.P., Meyer, W., and BÖrner, T., *Mycologia*, 1997, **89**, 442-460.

13. Bulat, S.A., Lübeck, M., Mironenko, N., Jensen, D.F., and Lübeck, P.S., *Mycol. Res.*, 1998, **102**, 933-943.
14. Castle, A., Speranzini, D., Rghei, N., Alm, G., Rinker, D. and Bissett, J., *Appl. Env. Microbiol.*, 1998, **64**, 133-137.
15. Kindermann, J., El-Ayouti, Y., Samuels, G.J. and Kubicek, C.P., *Fung. Genet. Biol.*, 1998, **24**, 298-309.
16. Lieckfeldt, E., Samuels, G.J., Nirenberg, H.I. and Petrini, O., *Appl. Env. Microbiol.*, 1999, **65**, 2418-2428.
17. Hermosa, M.R., Grondona, I., Iturriaga, E.A., Diaz-Minguez, J.M., Castro, C., Monte, E., and Garcia-Acha, I., *Appl. Env. Microbiol.*, 2000, **66**, 1890-1898.
18. Mukherjee, **P.K.,** *As-Pac. J. Mol. Biol. Biotechnol.* 1999, **7**, 95-96.
19. White, T.J., Bruns, T., Lee, S. and Taylor, J., In: *PCR Protocols. A Guide to Methods and Applications* (Eds. Innis, M.A., Gelfand, J.J., Sninsky, J.J. and White, T.J.), 1990, 315-322.

This paper received the Best Poster Award at the 70th Annual Meeting of the Society of Biological Chemists (India), held at Dept. of Biochemistry, Osmania University, Hyderabad, during December 27-29, 2001.

About the authors ...

Ms J. Latha, *M.Sc (Biotechnology), is from the 42nd batch of BARC Training School. She is the recipient of the "Homi Bhabha Award" for Biology-Radiobiology discipline in her batch, and is working in the Plant Pathology and Pesticide Residues Section of Nuclear Agriculture and Biotechnology Division (NABTD).*

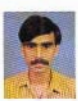

Dr P. K. Mukherjee, *M.Sc (Agriculture), completed his Ph.D. as a Krishnan DAE research fellow. He is working in the Plant Pathology and Pesticide Residues Section of Nuclear Agriculture and Biotechnology Division (NABTD), on the biocontrol mechanisms of plant diseases. He was awarded the "Pran Vohra Award" for agricultural sciences during 1998-1999 by the Indian Science Congress Association.*

Sensor for Remote Detection of Eccentricity between Coaxial Metallic Tubes

T. V. Shyam, S. K. Apraj and B.S.V.G. Sharma
Reactor Engineering Division
Bhabha Atomic Research Centre

Abstract

Eddy current sensor system along with associated signal conditioning electronic circuits for qualitative and quantitative detection of eccentricity between coaxial metallic tubes made of non ferrous and low electrical conducting material has been designed and is in advanced stage of further development at BARC. This miniature sensor can be kept in close proximity of metallic objects and is in-sensitive to the lift-off errors. The system can be used with 100 meters cable length and is expected to detect eccentricity between coaxial metallic tubes within overall accuracy of 0.5 mm. The design and developmental work involved design of sensor and associated signal conditioning hardware and software. This sensor is planned to be used as embedded sensing element in hydraulically actuated devices, that are subjected to heavy mechanical stresses, for detection of eccentricity between metallic tubes under operating conditions. This paper highlights general design and developmental aspects of Concentricity Detection Probe sensor along with associated Hardware.

Background

Precise measurement and correction of eccentricity between the two co-axial metallic tubes is essential in many industrial fields. One of such requirement in Indian nuclear reactors is need to measure and correct the eccentricity between highly radioactive non ferrous low electrical conductivity metallic tubes. An eddy current sensor based transducer and its associated hardware has been designed in order to check the eccentricity between metallic tubes in vertical axis ('Y' direction). These tubes are initially eccentric which needs to be corrected by using a **T**ube **F**lexing **T**ool (**TFT**). The sensor needs to be mounted in one of the bearings of TFT as an integral part of the tool, which will be inserted in the bore of inner tube. The TFT is hydraulically actuated in 'Y' direction generating vertical thrust to correct the eccentricity between the metallic tubes based on the eccentricity information feed back received from the transducer. This transducer needs to be operated from 100 meters cable distance and should be fairly insensitive to the lift-off errors. Further, since the TFT is subjected to very high mechanical stresses during eccentricity correction operation, the sensor needs to be protected against the damages. The transducer dimensions should be fairly small enough to fit in the bearing housing of TFT. The design constraints, constructional features and performance evaluation of the transducer system has been described in following sections .

Design Constraints And Salient Features

a) Mounting: The sensor being the integral part of the eccentricity correction tool TFT needs to be mounted in the bearing housing of the tool. The transducer should be designed such that the magnetic flux emerging out of the sensor should link the coaxial metallic tubes. The metallic body of TFT should not divert the flux. In order to achieve this, 'C'-clamp type pancake probes have been designed to ensure the flux linkage to both the tubes in spite of sensors being embedded in the tool bearing.

b) Size: The sensor size should be small enough to fit in the bearing of TFT.

c) Sensitivity: The sensor should be enough sensitive to detect precisely the eccentricity

between the metallic tubes. In order to improve the sensitivity of the sensor, the $\omega L/R$ ratio of the coil should be high. Mumetal has been used as the sensor material. One can also use ferrite core to improve the sensitivity, however mumetal has been used for higher sensitivity and better strength.

d) Tool Bearings: In order to reduce the diversion of flux generated in the sensor which is embedded in the bearing housing, the metallic bearings cannot be used for TFT. Non metallic high crushing strength Phenolic bearings have been used to serve the purpose. The sensor is embedded in one of the phenolic bearings and is protected by suitable potting.

e) Operating environment: The sensor system should be capable to work in RFI and EMI noisy environment.

Constructional Features And System Configuration

The schematic of the eccentricity measurement transducer sensor is shown in Fig.1 The transducer works on eddy current principle. The parameters such as conductivity, permeability, dimensions of the test object, spacing between the test object and test coil, spacing between the test objects and test frequency affecting eddy current are phase sensitive. It has been seen that the parameter like lift-off is less phase sensitive as compared to parameters like thickness variation and spacing between the components. In order to nullify the lift-off error, the phase measurement technique has been used in the system instead of amplitude measurement technique since the later is more sensitive to lift-off errors.

The eccentricity detection transducer consist of two eddy current sensors embedded in the bearing of the TFT. The sensors are located at 3 O'clock and 12 O'clock positions on the periphery of the bearing. The sensor at 3'o' clock position is used as reference sensor. The sensor in 12 O' clock position is used as the measurement sensor. These sensors are configured in differential mode by which the thickness variation and temperature variation of tube which in turn affects the conductivity will be compensated. By configuring the sensors in differential mode the common mode signals have been nullified.

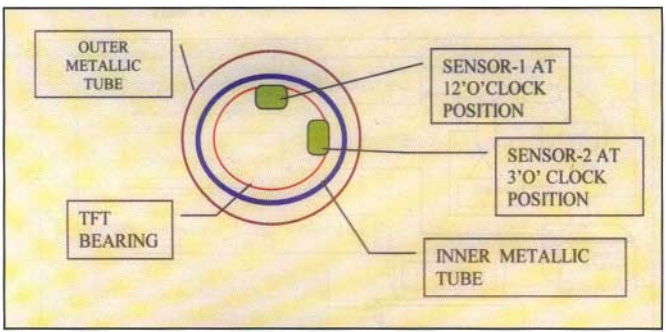

Fig. 1 : Schematic of eccentricity detection transducer

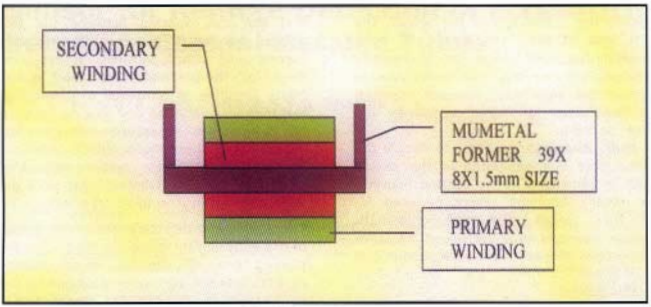

Fig. 2: Schematic of sensor

The schematic of the sensor used in the system is shown in Figure 2. It consists of C-Shape former made of mumetal surrounded by secondary and primary windings. The primary winding of the sensors will be excited by a constant current source. The outputs from the secondary windings are configured in series opposition mode and fed to the Sine to Square wave converters. The pulse width variation which is caused due to the change in the phase shift which in turn depends upon the eccentricity between the metallic tubes is measured by using XOR gate and micro-controller. The eccentricity information is displayed on DAS PC by DAS software. Figure 3 shows the schematic of the signal conditioning hardware associated with the transducer system.

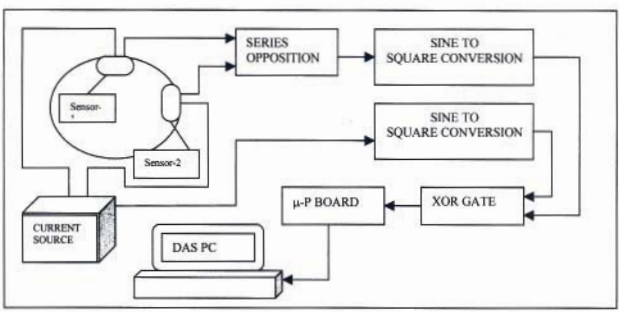

Fig. 3 : Schematic of signal conditioning hardware

Table-1

Sl No.	Test Frequency	%Lift-off Contribution
1.	2.5KHz	13.04
2	3.0KHz	10.83
3	3.5KHz	14.28
4	4.0KHz	19.2
5	4.5KHz	20
6	5.0KHz	23.8
7	5.5KHz	27.7
8.	6.0KHz	33.3

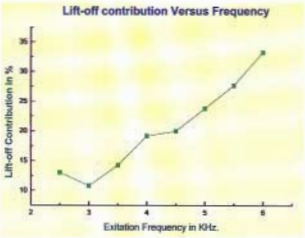

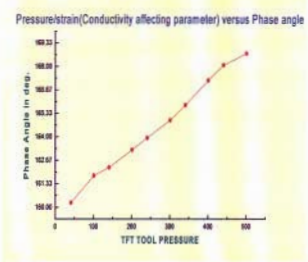

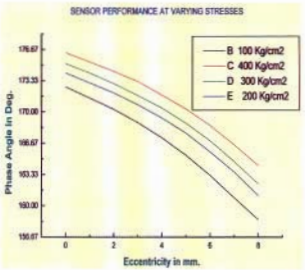

Table 2

Sl No.	Eccentricity Variation in mm	Phase angle variation in Deg.
1.	-7	134.13
2.	-6	134.4
3.	-5	134.93
4.	-4	135.4
5.	-3	136
6.	-2	136.6
7.	-1	137.26
8.	0	137.66
9	+1	138.26
10	+2	139
11	+3	140.46
12	+4	141.53
13.	+5	142.66
14.	+6	144.2
15.	+7	145.73
16.	+8	147.73

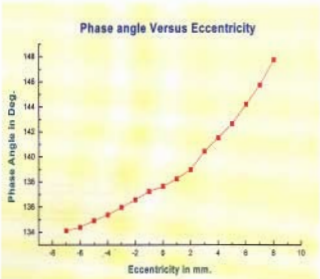

Experimental Observations Using Prototype System

The prototype transducer system developed has been used to measure the effect of lift off error at various frequencies in order to optimise the operating parameters for the transducer system. The Phase angle variation of signal while varying the full range of eccentricity between the tubes (0 to 16mm) for a typical setup have been studied.

(a) The results of Test Frequency Vs Worst possible Lift Off % is given in Table-1.
(b) The results of Eccentricity (-8 mm to +8mm) variation verses Phase angle variation is given in Table-2.

The following observations have been noted:

(a) Lift-Off Error: By using phase measurement techniques, the parameters like lift off are less sensitive. The parameter like annular gap variation between the tubes is more predominant.

(b) Transducer Signal Variation Due To Effect Of Mechanical Stress on Tubes : It has been observed that when TFT is operated to correct the eccentricity between the metallic tubes, the mechanical stresses are generated in the inner metallic tube due to flexing. These stresses will affect the signal out put of the transducer. As such the signal contribution due to the affect of mechanical stress generated in the tube should be compensated by using look-up table or by going for multi parameter technique.

Conclusion

The prototype of the transducer has been fabricated and tested. The experimental results are found highly encouraging. The transducer can be operated from a distance of 100 meters. Its performance is least effected by lift off errors. It has been observed that by using high permeability pancake probes, intense magnetic fluxes can be produced and application where remote field in non ferrous tubes is used, this type of design is having advantage.

INTRODUCTION

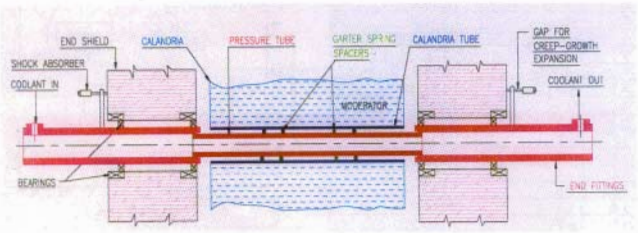

Schematic of PHWR Coolant Channel

System Highlights

- ★ Low cost system for precise measurement of eccentricity between the two co-axial metallic tubes.
- ★ Can be used to measure the eccentricity between non ferrous low electrical conductivity coaxial metallic tubes.
- ★ Miniature size to get accommodated in the bearing of the Eccentricity Correction Tool
- ★ Employs phase measurement technique to minimise lift-off errors

WORK DONE

Eddy current sensor namely Concentricity Detection Probe (CDP) has been devised to be used as embedded sensing element in hydraulically actuated Eccentricity Correction Tool (Tube Flexing Tool (TFT) which is subjected to heavy mechanical stresses), for detection of eccentricity between metallic tubes under operating conditions & subsequent correction of eccentricity (By actuating TFT based on feedback received from sensor). These posters highlights general design and developmental aspects of CDP sensor along with associated hardware. The experimental results showing the performance of the sensor are also highlighted.

Tube Flexing Tool (TFT) Modules used in Typical Tool

APPLICATION

A typical sensor for measuring eccentricity between the two coaxial metallic tubes has been designed and used in order to check the eccentricity between metallic tubes of coolant Channels of Indian 220 Mwe PHWR's in vertical axis ('Y' direction). These tubes are initially eccentric which needs to be corrected by using a Tube Flexing Tool (TFT) where the sensor is mounted in one of the bearings of TFT as an integral part of the tool. The TFT along with embedded sensor will be inserted in the bore of inner tube. The TFT is hydraulically actuated in 'Y' direction generating vertical thrust to correct the eccentricity between the metallic tubes based on the eccentricity information feed back received from the transducer.

This transducer can be operated from 100 meters cable distance and will be fairly insensitive to the lift-off errors.

This application can be extended for detecting eccentricity between any of coaxial metallic tubes.

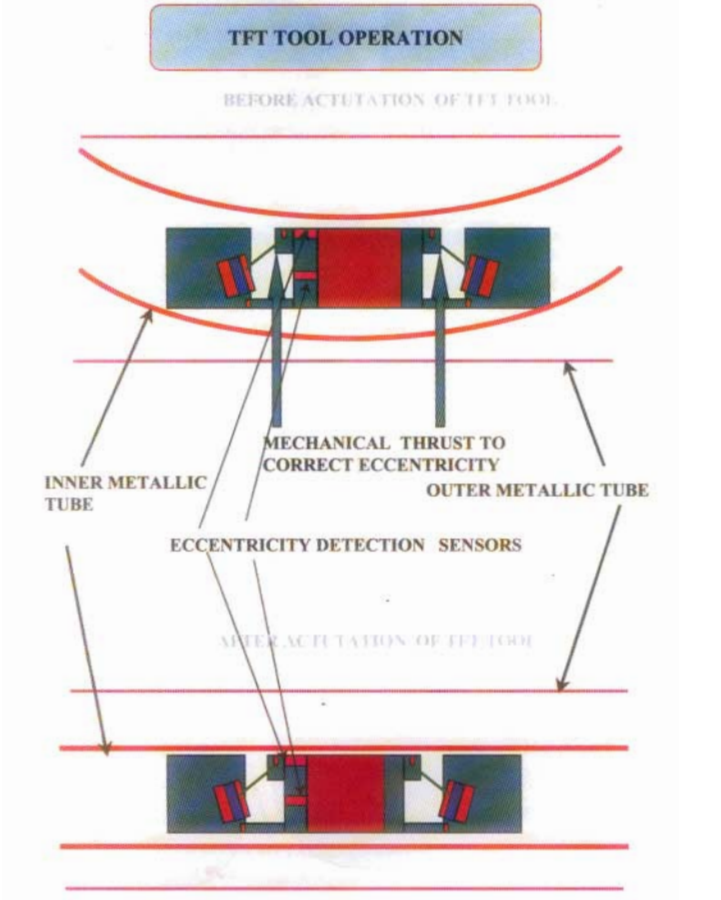
TFT TOOL OPERATION
BEFORE ACTUTATION OF TFT TOOL
MECHANICAL THRUST TO CORRECT ECCENTRICITY
INNER METALLIC TUBE
OUTER METALLIC TUBE
ECCENTRICITY DETECTION SENSORS
AFTER ACTUTATION OF TFT TOOL

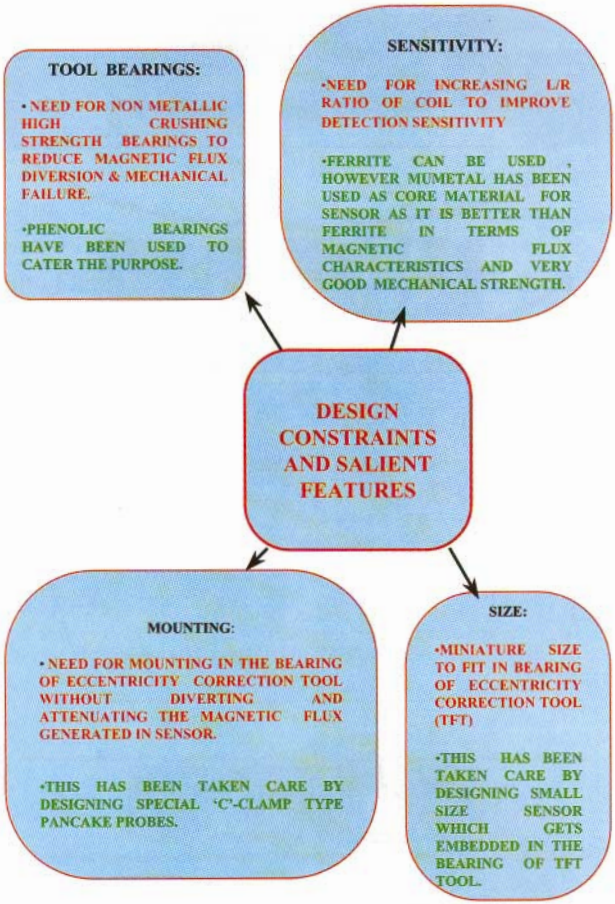
TOOL BEARINGS:
• NEED FOR NON METALLIC HIGH CRUSHING STRENGTH BEARINGS TO REDUCE MAGNETIC FLUX DIVERSION & MECHANICAL FAILURE.
•PHENOLIC BEARINGS HAVE BEEN USED TO CATER THE PURPOSE.
SENSITIVITY:
•NEED FOR INCREASING L/R RATIO OF COIL TO IMPROVE DETECTION SENSITIVITY
•FERRITE CAN BE USED , HOWEVER MUMETAL HAS BEEN USED AS CORE MATERIAL FOR SENSOR AS IT IS BETTER THAN FERRITE IN TERMS OF MAGNETIC FLUX CHARACTERISTICS AND VERY GOOD MECHANICAL STRENGTH.
DESIGN CONSTRAINTS AND SALIENT FEATURES
MOUNTING:
• NEED FOR MOUNTING IN THE BEARING OF ECCENTRICITY CORRECTION TOOL WITHOUT DIVERTING AND ATTENUATING THE MAGNETIC FLUX GENERATED IN SENSOR.
•THIS HAS BEEN TAKEN CARE BY DESIGNING SPECIAL 'C'-CLAMP TYPE PANCAKE PROBES.
SIZE:
•MINIATURE SIZE TO FIT IN BEARING OF ECCENTRICITY CORRECTION TOOL (TFT)
•THIS HAS BEEN TAKEN CARE BY DESIGNING SMALL SIZE SENSOR WHICH GETS EMBEDDED IN THE BEARING OF TFT TOOL.

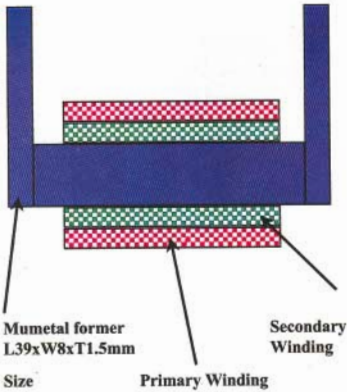

SCHEMATIC OF SENSOR OF ECCENTRICITY DETECTION TRANSDUCER

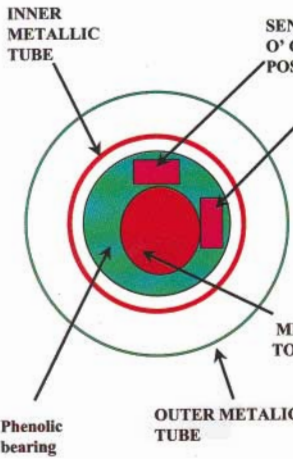

SCHEMATIC OF ECCENTRICITY DETECTION TRANSDUCER

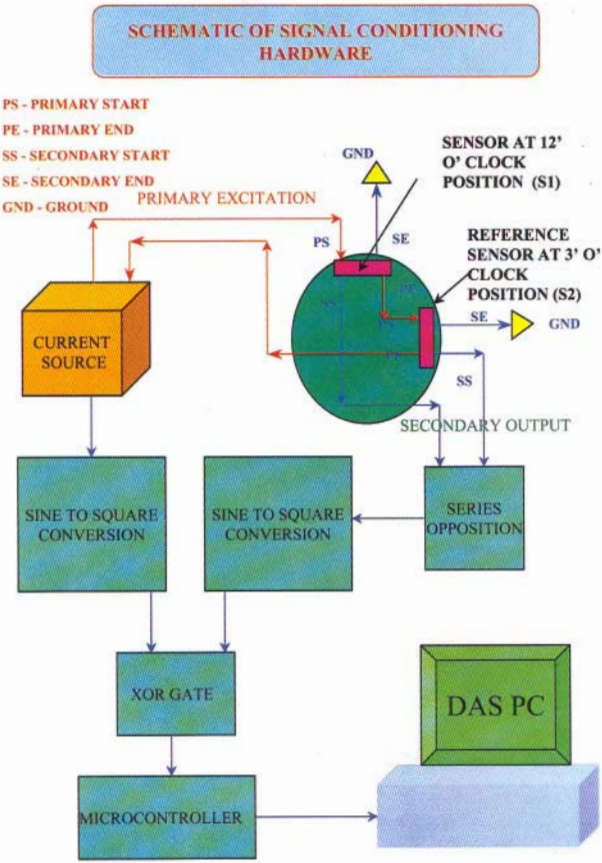
SCHEMATIC OF SIGNAL CONDITIONING HARDWARE
PS - PRIMARY START
PE - PRIMARY END
SS - SECONDARY START
SE - SECONDARY END
GND - GROUND
PRIMARY EXCITATION
GND
SENSOR AT 12' O' CLOCK POSITION (S1)
PS
SE
REFERENCE SENSOR AT 3' O' CLOCK POSITION (S2)
SE
GND
CURRENT SOURCE
SS
SECONDARY OUTPUT
SINE TO SQUARE CONVERSION
SINE TO SQUARE CONVERSION
SERIES OPPOSITION
XOR GATE
DAS PC
MICROCONTROLLER

RESULTS & CONCLUSION

THE PERFORMANCE RESULTS OF THE PROTOTYPE EDDY CURRENT TRANSDUCER FOUND HIGHLY ENCOURAGING AS INDICATED BELOW.

- **The Transducer can be operated from a distance of 100 metres.**
- **Phase measurement technique minimises the lift-off errors.**
- **The signal contribution due to effect of mechanical stresses on the metallic tubes (Conductivity change) is linear and can be compensated by using look-up table or by going for multi-parameter technique.**
- **Due to use of high permeability pancake probes, the system is a better substitute for Remote Field Technique Application in Non Ferrous Tubes**

This paper received the Best poster presentation award at the 8th National Seminar on "Physics and Technology of Sensors" held at BARC, Mumbai, during February 27 - March 1, 2001

About the authors ...

Mr T.V. Shyam *is actively working on design and development of eddy current sensors associated signal conditioning circuits and micro-controller based systems which are being used in rehabilitation tools for repair, and life-extension replacement of coolant channels of Indian Pressurised Heavy Water Reactors.*

Mr S.K. Apraj *is actively working on fabrication of various types of probes, associated signal conditioning circuits and control systems which are being used in rehabilitation tools repair, and life-extension replacement of coolant channels of Indian Pressurised Heavy Water Reactors.*

Mr B.S.V.G. Sharma *is Group Leader, Electrical Devices & Automation Group, Reactor Coolant Channel Section, Reactor Engineering Division. He has taken a leading role in design and development of Unconventional Tubular Linear Induction Motors, instrumentation and control systems for innovative tools, systems and techniques required for in service inspection, repair, life extension and replacement of coolant channels of Indian Pressurised Heavy Water Reactors.*

Synthesis of Chalcogenolate Complexes of Platinum Group Metals as Molecular Precursor

Sandip Dey
Novel Materials & Structural Chemistry Division
Bhabha Atomic Research Centre

Abstract

Several complexes of palladium(II) and platinum(II) containing benzylselenolate of the types $[M(SeBz)_2]_n$, $[M(SeBz)_2(P^nP)]$, $[M_2X_2(\mu\text{-}SeBz)_2(PR_3)_2]$ (X = Cl or Me) and $[M_2Cl_2(\mu\text{-}Y)(\mu\text{-}SeBz)(PR_3)_2]$ (Y = Cl, pz, Bu^{t}S) have been prepared. Similarly variety of products such as $[PdCl(Se^{\frown}N)]_2$, $[MCl(Se^{\frown}N)(PR_3)]$, $[M_2Cl_2(Se^{\frown}N)(PR_3)_2]$, $[Pt(Se^{\frown}N)_2(P^nP)]$ and $[Pt_2(\mu\text{-}Se^{\frown}N)_2(P^nP)_2]^{++}$ have been synthesized using the ligand 2-(dimethylamino)ethylselenolate ($Me_2NCH_2CH_2Se^{-}$ = $Se^{\frown}N$). All these complexes were characterized by elemental analyses, IR, NMR (^1H, ^{13}C, ^{31}P, ^{77}Se, ^{195}Pt) and UV/Vis spectroscopy. Structures of $[Pt_2Cl_2(\mu\text{-}SeBz)_2(PPr^n{}_3)_2]$ and $[PdCl(SeCH_2CH_2NMe_2)]_2$ were established by X-ray diffraction analyses. The thermal behaviour of a few complexes has been investigated.

Introduction

Materials growth techniques like MOCVD, plasma CVD, *etc.* employ molecular precursors rather than the elements to synthesize low temperature solid state inorganic materials for electronic devices [1]. During the last decades platinum group metal chalcogenolates have attracted considerable attention as molecular precursors for the synthesis of metal chalcogenides for electronic devices [2]. The area of metal chalcogenolates has been dominated by thiolato complexes which in most cases have been isolated as non-volatile, insoluble (sparingly soluble) and polymeric complexes thus making them inconvenient as precursor for the preparation of metal chalcogenide [3]. To suppress polymerization several strategies have been explored such as, (a) strongly coordinating ligand such as tertiary phosphines, (b) sterically demanding chalcogenolate ion, (c) internally functionallised ligands containing both soft chalcogen and hard N donors [4-6]. The later class of ligands not only yield low nuclearity complexes but also enhance complex stability. With the current interest in selenium containing inorganic materials and in pursuance of our program on the design and development of molecular precursors in NM&SCD, BARC, dibenzyl diselenide (Bz_2Se_2) and 2-dimethylaminoethyldiselenide ($Me_2NCH_2CH_2Se)_2$ were prepared and their palladium and platinum chemistry was explored.

Discussion

1 (i) Synthesis and characterization of benzylselenolate complexes

Sodium benzylselenolate has been prepared by the reductive cleavage of the Se-Se bond in Bz_2Se_2 (due to slow photo-decomposition it was recrystallised every month from petroleum ether) with $NaBH_4$ and the following Pd(II)/Pt(II) complexes have been prepared (scheme 1) [7]. The compound is a sparingly soluble polymeric complex. Strong neutral donor ligands like tertiary phosphines can easily cleave the selenolato bridge of 1 with the formation of monomeric *cis* isomer 2. In the case of binuclear complexes (4-6) three isomers, *viz.* one *trans* and two *cis* isomers are posiible.

On the basis of NMR spectroscopy, except in few cases, binuclear complexes (4-6) were formed exclusively as a *cis* isomer.

The ^{77}Se NMR spectrum of $[Pt_2Cl_2(\mu\text{-}SeBz)_2(PPr^n{}_3)_2]$ (Fig 1) shows that two Se

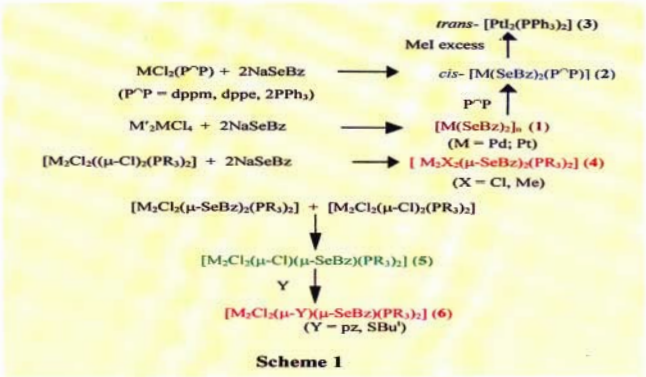

Scheme 1

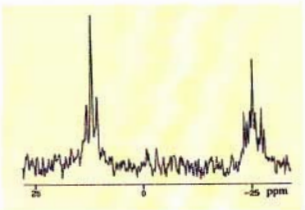

Fig. 1 : ^{77}Se NMR spectrum of [$Pt_2Cl_2(\mu\text{-}SeBz)_2(PPr^n{}_3)_2$]

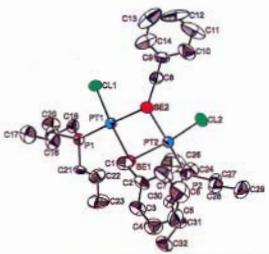

Fig. 2 : Molecular structure of [$Pt_2Cl_2(\mu\text{-}SeBz)_2(PPr^n{}_3)_2$]

atoms are magnetically in-equivalent, one is *trans* to P atoms and other is *trans* to chlorides. The X-ray structure of this complex (Fig 2) revealed that it consists of two distorted square planar platinum atoms Pt(1) and Pt(2) which show deviation of 0.046 and 0.032 Å, respectively from the mean planes defined by P(1)Cl(1)Se(1)Se(2) and P(2)Cl(2)Se(1)Se(2). This suggests pyramidization of platinum atoms. The molecule has a sym-*cis* configuration with a non planar four-membered "Pt_2Se_2" ring (hinge angle 131.1°).

1 (ii) Thermal studies

The TG trace of $[Pd(SeBz)_2]_n$ showed two stage of decomposition. The product forms after the first stage of decomposition (in the temperature range 210 to 500°C) has been identified as a mixture of products $PdSe_2$ and $Pd_{17}Se_{15}$ contaminated with carbon (typical analysis of a sample heated at 300°C : C, 7.7; H, 0.6; Se, 49.1; Pd, 40.4%, XRD pattern showed peaks due to $PdSe_2$ and $Pd_{17}Se_{15}$). In the second of decomposition (above 600°C) selenium is eliminated leading to the formatuon of $Pd_{17}Se_{15}$ as indicated by

the weight loss and XRD pattern. The carbon contents (C 5.7%) in this product has been reduced slightly.

2. (i) Synthesis and charaterization of 2-(dimethylamino)ethaneselenolate complexes

Using this ligand and it's sodium salt i.e. $NaSeCH_2CH_2NMe_2$ several Pd(II)/Pt(II) complexes have been prepared (scheme 2).

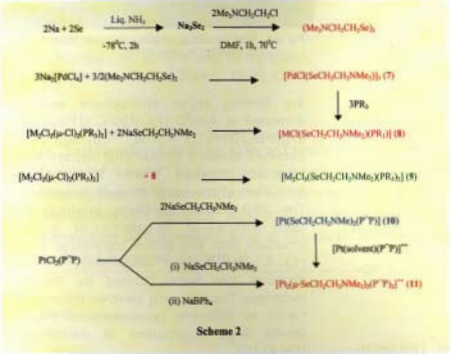

Scheme 2

The compound $[PdCl(SeCH_2CH_2NMe_2)]_n$ (**7**) was established as trimeric according to FAB mass spectrum and more confirmly by X-ray diffraction analysis (Fig 3).

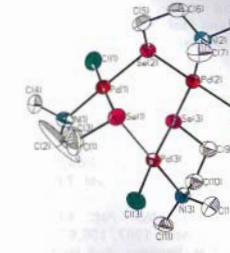

Fig. 3 : Molecular structure of $[PdCl(SeCH_2CH_2NMe_2)]_3$

The molecule contains three distorted square planar palladium centers held together by three bridging selenium atoms of the chelating dimethylaminoethane selenolate ligand. The resulting six-membered Pd_3Se_3 ring adopts a twist conformation. The dimethylaminoethyl selenolate ligands form "exocyclic" five-membered $PdSeC_2N$ chelate ring, with envelope conformations.

Tertiary phosphines react with 7 and results pink to violet coloured Pd complexes 8. According to NMR spectroscopy and X-ray structural analysis these complexes are monomeric with Se *cis* to phosphorus ligand.

The series $[M_2Cl_3(SeCH_2CH_2NMe_2)(PR_3)_2]$ (9) showed two major ^{31}P signals the one at lower frequency is attributed to the phosphine attached to the metal atom containing the chelating Se^N ligand. The second signal is due to the phosphine attached to MCl_2 fragment. The series $[Pt_2(\mu\text{-}SeCH_2CH_2NMe_2)_2(P^P)_2]^{2+}$ (11) show two sets of $^{31}P\{^1H\}$ and $^{195}Pt\{^1H\}$ (Fig 4) NMR peaks indicate that the non-equivalence of phosphorus nuclei of P^P ligand. In case of Se bridged binuclear complexes the Pt-Se bond distances are not equal (diff. ≈ 0.065 Å) thus making the Pt_2Se_2 fragment an asymmetric ring (Fig 5) in contrast to symmetric Pt_2S_2 ring [8].

The absorption spectra of the series $[MCl(SeCH_2CH_2NMe_2)(PR_3)]$ 8 showed week (ε = 100 $M^{-1}cm^{-1}$) long wavelength band at about 514 nm for Pd complexes, at ca. 400-430 nm for Pt derivatives. The band is hypsochromically shifted on replacing the phenyl substituents on the PR_3 group by donating alkyl groups. This absorption is due to a HOMO (Se) - to - LUMO (PR_3), *i.e.*, ligand - to - ligand charge transfer (LLCT) transition and is responsible for the unusual colour of the complexes. This is further

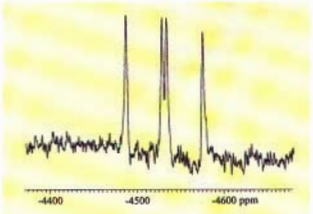

Fig. 4 : ^{195}Pt NMR spectra of $[Pt_3(\mu SeCH_2CH_2NMe_2)_2(dppp)_3]^{++}$

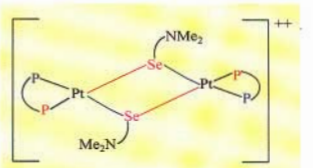

Fig. 5 : Structure of $[Pt_3(\mu\text{-}SeCH_2CH_2NMe_2)_2(dppp)_3]^{++}$

confirmed by electrochemical data and TD-DFT calculations [9, 10].

2 (ii) Thermal studies

Thermogravimetric analyses of $[Pd(SeCH_2CH_2NMe_2)Cl]_3$ (7) and $[PdCl(SeCH_2CH_2NMe_2)(PPh_3)]$ have been carried out under flowing argon atmosphere. The TG curve of 7 shows closely spaced two-step decomposition (284^{0}C), leading to the formation of $Pd_{17}Se_{15}$ as inferred from the calculated mass loss. The XRD patterns of the product and the elemental analyses [Found : Pd 59.0, Se 41.0 (±2%), C 3.9, H and N not detected (detection limit 0.2%); calcd for $Pd_{17}Se_{15}$: Pd, 60.9; Se, 39.6%] are in agreement with the $Pd_{17}Se_{15}$ formulation. The complex $[PdCl(SeCH_2CH_2NMe_2)(PPh_3)]$ also decomposes via two steps resulting in $Pd_{17}Se_{15}$ at 350^{0}C (from calculated mass loss), as confirmed by the XRD pattern.

To prepare large quantities of palladium selenide, a substantial amount of precursors (7, $[PdCl(SeCH_2CH_2NMe_2)(PPh_3)]$) (100-500 mg) have been heated in a furnace under a dry flowing argon atmosphere and then annealed at 400^{0}C (7), 450^{0}C ($[PdCl(SeCH_2CH_2NMe_2)(PPh_3)]$). The $Pd_{17}Se_{15}$ thus obtained shows a similar XRD pattern as the samples obtained from TG, indicating formation of the same product in each case. The XRD pattern of these products have been interpreted in terms of a cubic structure with the lattice parameter 10.584 (1) Å. The surface morphology of these products has been studied by the SEM technique.The scanning electron micrographs taken at different resolutions of $Pd_{17}Se_{15}$ shows large aggregates of microcrystals (Fig 6) [6].

Fig. 6 : SEM picture of $Pd_{17}Se_{15}$ obtained from $[PdCl(SeCH_2CH_2NMe_2)(PPh_3)]$

Acknowledgements

I would like to thank Dr. V. K. Jain for his guidance and encouragement of the work. I am grateful to Dr. B. Varghese, RSIC, Madras IIT and Prof. W. Kaim, University of Stuttgart, Germany for X-ray diffraction analysis.

References

1. Proceedings of the Third International Conference on Metal-Organic Vapor Phase Epitaxy. *J. Cryst. Growth*, G. B. Stringfellow, Ed. 1986, vol **77**, entire volume.
2. T. Yamamoto, *Jap. Pat.* 61215661, 1986, *Chem Abst*, 1987, 106,87694h; Y. Idota and M. Yagihara, *Fuji Photo Films Co. Ltd, Jap Pat*, 1986, 61186959, *Chem*

Abst 1987, **106**, 166325s; T. Oota, K. Yoshioka, T. Akyama and S. Mori, *Jap Pat*, 1995, 07205548, *ChemAbst*. 1995, **123**, 325855j.
3. I. G. Dance, *Polyhedron*, 1986, **5**, 1037; P. J. Blower and J. R. Dilworth, *Coord. Chem.Rev.*, 1987, **76**, 121.
4. M. Capdevila, W. Clegg, P. Gonzalez Duarte, B. Hanis, I. Mira, J. Sola and I. C. Taylor, *J. Chem. Soc. Dalton Trans.*, 1992, 2817; M. A. Ciriano, J. J. Perez-Torrente, L. A. Oro, A. Tiripicchio and M. J. Tiripicchio-Camellini, *J. Chem. Soc. Dalton Trans.*, 1991, 225.
5. S. Narayan, V. K. Jain and B. Varghese, *J. Chem Soc. Dalton Trans.*, 1998, 2359.
6. S. Dey, V. K. Jain, S. Chaudhury, A. Knoedler, F. Lissner and W. Kaim, *J. Chem. Soc. Dalton Trans.*, 2001, 723.
7. S. Dey, V. K. Jain and B. Varghese *J. Organomet. Chem.* 2001, **623**, 48.
8. S. Dey, V. K. Jain, A. Knoedler, W. Kaim and S. Zalis, *Eur. J. Inorg. Chem.*, 2001, 296
9. S. Dey, V. K. Jain, A. Knoedler, A. Klein, W. Kaim and S. Zalis, *Inorg. Chem.*, 2002, **41**, 2864.
10. S. Dey, V. K. Jain, J. Singh, V. Trehan, K. K. Bhasin and B. Varghese, *Eur. J. Inorg. Chem.*

Mr. Sandip Dey has been selected twice for "The Professor B. C. Halder Memorial Award" in Inorganic Chemistry Section for the best paper presentation in "International Conference on Chemistry and 36th Annual Convention of Chemists" held at Calcutta in Decemeber 1999 and "37th Annual Convention of Chemists" held at Hardwar in November 2000, organized by "Indian Chemical Society".

About the author ...

Mr Sandip Dey *passed out from the 41st batch of BARC Training School and is working in Novel Materials & Structural Chemistry Division, BARC, on the design and development of molecular precursors of platinum group metals for the synthesis of advanced materials.*

Strategies for *in vitro* Propagation and Synthetic Seeds in Banana

T.R. Ganapathi, P.Suprasanna, V.M. Kulkarni, V.A. Bapat and P.S. Rao
Nuclear Agriculture and Biotechnology Division
Bhabha Atomic Research Centre

Abstract

Bananas and plantains are one of the world's major fruit crops and staple food crops for hundreds of millions of people. Although more than 300 kinds of bananas exist, only a few are commercially important. Improving plant productivity is a necessity as several biotic and abiotic constraints impede its cultivation and production. In our laboratory, protocols have been established for the in vitro propagation of twelve commercially important cultivars of banana. Tissue culture derived plants have been field planted and the performance of these plants has been encouraging with increase in yield, early maturity and quality fruits. In the seed propagated Enset (Ensete superbum), protocols for in vitro propagation have been established using male inflorescences. Low cost procedures for in vitro propagation have been developed using commercial grade sugar and simplified nutrient media. Shoot tips have been encapsulated to prepare synthetic seeds that offer as novel delivery system for tissue cultured plants. Future prospects for the improvement of banana using biotechnological tools are also described.

Introduction

The word banana is derived from the Arabic word for finger. There are more than 300 kinds of banana but only a few are commercially important. Banana is the man's oldest and most valued fruit crop. It is prized for its nutritive value with high carbohydrates (22.2%), fibre (0.84%) and protein (1.1%) with less fat (0.2%) and water (75.7%). The World production of banana is about 95 million tons and most of the production is consumed locally.

In India, it is the most important fruit crop and is grown in 4.3 million hectare with a total production of 13.9 million tonnes. Several cultivars of banana are cultivated in the country among which, Dwarf Cavendish and Robusta are predominantly grown because of higher yields, resistance to strong winds and short cropping duration besides a good profit margin (Singh 1990). In addition to these, cultivars such as Poovan, Rasthali, Lalkela, Safed velchi and Karibale monthan are also grown. Banana is severely affected by viral (bunchy top virus, cucumber mosaic virus, banana streak virus), bacterial (moko or bacterial wilt, bacterial soft rot), fungal (black sigatoka, Fusarium wilt) agents besides insects/pests and nematodes.

Banana is a long duration crop of one and a half years and is propagated vegetatively by suckers. The production of suckers varies in different genotypes ranging from 5-10 per plant per year. Crop productivity and maturity is dependent on the size and age of suckers and uneven maturity extends the duration by 3-4 months. Suckers also carry soil nematodes, disease causing organisms such as bunchy top virus, leaf spot etc., thereby affecting the crop production considerably. In this regard, biotechnological approaches such as cell and tissue culture, protoplast fusion and gene transfer offer as useful tools (Novak *et al* 1993, Ganapathi *et al.*,. 2002). *In vitro* propagation of banana through shoot tip cultures is useful in the rapid multiplication of desirable disease free plantlets. In addition careful selection and updating of mother plants results in improved crop yield (Vuylsteke, 1989).

Enset [*Ensete superbum*] is the Indian wild banana, propagated by means of seeds and does not produce vegetative side suckers naturally. The Ensets are the staple food of almost 10 million people in Ethiopia. These have capacity to withstand severe draught, and have also been used to help ward off famine in Ethiopia. The wild counterparts are

known for their broad genetic base and carry several desirable genes and thus the Ensets could be utilized for improvement of cultivated bananas by employing various *in vitro* techniques (Vuylsteke and Swennen, 1993; Novak *et al.*, 1992). Conventional propagation of *Enset* is time consuming and hence there is a need for optimization of tissue culture techniques for the rapid propagation of enset.

We describe here our studies on *in vitro* propagation of banana and enset, low cost strategies for in vitro propagation and synthetic seeds in banana.

Materials and Methods

Suckers of ten varieties viz., Basrai, Shrimanthi, Rasthali, Lalkela, Poovan, Ardhapuri, Karibale monthan, Safed Velchi, Mutheli and Hazari were collected and established in the departmental green house. Cultivars, Williams and Grande Naine were obtained in the form of sterile cultures from INIBAP's Germplasm Transit Centre, Belgium. Male inflorescences of enset were collected from the wild plants growing on the steep hill slopes of Sinhagad hill fort of the Western Ghats, at an altitude of 800 m. Shoot tips were isolated from suckers by removing the sheathing leaf bases and were established in liquid MS medium (Murashige and Skoog 1962) supplemented with 5 mg/l benzyl adenine (BA). After 3 weeks these were transferred to semi-solid medium comprising of 2 mg/l BA and 30 mg/l adenine sulphate (AS) and 3% sucrose. Each shoot tip produced 3-5 shoots within a span of 3-4 weeks. Multiplication of shoots was carried out by isolating individual shoots and subculturing them on the same medium till a sufficient number of shoots were obtained. The individual shoots isolated from these multiple shoot cultures were used for various experiments. Individual shoots were transferred to medium with napthaleneacetic acid (NAA) for root induction.

Investigations on the effect of cyanobacterial extracts (CYE) were conducted with cyanobacterial strain (*Plectonema boryanum* UT x 594) grown on BG11 medium. The detailed procedures are given in Ganapathi *et al.*, (1994). Shoot tips were grown on medium with CYE (10, 20, 40, 80 %) and also CYE (100%) alone, along with growth regulators.

Experiments were conducted with commercial grade sugar (CGS) and tap water (TW) in place of sucrose and distilled water, respectively. Multiplication of shoots and rooting of shoots was tested on medium with CGS (3%) and TW. Shoots were also encapsulated in sodium alginate (3%) and their conversion into plants was examined in the above media combinations (Ganapathi *et al.*, 1995). For each treatment 24 shoots were used and all the experiments were conducted under controlled conditions of light (1000 lux), temperature (25$\pm$2° C) and relative humidity of 65%. Rooted plantlets were transferred to poly bags containing good horticultural soil and farm yard manure (1:1) in the green house at high humidity. About 8 week old hardened plants were used for field planting at Experimental Field Facility, Trombay, BARC and Gujarat State Fertilizers Company (GSFC) Ltd., Vadodara, Gujarat.

Results and Discussion

In vitro *propagation of banana*

Initially shoot tip cultures were established *in vitro* for the induction of multiple shoots (Fig.1A). The multiple shoots showed elongation and produced roots in liquid media (Fig.1B). Individual shoots transferred to rooting media formed complete plantlets within 4 weeks (Fig.1C). After another period of 4 weeks, plantlets transferred to polybags in the green house exhibited good growth by the emergence of new leaves (Fig.1D).

More than 15,000 plants were regenerated *in vitro* and around 4,500 plants were planted at multilocations in the states of Maharashtra and Gujarat for field trials. A field trial was conducted at R&D farm Gujarat State Fertilizers Company, Baroda (Fig. 1E) and the data suggested an early maturity by about 6 weeks and an increase in yield of 33% in the tissue cultured plants of cv. Basrai as compared to control. The tissue culture raised

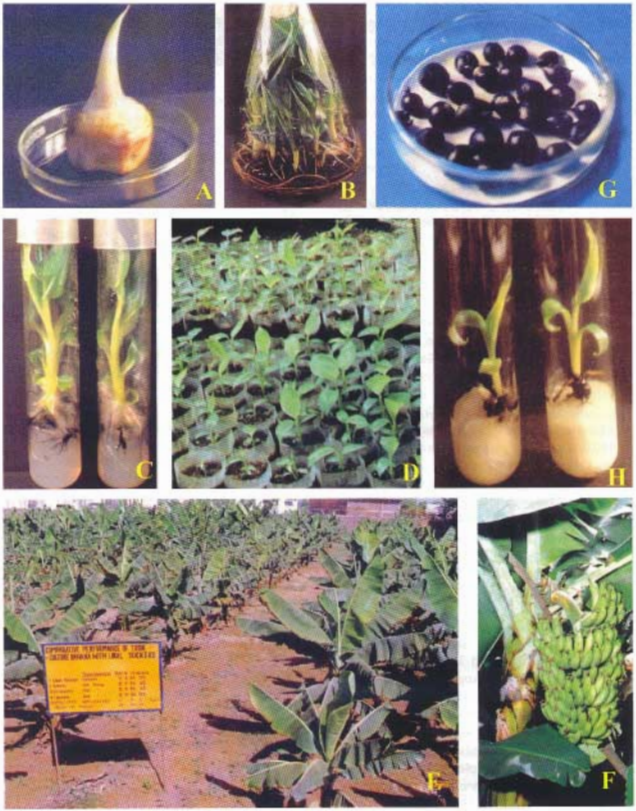

Fig. 1 :

A. *Isolated shoot tip used to initiate in vitro shoot cultures*
B. *Multiple shoots developed in liquid medium.*
C. *Rooted shoots*
D. *Hardened plants in the greenhouse.*
E. *Tissue cultured plants undergoing field trial at GSFC experimental field, Vadodara.*
F. *Tissue culture derived banana plant bearing a fruit bunch.*
G. *Encapsulated shoot tips of banana (synthetic seeds).*
H. *Plantlet development from synthetic seeds of banana.*

plants grown at the Experimental Field Facility at BARC, Trombay, showed more vigorous growth, early maturity and increase in bunch weight with good quality fruits (Fig.1F).

In vitro *propagation of Enset*

Male inflorescences were cultured on MS medium supplemented with BA (2 mg/l) and gibberellic acid (GA_3 1 mg/l). The extreme apical region of male inflorescences necrosed, but the surrounding floral primordia showed growth and produced profuse leafy structures initially. After 2 subcultures, the proportion of leafy structures decreased substantially (<10 %) and a mixture of corm tissue and multiple shoots became predominant (>90%). Longer shoots (2.9 cm) were induced on MS + BA (2 mg/l) + AS (30 mg/l) + GA_3 compared to shoots of 1.7 and 1.8 cm length on MS + BA (2 mg/l) + AS (30 mg/l) with and without caesin hydrolysate (500 mg/l) respectively (Kulkarni *et al.*, 1997a).

Efficacy of various media tested for root induction showed that MS medium alone was ineffective, whereas MS medium with NAA (1mg/l) gave highest number of roots followed by MS + indole-3-acetic acid (IAA) or indole-3- butyric acid (IBA). Addition of charcoal (0.1%) to these media did not improve rooting efficiency. Rooted plantlets exhibited normal growth upon transfer to polybags in the greenhouse and in the field.

There have been very few reports concerning micropropagation of Ensets. Afza *et al.*, (1996) reported micropropagation of *E. ventricosum* using shoot-tips from vegetative corms. Mathew and Philip (1997) reported regeneration using vegetative shoot apices in *Ensete superbum*. In the this study, cultured floral apices were employed as an alternative method for the *in vitro* propagation of enset. In the case of triploid banana cultivars, floral apices have successfully been used for the propagation of Chandrabale, Rasthali, Robusta (Doreswamy and Shahijram, 1989) and cvs. Monthan and Robusta (Balakrishnamurthy and Sree Rangasamy, 1988). The protocol for the regeneration *E. superbum* using male inflorescences will be useful for rapid *in vitro* propagation.

Low cost strategies for in vitro *propagation*

The main objective of this investigation was to develop a low cost *in vitro* technique for the micropropagation of banana by substituting laboratory grade sucrose and distilled water with commercial grade sugar and tap water, respectively, for minimizing the use of the expensive components of the nutrient media.

The shoot tips grown on media prepared in distilled water containing lab grade sucrose or commercial grade sugar showed the formation of multiple shoots (4-5 shoots/ hoot tip) in four weeks. There was no significant change in the frequency of multiple shoot formation in both the media and almost 100 % of the shoots responded. In an another experiment when tap water was used instead of distilled water, more time was required for the induction of multiple shoots and proliferation and the time of the subculture passage had to be extended to 6 weeks.

As presented in the Table 1, the excised shoots from multiple shoot cultures were transferred on various media for plantlet regeneration. The shoots cultured on MS medium prepared in distilled water and containing either laboratory grade sucrose or commercial grade sugar showed a good shoot growth having 2-4 roots with laterals in three weeks. The hoots showed comparatively slow growth on similar medium prepared in tap water. The frequency of plantlet formation was almost 95% and there was no change in the number of roots and their laterals.

Plantlets regeneration was also observed on Knop's salts with MS minor, iron and vitamins with lab grade sucrose or commercial grade sugar, in medium prepared either with distilled water or tap water. The response was comparatively better in medium prepared in distilled water, as has been shown in Table 1. The frequency

Table 1 : Effect of different media on plantlet formation from shoot tips of banana

Media + carbon source (3%) + NAA (1 mg/l)	% cultures forming plantlets	No. of roots/ plantlet	Plantlet height after 4 weeks (cm)
A. MS basal salts +			
I) sucrose/commercial grade sugar in distilled water	100	2-4	7-9
II) sucrose/commercial grade sugar in tap water	95	2-3	7-8
B. Knop's salts +MS minor, iron & vitamins+			
III) sucrose/commercial grade sugar in distilled water	85	2-3	6-8
IV) sucrose/commercial grade sugar in tap water	85	2-3	6-8
C. Knop's salts +			
V) sucrose/commercial grade sugar in distilled water	75	2-3	6-7
VI) sucrose/commercial grade sugar in tap water	75	2-3	6-7
Data obtained after 4 weeks; 24 explants per treatment.			

of plantlet formation was around 75-80% on Knop's salt alone with lab grade sucrose or commercial grade sugar.

The rooted plantlets (7-9 cm in length) thus produced were transplanted into ploybags for hardening in the green house for about two months before field planting.

In the present study with banana tissue cultures, laboratory grade sucrose was totally eliminated by using 3 % commercial grade sugar and for the preparation of media clean tap water of good quality was employed instead of distilled water. Though all the components of MS medium were necessary for shoot multiplication, rooting and regeneration of plantlets was achieved only on Knop's salts (KNO_3, $Ca(NO_3)_2.4H_2O$, $MgSO_4.7H_2O$, KH_2PO_4) with NAA and commercial grade sugar. These alterations in the medium would be useful in lowering the total cost of tissue cultured bananas without affecting the rate of multiplication and quality of plants.

Effect of cyanobacterial extract (CYE)

The effect of cyanobacterial extracts (*Plectonema boryanum* UT x 594) was tested on growth and multiplication of shoots from shoot tips as well as encapsulated shoot tips of banana. Shoot tips reared on MS medium containing different concentrations of CYE (10, 20, 40 and 80% v/v), showed induction of multiple shoot formation (2-4). Higher concentrations (40 or 80%) exhibited increased frequency of multiple shoot formation (Fig.2) and shoot growth compared to other concentrations. In one treatment, with complete elimination of MS basal medium, shoot tips were cultured on CYE supplemented with 3% sucrose, 5 mg/l BA and 0.8% agar. Although multiple shoot formation was noted in all the concentrations with varying frequencies, the shoots exhibited slow growth.

Liquid cultures were also initiated with different concentrations of CYE (10-100% v/v) to minimize the use of nutrients and growth regulators. Among these, 10 and 20 % CYE induced 2-4 shoots while 100% CYE gave as many as 8 shoots and the shoots elongated with 2-3 pairs of leaves. To regenerate complete plantlets, the elongated shoots were cultured on MS medium with CYE (10, 20, 40 and 80% v/v) and plants were regenerated on all the four concentrations with varying frequencies

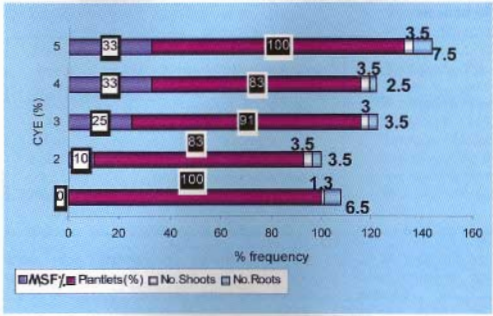

Fig. 2 : Effect of Cyanobacterial Extract (CYE) on multiple shoot cultures and planet formation in banana

(Fig.2). Similar to the controls (shoots on MS medium with 1 mg/l NAA), 100% of shoots cultured on MS medium with 80% CYE developed into plantlets within 4 weeks and all the plants were transplantable.

Cyanobacterial extracts are known to stimulate somatic embryogenesis and the conversion of synthetic seeds in carrot (Wake *et al.*, 1991, 1992) and sandalwood (Bapat *et al.*, 1996). Although the exact factors that are involved in such a response are unknown, it has been postulated that cyanobacterial extracts may synthesize a wide variety of compounds including plant growth regulating substances (Metting and Pyne 1986). In the present study, CYE has shown promotive effects on shoot multiplication and plantlet development suggesting that CYE can be employed in the *in vitro* propagation of banana.

Synthetic seeds

Shoot tips excised from the shoot cultures of bananas cv. Basrai were encapsulated to prepare synthetic seeds, in 3% sodium alginate solution prepared either in distilled water or MS medium with 0.1% activated charcoal (Fig.1G) and an antibiotic mixture (Ganapathi *et al.*, 1992). Encapsulated shoot tips were placed on MS or White's media with 1 mg/l NAA or 5 mg/l BA and also on different substrates like sterile absorbent cotton (Fig. 1H), soil, filter paper and soilrite (all moistened with 1/4th MS salt solution) for germination. Among these, White's medium gave high frequency (100%) plantlet development within a week compared to other substrates and MS media. Encapsulated shoot tips directly sown in petri plates containing autoclaved soil showed the emergence of shoots (10%) but failed to form complete plantlets.

The results revealed that the encapsulated shoot tips can be handled like a seed and could be useful in minimizing the cost of production as 1 ml of medium is sufficient for encapsulation of a single shoot tip compared to 15-20 ml for conversion of shoot tips into plantlets. By directly sowing the encapsulated shoot tips in soil, the two stage process such as rooting and hardening can be eliminated. As compared to suckers, encapsulated shoot tips present as inexpensive, easier and safer material for germplasm exchange, maintenance and transportation (Rao *et al.*, 1993).

Prospects for the improvement of banana

Banana has assumed an important status among fruit crops owing to the significant research inputs in the areas of cellular and molecular biology. Globally research is being focussed on aspects relevant to the needs of the developing countries. Mutation induction using physical as well as chemical mutagens can be useful for the induction of genetic variability. Towards this goal, we have conducted research as part of the Coordinated Research Project (CRP) of

Table 2 : Biotechnological approaches for the improvement and increasing productivity in banana

• Productivity	Cloning of high yielding varieties
• Germplasm storage & Transportation	Cryopreservation, Synthetic seeds
• Fungal diseases	Antifungal proteins, Antimicrobial compounds, Toxins
• Viral diseases	Coat protein genes, Replicase
• Nematodes	Bt genes, Chitinases
• Post harvest life	Anti polygalacturonase (PG), Anti-ethylene biosynthetic genes (ACC Synthase, ACC Oxidase)

International Atomic Energy Agency (IAEA), Vienna, on the 'Mutation breeding and related biotechnologies for banana improvement (Kulkarni *et al.*, 1997b, Rao *et al.*, 1999).

Somatic embryogenesis offers as an ideal system for the production somatic embryos on a large scale for use in the preparation of synthetic seeds, propagation and genetic transformation. In this direction, somatic embryogenesis has already been established in our laboratory from immature male flowers and proliferating shoot tips (Ganapathi *et al.*, 1999, 2001). Embryogenic cell suspension cultures developed from proliferating shoot tips have been useful as the best target tissue for genetic transformation using *Agrobacterium tumefaciens* (Ganapathi *et al.*, 2001).

Introduction of genes for fungal disease resistance may enable the development of new lines with disease resistance in banana. One of the approaches includes the expression of antimicrobial peptides. Improving fruit quality with options for delayed fruit ripening can have significance to boost banana exports from developing countries. Another dimension in the genetic engineering is the production of recombinant proteins or peptides of pharmaceutical importance in transgenic plants. Production of edible vaccines in an edible plant tissue, for example, in fruits of banana can be of great benefit to the developing countries to gain access to the much-needed health care. Studies in this direction have already shown some success towards obtaining transgenic plants of banana incorporated with useful characters like disease resistance and for developing edible vaccines (Ganapathi *et al.*, 2002).

Acknowledgements

Authors thank Dr. R.K. Iyer, Molecular Biology and Agriculture Division, BARC, for providing the cyanobacterial strain (*Plectonema boryanum* UT x 594).

References

1. Afza R., von Durren M. and Morpurgo R. 1996. Regeneration of *Ensete ventricosum* through somatic embryogenesis and adventitious buds. Plant Cell Rep. 15:445-448.
2. Balakrishnamurty G. and Sreerangaswamy S.R., 1988. Regeneration of banana plantlets from *in vitro* culture of floral apices. Curr. Sci. 57: 270-272.
3. Bapat V.A., Iyer R.K. and Rao P.S., 1996. Effect of cyanobacterial extracts on somatic embryogenesis in tissue cultures of sandalwood (*Santalum album* L.). J. Med. & Aromatic Plant Sci., 18 : 10-14.
4. Doreswamy R. and Shahjiram L. 1989. Micropropgation of banana from male floral apices cultured *in vitro*. Sci. Hort. 40:181-188.
5. Ganapathi T.R. Suprasanna P, Bapat V.A. and Rao P.S. 1992. Propagation of banana through encapsulated shoot tips. Plant Cell Reports 11 : 571 - 575.

6. Ganapathi T.R., Suprasanna P., Bapat V.A., Kulkarni V.M. and Rao P.S. 1999. Somatic embryogenesis and plant regeneration from male flower buds in banana. Curr. Sci. 76 (9) : 1228-1231.
7. Ganapathi T.R., Suprasanna P, Bapat V.A. and Rao PS, 1994. Stimulatory effect of cyanobacterial extracts on banana shoot tip cultures. Trop. Agri. 71: 299-302.
8. Ganapathi T.R., Chakrabarti A., Suprasanna P and Bapat V.A. 2002. Genetic transformation in banana. In : Plant Genetic engineering. Vol. 6: Improvement of fruits. Ed. PK Jaiwal and RP Singh. Sci-Tech Publ. Houston Texas, USA. (In press)
9. Ganapathi T.R., Higgs N.S., Balint-Kurti PJ, Arntzen C.J., May G.D. and Van Eck J.M. 2001. *Agrobacterium* -mediated transformation of embryogenic cell suspensions of the banana cultivar Rasthali (AAB). Plant Cell Reports 20:157-162.
10. Ganapathi T.R., Mohan J.S.S., Suprasanna P., Bapat V.A. and Rao P.S., 1995. A low cost strategy for *in vitro* propagation of banana. Curr. Sci., 68 : 646-649.
11. Kulkarni V.M., Ganapathi T.R., Suprasanna P., Bapat V.A. and Rao P.S. 1997b. Effect of gamma irradiation on *in vitro* multiple shoot cultures of banana. (*Musa* species). Jour. Nuclear Agri. Biol. 26(3) : 168-174.
12. Kulkarni V.M., Ganapathi T.R., Suprasanna P., Bapat V.A. and Rao P.S. 1997a. *In vitro* propagation in *Ensete superbum* (Roxb.) Cheesman, a species closely related to *Musa*. Ind. Jour. Exptl. Biol. 35 : 96-98.
13. Mathew M.M. and Phillips V.J. 1997. Clonal propagation of enset [*Ensete superbum* (Roxb.) Cheesman] through shoot tip culture. Plant Cell Rep. 16:232-234.
14. Metting B. and Pyne J., 1986. Biologically active compounds from microalgae. Enzyme Microbiol. and Technol., 8 : 386-394.
15. Murashige T. and Skoog F., 1962. A revised medium for repid growth and bioassays with tobacco tissue cultures. Physiol. Plant. 15 : 473-479.
16. Novak F.J., Brunner H., Afza, R., Morpurgo, R., Upadhyay R.K., Van Duren M., Sacchi M., Hawz J.S., Khatri A., Kahl G., Kaemmer D., Ramser J. and Weising K., 1993. Improvement of *Musa* through biotechnology and mutation breeding. In: Biotechnology applications for banana and plantain improvement . Proc. Of the Workshop. INIBAP, pp 143-158.
17. Rao P.S., Ganapathi T.R., Suprasanna P. and Bapat V.A. 1993 Encapsulated shoot tips of banana : a new propagation and delivery system. InfoMusa 2(2):4-5.
18. Rao P.S., Ganapathi T.R., Bapat V.A., Kulkarni VM and Suprasanna P. 1999. Improvement of banana through biotechnology and mutation breeding. IAEA Tecdoc 1047 on Use of Novel DNA fingerprinting techniques for the detection and characterization of genetic variation in vegetatively propagated crops. IAEA, Vienna. pp 107-118.
19. Singh H.P, 1990. Country paper report on banana and plantain - India. In: Banana and plantain R & D in Asia and the Pacific. INIBAP, pp. 161-185.
20. Vuylesteke D.R., 1989. Shoot tip culture for the propagation, conservation and exchang of *Musa* germplasm. Practical Manual for Handling Crop Germplasm *in vitro* 2, IBPGR, Rome, Italy.
21. Vuylesteke D.R. and Swennen R. 1993. Biotechnology: enhancing research on tropical crops Africa. In: Ed. Thotapilly G, Monti LM, Mohanraj DR., Moore AW, IITA. Pp. 143.
22. Wake H., Umetsu H., Ozeki Y, Shimamura K. and Matsunaga T. 1991. Extracts of marine cyanobacteria stimulated somatic embryogenesis of *Daucus carota* L. Plant Cell Rep. 9 : 655-658.
23. Wake H., Akasaka A., Umetsu H., Ozeki Y, Shimamura K. and Matsunaga T. 1992. Enhanced germination of artificial seeds by marine cyanobacterial extract. Appl. Micro. Biotechn. 36 : 684 - 688.

This paper was presented the Best Poster award in micropropagation in the National Symposium on "Plant Tissue Culture : Commercialization, Diversification of Agriculture and Preservation of Fragile Ecosystems", held during April 10-12, 1996, at G.B. Pant University of Agriculture and Technology, Pantnagar

About the authors ...

Dr T.R.Ganapathi *did his Ph.D. from Karnatak University,Dharwad, and joined BARC in 1991. He is working in the Plant Cell Culture Technology Section of Nuclear Agriculture and Biotechnology Division. His specialization is in the field of Plant tissue culture. He has standardized micropropagation protocols in banana and the technique has been transferred to user agencies. He has also established methods for somatic embryogenesis and agrobacterium mediated transformation in banana using embryogenic cell cultures. Currently, he is working on Genetic Transformation for the incorporation of useful traits into crop plants.*

Dr P. Suprasanna *joined BARC in 1991 after obtaining his Ph.D. degree in Genetics from Osmania University, Hyderabad. He is working in the Plant Cell Culture Technology Section of NA & BTD and is engaged in plant biotechnological research on rice, banana and sugarcane. His contributions have been in the areas of cell and tissue culture, somatic embryogenesis, in vitro selection and synthetic seeds. Dr Suprasanna has to his credit, more than 60 research publications in journals and books published by national and international publishers. His interests are in using plant cell cultures for understanding mechanism of differentiation as well as for genetic manipulation.*

Dr Vishvas M. Kulkarni *joined BARC in 1993 and subsequently obtained Ph.D. (Biotechnology) degree from Mysore University. In the Plant Cell Culture Technology Section of NA & BTD, he has been working on the use of tissue culture, molecular biological approaches in Banana and Pearl Millet and on mutagenesis in vitro using gamma irradiation for the isolation of banana mutants. He has also been involved in collaborative research projects, and has guided graduate and postgraduate students for the completion of their research projects. He has published several research papers in National and International Journals/Symposia/Workshops.*

Dr V.A. Bapat *is working in the area of plant tissue culture for the last 31 years. The main thrust area of his work is on Micropropagation and Genetic Transformation of Plants. He has effectively contributed for clonal propagation, suspension cultures, protoplasts, synthetic seeds and bioreactor production of somatic embryos in a precious forest tree - Sandalwood. He has also done extensive work on micropropagation of Banana and Mulberry. He has several publications in National and International journals to his credit. Currently he is heading the Plant Cell Culture Technology Section.*

Dr P. S. Rao*, former Head, Nuclear Agriculture and Biotechnology Division, joined BARC in 1966. and subsequently obtained his Doctorate in Botany from Delhi University in 1967. As a Visiting Scientist, he did advanced research in plant morphogenesis at the CNRS labs in Gif-sur-Yvette, France and in protoplast culture (1981-82) at the Max-Planck Institute, Koln, Germany. He is a Fellow of the National Academy of Sciences of India, and National Academy of Agricultural Sciences. Dr. Rao has guided several students for M.Sc., M.Tech. and Ph.D. He has published more than 170 research papers/articles. He has been the member of advisory board of several national research centres, universities and government bodies such as Department of Biotechnology (DBT), Department of Science & Technology (DST). He is a member of several professional societies in India and abroad, and is serving on the editorial board of scientific journals. Currently, Dr.Rao is the Vice-President (Biotechnology) of Indo-American Hybrid Seeds (India) Pvt. Ltd., Bangalore.*

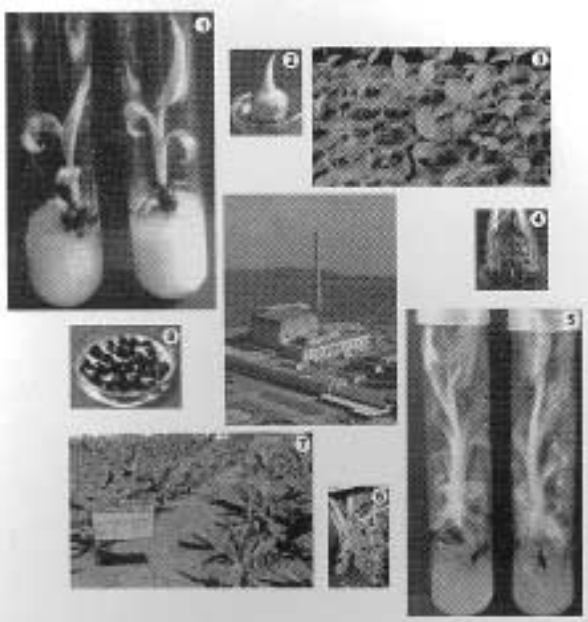

1. Plantlet development from synthetic seeds of banana.
2. Isolated shoot tip used to initiate in vitro shoot cultures.
3. Hardened plants in the greenhouse.
4. Multiple shoots developed in liquid medium.
5. Rooted shoots.
6. Tissue culture derived banana plant bearing a fruit bunch.
7. Tissue cultured plants undergoing field trial at GSFC experimental field, Vadodara.
8. Encapsulated shoot tips of banana (synthetic seeds).

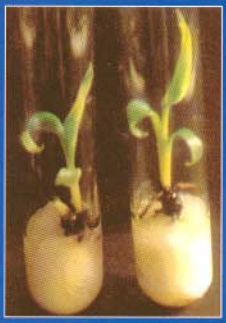


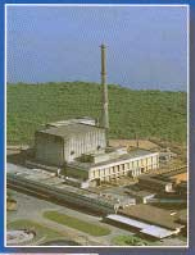




Edited and Published by
Dr. Vijai Kumar, Head, Library & Information Services Division
Bhabha Atomic Research Centre, Trombay, Mumbai 400 085, India
(For private circulation)

Editorial Management : T. C. Balan.
Computer Graphics, Design & Layout : P. A. S. Warrier
Available at URL : http\\www.barc.ernet.in